8-2010

Polymeric Loop Formation at Hard and Soft Interfaces

Earl Ashcraft
University of Tennessee - Knoxville, ashcraft@utk.edu

To the Graduate Council:

I am submitting herewith a dissertation written by Earl Ashcraft entitled "Polymeric Loop Formation at Hard and Soft Interfaces." I have examined the final electronic copy of this dissertation for form and content and recommend that it be accepted in partial fulfillment of the requirements for the degree of Doctor of Philosophy, with a major in Chemistry.

Mark D. Dadmun, Major Professor

We have read this dissertation and recommend its acceptance:

Jimmy W. Mays, Charles S. Feigerle, Kevin M. Kit

Accepted for the Council:

Carolyn R. Hodges

Vice Provost and Dean of the Graduate School

(Original signatures are on file with official student records.)

To the Graduate Council:

I am submitting herewith a dissertation written by Earl C. Ashcraft entitled “Polymeric Loop Formation at Hard and Soft Interfaces.” I have examined the final electronic copy of this dissertation for form and content and recommend that it be accepted in partial fulfillment of the requirements for the degree of Doctor of Philosophy, with a major in Chemistry.

Mark Dadmun, Major Professor

We have read this dissertation
and recommend its acceptance:

Jimmy Mays

Charles Feigerle

Kevin Kit

Accepted for the Council:

Carolyn R. Hodges

Vice Provost and Dean of the Graduate School

(Original signatures are on file with official student records.)

POLYMERIC LOOP FORMATION AT HARD AND SOFT INTERFACES

A Dissertation

Presented for the

Doctor of Philosophy Degree

The University of Tennessee, Knoxville

Earl Ashcraft

August 2010

Acknowledgements

I would like to thank my advisor, Dr. Mark Dadmun, for supporting this project and for all the time and effort he put into critically reviewing my work. I would also like to thank him for letting me work independently on this project, thus enabling me to pursue my own interests. The guidance and time committed to reviewing this document by my other committee members, Dr. Jimmy Mays, Dr. Charles Feigerle, and Dr. Kevin Kit, is also greatly appreciated. The completion of this study would have been much more difficult without the expertise, advice, and friendship of my lab mates. I would like to thank past and present group members. They include Kevin Rice, Sudesh Kamath, Steve Wargacki, Scott Fontana, Asif Rasheed, Deepali Kumar, Michael Lay, Nate Crawford, Nathan Henry, Shraddha Deodhar, Rujul Mehta, Dias Linton, Chang-Uk (Jack) Lee, Caleb Dyer, Brian Bachner, Brad Miller, Leslie Thompson, Zhenyu Huang, Huimin Li, Onome Swader, Say-Lee Teh, Mary Mutz, Wen Yin, Raghu Hegde, Brandi Weigand, and Adam Imel.

The work and determination put into this project is dedicated to my father, Robert Ashcraft. May he rest in peace. 11/14/44 – 03/02/94

Financial support of this project was provided by NSF grant CHE-0304807.

Abstract

Copolymers are used to increase the interfacial strength of immiscible components and suppress recombination of the minor phase by steric hindrance. The experiments conducted in these studies are designed to investigate *in situ* polymer loop formation at soft interfaces and functionalized nanotube surfaces. Block copolymers are the most effective type of copolymer for compatibilization because they extend perpendicular to the interface, allowing good entanglement with the homopolymer chains. Multiblock copolymers are more effective than diblock copolymers for strengthening the interface because they can cross the interface multiple times, forming "loops" in each phase that provide entanglement points for the homopolymer.

The first part of this dissertation focuses on understanding how telechelic variables influence their effectiveness to compatibilize an immiscible polystyrene (PS)/polyisoprene (PI) homopolymer blend. A fast reacting anhydride and amine telechelic pair (anh-PS-anh/NH2-PI-NH2) are compared with a slower reacting epoxy and carboxylic acid pair (epoxy-PS-epoxy/COOH-PI-COOH). Different molecular weight pairs are used to investigate the influence of end group concentrations and steric effects. We also investigate how the loading level affects the conversion of one telechelic pair. The PI telechelic has a fluorescent tag, which enables gel permeation chromatography (GPC) with fluorescence detection to be used for determining the amount of tagged PI converted and the molecular weight of the copolymer formed *in situ* as a function of mixing time. The effectiveness of these telechelic pairs as compatibilizers is quantified by annealing the samples and using scanning electron

microscopy (SEM) to measure the domain size of the minor phase as a function of annealing time.

The second part of this study investigates the grafting of polymer loops to carboxylated multiwall nanotube (COOH-MWNT) surfaces and determining the reaction rate. These polymer loops will improve the nanotube dispersion by steric hindrance and improve energy transfer by creation of polymer chain entanglements. Fourier transform infrared spectroscopy (FT-IR) is used as a novel technique to measure the quantity of epoxy-PS-epoxy grafted to the nanotube surface. In addition, we determined the fraction of telechelics that form loops by further reacting the grafted nanotubes with monocarboxy terminated poly(4-methylstryrene) (COOH-P4MS), which only reacts with unbound epoxy-PS-epoxy chain ends.

TABLE OF CONTENTS

LIST OF TABLES

LIST OF FIGURES

Chapter 1

Introduction

1.1 Use of Polymer Blends

For nearly a century, our lives have been made easier by products composed of polymeric materials. With polymer-based components, it is possible to make products that are lightweight, strong, heat resistant, transparent, or environmentally inert, just to name a few advantages. More importantly, these products designed for mass consumption are also designed to be inexpensive. Polymers are large molecules composed of simple repeating units called monomers. The physical properties of a polymer depend on many factors, such as chain length, crystallinity, monomer structure, and interchain bonding forces. Many polymer-based products require physical properties that cannot be found in a single polymer; for instance it may be desirable to have a material that is both strong and impact resistant. In order to obtain a desired physical property, it may be necessary to design and synthesize a new polymer for one specific purpose. This is expensive and time consuming. It is much easier and cost effective to take commercially available polymers and mix them together, forming a polymer blend. Polymer blends can be used to tailor the properties of a material.[1] By mixing different polymers together in varying ratios, favorable properties of each individual polymer can be incorporated into the final material. Polymer blends are very important for industrial purposes since it is much more cost effective to blend commercially available polymers than it is to synthesize a new polymer for one specific application. Polymer blends are essential to the plastics market, exemplified by the fact that 1.5 million tons of polymer blends were made in 1998.[1]

1.2 Thermodynamics of Polymer Blends

However, making usable blends is not trivial because most polymers are immiscible due to their positive enthalpy of mixing.[2] Polymer blends exhibit a free energy of mixing described by:

$$\Delta G_{mix} = \Delta H_{mix} - T\Delta S_{mix} \tag{1.1}$$

where ΔG_{mix} is the Gibbs free energy of mixing, ΔH_{mix} is the enthalpy of mixing, ΔS_{mix} is the entropy of mixing, and T is the absolute temperature. For a blend to be miscible, ΔG_{mix} must be negative,[3] indicating a lowering of the free energy upon mixing. The entropy of mixing is only slightly increased during blending since polymer chains are already disordered to begin with,[2] meaning that miscibility of polymers is primarily controlled by the enthalpy of mixing. Another way to understand the enthalpy of mixing is to express ΔH_{mix} in terms of the polymer-polymer interaction parameter, χ. The parameter χ is negative for favorable inter-polymer interactions, 0 for athermal interactions, and positive for unfavorable interactions. The role of the χ parameter in the free energy of mixing can be best understood through the Flory-Huggins theory of polymer solutions. This lattice model theory calculates the entropy of mixing by considering the number of ways a polymer chain can be placed in a lattice and calculates the enthalpy of mixing by determining the interaction energy between neighboring segments of different types.[4] This equation can be applied to polymers in the melt as well,[2] and the free energy of mixing can be expressed by:

$$\Delta G_{mix} = (RTV/V_r)[\, \chi_{ab}\, \varphi_a\, \varphi_b + (\varphi_a/N_a) \ln \varphi_a + (\varphi_b/N_b) \ln \varphi_b] \tag{1.2}$$

where R is the ideal gas constant, V is the total volume, V_r is the reference volume which is taken as the molar volume of the smallest polymer repeat unit, χ_{ab} is the interaction

parameter between polymer *A* and *B*, φ_a and φ_b are the volume fraction of polymer *A* and *B*, respectively, and N_a and N_b are the degrees of polymerization of polymer *A* and polymer *B* in terms of the reference volume, respectively. The contribution of ΔS_{mix} *to* the energy of mixing is always positive, leading to a negative contribution to ΔG_{mix}. Therefore, the sign of the Gibbs free energy of mixing depends on the enthalpy of mixing, ΔH_{mix}. An immiscible polymer blend will have a large positive χ parameter, leading to large positive ΔH_{mix} value, making the Gibbs free energy of mixing positive and therefore unfavorable.

A polymer blend can be compatibilized by adding a copolymer, a molecule that contains the same or similar repeat units as the homopolymers in the blend. Ideally, the copolymer will reside at the interface between the immiscible polymers, as will be discussed later in this chapter. When the copolymer is at the interface, it displaces the unlike homopolymers from the interfacial region. Assume the copolymer is composed of repeat units *C* and *D*, and unit *C* is compatible with homopolymer *A* while unit *D* is compatible with homopolymer *B*. The addition of the copolymer separates the homopolymers at the interface, minimizing interactions between the unlike homopolymer chains. The Gibbs free energy of mixing will now contain the parameters χ_{AC} and χ_{BD}, which are much more favorable than χ_{AB}.

1.3 Blend Morphology during Processing

Because most polymer pairs have a positive χ value, they will phase separate in order to minimize interactions between components, resulting in a sharp and narrow interface between the unlike phases. Subsequently, a weak interface is formed due to the minimization of chain entanglements between the unlike phases,[5] often yielding a

polymer blend with poor mechanical properties.[6] The final blend morphology of two immiscible polymers mixed together depends on several factors such as the shear rate, viscosity ratio, interfacial tension, elasticity ratio, and processing conditions.[7-9] At low concentrations of the immiscible homopolymer, the blend morphology usually consists of minor phase droplets dispersed in the major phase matrix. These droplets continue to increase in size as the minor phase blend composition is increased.[10] Upon reaching a nearly equal homopolymer composition, a co-continuous morphology is attained.[10,11] The viscosity ratio has a significant effect on the final morphology, as ellipsoid and fiber shapes have also been observed.[12,13] In addition, the viscosity ratio also greatly affects the concentration at which the blend becomes co-continuous.[13]

In industry, blends are most often prepared by mixing the polymers together in an extruder at an elevated temperature. According to Scott and Macosko,[14,15] the blend morphology evolves rapidly during mixing. The two components are added together into the mixer as solid pellets. In the first stage of softening and melting, the polymers become deformable solids and then viscoelastic liquids. There is a large fluctuation in the temperature, stress, and strain within the sample during this stage, due to variation in heat transfer at very short mixing times. Large deformations and reduction of the minor phase domain size occurs in regions above the softening or melting points of the polymer during this stage. During the second stage of mixing, a sheet or ribbon of the minor phase is formed due to either field flow or from a piece of the sample being dragged across a hot surface in the mixer. Holes form in the ribbon as a result of the interfacial tension and flow, and the matrix subsequently fills these holes. This results in a lace structure, which then breaks apart into irregular sized pieces due to the interfacial tension

and flow. Finally, these pieces further break down into spherical droplets on the micron to sub-micron size scale. A schematic of this process is seen in Figure 1.1, from ref. 9. During the mixing of these immiscible polymers, a sharp interface forms between the matrix and dispersed phase, as each species tries to minimize its interaction with the other. During mixing, the droplet size is determined by the balance between droplet breakup by shear forces and droplet recombination due to coalescence, a process which will be more thoroughly discussed later. If the mixing is stopped, the particles will readily coalescence. Controlling the coalescence is critical for tuning polymer blends to have specific properties because the size of the droplets and their interactions with the matrix control the physical properties of the polymer blend. A system with poor interaction between immiscible polymer chains leads to poor stress transfer and adhesion; since it is energetically unfavorable for the polymers to mix with each other, there will be few entanglements between them. This is the primary cause of mechanical failure in polymer blends. A useable polymer blend requires a method to increase the interactions between unlike polymers and to prevent the droplets from recombining.

1.4 Effect of Copolymer Architecture on Compatibilization Ability

In order to create a usable polymer blend composed of immiscible homopolymers, a copolymer may be added during the mixing phase. The copolymer that is added to the blend is composed of monomer units that are identical or compatible with each of the homopolymers. The ordering of these monomer units can be random (no order in the sequence of monomer units: *ABBABAAABABB*), alternating (ordered repetition of single monomer units: *ABABAB*), block (a sequence of one type of monomer followed by a sequence of another type: *AAAAABBBBB*), or graft (one or more blocks of polymer *B* is

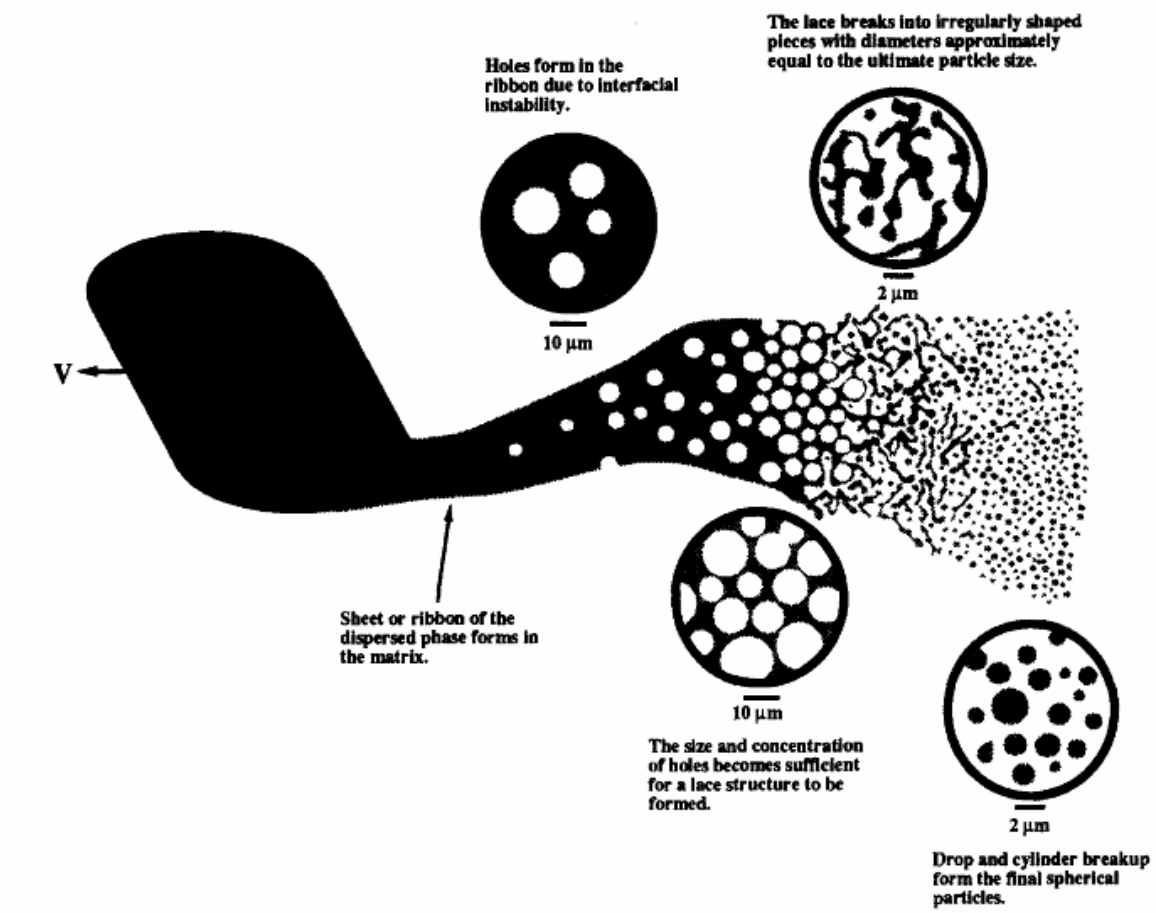

Figure 1.1. The proposed mechanism by Scott and Macosko for droplet formation of the minor phase in a polymer blend during melt mixing.

grafted as branches onto a backbone of polymer *A*). A copolymer will ideally reside at the interface between the homopolymers because unfavorable interactions with unlike homopolymers are minimized.[16-18] For example, an *A*-*B* block copolymer initially dispersed in homopolymer *A* will migrate to the interface so that the *B* component of the copolymer can avoid an unfavorable *A*-*B* interaction. This repulsion between unlike phases is the driving force for copolymer migration to the interface. This enthalpy reduction must compensate for the reduction of the entropy of the system that results from confining the copolymer to the interface.[16,17,19] When the copolymer resides at the interface, it displaces unlike homopolymers away from each other, making ΔH_{mix} between the unlike homopolymers less unfavorable.[17,20] The like chains can become entangled with each other, thus strengthening and broadening the interface between the immiscible homopolymers.

In this discussion, it is has been assumed that all of the copolymer chains reside at the interface. However, if the copolymer concentration is above the critical micelle concentration (CMC), the concentration of non-aggregated free copolymer chains increases very slowly with copolymer concentration while the excess copolymer chains form micelles in one of the homopolymer phases.[21,22] Block and graft copolymers tend to form micelles in the bulk, while random copolymers do not have this tendency.[23] The component of the copolymer which is incompatible with the homopolymer phase forms the core of the micelle and the component of the copolymer which is compatible with the homopolymer phase chains forms the corona of the micelle. Micelle formation is undesirable because copolymers cannot modify interfacial properties while trapped as

micelles in the bulk phase. In addition, micelle formation may also lead to a reduction in mechanical properties of the blend.[24]

It is important that the definition of compatibilization now be addressed since there are multiple meanings. In thermodynamic compatibilization, the addition of a copolymer results in a blend with a completely miscible, single phase that exhibits one single glass transition temperature. This may be desirable for blending some systems, such as a low molecular weight plasticizer into a high molecular weight polymer in order to make processing easier. However, it may not be desirable to have complete miscibility, such as the case of rubbery polymers added to glassy, rigid polymers. In this case it is important for the separate rubbery phase to be able to absorb and dissipate impact energy. Here, efficient interfacial stress transfer is desirable. In order to transfer stress efficiently between the immiscible polymers, there must be sufficient interfacial contact between the two phases in order for the stress to be transferred. This can only happen with a strong interface. For instance, if a copolymer is present, it bridges the two unlike phases and allows energy to be transferred between chain entanglements. Thus, a second type of compatibilization is interfacial compatibilization. There are distinct separated phases in this blend, but the interface between them becomes broadened and highly entangled because the copolymer chains entangle with both homopolymers. Blends exhibiting interfacial compatibilization contain the physical properties of each component. Future references to compatibilization in this study refer solely to interfacial compatibilization.

The architecture of the copolymer will influence the extent to which it crosses the interface, and therefore the degree which it is able to interact with the homopolymer

chains. There have been several experimental and theoretical studies demonstrating how block copolymers cross the interface to the greatest extend, which maximizes the copolymer chain entanglements with the homopolymers. Fayt et al. were the first to experimentally show that when a premade diblock copolymer is melt blended with immiscible homopolymers, the copolymer may reside at the interface, with each block extending into its analogous homopolymer phase.[25] If the segment length of the copolymer is long enough, the homopolymer chains can become entangled with it, and interfacial adhesion is increased.[20] Monte Carlo simulations performed by Dadmun demonstrate that block copolymers extend across the interface to a greater extent than in the other two dimensions, whereas random and alternating copolymers extend more along the interface.[26] This suggests block copolymers are more effective interfacial compatibilization agents than random, alternating, and graft copolymers. Because the blocks of the copolymer can extend the furthest into the homopolymer phases, they may more readily become entangled with the homopolymer chains, improving stress transfer.

1.5 Role of Copolymer

A. Interfacial Adhesion

When a copolymer is added to a blend, it may locate at the interface. In the case of a block copolymer, type *A* blocks can intertwine with type *A* homopolymer chains, while type *B* blocks intertwine with type *B* homopolymer. The copolymer separates the unlike homopolymers at the interface and allows them to relax in the like block of the copolymer. The copolymer therefore creates entanglements between the immiscible chains and strengthens the interface. Early studies on polymer blends experimentally demonstrated how copolymers strengthen the interface. Ide and Hasegawa[27] showed that

incorporating maleic anhydride grafted-polypropylene (MAH-PP) to an immiscible nylon 6/polypropylene (N6/PP) blend improves dispersion and increases the mechanical properties of the blend. This was attributed to the grafting of MAH-PP to the nylon via reaction of the maleic anhydride group with the terminal amine group on the nylon (N6). This results in chain entanglement between the PP homopolymer and grafted MAH-PP chains. Fayt et al. showed that the addition of a poly(hydrogenated butadiene-b-styrene) diblock copolymer to low density polyethylene/polystyrene (LDPE/PS) and high density polyethylene/polystyrene (HDPE/PS) blends increases the interfacial adhesion of the homopolymers, resulting in increased yield strength, ultimate strength, and elongation at break.[28,29] Additionally, Liu and Baker demonstrated that adding a diblock copolymer improves interfacial adhesion between the bulk phases and increases the impact resistance of polystyrene/butadiene rubber (PS/NBR) polymer blends.[30] Clearly, the copolymer's role of promoting entanglements between the homopolymers is critical to improving the mechanical properties of the blends. The discussion in this section suggests block and graft copolymers may contain segments long enough to become entangled with the homopolymer chains, while random and alternating copolymers do not have segments long enough to become entangled. Block copolymers are also more effective compatibilizers than graft copolymers. If the graft copolymers have a high degree of branching, the grafts will not effectively penetrate into the homopolymer phases and become entangled.[31] Thus if the segments of the copolymer chain are not long enough, the copolymer cannot effectively strengthen the interface of an immiscible polymer blend.

B. Interfacial Tension

The surface tension describes the energy present per unit area at the liquid/air interface. The interactions between a molecule and the bulk liquid are balanced by equally attractive forces in all directions. When the molecule is at the surface, there are not any attractive forces acting on the particle from the surface, leading to an overall unbalanced attractive force towards the bulk. These molecules at the surface are in a higher energy state than the molecules in the bulk. This subsequently leads to an excess of free energy at the surface called the surface free energy. In order to minimize the energy of the system, the liquid tries to minimize its surface area in order to decrease the number of molecules at the interface. To change the surface area A of the liquid by an amount δA, a quantity of work $\gamma \delta A$ must be applied, where γ is the surface tension in units of force per area.[32] Surfaces must be less energetically favored than the bulk, otherwise there would be a driving force for surfaces to be created. The surface energy can be described as the excess energy at the surface compared to the bulk. For a liquid, the surface energy and surface tension are the same.[33] When the surface being described is the interface between two liquids, this quantity is referred to as interfacial tension. For example, when a small quantity of oil is placed in water, oil droplets are formed. Oil does not mix with water, creating an interface between the liquids. To minimize this unfavorable interaction, the oil droplets reduce their surface area and form droplets in the water. The amount of work required to increase the surface area of the oil droplet is large since these unfavorable interactions must be overcome. In other words, the surface tension γ is high. Likewise, an immiscible polymer blend has a large interfacial tension due to unfavorable interactions of unlike polymers at the interface. When a block

copolymer is added and locates at the interface, the homopolymer chains are pushed away from each other, as previously discussed. As the homopolymer chains become entangled with the like blocks of the copolymer, ΔH_{mix} and the interfacial tension are reduced.[34] Because the homopolymer chains can relax in the like copolymer block and their interaction is not unfavorable, much less work is required to expand the interfacial area, thus the interfacial tension has been reduced. When sufficient copolymer is present at the interface, the interfacial tension may be driven to zero or even slightly negative.[35,36] Under these conditions, there is no longer a free energy penalty for increasing the interfacial area. Another benefit of reduced interfacial tension is the fact that droplet breakup by shear forces during mixing becomes much easier, creating a finer dispersion of particles.[37]

Earlier studies of polymer blends correlated the main role of diblock copolymers as compatibilizers to the observed decrease in interfacial tension. Anastasiadis et al. observed an initial linear decrease in interfacial tension with an increase in copolymer concentration, followed by a leveling off as the copolymer concentration increased further.[38] The leveling off was due to surpassing the critical micelle concentration (CMC), the concentration at which copolymers formed micelles in the homopolymers.[21,39] Above this concentration, the copolymers were not located at the interface where they lower the interfacial tension. Favis related the observed decrease in particle size to the decrease in interfacial tension upon addition of a diblock copolymer.[40] The particle size decreased linearly with the diblock concentration up to a certain point, then leveled off. The point at which the dispersed phase didn't show any further decrease in particle size was correlated to the saturation of the interface with copolymer.

C. Coalescence Suppression

A third role the copolymer plays is to prevent the droplets from recombining during mixing or annealing. The final size of the particles is governed by several variables at a given volume fraction. For a single Newtonian droplet in a Newtonian matrix, Taylor showed that the final droplet diameter can be estimated by:[41]

$$D = \frac{\gamma(16\eta_r + 16)}{G\eta_m(19\eta_r + 16)} \tag{1.3}$$

where D is the droplet diameter, γ is the interfacial tension, G is the shear rate, η_m is the matrix viscosity, and $\eta_r = \eta_d/\eta_m$ is the relative viscosity where η_d is the viscosity of the minor phase droplets. The Taylor equation cannot accurately predict particle size of polymer blends since they are viscoelastic fluids and not Newtonian fluids. The viscoelastic forces can further stabilize the droplet and prevent breakup into smaller particles.[42] In addition, the Taylor equation does not take droplet recombination into account, as blends with over a few percent minor phase show much larger droplet sizes than the Taylor equation predicts.[43,44] Despite this fact, the Taylor equation can still be used on polymeric systems to provide a comparative understanding of the behavior of blends.[44] Studies by Sundararaj and Macosko[43] showed that blends with 10 wt. % block copolymers had droplet sizes nearly identical to a blend without copolymer at low minor phase concentrations. When higher concentrations of the minor phase were used, the droplet size was reduced relative to the blend without copolymer. It was noted that if the primary role of the copolymer was to reduce the interfacial tension, then the droplet size at low minor phase concentrations should have been reduced significantly. Experimental results by Beck-Tan et al. came to the same conclusion about the role of the copolymer.[44]

The fact that the droplet size was not reduced at very low minor phase concentration suggests that the main role of the copolymer is to prevent the droplets from coalescence, a process in which smaller droplets combine to form larger droplets. At very low minor phase concentrations, there is a low probability of droplet collision due to the fact that there are so few droplets in the system. Coalescence occurs because the blend is not in a thermodynamically stable state, and therefore the system tries to reduce the interfacial energy as much as possible by increasing the particle size.[45] The attractive van der Waal forces between the minor phase particles is the driving force for coalescence in polymer blends.[46] When a block copolymer is present at the interface of an immiscible blend, one block extends into the minor phase droplets, and the other block extends into the matrix. Coalescence is suppressed when the compatibilized droplets try to recombine because the copolymer blocks extending into the matrix must be compressed in order for the droplets to meet. That is, the attractive van der Waals force between the droplets must be greater than the repulsive elastic force of the chains being compressed for coalescence to occur. A diagram of the steric effect of copolymers is shown in Figure 1.2, taken from ref 37. Coalescence is also possible if the copolymer can be moved out of the contact area. However, Sundararaj and Macosko assumed the copolymer was nearly immobilized at the interface due to the increase in viscosity as a result of entanglement between the homopolymer and its analogous copolymer block.

A second school of thought for the primary role of the copolymer is the Marangoni effect. In this mechanism, proposed by Milner and Xi,[47] the approaching droplets push out the matrix fluid between them. This sets up a recirculating fountain flow that sweeps away the copolymer in the collision of the droplets. Here the copolymer

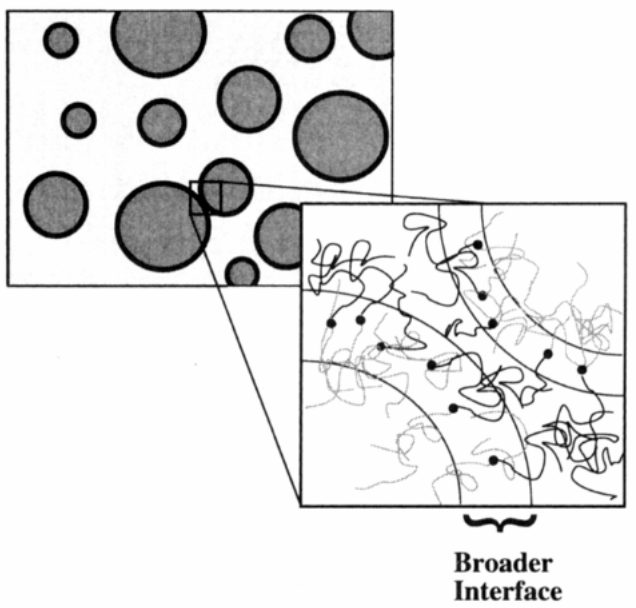

Figure 1.2. The Sundararaj and Macosko theory describes how copolymers prevent coalescence by steric hindrance, as the blocks extending into the matrix must be compressed before the droplets are able to recombine.

is assumed to have some mobility, unlike the immobile copolymer assumption of Sundararaj and Macosko. Due to this mobility, the copolymer can no longer prevent the collision of droplets by steric hindrance, but the work done removing the copolymer creates a repulsive force between the droplets. This repulsive force suppresses coalescence. Figure 1.3, from ref 41, shows the Marangoni effect.

Over the last decade, there have been several studies that support the Sundararaj and Macosko mechanism for coalescence suppression.[48-58] However, many studies support the Milner and Xi theory as well.[59-64] One primary difference between the mechanisms is the shear rate dependence of the amount of copolymer at the interface required to suppress coalescence. For coalescence suppression due to steric hindrance, the minimal interfacial surface coverage of copolymer needed to inhibit droplet recombination, Σ_{min}, is independent of shear rate:[49]

$$\Sigma_{\min} = \frac{20}{27\pi\left\langle r_0^{\,2}\right\rangle} \tag{1.4}$$

where $<r_0^2>$ is the average of the squares of the relaxed chain end – to – end distance of the copolymer block extending into the matrix. If the Marangoni effect is responsible for inhibiting droplet recombination, the amount of copolymer required to suppress coalescence is proportional to shear rate:[47,54]

$$\Sigma_{\min} = \frac{5}{32}\frac{D\eta_m G}{k_B T} \tag{1.5}$$

where D is the particle diameter, η_m is the matrix viscosity, G is the shear rate, k_B is the Boltzmann constant, and T is the absolute temperature. According to Lyu et al.,[54] it is believed that there are few experimental results supporting the Marangoni effect as the primary cause of coalescence suppression because this theory assumes the Marangoni force is weak and allows for a mobile drop surface, which is equivalent to a dilute concentration of copolymer at the interface. However, the fact that 25% – 80% copolymer coverage is needed in experiments by Lyu et al. and 20% copolymer coverage is needed in experiments by Macosko et al.[49] to suppress coalescence indicates the copolymer concentration at the interface is not dilute. Likewise, the small change in $\Sigma_{\min}$

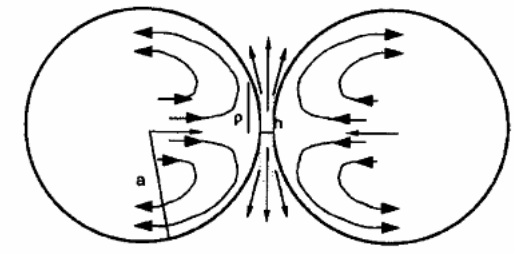

Figure 1.3. According to the Milner and Xi theory, the Marangoni effect prevents coalescence by creating a repulsive force between droplets due to the work required to create a recirculating fountain flow created when the matrix fluid is drained upon droplet recombination.

with shear rate observed in experiments by Lyu and Macosko also suggests that the main mechanism of coalescence suppression is due to steric hindrance and not Marangoni forces. In this study, the effects of shear rate have not been tested, and it is assumed that the copolymer inhibits coalescence due to steric hindrance.

1.6 Reactive Extrusion

It has been demonstrated that block copolymers are effective compatibilizers because they cross the interface, displace homopolymers at the interface, and promote entanglements of analogous chains. An effective way to compatibilize a blend is to create a block copolymer *in situ* by reactive extrusion.[65] This is accomplished by melt mixing polymers with reactive end groups along with their homopolymer analogs in an extruder. There are several reasons why reactively formed copolymers are more effective than premade copolymers. First, the only place that the reactive polymers can meet is at the interface between the immiscible homopolymers,[1,66] thus the copolymer is only formed in the desired region. Any unreacted polymer remains in its homopolymer analog. Although reactively formed copolymers can still form micelles, the probability of this occurrence is lower because the copolymer is only formed at the interface.[1] It has been shown that premade diblocks tend to form micelles in the bulk before saturating the interface.[67] This means there may not be sufficient copolymer present at the interface to prevent coalescence. In addition, the presence of micelles in the bulk is undesirable, since it will decrease the mechanical properties of the blend. Thirdly, reactively formed copolymers are made when lower molecular weight species react at the interface to form a higher molecular weight copolymer. Since the reactive polymers are smaller molecules

than the premade copolymer, they can get to the interface faster due to their lower viscosity and faster diffusion.[1] This allows the copolymer to be present at the interface more quickly than the premade polymer.[68]

1.7 Kinetics of Reactive Polymers

To effectively compatibilize a polymer blend during processing, the *in situ* creation of a significant quantity of copolymer needs to occur on the timescale of minutes. When polymer blends are made for industrial applications, the components are melt mixed in an extruder only for an average of 2 – 5 minutes, thus it is important to use functionalized polymers with highly reactive end groups or a high concentration of end groups (low molecular weight chains) in order to get a significant conversion in this time frame.[65] An important question to answer is whether the rate determining step in the formation of copolymer from reactive blends is the diffusion of the polymer to the interface or the reaction of the end groups at the interface. Fredrickson and Leibler conducted theoretical studies assuming that the diffusion of the chains to the interface is the rate determining step in a dilute quiescent (zero shear) system, and that the reaction occurs quickly when the reactive groups are inside of a reaction sphere.[69] In other words, the reaction of the functional groups at the interface occurs instantaneously, and any further reaction is dependent on the time it takes for the reactive polymer to diffuse to the interface. Fredrickson and Leibler then incorporated the effects of shear, where the reaction rate becomes dependent on the shear rate:

$$k_{shear} = 50.26 D_0 R[1 + 0.8068 De^{1/2} + \ldots] \quad (1.6)$$

where D_0 is the diffusion coefficient, R is the radius of gyration of the reaction sphere, and De is the Deborah number, $De = \kappa\tau$. The coefficient κ is the characteristic time scale

of the velocity tensor, and is equal to the shear rate in case of simple shear flow, and τ is the longest polymer chain relaxation time. Thus the reaction rate under shear is limited by how fast the chains can be brought to the interface by shear forces, and the reaction is therefore still diffusion controlled.

In real world applications, the reactivity of functional groups is much lower, as measurable reactions take place on the second or minute time scale. A more recent theory by O'Shaughnessy and Vavylonis[70,71] assumed that for a quiescent, dilute system at short reaction times, the chemical reactivity of "weak" reactive pairs (which includes anhydride/amine and epoxy/carboxylic acid reactive pairs[72] used in this study) inside a reaction sphere is the rate determining step and follows 2nd order kinetics. When the interface becomes crowded with copolymer, there is a decrease in reaction rate caused by a crossover to 1st order kinetics which is controlled by the diffusion of the reactive polymer chain to the interface. Oyama and Inoue proposed a new model in which the copolymer formation is reaction controlled and followed pseudo 1st order kinetics.[73] When they plotted experimental data from other research groups, their model fit the data very well. Further support for reaction controlled kinetics was displayed by determining the activation energy, E_A, of the reaction. The reaction was conducted at various temperatures, and an Arrhenius plot was constructed to determine E_A. Oyama and Inoue noted the activation energy of diffusion controlled reactions is usually < 30 kJ/mole because only a physical process is involved, but E_A is much larger for reaction controlled kinetics because a chemical reaction takes place. The activation energy found in this study was 120 kJ/mole, which strongly suggests that the process is controlled by the chemical reaction of the functional groups at the interface.

Numerous experimental results have shown that the reaction between end groups on functionalized polymers at an interface is controlled by the reactivity of the species, and not the diffusion of the polymer to the interface. Smoluchowski's equation for a diffusion-limited reaction rate, k_d, is given by:[74]

$$k_d = 4\pi(r_1 + r_2)(D_1 + D_2)N_A \quad (1.7)$$

where r_i is the radius of the reaction sphere of reactive species i, D_i is the diffusion coefficient of reactive component i, and N_A is Avogadro's number. The fact that the experimentally calculated reaction rates for melt mixed blends are several orders of magnitude lower than the diffusion-limited reaction rate[72,74-77] means that the reaction can only proceed as fast as the end groups can react. It is also interesting to note that the interfacial reaction rate for heterogeneous reactive polymers was found to be greater than for homogeneous reactive polymers when the same reactive pairs were used. It is believed that the end groups prefer the interface, and thus are more concentrated and have a higher reaction efficiency in the heterogeneous blend.[74,75] Rice also showed that grafting difunctional polymers to a functionalized surface is reaction controlled.[78] When reactive polymers of similar molecular weight but different end groups were used, the grafting rate was greatly altered, providing further strong evidence of a reaction controlled process.

Yin et al.[79] studied the effects of molecular weight on reactivity, and showed that there was little difference in conversion of low and high molecular weight reactive polymers during the first minute of mixing (13% vs. 11%, respectively). However, the conversion of low molecular weight reactive polymers increased an additional 5% during the next 20 minutes of mixing, whereas there was no increase in conversion for the high

molecular weight reactive polymers. This was interpreted to indicate that the high molecular weight reactive polymers could not approach the interface at these later reaction times because of the presence of the large copolymers already there. This was associated with a buildup of an energy barrier of the diffusion of reactive polymers towards the interface.[80] As the copolymer concentration at the interface increases, there is an entropy loss associated with the confinement of the copolymer at the interface and the stretching of the copolymer blocks towards the bulk phase. This energy barrier increases with molecular weight, making further reaction of high molecular weight reactive polymers difficult. However, a Monte Carlo study by Smith et al. showed that the polymer chain height does not change much with increasing surface coverage, meaning the chains are not in a highly stretched configuration.[81] The reduction in reaction rate at high grafting density was therefore attributed to steric hindrance due to the growing brush, and not thermodynamic barriers associated with highly stretched chains. Smith el al. noted that thermodynamic barriers would become the primary factor affecting reaction rate at very high interfacial copolymer concentrations which are not attainable in simulations or experimental conditions due to the excessive amount of time required for the reaction to occur.

1.8 Multiblock Copolymers

As previously stated, copolymers increase interfacial adhesion by extending their blocks into their homopolymer analogs, and the chains become entangled if the molecular weight is high enough. As diblocks readily form micelles, the behavior of other linear copolymers may provide insight into improved compatibilization schemes. Russell et al. have experimentally shown that a triblock copolymer has a hairpin configuration at the

interface between two immiscible homopolymers.[82] The central block is anchored at both ends, and extends into the matrix in a manner similar to a diblock. Provided this insight, a logical conclusion is that a multiblock copolymer may provide better interfacial adhesion in a blend than a diblock, since a multiblock copolymer composed of *n* blocks crosses the interface *(n – 1)* times, forming several of these hairpin loops while a diblock only crosses the interface once, as illustrated in Figure 1.4. Theoretical studies by Noolandi have shown that diblock and triblock copolymers extend perpendicular to the interface and have a dumbbell-like shape, while multiblock copolymers occupy a larger interfacial area and have a pancake configuration along the interface.[18] Balazs et al. conducted a Monte Carlo study showing that multiblock copolymers covered a larger surface area than diblock copolymers.[83] Therefore fewer multiblock copolymers are required to saturate the same interfacial area than di- or triblock copolymers. In addition, multiblock copolymers do not form micelles as readily as di- and triblocks.[18] Previous experimental studies by Eastwood and Dadmun[84] have shown that a premade multiblock copolymer increases interfacial strength between PS and PMMA more than a diblock copolymer due to the fact that a multiblock crosses the interface several times, helping to stitch the two phases together by forming loops that can become entangled in each homopolymer phase. Asymmetric dual cantilever beam (ADCB) tests showed that the fracture toughness for copolymers of similar molecular weight followed pentablock > triblock > diblock > heptablock. The heptablock performed more poorly than the diblock due to the fact that its block lengths were not long enough to effectively entangle with the homopolymers. A pentablock forms more loops than a triblock, increasing the amount of entanglements and thus fracture toughness. It has been shown that a block copolymer

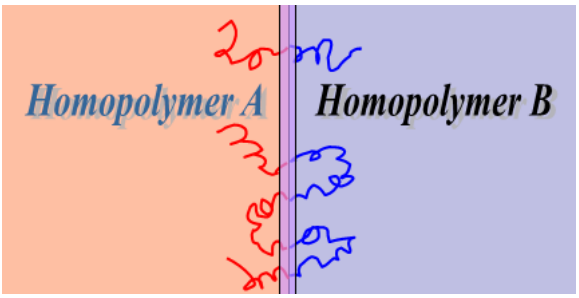

Figure 1.4. A diblock copolymer crosses the interface between two immiscible homopolymers once (top), whereas a multiblock copolymer can cross the interface many times (bottom).

must entangle with both homopolymers to act as a mechanical reinforcer. If the molecular weight of the blocks is too low, the copolymer will only act as a surfactant and lower the interfacial tension, but will poorly prevent mechanical failure at the interface.[85] Experimental studies by Kroeze et al. demonstrated that multiblock copolymers most efficiently improved the tensile strength and breaking energy of phase separated polymer blends when compared to the behavior of diblock, triblock, graft, and star copolymers.[86] The use of multiblock copolymers is the most appealing route for polymer blend compatibilization, as they provide multiple entanglement points to stitch the homopolymer phases together, resulting in improved interfacial strength and stress transfer. Multiblock copolymers are expected to offer superior compatibilization effects, while at the same time requiring a smaller amount of copolymer to be effective, which is typically about 1 – 2 wt.% for premade diblocks.[6]

1.9 Factors Affecting Compatibilization

A. Interfacial Coverage

The amount of an interfacial modifier copolymer that resides at the interface is important and must be considered in optimizing the compatibilization of polymer blends. It is imperative to note that in this study, Macosko's definition of compatibilization is

employed, the stabilization of blends against coalescence.[49] There are two types of coalescence: dynamic and static. In dynamic coalescence, the shear forces in the mixer break apart the minor phase into droplets. The droplets can recombine by coalescence as the convective flow in the system brings them together again. The final particle size is determined by the equilibrium between droplet breakup and dynamic coalescence. Because an external force is breaking apart the droplets and the flow keeps the contact time between droplets short, very little copolymer is needed in order to inhibit droplet recombination. Macosko et al. estimated that only ~1% coverage of interfacial area is required to suppress dynamic coalescence.[49] Static coalescence refers to zero shear conditions at temperatures above the T_g of all blend components. There is no force breaking up the droplets in this case. When Brownian motion brings the droplets in the vicinity of each other, the droplets will try to recombine due to the attractive van der Waals forces between the droplets in order to reduce the interfacial energy of the system. In this case, a larger quantity of copolymer is required to inhibit coalescence. This is because with few copolymer chains present, allowing contact between droplets that leads to coalescence. At higher interfacial concentrations of copolymer, there is enough crowding for the copolymer to become immobile.[49] In order to suppress static coalescence, Macosko et al. estimates the required interfacial coverage is 15% – 20%.[49]

B. Molecular Weight of Reactive Polymers

In addition to the interfacial coverage, the molecular weight of the reactive polymer plays an important role in coalescence suppression.[49] A reactive polymer of low MW can get to the interface quickly and form a copolymer, aiding in droplet breakup and dynamic coalescence suppression. However, it may not entangle with the matrix, and the

repulsive force of compressing short blocks may not be large enough to overcome the attractive forces of the approaching droplets. These low MW reactive polymers are good at preventing dynamic coalescence but act as poor compatibilizers for static coalescence. On the other hand, high molecular weight reactive polymers work best in static conditions because they form highly entangled copolymers that are immobilized at the interface, and their chain length is sufficiently long such that compression becomes difficult, thus hindering the recombination of approaching droplets. Thus there exists an optimum molecular weight of the compatibilizing polymer that will provide adequate dynamic and static coalescence suppression. Other experimental studies have confirmed this theory; an intermediate molecular weight copolymer proved to be the most effective for coalescence suppression.[54,55,87,88]

The molecular weight of the compatibilizing polymers relative to the homopolymers is also important. According to Leibler's brush theory,[89] a diblock copolymer locates at the interface and the blocks extend into the analogous homopolymers, with each block forming a "brush", or extended chain. If the degree of polymerization of the copolymer block N_i is less than the analogous homopolymer degree of polymerization $P_i^{3/2}$, a dry brush forms. In a dry brush, the homopolymer cannot penetrate into the brush. However, if $N_i > P_i^{3/2}$, a wet brush results in which the homopolymer penetrates into the copolymer block. In a wet brush, the copolymer block prefers to stay in the bulk and interact with the homopolymer, whereas in a dry brush it is energetically more favorable for the copolymer to remain at the interface. Therefore, dry brush conditions can be employed to modify homopolymer chain penetration into the

copolymer block segments, which can help discourage the formation of micelles in the bulk phase.[55]

C. Symmetry of Copolymer

Riess and Jolivet presented experimental results that indicated that a diblock copolymer with a symmetric composition is the most efficient interfacial modifier for immiscible polymers of equal molecular weight since the symmetric copolymer has no preference of bulk phases, so the interface is preferred.[90] This study also demonstrated that when the molecular weight of the copolymer blocks was less than the homopolymer molecular weight, dry brush conditions drove the copolymer to the interface. This can be explained by the reduced entropy of mixing between like chains. As the copolymer segment molecular weight increases and the brush becomes more dry, the copolymer is driven to the interface.[20] There are fewer interactions between the homopolymer chains and the like chains of the copolymer, while there is a repulsion between the homopolymer chains and the unlike chains of the copolymer. Therefore the copolymer prefers to reside at the interface in order to minimize these unfavorable interactions. Riess and Jolivet demonstrated that when the molecular weight of one of the homopolymers was less than the molecular weight of the copolymer block, forming wet brush conditions, the copolymer tended to form micelles in the homopolymer phase. They also showed that for an asymmetric copolymer composition, the copolymer preferred the homopolymer phase corresponding to the highest diblock volume fraction. For instance, a polystyrene/polyisoprene (PS/PI) diblock copolymer made mostly of PI prefers the homopolymer PI phase. Although symmetric copolymers are preferred for compatibilization, asymmetric copolymers can still be effective compatibilizers. Leibler

conducted a theoretical study which demonstrated that copolymers with a symmetry greater than $f = 0.31$ are efficient interfacial agents, with the symmetry given by:[89]

$$f = \frac{V_a^3 R_{G,a}^2}{V_a^3 R_{G,a}^2 + V_b^3 R_{G,b}^2} \tag{1.8}$$

where V_i is the molar volume of block i, and $R_{G,i}$ is the radius of gyration of block i. A perfectly symmetric copolymer has a symmetry of $f = 0.50$. Leibler showed that when the copolymer symmetry was between $f = 0.31$ and $f = 0.50$, it was possible to lower the interfacial tension to zero. He also showed that a copolymer with a majority of one block type will prefer that same bulk phase. Lyu et al. showed that when asymmetric copolymers were used, static coalescence was suppressed more when the longer chain extended into the matrix.[54] This is due to the fact that the longer chains are more difficult to compress than shorter chains, thus reducing the coalescence of minor phase droplets. Thus it is desirable to use symmetric copolymers for compatibilization, but asymmetric chains should still be effective if f is above 0.31.

1.10 Improving Dispersion of Nanotubes in Polymers

Literature review and results in our lab suggest that creating polymer loops via *in situ* multiblock copolymer formation at a soft, immiscible homopolymer interface provides an effective strategy for increasing interfacial strength and improving dispersion. The practical use of polymer loops is not limited to these applications. It stands to reason that polymer loops at a hard, polymer/nanoparticle interface should also improve dispersion of the nanotubes and enhance interaction with the polymer host. It is important to understand the role of polymer loops at the polymer/nanoparticle interface, as nanoparticles such as carbon nanotubes have been used extensively to improve the

physical properties of materials.[91,92] There are a myriad of commercial applications which could benefit from improving polymer/nanoparticle interactions. A prime example is the incorporation of carbon nanotubes into a polymer, resulting a nanocomposite which exhibits improved mechanical, electrical, and thermal properties while decreasing the weight of the material.[92]

Carbon nanotubes are cylindrical structures composed exclusively of sp^2 bonds, akin to rolled up sheets of graphite. Additionally, carbon nanotubes have a low density and exceptional strength. Nanotubes have an extremely large length to diameter ratio, with diameters on the order of 1 nm, and lengths that may extend into the mm range. At sizes on the order of nanometers, quantum confinement effects result in unique physical properties that are not observed at bulk size scales. For example, electrical and phonon conductivity through the nanotubes is significantly larger than in the bulk. However, in order for the nanotubes to optimally improve the properties of a polymer nanocomposite, they must be homogeneously dispersed throughout the material and also be able to interact well with the matrix in order to transfer stress effectively.[93] Unfortunately, nanotubes tend to agglomerate and form bundles,[94] and the expected large physical property enhancements in the polymer nanocomposite are not realized. It is expected that polymer loops grafted to a nanotube surface will entangle with the chains of the polymer host, improving nanotube dispersion and stress transfer between the matrix and nanotube. The polymer loops grafted to the nanotubes suppress aggregation of the nanotubes, which have short but very steep van der Waals attractive forces. Grafting sufficiently long polymer chains to the nanotube surface is expected to sterically hinder nanotube aggregation.

Increasing the dispersion of nanotubes can be achieved by a variety of methods. The functionalization of nanotubes provides a technique to achieve improved nanotube dispersion and interaction with the matrix. The functional groups on the nanotube surface may form covalent or noncovalent interactions with the polymer chains of the matrix. A disadvantage of this technique is that functionalization leads to the disruption of the extended π conjugation in the nanotubes, decreasing their mechanical, thermal, and electrical properties.[92] Another method to improve nanotube dispersion involves grafting polymer chains to the nanotube surface, which achieves two purposes. First, the matrix polymer chains may become entangled with the grafted polymer chains, creating a better polymer/nanotube interaction. Second, the polymer chains grafted to nanotubes hinder nanotube agglomeration[95,96] due to steric hindrance in the same manner copolymers suppress droplet coalescence. Incorporation of covalently bound polymer chains onto the nanotube surface can be achieved by either the "grafting from" technique, or the "grafting to" technique.[93] In the "grafting from" technique, a monomer and initiator are combined with the nanotubes. The initiator attacks one of the π-bonds of the nanotube. Subsequent *in situ* polymerization of the monomer ensues, resulting in covalently bound polymer chains grafted at one end onto the nanotube surface. High grafting density can be achieved using this technique. The main drawback is the fact that conditions must be tightly controlled to achieve the desired grafting density and molecular weight of the grafted polymers. In the "grafting to" technique, a pre-made polymer with reactive end groups reacts with functionalized nanotubes to form a covalent bond. High grafting density cannot be achieved using this method because the initially grafted polymers sterically hinder other polymers from finding a reactive site on the surface. An advantage

of this technique is that the grafted polymers have a controlled molecular weight and polydispersity. If a difunctional polymer chain is used in the "grafting to" technique, it may react at one end to form a "tail" or at both ends to form a "loop". Since it has been shown that polymer loops are better interfacial modifiers than diblock copolymers which form tails, it stands to reason that grafting polymer loops onto nanotubes will create a system with improved dispersion of the tubes in a polymer matrix relative to that of singly bound grafted polymer chains.

1.11 Purpose of This Study

A. Motivation

The purpose of this study is to understand how polymer loops at biphasic interfaces improve interfacial strength and dispersion in immiscible systems. The presented literature review suggests that multiblock copolymers are effective compatibilizers for immiscible polymer blends due to multiple interfacial crossings. The resulting polymer loops formed by each of the copolymer blocks in its respective homopolymer phase provide entanglement points for the homopolymer chains, improving interfacial strength. In addition, the polymer loops inhibit recombination of the minor phase component due to steric hindrance. Previous studies have only experimentally investigated the use of premade multiblock copolymers to study loop formation at immiscible interfaces. A problem with premade block copolymers is their tendency to form micelles in one of the bulk phases, where they are ineffective as interfacial modifiers. One way to circumvent this problem is to use difunctional reactive polymers, telechelics, to reactively compatibilize the polymer blend. These lower molecular weight telechelics efficiently approach the interface and react, forming a large multiblock

copolymer *in situ* in a short time period. These *in situ* formed copolymers have a great potential for use in industrial applications, where mixing times on the order of minutes is employed. However, there are no experimental studies which have investigated the use of telechelics as reactive compatibilizers. Therefore the effectiveness of these telechelics as compatibilizers is of prime interest. The experiments in this study are designed to develop methods for reactive modification of polymeric interfaces, as well as gain an understanding of how telechelics form polymer loops at biphasic interfaces. The proposed experiments examine the impact of varying the reactive groups, molecular weight, and telechelic loading level on the ability of each telechelic pair to effectively modify the interface. The effectiveness of polymer loops as interfacial modifiers is not limited to polymer/polymer interfaces. As such, experiments which investigate the formation of polymer loops on a functionalized nanotube surface via reaction with telechelic polymers have been designed as well. This loop formation process is expected to improve dispersion and polymer/nanoparticle interactions. By first proving that polymer loops have been grafted to the nanotube surface in these studies, future mechanical testing experiments which quantify the effectiveness of polymer loops can be explored. These experiments are designed to provide insight into the optimal parameters required for polymer loop formation, which will likely be beneficial for commercial applications.

B. Proposed Experiments

In this study, immiscible polystyrene and polyisoprene is chosen as the model homopolymer constituents. The former polymer offers good strength and the latter offers good impact resistance. The molecular weight of the bulk homopolymers are held

constant in these experiments. To create a multiblock copolymer *in situ*, anionically synthesized telechelics are used in order to accurately monitor molecular weight effects. This minimizes polydispersity variations in viscosity, diffusion coefficient, end group concentration, copolymer symmetry, etc., simplifying the interpretation of the experimental results. Reactive pairs that are studied include succinic anhydride-terminated polystyrene (anh-PS-anh) with primary amine-terminated polyisoprene (NH_2-PI-NH_2), as well as epoxide-terminated polystyrene (epoxy-PS-epoxy) with carboxylic acid-terminated polyisoprene (COOH-PI-COOH). The telechelic PI is fluorescently labeled at both ends so that gel permeation chromatography (GPC) with fluorescence detection determines both the conversion of the telechelic into multiblock copolymer and the molecular weight of the formed copolymer. In order to quantify the coalescence suppression effectiveness, scanning electron microscopy (SEM) monitors the domain size as a function of annealing time above the glass transition temperature of all the blend components. At this temperature, droplets coalesce to reduce the energy of the system. If a blend has been well compatibilized, coalescence will be suppressed due to steric hindrance of the copolymer blocks at the interface, inhibiting droplet recombination. In order to optimize copolymer formation and coalescence suppression, the telechelic functional groups, molecular weight, and concentration are examined in a systematic way. GPC and SEM data provides a means for quantifying the effectiveness of each telechelic pair. Preliminary studies on the mechanical properties of the blends are also conducted. Instron tests provide tensile properties of the uncompatibilized and compatibilized blends. Additionally, dynamic mechanical analysis (DMA) experiments determine *tan* δ (loss modulus/storage modulus) of the blends as a function of

temperature. *Tan δ* peaks of the individual components shift towards each other if the blend is well compatibilized, and the extent of this shift correlates to the extent of mixing on a molecular level.[97]

Grafting polymer loops onto oxidized multiwall is also examined to verify and monitor polymer loop formation at a polymer/nanotube interface. Carboxylated nanotubes are reacted with epoxy-PS-epoxy telechelic polymer in solution at high temperature in order to graft the polymer onto the nanotube surface. Fourier transform infrared spectroscopy (FT-IR) is used to confirm the formation of a new covalent bond, as well as to quantify the amount of polymer grafted to the nanotubes as a function of reaction time. In order to determine the fraction of polymer loops formed, the grafted nanotubes were further reacted with carboxy-terminated poly(4-methylstyrene) (COOH-P4MS), which only reacts with unbound epoxy-PS-epoxy chain ends. FT-IR of this system quantifies the fraction of telechelics that formed loops in the initial reaction. Thermogravimetric analysis (TGA) is used in conjunction with FT-IR to test the validity of FT-IR as a quantitative technique.

The experimental studies are designed to document the impact of the molecular weight and reactivity of telechelic pairs on the grafting of the telechelic to the surface, the size of the copolymer created *in situ*, and the ability of the resultant copolymer to suppress coalescence. Understanding the physics that governs these processes enables the rational optimization of the compatibilization properties of a phase separated polymer blend. Similarly, the experiments that monitor the grafting of polymer loops onto carbon nanotubes provide a method to controllably alter nanoparticle interfaces and optimize grafting density and loop formation.

Chapter 2

Experimental Materials and Techniques

2.1 Blend Materials and Sample Preparation

A. Bulk homopolymers and antioxidants

In the scanning electron microscopy (SEM) experiments, Instron tensile strength tests, dynamic mechanical analysis (DMA) experiments, and initial gel permeation chromatography (GPC) with fluorescence detection experiments, the homopolymers used were bulk materials. Polystyrene (PS) (M_n 77,000, M_w 196,000, PDI = 2.55) and polyisoprene (PI) (M_n 191,000, M_w 293,000, PDI = 1.53) were purchased from Aldrich. The PS pellets were first ground up into a coarse powder and placed in a vacuum oven at 130°C for one week to remove any residual solvent and monomer. To inhibit thermal degradation of the polyisoprene during mixing, 0.25 wt. % Tris(4-tert-butyl-3-hydroxy-2,6-dimethylbenzyl)isocyanate (Aldrich, 97%) and 0.25 wt. % Tris(2,4-di-tert-butyl-phenyl)phosphate (Aldrich, 98%) antioxidants were incorporated into the PI by dissolving all the components in HPLC grade toluene (Fisher) at room temperature, stirring overnight in a jar purged with argon, and then evaporating the solvent and drying in a vacuum oven at 50 °C for one week. The former antioxidant is a primary antioxidant commercially known as Cyanox 1790 (Ciba) and the latter is a secondary antioxidant commercially known as Irgafos 168 (Ciba). The role of a primary antioxidant is to donate H atoms to free radicals, preventing the radicals from propagating the free radical oxidation chain reaction, whereas secondary antioxidants act as hydroperoxide decomposers.[98] The addition of a secondary antioxidant has been shown to have a synergistic effect;[98] since it decomposes peroxides, there are fewer hydroperoxides that

the primary antioxidant needs to stabilize. The Aldrich equivalent of Cyanox 1790 was chosen because it has been proven to have better thermal stabilization properties than other common antioxidants such as butylated hydroxytoluene (BHT), Irganox 1076 (Ciba), and Irganox 1010 (Ciba).[98]

B. Free Radical Polystyrene

In later fluorescence experiments, it became necessary to use homopolymers of a higher molecular weight and lower polydispersity to minimize fluorescence interference. Homopolymer polystyrene was made by free radical synthesis. Any homopolymer PS used in this project made by free radical synthesis is referred to as FR-PS*x*, where *x* is the batch number.

The target molecular weight of FR-PS1 was 100k. The monomer to initiator ratio was estimated by:[99]

$$DP = C\frac{[M]}{[I]} \tag{2.1}$$

where *DP* is the degree of polymerization of the polymer, *C* is the percent conversion, *[M]* is the monomer concentration, and *[I]* is the initiator concentration. *C* was assumed to be 70%. It should be noted that this equation is used for atom transfer radical polymerization (ATRP), which is not the same as free radical polymerization. Since the equations are not exact, it was chosen as a basis to further modify the *[M]/[I]* ratio based on trial and error. The initiator 2,2-Azobisisobutyronitrile (AIBN) (Sigma, 98%) and styrene monomer (Sigma, 99+% ReagentPlus, stabilized) were used as received. The solvent was 1,4-Dioxane (Sigma, 99.8%, anhydrous), and a solvent to monomer ratio of 0.8:1 was used. Three freeze-pump-thaw cycles were completed before starting the

reaction and dry nitrogen was purged through the flask during the thawing cycle. After removal of oxygen from the system, the reaction was conducted at 65 °C for 24 hours under a dry nitrogen atmosphere. The polymer was precipitated in cold methanol (Fisher, ACS grade) (-25 °C) to remove the monomer and low molecular weight polymer species that are soluble in methanol. After the polymer was recovered, it was redissolved in tetrahydrofuran (THF) (Fisher, HPLC grade), and precipitated two more times to further remove impurities. The polymer was dried in a vacuum oven at 60 °C overnight. Gel permeation chromatography equipped with a differential refractive index detector was used to determine the molecular weight. FR-PS1 had a number average molecular weight M_n of 112,000, close to the target molecular weight. When used in fluorescence experiments, the molecular weight of FR-PS1 was still too low to avoid homopolymer fluorescence interference, so FR-PS2 was synthesized with a target weight of 300,000. However, the M_n of this polymer was only 134,000 despite the fact that three times less AIBN was used. Using less initiator will increase the molecular weight of the polymer because fewer radicals are formed, leading to a small number of large chains that are polymerized.

It was then decided to use the equation to precisely estimate the molecular weight of a polymer by free radical polymerization. For FR-PS3, the average kinetic chain length v in a free radical synthesis was used to calculate the monomer to initiator ratio required to make the polymer, with the equation:[100]

$$\nu = \frac{k_p[M]}{2(fk_i k_d[I])^{1/2}} \tag{2.2}$$

where k_p is the free radical propagation rate constant, *[M]* is the monomer concentration, f is the initiator efficiency, k_t is the termination rate constant, k_d is the initiator decomposition rate constant, and *[I]* is the initiator concentration. The degree of polymerization *DP* is related to the average kinetic chain length by $DP = 2v$ for polymers like polystyrene that terminate primarily by coupling.[100] The constants used for the polymerization of styrene at 60 °C were $k_p = 176\ L*mol^{-1}*sec^{-1}$, $f = 0.75$, $k_t = 7.2E7\ L*mol^{-1}*sec^{-1}$ and $k_d = 8.45E\text{-}6\ sec^{-1}$.[99,100] Even with the correct equation for a free radical synthesis, which required only 3.3 mg of AIBN for the synthesis (~17x less than FR-PS1), the M_n was only 123,000. Thus using the correct equation (i.e. correct *[M]/[I]*) for a free radical synthesis had little influence on the molecular weight of the polymer.

It was not possible to obtain a M_n above ~130,000 for FR-PS even when the AIBN concentration was significantly reduced. The most likely cause for this is the fact that the solvent used for the synthesis, 1,4-dioxane, has a chain transfer constant that is too large to allow high molecular weight FR-PS to be formed. The chain transfer constant indicates the solvent's ability to terminate the free radical reaction by means of a free radical polymer chain abstracting a hydrogen radical from the solvent molecule.[99] This stops the chain propagation, leading to a lower molecular weight product. A solvent with a low chain transfer constant should be chosen for synthesizing high molecular weight polymers. Therefore the reaction was attempted in cyclohexane (Sigma, 99.9+%, HPLC grade), which has strong C – H bonds that resist hydrogen abstraction by free radicals resulting in a very low chain transfer constant.[99] Benzene has a slightly lower chain transfer constant than cyclohexane, but was not chosen as a solvent because it is a carcinogen. When the reaction in cyclohexane was completed and the solution was

precipitated in cold methanol, polymer "goo" was formed instead of a fluffy precipitate. This is due to poor solvent interaction between polar methanol and non-polar cyclohexane, resulting in cyclohexane being trapped in the polymer. The polymer "goo" was quickly recovered by removing it from the beaker with a spatula. It is important to immediately remove the polymer from the methanol, otherwise the "goo" becomes more liquid-like within 1 – 2 minutes and is not recoverable. The polymer was redissolved in THF, with subsequent precipitation in cold methanol resulting in the formation of a white fluffy precipitate. The polymer dissolved in THF was precipitated in cold methanol a total of three times to remove impurities. The M_n of this polymer was ~350,000 for FR-PS4 and ~250,000 for FR-PS5. These results show solvent choice is critical for creating high molecular weight polymers by free radical synthesis.

Because the yield of the high molecular weight FR-PS was so low (~4%), several batches had to be made. When a new bottle of styrene (Acros, 99%, stabilized) was used for making high molecular weight FR-PS, the reaction no longer worked under otherwise identical conditions. The cause of this is most likely a difference in the inhibitor concentration or the types of inhibitors used in the two different monomer batches. The Acros styrene monomer was then distilled to remove the inhibitor. To prevent auto-initiation of the purified monomer, the styrene was distilled on the same day as the reaction, and was kept sealed in a freezer until it was added to the reaction flask. The M_n of FR-PS6 was even higher using distilled styrene, ~450,000. Doubling the AIBN mass in FR-PS7 did not significantly reduce the molecular weight. A summary of the number-average molecular weight (M_n), weight-average molecular weight (M_w), and polydispersity index (*PDI*) of the different FR-PS batches is shown in Table 2.1.

Table 2.1. Summary of the conditions used for free radical synthesis of polystyrene. All reactions were run at 65 °C for ~24 hours. Molecular weights were determined by GPC equipped with a differential refractive index detector.

Batch	AIBN (mg)	Styrene (g)	Styrene Comments	Solvent (g)	Solvent Comments	M_n	M_w	PDI
FR-PS1	57.6	49.98	Aldrich As-Is	39.86	1,4-Dioxane	112,000	204,000	1.82
FR-PS2	19.0	55.01	Aldrich As-is	40.00	1,4-Dioxane	134,000	258,000	1.92
FR-PS3	3.3	50.36	Aldrich As-is	40.00	1,4-Dioxane	123,000	241,000	1.96
FR-PS4	1.0	49.99	Aldrich As-is	39.74	Cyclohexane	356,000	574,000	1.61
FR-PS5	1.5	75.01	Aldrich As-is	60.01	Cyclohexane	261,000	534,000	2.04
FR-PS6	1.8	94.58	Acros Distilled	75.55	Cyclohexane	469,000	759,000	1.62
FR-PS7	3.5	87.52	Acros Distilled	70.02	Cyclohexane	432,000	719,000	1.67

C. Cold Mastication Polyisoprene

The sample jar containing bulk polyisoprene (PI) with 0.5% antioxidants was purged with dry nitrogen, sealed with Parafilm, and stored in a freezer after each use. Despite these precautions taken, after nearly four years of use, GPC analysis showed the PI was cross-linked. An identical product number of new PI was ordered from Aldrich, however the M_n was 189,000 and the M_w was 570,000 (PDI = 3.02). The significantly higher M_w and PDI will affect the physical properties of the PI, making direct comparisons with blends containing the original PI questionable. The large differences are seen in Figure 2.1. However, it was still possible to break down the new PI to a lower molecular weight similar to the original PI using a process called cold mastication. In industrial terms, mastication refers to softening or making a pulp by crushing or kneading.

When entangled polymers in bulk are subjected to a shearing force such as a mechanical mixer, they must become disentangled in order for flow to occur.[101] If the polymer cannot move quickly enough, shear forces exert a large force on the polymer. If enough energy is provided by the shear force, the polymer chain can be broken, forming two free radical chains. The breaking of these chains is not random. For a chemical bond linking monomer unit i and $i+1$, the force exerted on the $(i+1)^{th}$ group, F_{i+1}, is the sum of the viscous forces $f_{i+1} + f_{i+2} + \ldots + f_n$ exerted on each monomer unit from the end of the chain up to f_{i+1}. The force exerted on the i^{th} group, the monomer on the opposite side of the bond, has an equal magnitude and opposite direction of pull.[102] Thus the central link in a polymer chain is the most susceptible to rupture since it is subjected to the greatest shear force; for every 10 chains broken at the center, only 1 chain will

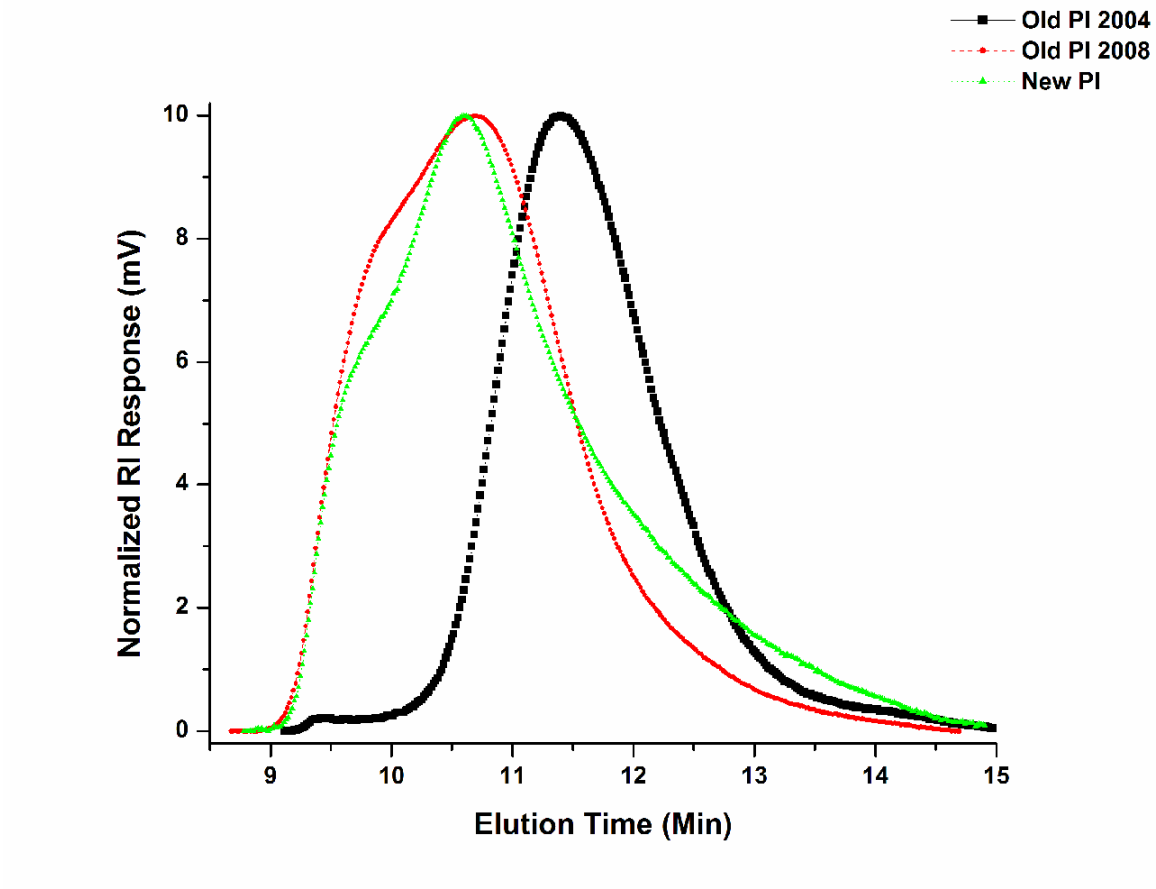

Figure 2.1. GPC analysis of the original polyisoprene used in this study shows the effects of cross-linking on the molecular weight. The new polyisoprene had a M_w nearly as high as the old cross-linked PI.

break 1/3 of the way out from the center.[101] These broken chains can subsequently be broken in half until shear forces no longer exert enough force on the central link to break the chain. That is, a limiting chain length is reached. In this manner, the molecular weight and polydispersity of a polymer are reduced.

An important parameter affecting the mechanical mastication of polymers is the melt viscosity. For an entangled polymer, the viscosity is proportional to $M_w^{3.4}$.[103] The higher the viscosity, the less quickly the polymer can respond to shear forces. Mastication occurs rapidly for high molecular weight polymers because they cannot respond fast enough to dissipate the shear energy. For a polymer of a given molecular weight, the melt viscosity η is greatly affected by temperature:[104]

$$\eta \propto \exp\left(\frac{E_A}{RT}\right) \tag{2.3}$$

where E_A is the activation energy for flow, R is the universal gas constant, and T is the temperature in Kelvin. Higher temperatures reduce the melt viscosity, allowing polymer chains to respond to shear forces more quickly and dissipate the energy more effectively. A reduced viscosity would require a higher shear rate to break the same number of polymer chains as in the lower temperature conditions. Therefore, masticating polymers at lower temperatures will result in more efficient mechanical degradation.

It was previously stated in this discussion that shear forces break a polymer chain near the center, creating two radical chains. It is possible for the radicals to react with a polymer molecule, causing branching or cross-linking. However, the activation energy of this process is higher than radical recombination,[105] so this occurrence is not as likely to happen. In most cases, the radicals will simply recombine, and no apparent change in

molecular weight will be observed. It is therefore necessary to stabilize the formed radicals so the shorter chains produced by mastication do not recombine. It is known that oxygen reacts with radicals and stabilizes them, as there is no softening of the polymer when it is masticated at low temperatures under an inert atmosphere.[105,106] Only a small percent of oxygen in the environment is needed to stabilize the radicals,[105] forming less reactive hydroperoxide species. At higher temperatures, thermooxidative degradation of the polymer chain occurs. Oxygen attacks unsaturated bonds, producing free radicals. However, chain scission is random,[105] and therefore breaking down polymers at high temperatures is not desirable.

Any homopolymer polyisoprene created by cold mastication in this project is referred to as CM-PI*x*, where *x* is the batch number. The effects of temperature, rotor speed, mastication time, and type of atmosphere were investigated. The goal of the cold mastication was to create a CM-PI that had a similar molecular weight and PDI as the original PI so that differences between systems made with both types of PI would still be attributed to a difference in the telechelics used and not the PI.

In experiments by Pike and Watson,[105] the lowest temperature used for cold mastication of rubber was 55 °C. In this study, the effects of temperature were first investigated. Cold mastication of polyisoprene in air with a rotor speed of 125 rpm was compared at 25 °C and 55 °C. The sample size was approximately 1 gram. In the case of the former temperature, the friction of the highly viscous PI being dragged across the mixing cup by the rotor caused the temperature to increase to ~30 °C by the end of the mixing time. Results of mixing times up to one hour are shown in Figure 2.2. Results in Figure 2.2 show rapid mechanical degradation during the first 30 minutes at 25 °C. The

peak molecular weight (M_p) is approximately equal to the original PI, but there is a significant low MW component as well, indicated by the significant signal between an elution time of 12 – 14 minutes. By increasing the temperature to 55 °C to reduce the viscosity of the PI, the mechanical shearing is slowed down in a more controlled manner. However, the distribution of molecular weights was still too broad compared to the original PI.

Next the sample was purged with argon by placing a stainless steel collar over the mixing cup to minimize the amount of oxygen present so more control of the mastication could occur. Due to the reduced amount of radical-accepting oxygen present in the cup, mixing times required to achieve the desired results were significantly increased. The results of PI masticated under argon at 55 °C at 125 rpm are shown in Figure 2.3. The results in Figure 2.3 show that purging the mixing cup with argon significantly slows down the radical stabilization of the masticated chains, as the molecular weight of the masticated PI is still higher than the original PI after 60 minutes of mixing. The presence of a high molecular weight shoulder near an elution time of 10 minutes suggests that the viscosity of the PI is too low at this temperature to break down these chains. The PI was then melt mixed at 25 °C under argon at 125 rpm in an attempt to break the high molecular weight chains. After 4 hours of mixing, the temperature in the cup was 33 °C. The results of the room temperature cold mastication are shown in Figure 2.4. The experimental results indicate that melt mixing for 240 minutes under argon at 25 °C yields a molecular weight distribution most similar to the original PI. The high MW shoulder has been greatly reduced and the M_p nearly matches the original PI. In addition, the cold mastication of PI was reproducible. Figure 2.5 shows the molecular weight

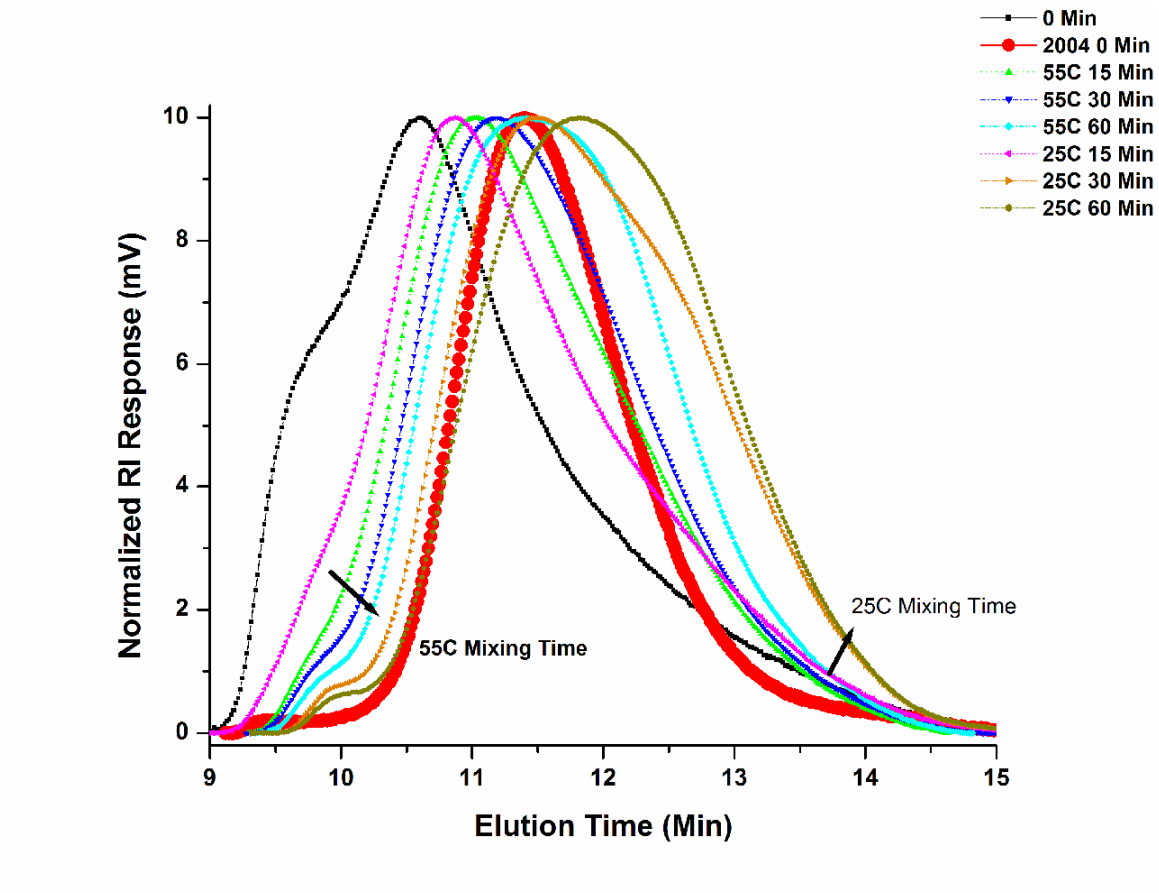

Figure 2.2. GPC results for cold mastication of PI for various mixing times at 125 rpm in air at 25 °C and 55 °C. *2004 0 Min* shows the molecular weight distribution of the original PI under zero shear conditions. *0 Min* is the new batch of PI under zero shear conditions.

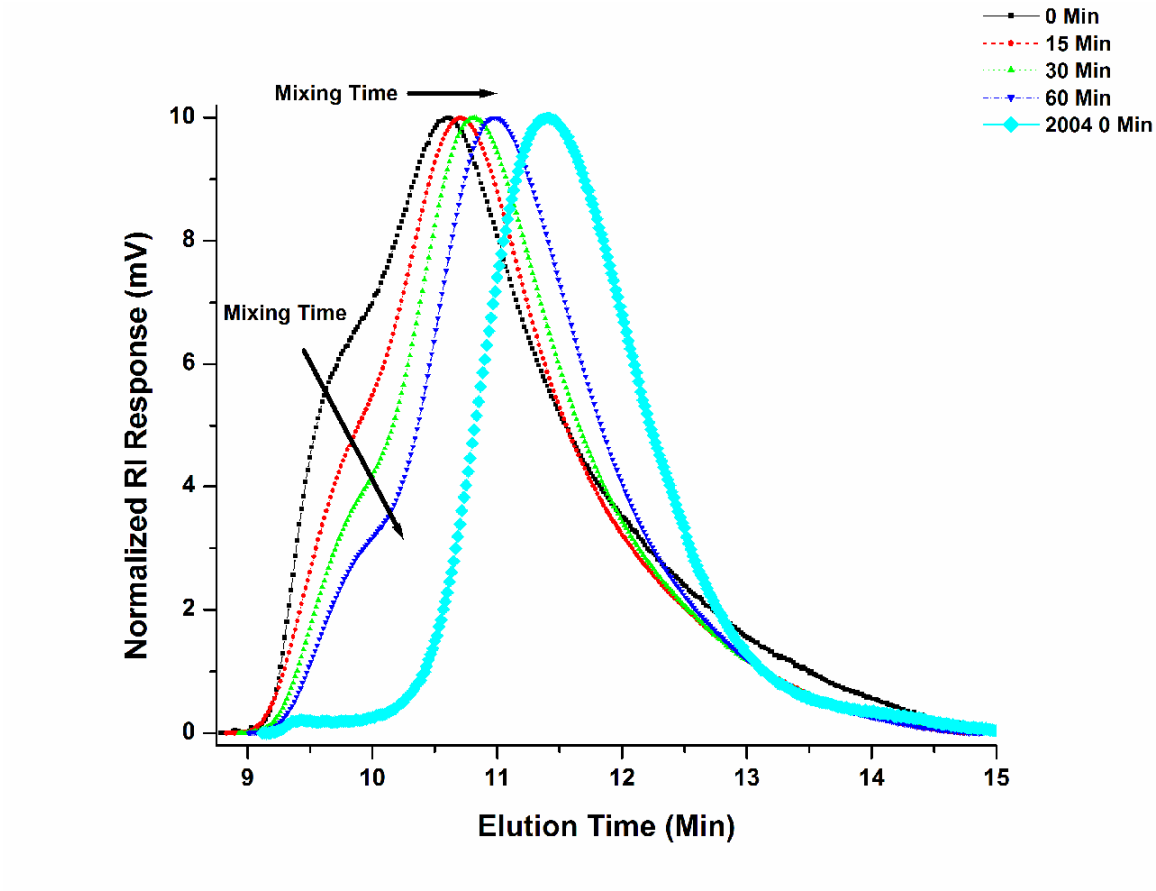

Figure 2.3. GPC results for the cold mastication of PI for mixing times up to one hour with argon purging at 125 rpm and 55°C.

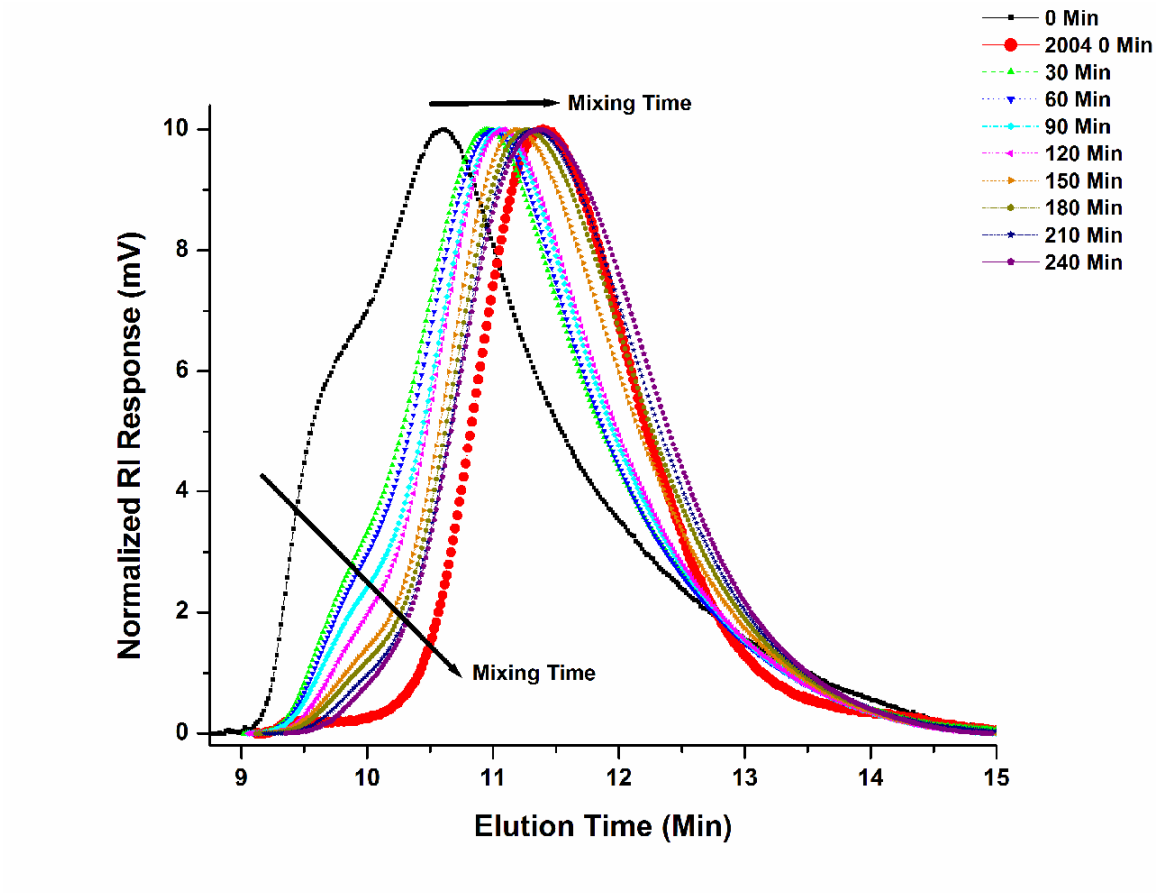

Figure 2.4. GPC results for the cold mastication of PI purged with argon at 125 rpm and 25°C.

distribution of four batches is nearly superimposable.

To see if mixing times shorter than 4 hours per batch could be obtained, the rotor speed was set to 25, 50, and 100 rpm for the mastication of PI in air at 25°C. The molecular weight distributions closest to that of the CM-PI mixed under argon at 25°C for 4 hours are shown in Figure 2.6.

The PI masticated in air at various reduced rotor speeds still had a significantly greater population of high molecular weight species than the original PI, exhibited by the shoulder near an elution time of 10 minutes. In addition, the PI masticated in air also had a greater population of lower molecular weight species than the original PI, demonstrated by the peak tailing from 12 to 15 minutes elution time. Therefore it was decided to create CM-PI under argon at 25°C for 240 minutes to best duplicate the molecular weight distribution of the original PI. The individual batches of CM-PI were dissolved together in toluene, and antioxidants were added as described in Chapter 2.1 A. The antioxidant loading level was slightly reduced to 0.3 wt. % for the CM-PI. The molecular weight of the CM-PI batches and the original PI are shown in Table 2.2 below. When the CM-PI batches were subsequently melt mixed under argon at 180 °C and 100 rpm, which were the conditions for melt blending, there was only a slight change in the fluorescence and RI response of the CM-PI. As previously discussed, high temperature mixing results in random chain scission by means of thermooxidation. The changes in molecular weight distribution determined by GPC with a differential refractive index detector are shown in Figure 2.7.

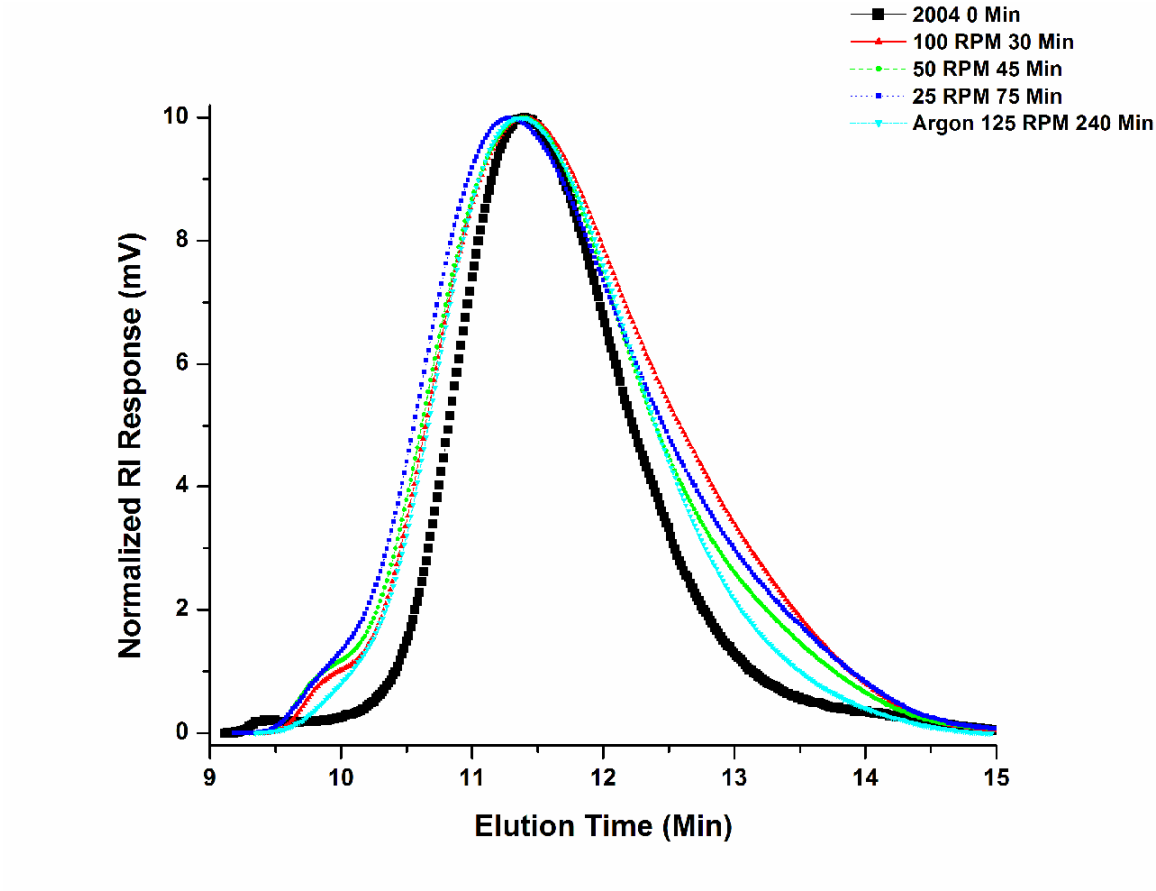

Figure 2.5. GPC results showing the reproducibility of CM-PI batches melt mixed under argon at125 rpm and 25°C for 240 minutes. All batches showed similar MW distribution to the original PI used in this study.

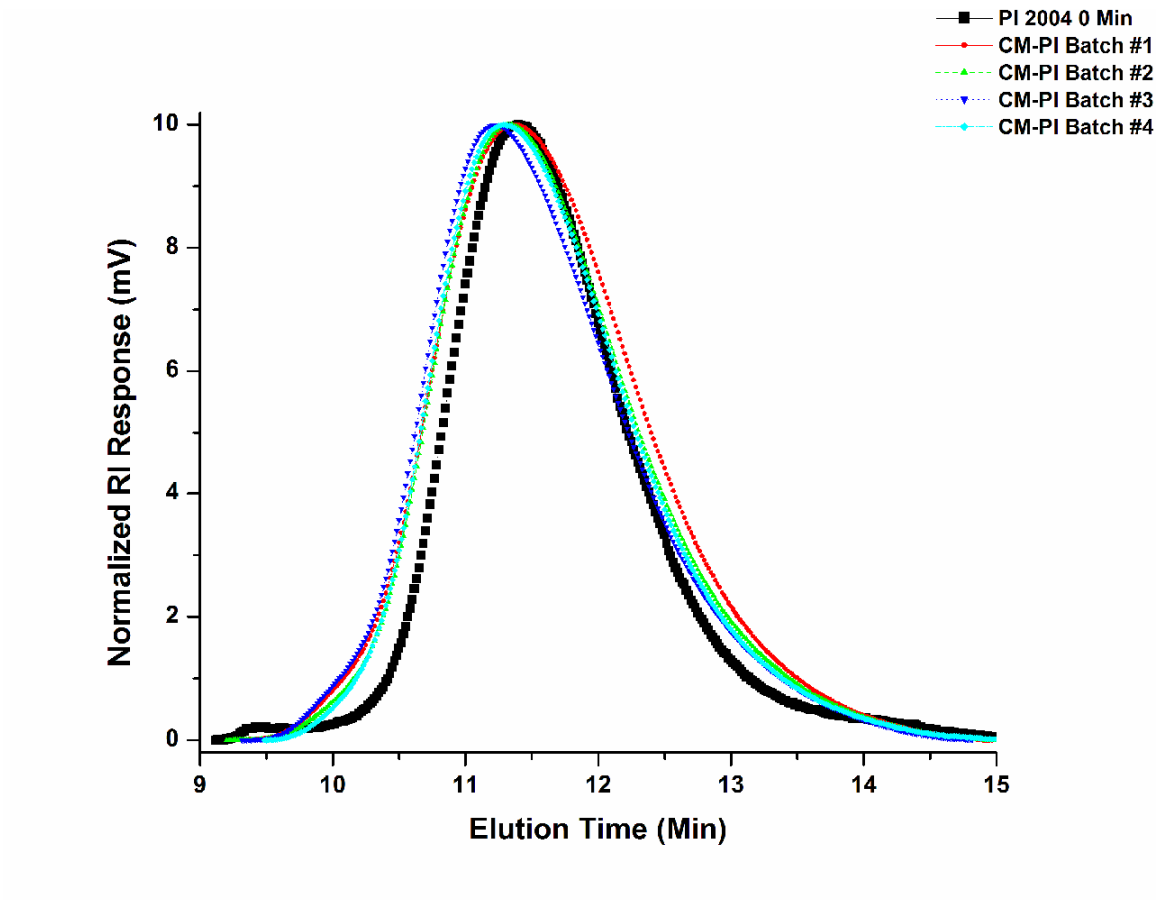

Figure 2.6. GPC results for PI masticated in air at 25°C at 25, 50, and 100 rpm compared to mastication under argon at 125 rpm and 25°C for 240 minutes.

Table 2.2. Number average (M_n), weight average (M_w), peak average (M_p), and polydispersity index (PDI) of original PI and CM-PI with 0.3 wt.% antioxidants determined by GPC with a RI detector.

Batch	M_n	M_w	M_p	PDI
PI	197,000	329,000	320,000	1.67
CM-PI1	158,000	298,000	335,000	1.88
CM-PI2	159,000	327,000	318,000	2.06

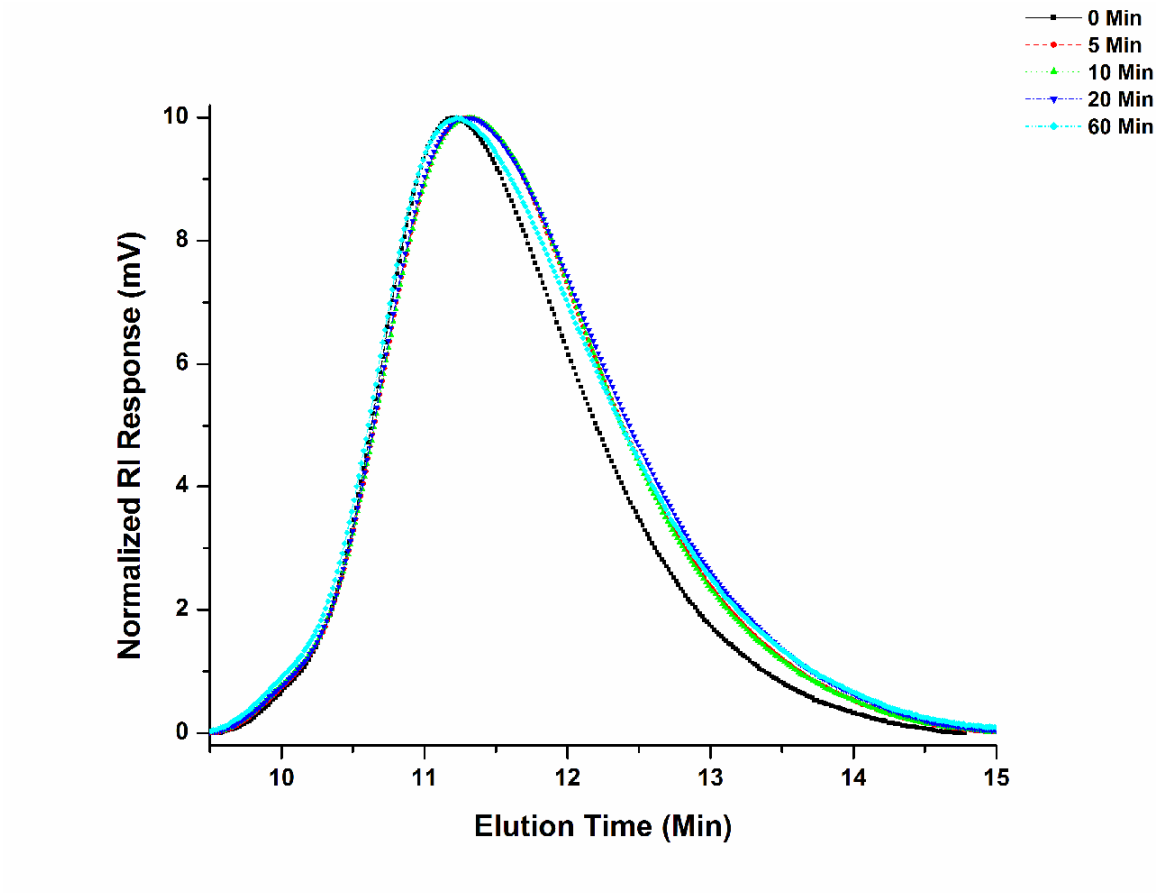

Figure 2.7. GPC normalized RI response as a function of elution time for CM-PI1 melt mixed under argon at 180 °C and 100 rpm for various times.

D. Telechelic Polymers

Difunctional reactive polymers called telechelics are used throughout this study. In order to control the molecular weight and functionality of the telechelic polymers, they were anionically synthesized.[107] The use of a dilithium initiator yields a negative charge on both ends of the living chain, allowing α,ω difunctional polymers to be created.[108] All telechelic polymers were synthesized at the University of Tennessee by Haining Ji. Antioxidants were added to the telechelic PI in the same manner as the homopolymer PI described in Chapter 2.1 A. Reactive pairs used in this study include succinic anhydride-terminated polystyrene (anh-PS-anh) with primary amine-terminated polyisoprene (NH_2-PI-NH_2), as well as epoxide-terminated polystyrene (epoxy-PS-epoxy) with carboxylic acid-terminated polyisoprene (COOH-PI-COOH).[109-112] The functionality of the anh-PS-anh was 1.6, and the functionality of the remaining telechelics was 1.9. In addition, the polyisoprene telechelics were prepared with 1-(1-anthryl)-1-phenylethylene[113] (APE) fluorescent labels adjacent to each functional group in order to calculate conversion of the reactive polymers into multiblock copolymer by using fluorescence detection size exclusion chromatography. A drawing of the APE tag is shown in Figure 2.8. The number average molecular weight (M_n) and polydispersity index (PDI) of the telechelic reactive pairs used in this study are shown in Table 2.3. Additionally, a telechelic NH_2-PI-NH_2 polymer with M_n = 19,000 and PDI = 1.21 was synthesized with a 9-vinyl anthracene fluorescent tag. The structure of this tag is shown in Figure 2.9. This polymer is referred to as 9-VA NH_2-PI-NH_2 in experimental work.

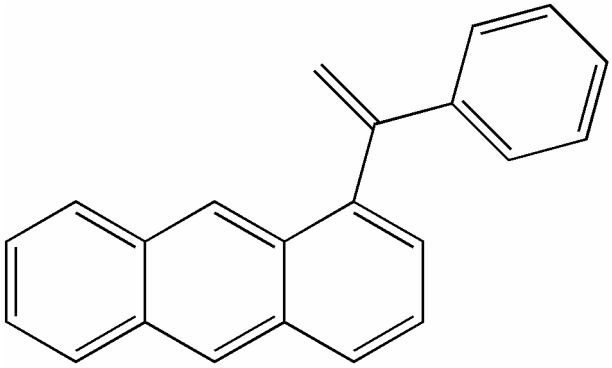

APE

Figure 2.8. The structure of the APE fluorescent tag used in this study.

Table 2.3. Molecular weight and polydispersity of reactive polystyrene and polyisoprene polymers used in this study.

Telechelic	M_n	PDI	Telechelic	M_n	PDI
anh-PS-anh	16,000	1.11	NH_2-PI-NH_2	16,000	1.28
anh-PS-anh	37,000	1.02	NH_2-PI-NH_2	32,000	1.27
anh-PS-anh	83,000	1.02			
epoxy-PS-epoxy	18,000	1.04	COOH-PI-COOH	18,000	1.14
epoxy-PS-epoxy	44,000	1.04	COOH-PI-COOH	54,000	1.18

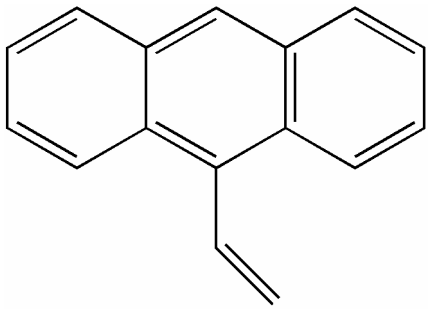

9-Vinyl Anthracene (9-VA)

Figure 2.9. Structure of 9-vinyl anthracene used to tag the 19k NH_2-PI-NH_2 telechelic.

In Figure 2.10, the reactions between the functional groups of these telechelics at elevated temperatures are shown. The second order reaction between the carboxylic acid and epoxy forms an ester,[74,114] and has been shown to be relatively slow, with only 9% conversion after 2 minutes of mixing monofunctional epoxy-PS and COOH-PS at 180°C.[115,77] The second order reaction between a cyclic anhydride and an aliphatic amine first yields amic acid after a ring opening step, and then an imide and water are formed after a condensation step.[116] This reaction is very fast, with 99% conversion between monofunctional anh-PS and NH_2-PS after 2 minutes of mixing at 180°C.[115,77]

2.2 General Blending Procedure

Blends initially contained 5.0% telechelics by weight, while the remaining 95% of the sample consisted of a 90% PS/10% PI homopolymer composition. Stoichiometric amounts of anh-PS-anh/NH_2-PI-NH_2 and epoxy-PS-epoxy/COOH-PI-COOH constituted the telechelic contribution of the blend. The maximum sample size was 1200 mg. For example, a blend of 90% PS/10% PI + 5.0% 37k anh-PS-anh/16k NH_2-PI-NH_2 contains

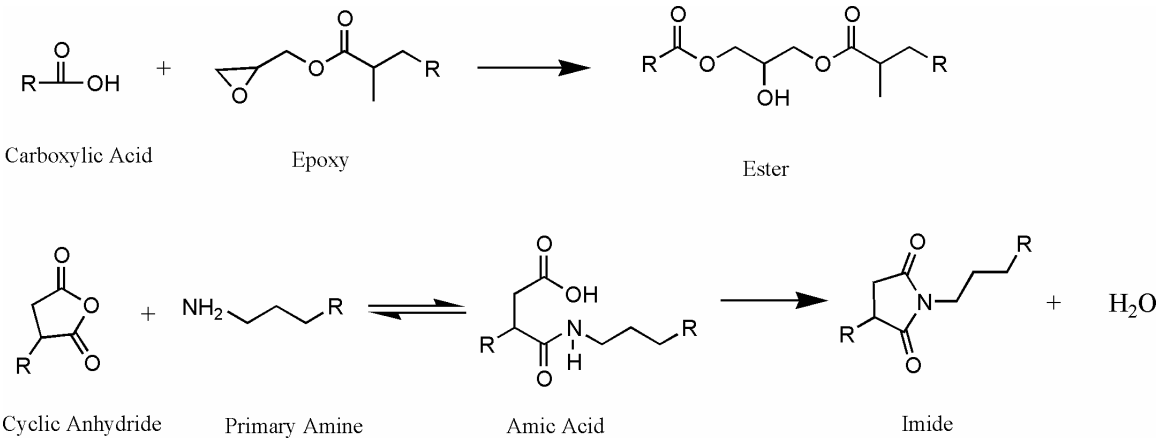

Figure 2.10. Reaction between carboxylic acid and epoxy groups yields an ester (top). Reaction between a cyclic anhydride and a primary amine results in an imide (bottom).

1026.0 mg PS, 114.0 mg PI, 37.8 mg 37k anh-PS-anh, and 22.3 mg 16k NH_2-PI-NH_2. The ratio of telechelics is determined by the concentration of reactive end groups, which depends on the molecular weight and functionality of the telechelic. Unless otherwise stated, the homopolymer composition was 90% PS/10% PI. In later experiments, the telechelic loading was reduced. The homopolymer content was adjusted accordingly, while the ratio remained 90% PS/10% PI. The blend constituents were first placed together in an aluminum weighing pan and were premixed by hand. The four components were then placed in an Atlas Laboratory Mixing Molder heated to 180 °C, with a rotor speed of 100 rpm. The shear rate G was calculated by:[117]

$$G = \frac{2\pi N}{\ln\left(R_{cup} / R_{rotor}\right)} \tag{2.4}$$

where N is the number of revolutions per second, R_{cup} is the radius of the mixing cup, and R_{rotor} is the radius of the rotor. Using this calculation, the shear rate is 2655 sec^{-1} at outer edge of the rotor and 15 sec^{-1} at the midpoint of the rotor radius at 100 rpm. This type of mixer has an extremely tight fit between the cup and rotor, and therefore can generate a very high shear rate at the outer edge of the rotor. It has been demonstrated that antioxidants alone will not prevent the thermal degradation of PI polymers, and an inert gas must also be used during mixing.[115] A stainless steel collar was made to sit on the mixing cup and surround the rotor, where dry argon was purged through the collar to minimize thermal oxidation of the PI. Samples initially extruded from the mixing molder were inhomogeneous due to poor blending in the pathway between the bottom of the cup and where the blend was extruded. To ensure homogenous samples, the four components

were first blended in the mixing molder for the shortest possible time and extruded twice, followed by melt blending for 15, 30, 60, and 180 minutes. A small aliquot of the blend, approximately 5 mm in diameter, was extruded and then quenched at room temperature, where it was cool to the touch after a few seconds.

2.3 Forming Polymer Loops on Nanotubes

A. Functionalized Nanotubes

Carbon nanotubes with > 50% single wall content and < 35% multiwall content were purchased from Cheap Tubes, Inc., and are referred to as MWNT in this study. To oxidize the nanotubes and thereby introduce COOH groups to the nanotube surface, 1500 mg of MWNT were added to a two neck round bottom flask containing 500 ml of 6 M HNO_3 (Fisher, Certified ACS Plus). The nanotubes were stirred and refluxed under dry nitrogen at 120 °C for 16 hours. The nitric acid not only introduces oxygen-bearing functional groups, but also removes metal catalysts and amorphous carbon from the nanotubes.[118,119] After cooling, the solution was diluted with 500 ml of deionized water. The nanotubes were then centrifuged (Eppendorf 5702 Centrifuge) for 8 minutes at 4400 rpm. The collected nanotubes were then placed in approximately 200 ml of a 0.5 M NaOH solution and stirred for 30 minutes at room temperature. The NaOH is used to remove carboxylated amorphous carbon impurities that coat the nanotubes, which are soluble in aqueous metal hydroxide solutions.[119-121] After centrifugation, the nanotubes were rinsed with approximately 300 ml of nanopure water and centrifuged again. The nanotubes were then placed in a two neck round bottom flask containing 400 ml of piranha solution, which is composed of 3 parts H_2SO_4 (Fisher, Certified ACS Plus) to 1 part H_2O_2 (Fisher, 30 vol. %, sodium stannate stabilized). The nanotubes were then

stirred and refluxed under dry nitrogen at 70 °C for 30 minutes. This step is used to introduce defect sites on the nanotubes and to further cut the tubes.[118] After cooling the piranha solution, 500 ml of deionized water was used to dilute the solution. The functionalized nanotubes were centrifuged for 3 minutes at 4400 rpm. After collection, the nanotubes were again placed in approximately 200 ml of 0.5 M NaOH and stirred for 30 minutes at room temperature in order to remove any additional amorphous carbon impurities. The functionalized nanotubes were then rinsed with nanopure water and centrifuged repeatedly until the pH of the solution was neutral. The nanotubes were then dried in a vacuum oven at 80 °C overnight. The functionalized multiwall nanotubes are named COOH-MWNT in this study.

It should be noted that COOH groups are not the only oxygen-bearing functional groups introduced to the nanotube surface by the HNO_3 acid reflux treatment. Zhang et al. used FT-IR to show that HNO_3 treatment first introduces hydroxyl groups, which are then converted into quinones, followed by further conversion to COOH groups at later reaction times.[122] The C=O stretch of the COOH group shifted to a lower wavenumber as the reflux time increased, which indicates the formation of hydrogen-bonded COOH groups. X-ray photoelectron spectroscopy (XPS) and titration studies on HNO_3-treated nanotubes support the theory that hydroxyl and quinonyl groups are precursors to the formation of COOH groups as well.[118,123-126] González-Guerrero et al. used titration methods to monitor the formation of COOH groups on HNO_3-treated multiwall nanotubes as a function of reflux time.[127] It was discovered that COOH groups consisted of ~75% of the total acidic sites up to 6 hours of reflux time. After 6 hours, the total number of acidic sites did not increase, whereas the amount of COOH groups continued

to increase and approached the total number of acidic sites after 12 hours of refluxing. This supports the hypothesis that once the surface is covered with acidic sites, these sites are eventually converted to COOH groups. Fluorescence studies, which are much more sensitive than FT-IR, XPS, and titration methods, showed that there was a higher concentration of carbonyl functionalities (aldehyde and ketone) present than COOH or OH groups on HNO_3-treated nanotubes.[128] The nanotubes were treated in concentrated HNO_3 for 2 hours at room temperature in this study, which may not be enough time for full conversion to COOH groups. Therefore, there are likely several different oxygen-bearing functional groups present on the acid-treated nanotubes, including substantial carboxylic acid groups.

B. Grafting Telechelics to Functionalized Nanotubes

To study the grafting of loops on a nanotube surface, telechelic epoxy-PS-epoxy anionically synthesized at the University of Tennessee by Haining Ji (M_n = 17,800, PDI = 1.05, functionality = 1.9) was reacted with the COOH-MWNT in solution. Approximately 500 mg of COOH-MWNT were added to a two neck round bottom flask containing ~ 250 ml of 1-methyl-2-pyrrolidinone (NMP) (Sigma, Chromasolve Plus HPLC). The solution was sonicated for 15 minutes to disperse the nanotubes. Then ~500 mg of epoxy-PS-epoxy which was dissolved in ~50 ml of NMP was added to the round bottom flask. The solution was stirred and refluxed under dry nitrogen at 150 °C. 50 ml aliquots were removed from the reaction flask at time intervals of 1, 2, 3, and 6 days. After the solution was cooled, the nanotubes were collected by centrifugation at 4400 rpm for 3 minutes. The NMP supernatant was then decanted from the centrifuge tube and collected. To ensure any remaining unreacted epoxy-PS-epoxy was removed,

50 ml of N,N-dimethylformamide (DMF) (Acros, HPLC) was added to the centrifuge tube. The tube was shaken to redisperse the nanotubes, and after subsequent centrifugation, the DMF supernatant was decanted and collected. To test for the presence of unreacted epoxy-PS-epoxy, both the NMP and DMF supernatant were precipitated in cold methanol (-20 °C). After centrifugation, a white precipitate formed in the NMP supernatant indicating the presence of epoxy-PS-epoxy, but no precipitate was visible in the DMF supernatant. It was therefore assumed that 50 ml of DMF was adequate for rinsing the nanotubes to remove excess telechelic PS. The reacted nanotubes were then dried in a vacuum oven at 80 °C overnight to remove the residual solvent. A temperature below the T_g of polystyrene was used to ensure no further grafting reaction occurred during this step of the experiment.

To examine the ability to increase loop formation with heating, the grafted nanotubes were annealed in a vacuum oven at 150 °C for 1 – 6 days. This allows grafted polymer chain end diffusion, allowing any untethered telechelic chain ends to form loops upon reaction with COOH groups on the nanotube surface. In order to quantify the amount of telechelics that only formed tails, a new sample of ~100 mg of COOH-MWNT and epoxy-PS-epoxy was reacted for 1 day in NMP at 150 °C. After removal of the unreacted epoxy-PS-epoxy, the grafted nanotubes were redispersed in ~50 ml of NMP by sonication for 15 minutes, and ~100 mg of monocarboxy terminated poly(4-methylstyrene) (COOH-P4MS) (Scientific Polymer Products, Inc.) (M_n = 19,400, PDI = 1.09) was dissolved in ~100 ml NMP. The polymer solution was added to the dispersed nanotubes, and the polymer grafting reaction in NMP proceeded at 150 °C under dry nitrogen as previously described for the epoxy-PS-epoxy reaction. At reaction time

intervals of 1, 2, 3, and 6 days, 50 ml aliquots were removed from the reaction flask for analysis. The unreacted COOH-P4MS was removed in the same manner as the unreacted epoxy-PS-epoxy. To determine if there was any reaction between the COOH-P4MS and the various functional groups introduced onto the nanotubes, COOH-MWNT and COOH-P4MS were reacted for 1 day at 150 °C. The sample preparation was the same as the previously described samples.

2.4 Sample Preparation and Instrumental Analysis

A. Gel Permeation Chromatography (GPC)

Gel permeation chromatography (GPC) was used to determine the number average molecular weight (M_n), weight average molecular weight (M_w), and polydispersity index (PDI), M_w/M_n, of the samples relative to polystyrene standards. The GPC columns are composed of a stationary phase consisting of polystyrene crosslinked with divinylbenzene.[129] Larger size polymers elute first, as they are too big to explore the smaller size pores of the gel in the column. A calibration curve is made by determining the peak elution time of polymer standards with a narrow molecular weight distribution. The unknown samples are then analyzed. From the measured elution time, their molecular weight is reported relative to the standard used. However, the elution time of a polymer not only depends on molecular weight M, but on the intrinsic viscosity $[\eta]$ of the polymer as well. The product of the two parameters, $M[\eta]$, is proportional to the hydrodynamic volume.[130] If the hydrodynamic volume is plotted against elution time, differences in polymer structure are taken into account. This is known as universal calibration. A viscometer connected to the GPC is required to measure $[\eta]$. The intrinsic viscosity can be measured in a separate experiment, but this is very time consuming. If

the GPC system is not equipped with a viscometer, it is still possible to obtain the corrected molecular weight of the polymer sample if the type of polymer and the hydrodynamic correction factor are known. The correction factor is simply based on the fact that two different polymers that elute at the same time are related by the equation

$$M_1[\eta_1] = M_2[\eta_2] \quad (2.5)$$

In order to determine the molecular weight of PI samples in this study, the molecular weights calculated relative to the PS standards were divided by 1.60, which is the PI hydrodynamic radius correction factor in THF at 23 °C.[131]

Polystyrene is weakly fluorescent, and standards were used to create a calibration curve for the fluorescence detector when the detector gain was set to the highest level. The tagged PI telechelics enables the amount of telechelics converted into a higher molecular weight copolymer and the percent of tagged PI converted to be determined. Fluorescence detection is advantageous because a fluorescence detector is about 100 times more sensitive than a differential refractive index detector,[132] and can easily detect species on the μM scale. Samples were analyzed with a Polymer Labs GPC-20 instrument containing two 300 mm x 7.5 mm Polymer Labs 5 μm Mixed C columns and a 50 mm x 7.5 mm Polymer Labs 5 μm guard column. The GPC was equipped with a Knauer K-2301 differential refractive index detector and a Jasco FP-920 fluorescence detector. Tetrahydrofuran (THF) (Fisher, HPLC grade) stabilized with 100 ppm butylated hydroxy toluene (BHT) (Fisher) was used as the mobile phase. Experiments were run at room temperature with a flow rate of 1 ml/min. The concentration of the samples was 2 mg/ml. Two drops of phenyl isocyanate (Acros, 99+%) per ml of sample were added to cap any unreacted amine groups[76] or COOH groups[1] in order to prevent

peak tailing due to column adsorption of functional groups, and to act as the flow rate marker. A flow rate marker is used because thermal fluctuations and variation in pump speed can alter the elution time. By multiplying the observed elution time by a correction factor, the actual elution time can be obtained. The correction factor is calculated by the ratio of the peak elution time of the marker during calibration to the peak elution time of the marker during analysis of the unknown sample. Samples were filtered through a 0.20 μm polytetrafluoroethylene (PTFE) syringe filter (Fisher) prior to injection. For analysis of blends containing the APE tag, the fluorescence detector was set to an excitation wavelength (λ_{ex}) = 295 nm, emission wavelength (λ_{em}) = 385 nm, gain = 1000, and attenuation = 1. For the analysis of samples containing the 9-VA tag, the instrument settings were λ_{ex} = 389 nm, λ_{em} = 460 nm, gain = 1000, and attenuation = 1. The slit width was 10 nm for excitation and 18 nm for emission. The gain was automatically reduced to 10 prior to the elution of the phenyl isocyanate marker to prevent detector saturation by using a timed program on the fluorescence detector.

B. Instron Tensile Strength

For Instron tensile strength tests, samples contained a homopolymer ratio of 95% PS/5% PI, 90% PS/10% PI, and 80% PS/20% PI. All homopolymers were bulk materials described previously in Chapter 2.1 A. Each of these samples contained stoichiometric amounts of either 5 wt.% 37k anh-PS-anh/16k NH_2-PI-NH_2, 5 wt.% 83k anh-PS-anh/32k NH_2-PI-NH_2, or no compatibilizer. A total sample size of 1200 mg was melt mixed at 160 °C for 20 minutes at 100 rpm under argon and extruded into a dog bone shaped stainless steel die. The die was held together with two d-clamps to make sure none of the polymer blend leaked out of the sides of the mold during extrusion. The die was warmed

with a heat gun for 5 minutes prior to extrusion to prevent the sample from cooling below the T_g of PS (~100 °C) before filling the entire mold. The dimensions of the dog bone mold did not meet *ASTM D 638* standards[133] because the angle between the narrow section of the sample and the wide section at both ends of the sample was 90°, whereas it should have been tapered in order to meet the standards. This subsequently led to the sample breaking at the neck during mechanical testing, which was undesirable. The sample was removed from the die by heating the mold to 120 °C, which is slightly above the T_g of the PS matrix, and then prying the sample out with a screwdriver. If the samples became deformed in this process, they were straightened out in a Carver press heated to 120 °C. The sample was sandwiched between two pieces of Kapton film, and then the press was gently compressed until the sample was flatted without being deformed.

To analyze the sample, the Instron 1122 machine was first calibrated with standard weights. Then the specimen was secured in the grips of the Instron 1122 machine, and the distance between the grips and width of the narrow section were measured with digital calipers in order to determine the surface area of the sample between the grips. The tensile strength was determined by measuring the force required to move the grips a measured distance ΔL from the initial clamp distance L_0. The grips were moved at a rate of 0.5 mm/min. Seven samples of each composition were analyzed at room temperature and the average values and standard deviation were calculated.

For tensile strength tests, the force F required to move the clamps is measured in *kg*. The relative distance the clamps, and therefore the secured sample, moves in *mm* from the initial distance as a function of this applied force is the strain, $\Delta L/L_0$. Tensile

strength tests are generally used to investigate the elastic response of a material. This elastic behavior is described by Hooke's law,

$$\sigma = k*\gamma \tag{2.6}$$

where σ is the stress, or force per area, required to extend the sample a given distance $\Delta L/L_0$, which is known as the strain γ. The amount of force required to move the sample also increases linearly with the spring constant, k. The stress-strain curve initially gives a linear response, with the slope of the line being equal to the material's elastic modulus, E.[134] The elastic modulus describes the stiffness of the material, or its resistance to deformation. The yield point is the amount of force required to cause the stress-strain curve to become nonlinear, as the material begins to deform and draw out.[134] Finally, after the material is deformed, the sample breaks, and the amount of force required to move the grips drops precipitously. The total area under the stress-strain curve is proportional to the amount of energy required to break the sample, and describes the toughness of the material.[134] An example of a stress-strain curve is shown in Figure 2.11, from ref. 41. When Instron tests are conducted, the initial response observed is usually not linear because there is some slack in the hanging clamp, and the sample may not initially be fully secured in the clamps. Therefore corrections to the data must be applied to make the initial response linear.[133] This is accomplished by examining the stress-strain response in the linear regime, and determining the slope of the line. The line is then extrapolated through the zero stress axis. The point on the strain axis where the extrapolated stress is zero is the correct zero strain point. All strain values are then calculated from this corrected data point. This procedure is demonstrated in Figure 2.12, from ref. 40. After the correct zero point stress and strain values have been obtained, the

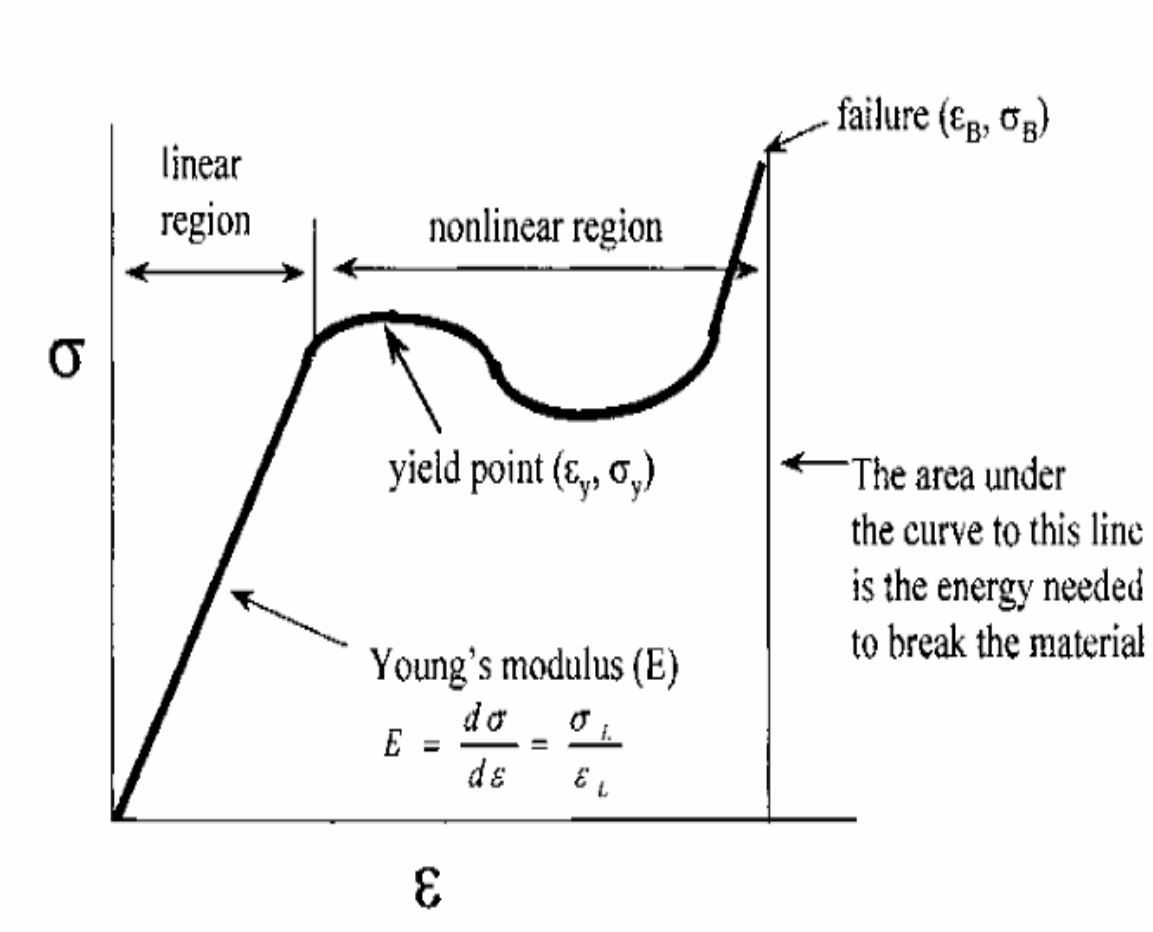

Figure 2.11. Stress-strain curve showing the various regimes of the curve. The initial elastic response of the curve gives a linear response, with the slope of the line describing the elastic modulus, *E*. The point where the curve becomes non-linear is the yield point, and the total area under the curve is the toughness of the material.

measured applied force is converted into applied stress. The stress is the force applied per area, and is reported in units of Pascals (*Pa*), which is equivalent to N/m^2. By measuring the sample cross sectional area (*CSA*) between the grips in mm^2, and using the corrected measured force in *kg*, the stress is calculated:

$$\sigma = \frac{kg * 9.80665}{CSA(mm^2)} * \frac{1E6mm^2}{1m^2} \tag{2.7}$$

After data correction, the modulus *E* was calculated from the slope of the stress-strain curve in the linear regime of $\Delta L/L_0 = 0.000 - 0.010$. The toughness was calculated by integrating the area under the stress-strain curve using *Origin 6.0* graphing software.

C. Dynamic Mechanical Analysis (DMA)

Dynamic mechanical analysis (DMA) was used to measure the storage modulus *E'*, loss modulus *E"*, and *tan δ* (*E"/E'*) of polymer blends as a function of temperature. *E'* is a characteristic of the elastic component of the material, which responds in phase to an applied oscillatory force. *E"* is characteristic of the viscous component, and is associated with the out of phase response of the material. The peak of E" is generally used to determine the T_g of the material.[134] The parameter *tan δ* is the damping peak. The *tan δ* peak can provide information on the mixing at the molecular scale, as the peak broadens upon interpenetration of polymer chains.[97] Therefore DMA can be used to demonstrate mixing on a molecular level, as compatibilizers increase chain entanglements at the interface between immiscible phases. Samples were prepared for analysis under the same conditions and in the same manner as described above for Instron mechanical testing. The ends of the dog bone sample were cut off with a razor blade, leaving the sample in the shape of a bar. Fine sandpaper was used to smooth the sample and ensure all

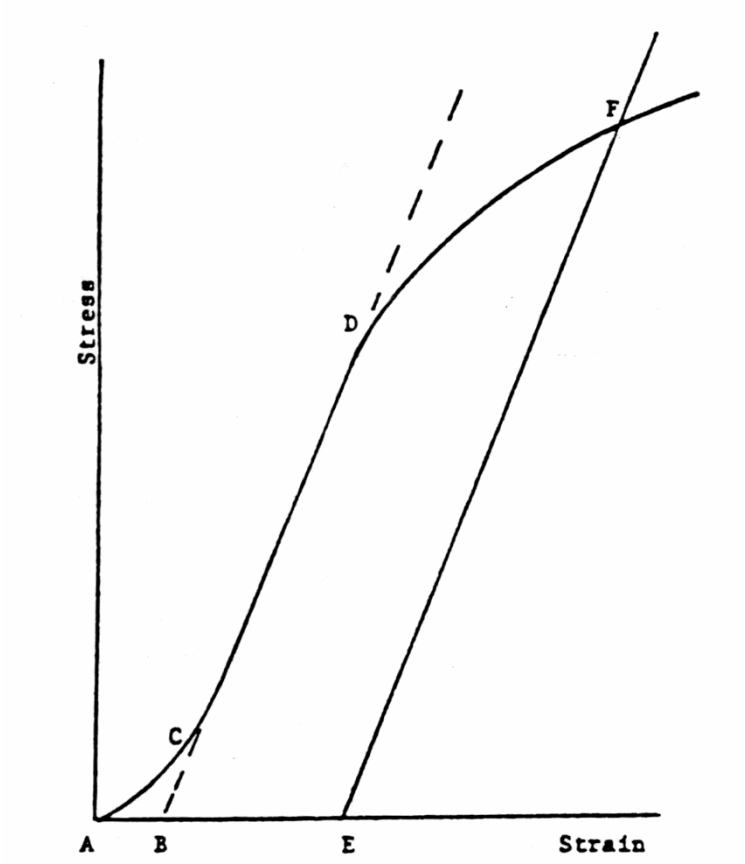

Figure 2.12. Method for determining correct zero strain point in a tensile strength test. The slope of the line in the linear regime between points *C* and *D* is determined. The line is then extrapolated to point *B*, which is the correct zero strain point from which the sample strain is measured.

dimensions were uniform, which were measured using digital calipers. A Thermal Analysis Q800 DMA was used to analyze the sample using the single cantilever sample stage for measurement. The samples were heated at 5 °C/min from -90 °C to 120 °C. A frequency of 1 Hz and a sample amplitude of 20 μm were the parameters used for the oscillatory forces applied to the sample.

D. Scanning Electron Microscopy (SEM)

Scanning electron microscopy (SEM) was utilized to determine the PI domain size of the blends. In SEM, an electron beam is rastered over the sample by means of a magnetic field which deflects the beam. When the electrons of the beam strike the sample, they are backscattered. These electrons are collected by a backscattering detector positioned at a high angle from the sample plane. Heavier atoms have higher backscattering efficiency, which means the detector signal intensity will be higher for these heavier atoms than for lighter atoms. As a result, heavier atoms appear brighter in the SEM micrograph. Samples containing different species with large differences in atomic mass can be easily distinguished by SEM. Contrast can also be induced by selective staining with highly reactive heavy metal oxidizing agents such as OsO_4 or RuO_4.

For SEM studies, all samples were melt blended at 180 °C for 10 minutes at 100 rpm under argon. Extruded samples were placed in an argon purged oven at 150 °C for 15, 30, 60, and 180 minutes in order to anneal them. To prepare the samples for analysis, the specimens were placed in liquid nitrogen for at least 90 minutes, and then shattered with a hammer. The smallest pieces were placed in HPLC grade n-heptane (Acros) overnight at room temperature to remove the polyisoprene. After rinsing with fresh n-

heptane, the samples were dried under vacuum at room temperature for at least 4 hours. The samples were mounted onto homemade 3 mm aluminum discs using double sided carbon tape (Electron Microscopy Sciences). Discs were knocked out of an aluminum weighing dish using a paper hole punch. These discs are much more economical and durable than copper TEM grids which are traditionally used for mounting SEM samples analyzed with this microscope. Because polymers are insulators, the samples were sputter coated with gold for 10 seconds to prevent charge buildup during scanning. In the initial experiments, the PI phase of the sample was selectively stained with OsO_4[135] before the gold coating process in order to create contrast in the SEM image, as previously described. Samples that had already been mounted on aluminum discs were secured to the bottom of a vial cap with double sided carbon tape. The cap was tightened on the vial containing a 4% aqueous solution of OsO_4 (Electron Microscopy Sciences), and the samples were stained by the OsO_4 vapor for 30 minutes. Samples were then sputter coated with gold as previously described. The staining method was not used because annealing caused "rivers" of PI to form throughout the sample, making domain size analysis impossible. Therefore the holes where the PI once resided were analyzed instead.

A Delong Instruments LV-EM5 low voltage SEM (5 kV) was used to analyze the samples. At least 300 particles per sample, consisting of a collection of several micrographs, were analyzed using Image J 1.36b software (NIH) to determine the area of the holes where the polyisoprene once resided. Only hole areas with a circularity greater than 0.7 were considered, where a circularity of 1.0 represents a perfect circle. From the area of the holes, A, an equivalent diameter of each hole, D_i, was calculated by:

$$D_i = 2*(A/\pi)^{0.5} \quad (2.8)$$

Since the center of the holes is not necessarily being observed by SEM, geometric corrections were applied, and the number average *(D_n)*, weight average *(D_w)*, and volume to surface area average *(D_{vs})* diameters were calculated.[136] In this analysis, the diameter is defined as the largest chord on a given circle. This layer chord length, l_i, was used to calculate the weighted chord lengths:

$$l_h = \Sigma N_i / \Sigma N_i/l_i;\ l_n = \Sigma N_i l_i / \Sigma N_i;\ l_w = \Sigma N_i l_i^2 / \Sigma N_i l_i \quad (2.9)$$

where the subscript *h* refers to the harmonic average, and N_i is the number of chords of size *i*. Applying geometric corrections gives the weighted diameters:

$$D_n = l_h(\pi/2);\ D_w = l_n(4/\pi);\ D_{vs} = l_w(3\pi/8) \quad (2.10)$$

E. Fourier Transform Infrared Spectroscopy (FT-IR)

A Varian 4100 Fourier Transform Infrared Spectrometer (FT-IR) was used to measure the signal intensity of characteristic vibrational modes of oxidized nanotubes and the grafted polystyrene. Each vibrational mode has a distinct resonant frequency which can be used for identification. If a vibrational mode has the same resonant frequency of energy as the incident light from the source, it will be excited and energy will be absorbed by the sample. After subtracting out the absorbance from the matrix, the sample absorbance *A* of energy at a given frequency follows Beer's law:

$$A = \varepsilon bc \quad (2.11)$$

where ε is the molar extinction coefficient that describes how strongly a material absorbs light, *b* is the sample pathlength, and *c* is the sample concentration. This linear dependence of absorbance on concentration means a calibration curve can be constructed with known amounts of a material in order to use FT-IR for quantification in a test

sample. In this manner, the amount of telechelic polymers grafted to COOH-MWNT could be determined by FT-IR.

Pellets were made using FT-IR grade KBr (Sigma, 99+%). The total sample size was 100 mg. The carbon nanotube content was ~0.75% by mass. All samples were dried in a vacuum oven at 80 °C for at least one hour to remove atmospheric water. The auto gain feature of the FT-IR laser was utilized to optimize the laser power and detector response. For each sample, 8192 (2^{13}) scans were taken at a resolution of 4 cm^{-1}. A KBr background sample was analyzed with the same number of scans and resolution in order to automatically subtract out the matrix contribution of the absorption.

F. Thermogravimetric Analysis (TGA)

The amount of polystyrene grafted onto carboxylated nanotubes was also quantified with a TA Instruments Q50 thermogravimetric analyzer (TGA). A TGA uses a furnace to heat a sample placed in a platinum pan which hangs on a sensitive balance. A purge gas is blown over the sample to create an inert (N_2) or oxidizing (air or O_2) environment. TGA only determines the change in sample weight as a function of temperature or time, and cannot identify the species associated with the weight change unless it is coupled to a mass spectrometer, in which case the evolved gases can be characterized.

Samples were first crushed into a powder with a mortar and pestle and then heated under nitrogen at 10 °C/min from room temperature up to 550 °C and then 20 °C/min from 550 °C up to 900 °C. Samples of COOH-MWNT, epoxy-PS-epoxy, COOH-P4MS, and the grafted nanotube samples were analyzed. Many samples from the same batch were analyzed twice to test for reproducibility.

Chapter 3

Quantifying the Effectiveness of Multiblock Copolymer Coalescence Suppression

3.1 Introduction

Many polymer blends must be heated above the T_g of the individual components during processing, during which time minor phase recombination occurs if the blends are immiscible. Here we assume the minor phase consists of less than 15 vol.% of the blend, resulting in a droplet morphology. The recombination of these droplets, called coalescence, results in the reduction of interfacial energy because the blend is not in a thermodynamically stable state.[45] By reducing its interfacial area in the blend upon coalescence, the immiscible minor phase can minimize its unfavorable interactions with the matrix. In Chapter 1, the critical role that copolymers play in droplet coalescence suppression was discussed in detail. When the copolymer resides at the interface of the matrix and the minor phase droplets, one of the copolymer blocks extends into the matrix. Droplet coalescence is suppressed with addition of compatibilizer because the copolymer chains that extend into the matrix must be compressed before the droplets are able to coalesce.[43,49] If the elastic repulsive force required for this compression of the copolymer is greater than the attractive van der Waals force between the droplets, coalescence will be inhibited.[49] In Chapter 1, sufficient evidence was provided that suggests a very effective way to compatibilize a blend is to form the copolymer *in situ* using polymers with reactive end groups.[43,74,76] This forms a diblock via a reaction between the end groups of two chains which can occur only at the interface. In comparison, a premade copolymer may become trapped as a micelle in one of the homopolymer phases of the blend. It must then diffuse through the bulk to the interface, decreasing its efficiency as a

compatibilizer.[68] Both theoretical and experimental studies presented in Chapter 1 demonstrate that a pre-made multiblock copolymer offers enhanced compatibilization effects relative to a diblock copolymer due to the fact that a multiblock copolymer will cross the interface several times, forming loops.[18,83,84] The interfacial strength is increased as the homopolymer chains become entangled with the loops of the copolymer. The work presented in Chapter 1 indicates that forming multiblock copolymers *in situ* from difunctional reactive polymers should be an extremely effective method for compatibilizing immiscible polymer blends since the copolymer can be formed quickly at the interface and the resulting multiple interfacial crossings greatly will improve interfacial strength. Our group and others have recently begun a collaborative effort to study the formation of loops at interfaces,[78,81,137-139] in order to investigate the enhanced properties these loops should afford.

In this project, we report results of our studies which examine the ability of telechelic polystyrene and polyisoprene to compatibilize a polystyrene (PS)/polyisoprene (PI) blend by forming a multiblock copolymer *in situ* at the interface between the immiscible homopolymers. Verification of *in situ* multiblock copolymer formation is presented in detail in Chapter 5.3, while Appendix A discusses attempts to quantify the PI telechelic conversion into multiblock copolymers for telechelic pairs of various molecular weight and functional groups. The goal is to quantitatively determine the most effective telechelic pair for compatibilization of a PS/PI immiscible homopolymer blend. To quantify the compatibilization efficiency of this process, the blends are annealed for various times and scanning electron microscopy (SEM) is used to determine the domain size of the dispersed phase. Here, we use Macosko's definition of compatibilization, the

stabilization of blends against coalescence.[49] Upon annealing, the domain sizes are expected to grow with time by the following relationship:[45]

$$D^3(t) = D_0^3 + Kt \quad (3.1)$$

where $D(t)$ is the diameter of the dispersed phase at annealing time t, D_0 is the diameter of the particle at zero minutes of annealing, and K is the coarsening constant. The coarsening constant in polymer blends describes the rate of coalescence of the minor phase. In the coalescence process, Brownian motion first brings two droplets towards each other. The matrix film between the droplets is then drained as the droplets push out the fluid, and the van der Waals attractive force between the droplets causes them to merge together into a larger droplet.[43,57] For coalescence, $K \propto \varphi_d T/\eta_m$, where φ_d is the volume fraction of the dispersed phase, T is the temperature, and η_m is the matrix viscosity.[45] It has also been shown that $K \propto A/\eta_m$,[140] where A is the Hamaker constant. The Hamaker constant describes the strength of the van der Waals forces between the droplets, and decreases with an increase in the energy barrier between coalescing droplets.[140,141] Thus copolymers located at the interface can suppress coalescence due to steric hindrance, as the chains extending into the matrix results in a large repulsive force when compressed, creating a energy barrier that must be overcome for droplet recombination to occur.

As mentioned in Chapter 1.9 B, the choice of telechelic molecular weight plays an important role in the compatibilizer's ability to sterically hinder coalescence. To determine the overall effectiveness of this compatibilization scheme to improve blend properties, the right balance of static and dynamic coalescence suppression must be realized. Lower molecular weight telechelics offer the advantage of a higher

concentration of end groups per given volume and the ability to approach the interface quickly, readily forming a copolymer and providing good suppression of dynamic coalescence during mixing.[49,79] However, higher molecular weight telechelics should provide better suppression of static coalescence during annealing, as it is more difficult to compress longer chains between two coalescing droplets.[49] An optimal telechelic molecular weight can thus be defined as that which results in a system where the blend will be well compatibilized and the coarsening constant K is small. It is therefore the goal of this study to determine the role of telechelic loading and chain length on its ability to reactively compatibilize a phase separated polymer blend. In addition, we wish to determine whether telechelics possessing less reactive complementary functional groups can still produce sufficient copolymer at short reaction times to suppress coalescence.

3.2 Experimental

A. Materials

Bulk polystyrene (PS) (M_n = 77,000, M_w = 196,000, PDI = 2.55) and polyisoprene (PI) (M_n = 191,000, M_w = 293,000, PDI = 1.53) were used in this SEM study. Preparation of the homopolymers is described in Chapter 2.1 A. Various molecular weight anh/NH_2 and epoxy/COOH telechelic pairs, described in detail in Chapter 2.1 D, are used in this study. The M_n and PDI of the telechelics are shown in Table 3.1. Recall from Chapter 2.1 D that the reaction between an anhydride and primary amine is very fast, while the reaction between an epoxide and carboxylic acid is considerably slower.

B. Blending and Annealing Procedure

The blends studied initially contained 5.0% telechelics by weight, while the remaining 95% of the sample consisted of a homopolymer composition that was 90%

Table 3.1. Number average molecular weight and polydispersity index of difunctional polystyrene and polyisoprene polymers used in this study.

Telechelic	M_n	PDI		Telechelic	M_n	PDI
anh-PS-anh	16,000	1.11		NH_2-PI-NH_2	16,000	1.28
anh-PS-anh	37,000	1.02		NH_2-PI-NH_2	32,000	1.27
anh-PS-anh	83,000	1.02				
epoxy-PS-epoxy	18,000	1.04		COOH-PI-COOH	18,000	1.14
epoxy-PS-epoxy	44,000	1.04		COOH-PI-COOH	54,000	1.18

PS/10% PI. For one telechelic pair, the loading level was decreased to 2.5 wt.%, 1.3 wt.%, 0.5 wt.%, and 0.1 wt.%. The blending procedure is described in Chapter 2.2. A small aliquot of the blend, approximately 5 mm in diameter, was extruded after 10 minutes of melt mixing. The sample was quenched at room temperature, where it was cool to the touch after a few seconds. These small samples were then placed in an argon purged oven at 150 °C for 15, 30, 60, and 180 minutes to anneal the samples.

C. SEM Analysis

Samples for SEM were prepared according to Chapter 2.4 D. A Delong Instruments LV-EM5 low voltage SEM (5 kV) was used to analyze the samples. Micrographs were analyzed using Image J 1.36b software (NIH) to determine the area of the holes where the polyisoprene once resided. The number average hole diameter (D_n), weight average hole diameter (D_w), and volume to surface area average hole diameter (D_{vs}) were calculated. Geometric corrections were applied to account for the fact that the holes may not be examined in the center. A full description of this procedure is discussed in Chapter 2.4 D. Several micrographs, each containing approximately 100 – 400 holes, from different areas of a single sample were analyzed, and the average weighted diameter and standard deviation were calculated.

3.3 Calculation of Coarsening Constant

A. Visual Results

SEM images of representative samples melt blended for 10 minutes and then annealed at 150°C under argon for 0 and 180 minutes are shown in Figure 3.1. From Figure 3.1, one can visually observe that the blends with the telechelics have a larger initial droplet size than the uncompatibilized blend.

B. Coarsening Constant Quantification

In Figure 3.2, D^3, expressed as $D_n*D_w*D_{vs}$, is plotted as a function of annealing time in order to determine the coarsening constant K. The results show that the slope of the line is reduced in the compatibilized blends due to the suppression of coalescence by steric hindrance of the copolymer. In addition, the results in Figure 3.2 agree with the visual results shown in Figure 3.1, in that the initial droplet size in the compatibilized blends is actually larger than the uncompatibilized blend. The initial size of the droplets varies widely in the compatibilized blends. However, the coarsening constant does not depend on the initial size of the particle, only the rate of growth. Thus it may be more useful to quantify the rate of coalescence of PI droplets using the relative cubed diameter, $D(t)^3/D_0^3$. The data in Figure 3.2 is replotted as the relative cubed diameter as a function of annealing time in Figure 3.3. The results in Figure 3.3 show that the droplets in the blend without telechelics coalesce rapidly, as the relative size increases by a factor of ~6 after only 10 minutes of annealing. The 18k epoxy-PS-epoxy/20k COOH-PI-COOH telechelics also did not compatibilize the blend, as the domain size increased rapidly for the entire 180 minutes of annealing and its relative droplet size surpassed that of the uncompatibilized blend. All of the other telechelic pairs suppress coalescence relative to

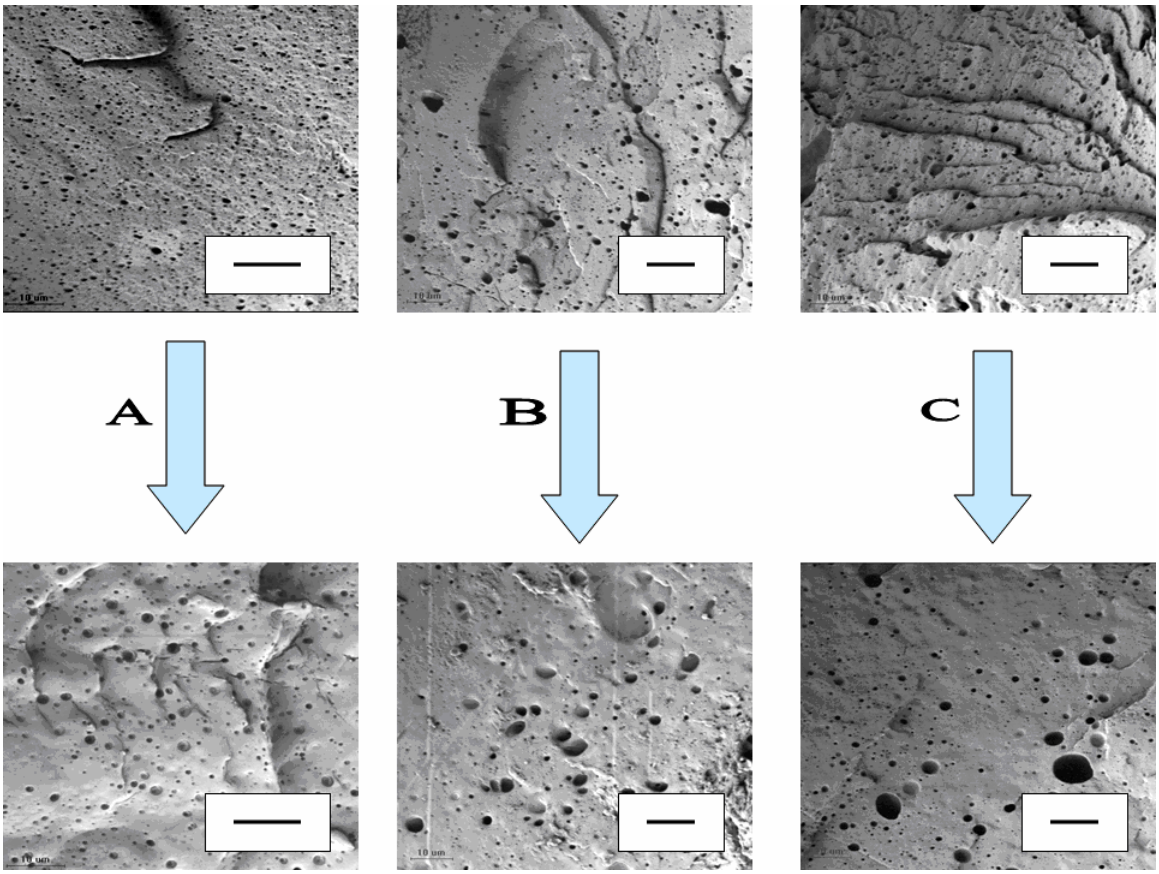

Figure 3.1. SEM images of 90% PS/10% PI blends annealed at 150°C for 0 minutes (top) and 180 minutes (bottom): (A) Uncompatibilized, (B) 37k anh-PS-anh/32k NH_2-PI-NH_2, (C) 44k epoxy-PS-epoxy/54k COOH-PI-COOH. The scale of the bar in each image is 10 μm.

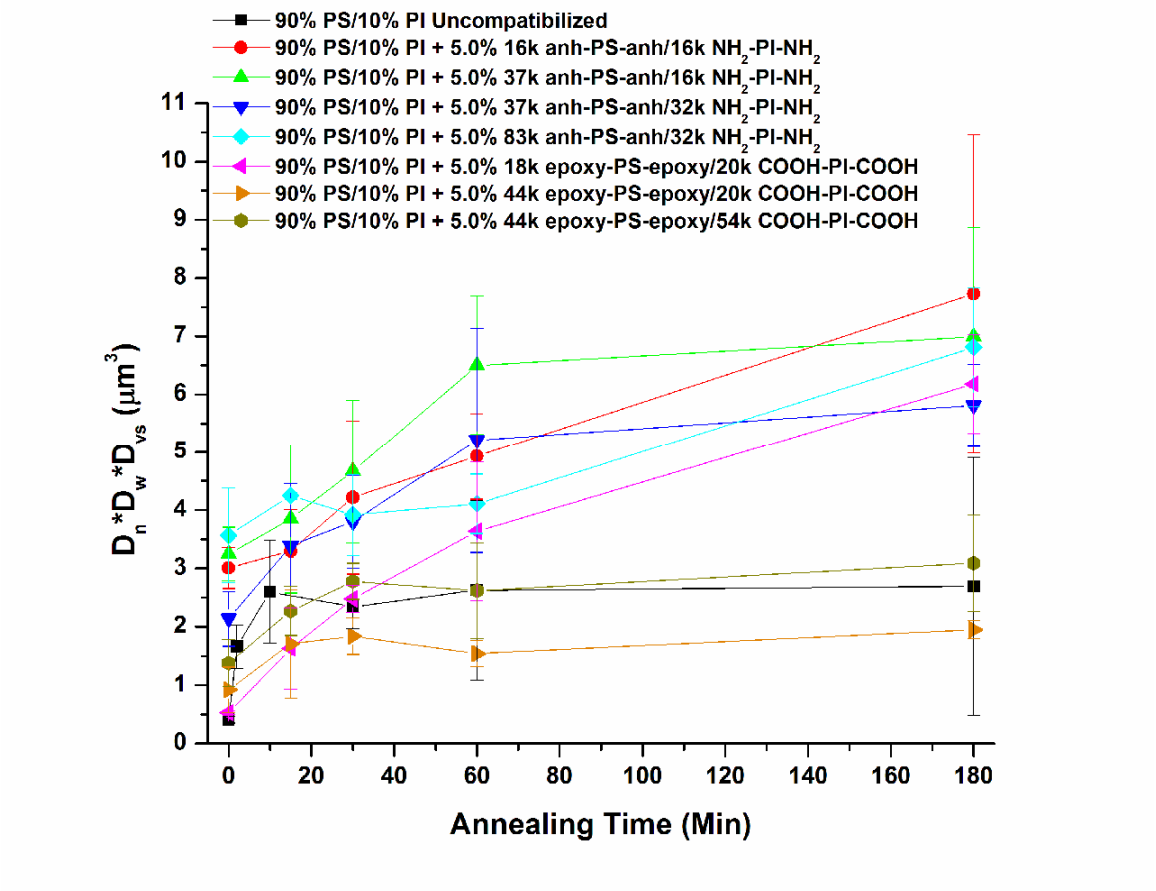

Figure 3.2. D^3 as a function of annealing time for 90% PS/10% PI blends with 5.0 wt.% telechelics.

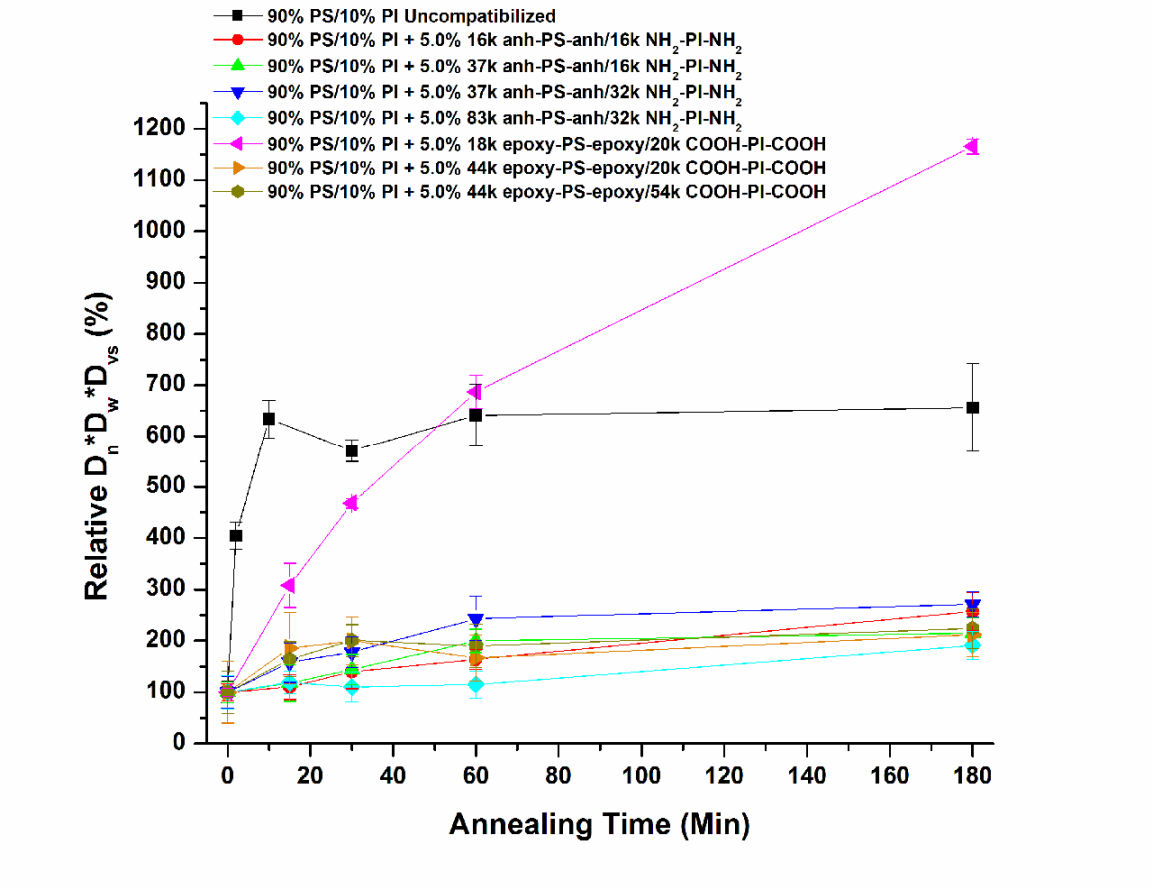

Figure 3.3. Relative D^3 $(D(t)^3/D_0^3)$ as a function of annealing time for 90% PS/10% PI blends with 5.0 wt.% telechelics.

the uncompatibilized blend, as their droplet size increases only by a factor of ~2 after 180 minutes of annealing.

The coarsening constant K in Equation 3.1 was determined from the slope of a linear fit of $D(t)^3 - D_0^3$ as a function of annealing time, with D^3 expressed as $D_n*D_w*D_{vs}$. The slope of the line was determined by fitting the data from zero time to the stabilization time of the droplets to a line. In a study of polystyrene/poly(dimethylsiloxane) blends by Macosko et al., the system was described as stable to coalescence if the particle size changed less than 25% after 30 minutes of annealing.[55] We use a similar criterion, defining the droplets as stabilized when the D_{vs} increase is less than 25% between annealing time intervals. Table 3.2 shows the stabilization time, absolute coarsening constant K, total growth expressed as $K*t_{stable}$, and R^2 of the linear fit of the data. Table 3.2 shows that the blends have various stabilization times. The coarsening before the stabilization time nearly fits the linear model of Equation 3.1. The uncompatibilized blend fit poorly to Equation 4.1 due to a rapid slowdown in coarsening between 2 and 10 minutes. In addition, the 18k epoxy-PS-epoxy/20k COOH-PI-COOH blend also demonstrated a reduction in the coarsening rate between 60 minutes and 180 minutes of annealing, observed in Figure 3.2 and Figure 3.3, leading to a poor R^2 value shown in Table 3.2. Comparing the data in Table 3.2 with Figure 3.2 and Figure 3.3, it is clear that the lowest K value does not describe the best compatibilized blend, as the 83k anh-PS-anh/32k NH_2-PI-NH_2 blend has the lowest K value but is not stabilized after annealing. Since all the blends have various stabilization times, it may be more instructive to use $K*t_{stable}$, the coarsening constant multiplied by the stabilization time, as a measure of the telechelics' ability to compatibilize the blends. This provides a measure of the total

Table 3.2. Coarsening constant K determined from a linear fit of $D(t)^3 - D_0^3$ as a function of annealing time. A * indicates the droplets were not stabilized, and a time of 180 minutes was used in the calculation.

90% PS / 10% PI 5.0 wt% Telechelics	Stabilization (Min)	K (μm^3/Min)	K*t_{stable} (μm^3 Growth)	R^2
Uncompatibilized	10	2.3E-01	2.3	0.737
16k anh-PS-anh / 16k NH_2-PI-NH_2	180*	2.7E-02	4.9	0.980
37k anh-PS-anh / 16k NH_2-PI-NH_2	60	6.6E-02	3.9	0.988
37k anh-PS-anh / 32k NH_2-PI-NH_2	60	5.0E-02	3.0	0.915
83k anh-PS-anh / 32k NH_2-PI-NH_2	180*	1.7E-02	3.1	0.930
18k epoxy-PS-epoxy / 20k COOH-PI-COOH	180*	3.4E-02	6.2	0.863
44k epoxy-PS-epoxy / 20k COOH-PI-COOH	15	5.3E-02	0.8	1.000
44k epoxy-PS-epoxy / 54k COOH-PI-COOH	30	4.9E-02	1.5	0.972

growth, so different stabilization times are accounted for. The K^*t_{stable} value for 18k epoxy-PS-epoxy/20k COOH-PI-COOH has the largest value in the table, agreeing with the data in Figure 3.3. The 44k epoxy-PS-epoxy/20k COOH-PI-COOH and 44k epoxy-PS-epoxy/20k COOH-PI-COOH have the smallest K^*t_{stable} values, which also agrees with the results in Figure 3.2 and Figure 3.3. However, the uncompatibilized blend has a smaller K^*t_{stable} value than the remaining anh/NH_2 telechelic pairs, which undoubtedly suppress coalescence. Thus, it is clear that this analysis of the data in Figure 3.2 does not provide a quantifiable measure of the ability of the telechelics to compatibilize these blends.

Inspection of Figure 3.2 shows that the blends have different initial droplet sizes, and all compatibilized blends have an initial D^3 greater than the uncompatibilized blend, which may explain the failure of the analysis of the data in Figure 3.2 to accurately describe the effectiveness of the telechelics as compatibilizers. For instance, if the droplets are large to begin with, annealing will lead to even larger droplets being formed, and the absolute K value of these blends will be larger than the uncompatibilized blend.

Therefore accurately quantifying the effectiveness of the compatibilizers will require the analysis of the relative size increase of the droplets, as shown in Figure 3.3. If D^3/D_0^3 is plotted as a function of annealing time, the slope is the relative coarsening constant, K_{rel}, in units of % growth/min. The value $K_{rel}*t_{stable}$ then provides a measure of the total percent growth up to stabilization. The results of these analyses are shown in Table 3.3. Table 3.3 shows that the 44k epoxy-PS-epoxy/20k COOH-PI-COOH, 44k epoxy-PS-epoxy/54k COOH-PI-COOH, 37k anh-PS-anh/16k NH_2-PI-NH_2, and 37k anh-PS-anh/32k NH_2-PI-NH_2 exhibit the lowest $K_{rel}*t_{stable}$ values of stabilized blends, in agreement with the data in Figure 3.3. The results show that the slower reacting epoxy/COOH pair produced sufficient copolymer in the 10 minute mixing time to suppress coalescence as effectively as the highly reactive anh/NH_2 pair.

It is also interesting to note that the low molecular weight pairs of both the anh/NH_2 and epoxy/COOH systems both suppress coalescence poorly relative to the intermediate molecular weight telechelic pairs. Since this is the case for both the high

Table 3.3. Relative coarsening constant K_{rel} determined from a linear fit of $(D(t)^3/D_0^3) - 1$ as a function of annealing time. A * indicates the droplets were not stabilized, and a time of 180 minutes was used in the calculation.

90% PS / 10% PI 5.0 wt% Telechelics	Stabilization (Min)	K_{rel} (%/Min)	$K_{rel}*t_{stable}$ (% Growth)	R^2
Uncompatibilized	10	5.7E+01	570	0.737
16k anh-PS-anh / 16k NH_2-PI-NH_2	180*	9.0E-01	162	0.980
37k anh-PS-anh / 16k NH_2-PI-NH_2	60	1.6E+00	96	0.988
37k anh-PS-anh / 32k NH_2-PI-NH_2	60	2.3E+00	138	0.915
83k anh-PS-anh / 32k NH_2-PI-NH_2	180*	4.8E-01	86	0.930
18k epoxy-PS-epoxy / 20k COOH-PI-COOH	180*	6.5E+00	1170	0.863
44k epoxy-PS-epoxy / 20k COOH-PI-COOH	15	5.7E+00	86	1.000
44k epoxy-PS-epoxy / 54k COOH-PI-COOH	30	3.5E+00	106	0.972

and low reactivity pairs, this observation can be explained as a molecular weight effect, where the blocks of the copolymer formed from the telechelic are too short to effectively entangle with the homopolymer chains as a compatibilizer. For entangled chains, the polymer viscosity is proportional to $M_w^{3.4}$ when $M_w > M_c$, where M_c is the critical molecular weight.[103] M_c is approximately equal to twice the entanglement weight, M_e.[85] At a temperature of 140 °C, M_e of polystyrene is ~13,000, whereas M_e of polyisoprene is only ~6,000.[142] For the 16k anh-PS-anh/16k NH_2-PI-NH_2 and 18k epoxy-PS-epoxy/20k COOH-PI-COOH blends, the PS telechelic molecular weight is below M_c, which results in poor entanglement between the PS block of the copolymer and the PS matrix. The PS copolymer blocks therefore have significant mobility, and can be readily squeezed out of the way of the recombining droplets,[49,55] leaving the concentration of copolymer at the interface too low to effectively suppress coalescence.

This observation agrees with previous compatibility studies using premade multiblock copolymers. In a study by Eastwood and Dadmun, premade block copolymers with a similar molecular weight but different block numbers were used to compatibilize PS and PMMA.[84] It was found that the order of interfacial strength was pentablock > triblock > diblock > heptablock. Increasing the number of blocks in the copolymer increases the number of interfacial crossings, strengthening the interface. However, the heptablock copolymer provided the least increase in interfacial strength despite having the most interfacial crossings. This was due to the fact that the block size of this copolymer was below the entanglement weight of the homopolymers. Since the copolymer blocks could not entangle well with the homopolymers, the interfacial strength was not effectively increased. These previous results and the complimentary results

demonstrated in this study show it is critical that each copolymer block size is larger than the entanglement weight of the homopolymer. Otherwise the copolymer will not be an effective interfacial modifier, regardless of how many times it crosses the interface. In this study, we only observed the suppression of droplet coalescence for blends that were mixed for 10 minutes. This project could be expanded to include blends mixed for different times to see if there is a difference in the effectiveness of coalescence suppression, since the telechelics first form diblock copolymers, then triblock copolymers, etc.

C. Specific Interfacial Area

The change in specific interfacial area (interfacial area per unit volume) as a function of annealing time also provides a method to quantify the effectiveness of telechelic pairs to compatibilize a polymer blend. As the blend anneals, smaller droplets coalesce into larger ones, reducing the surface area of the droplets, causing the volume to surface area ratio to increase. Therefore, a well compatibilized blend will lose less specific surface area during annealing than a poorly compatibilized blend. The specific surface area of the droplets in the blend can be calculated by:[49]

$$S_{sp} = 6\varphi_{minor}/D_{vs} \tag{3.2}$$

where φ_{minor} is the volume fraction of the minor phase in the blend, and D_{vs} is the volume to surface area droplet diameter determined by SEM. The specific surface area is the ratio of the surface area to the mass of a sphere, and is expressed as

$$S_{sp} = \frac{A_{sphere}}{V_{sphere}\rho} = \frac{4\pi r^2}{4/3\,\pi r^3 \rho} = \frac{3}{r\rho} \tag{3.3}$$

Since D_{vs} is equal to $2r_{vs}$, Equation 3.2 is derived from this relationship.

Figure 3.4 shows the change in specific surface area as a function of annealing time for the blends containing 5.0 wt.% telechelics, while the relative change in specific surface area, $S_{sp}(t)/S_{sp,0}$ is plotted as a function of annealing time in Figure 3.5. In addition, the relative specific surface area at the times the droplet morphology has been stabilized is shown in Table 3.4. The results show that the uncompatibilized blend loses more than half of its specific surface area when the droplets coalesce during annealing. When the 18k epoxy-PS-epoxy/20k COOH-PI-COOH telechelic pair is used, only one third of the original specific surface area remains after annealing, showing these telechelics mainly act as plasticizers that make coalescence easier. The most effective telechelic pairs, which have the lowest $K_{rel}*t_{stable}$ values shown in Table 3.3, only lose ~15% – 25% of their specific surface area before stabilization is achieved.

Another point of interest is that the droplets in the blends compatibilized with 44k epoxy-PS-epoxy/20k COOH-PI-COOH and 44k epoxy-PS-epoxy/54k COOH-PI-COOH rapidly grow and lose specific surface area in the first 15 minutes of annealing, but then become stabilized. This is most clearly demonstrated in Figure 3.3 and Figure 3.5. With the exception of the 37k anh-PS-anh/32k NH_2-PI-NH_2 telechelic pair, the blends stabilized with the anh/NH_2 telechelics do not lose a significant amount of specific surface area until after 30 minutes of annealing. This suggests that the slower conversion of telechelics into multiblock copolymers for the less reactive epoxy/COOH pair impacts the morphology development. Because of the lower initial copolymer concentration at the interface for the slow epoxy/COOH reaction, the droplets can initially coalesce quickly and reduce the droplet surface area. As the droplets grow and their surface area decreases, the local copolymer concentration increases until a critical copolymer surface

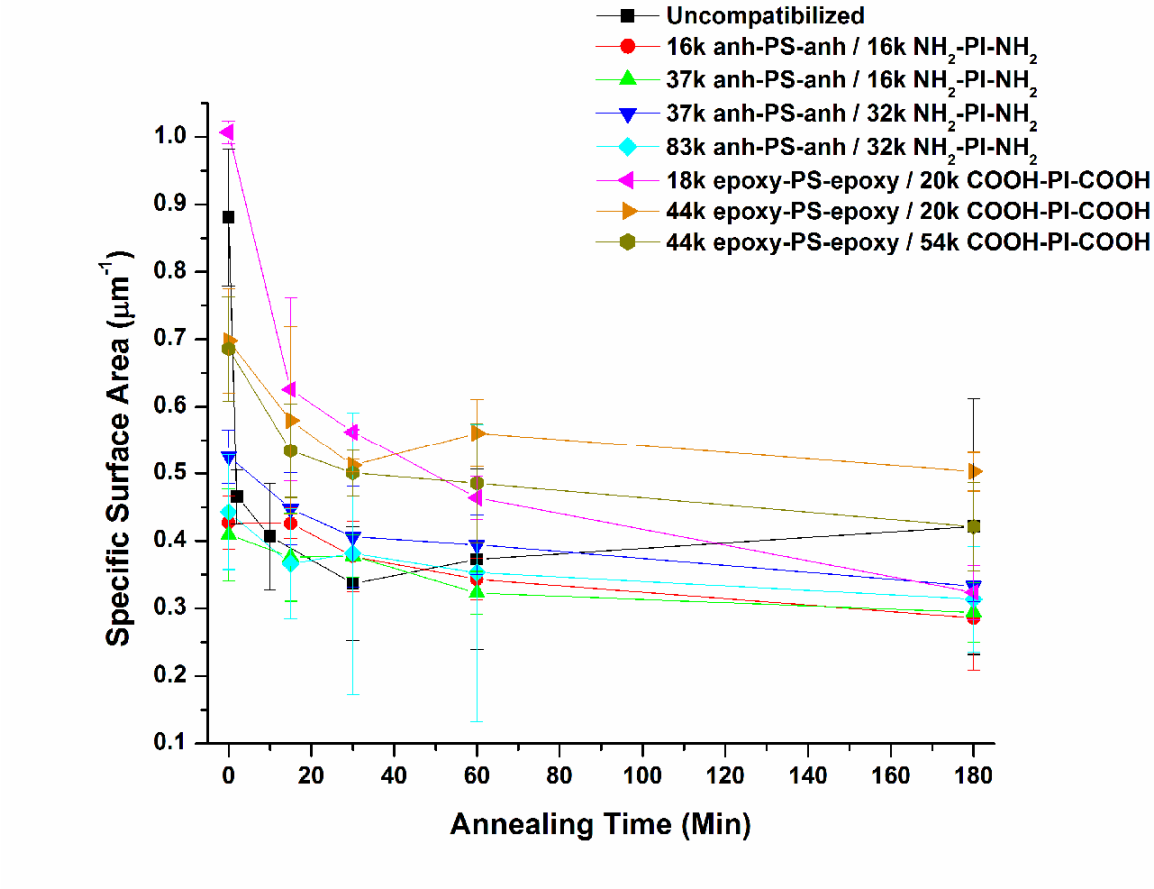

Figure 3.4. The change in the specific surface area as a function of annealing time for blends composed of 90% PS/10% PI with 5.0 wt.% telechelics.

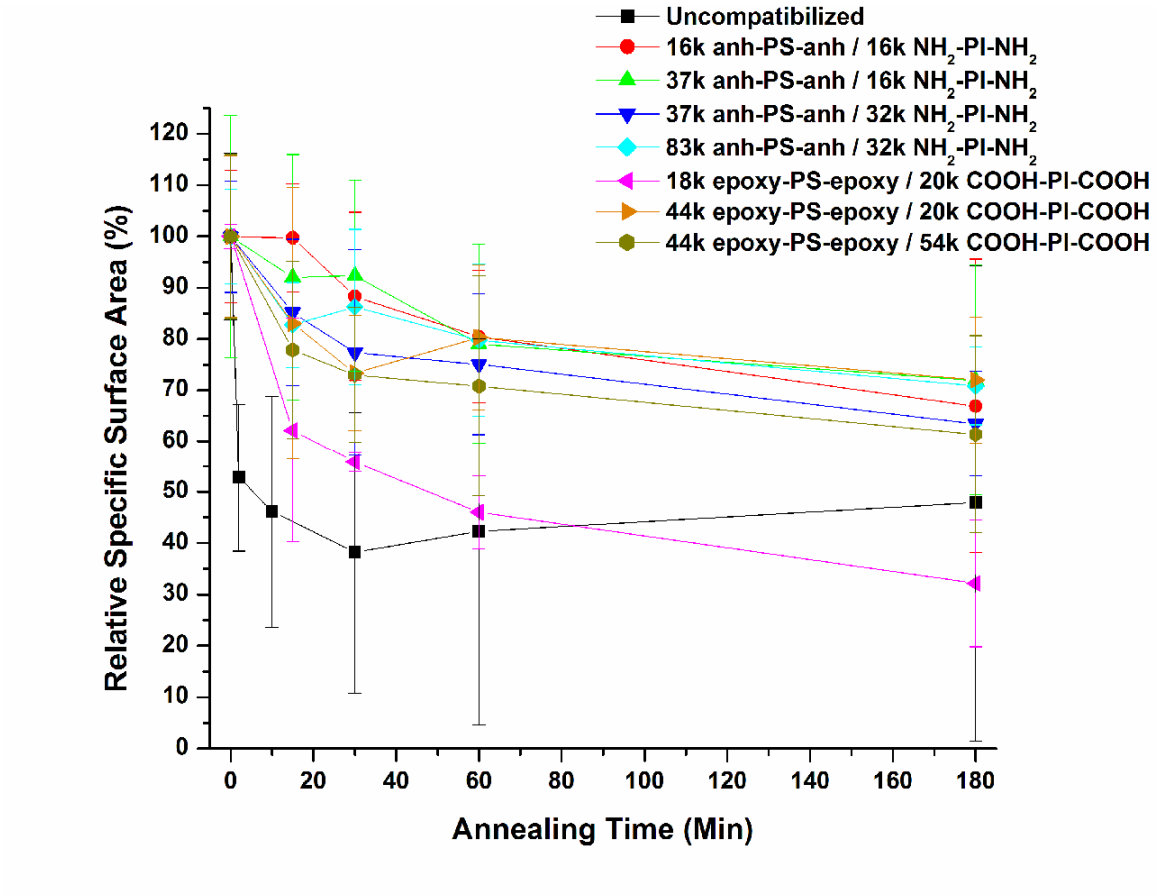

Figure 3.5. The relative change in specific surface area as a function of annealing time for blends composed of 90% PS /10% PI with 5.0 wt.% telechelics.

Table 3.4. Percent of original relative specific surface area (Rel SA) remaining in 90% PS/10% PI blends with 5.0 wt.% telechelics after droplet stabilization time. A * indicates the blend was not stabilized, and the D_{vs} at 180 minutes was used in the calculation.

Blend	Rel SA (%)	Stabilization Time (Min)
44k epoxy-PS-epoxy/20k COOH-PI-COOH	83.0	15
37k anh-PS-anh/16k NH_2-PI-NH_2	79.0	60
37k anh-PS-anh/32k NH_2-PI-NH_2	75.0	60
44k epoxy-PS-epoxy/54k COOH-PI-COOH	73.0	30
83k anh-PS-anh/32k NH_2-PI-NH_2	70.8	180*
16k anh-PS-anh/16k NH_2-PI-NH_2	66.9	180*
Uncompatibilzed	46.2	10
18k epoxy-PS-epoxy/20k COOH-PI-COOH	32.1	180*

coverage has been reached, stabilizing the droplets against further coalescence. The epoxy/COOH reaction is known to be slower than the anh/NH_2 reaction, which allows initial morphology coarsening, however our results clearly show that it produces sufficient copolymer to ultimately stabilize the blends, as the blends remain stabilized after short annealing times.

3.4 Effects of Telechelic Loading

It is important to understand why the initial droplet size is not reduced with addition of telechelics. As discussed in Chapter 1, one role of the copolymer is to reduce the interfacial tension of the minor phase droplets and assist in their breakup by shear forces into a finer dispersion. However, our results show that the initial droplet size is actually larger in the 90% PS/10% PI blends with telechelics than the uncompatibilized blend. One explanation for this is that the telechelics, except for the 83k anh-PS-anh, have lower molecular weights than the homopolymers, 77k M_n for PS and 191k M_n for PI. This results in a decrease of the viscosity of the sample, which alters droplet formation during melt blending, where there is an equilibrium between the rate of droplet breakup by shear forces and recombination by coalescence. The final droplet size is predicted to be:[143]

$$\frac{1}{R} = A\frac{\eta_a G}{\phi_d \sigma} + \frac{B}{\sigma} \tag{3.4}$$

where R is the droplet radius, η_a is the apparent blend viscosity, G is the shear rate, φ_d is the volume fraction of the dispersed phase, σ is the interfacial tension, A is a constant related to the coalescence probability, and B is a constant related to the macroscopic bulk breaking energy. Thus, even though high molecular weight multiblock copolymers are being formed during mixing, any remaining unreacted telechelics remain in the

homopolymers lowering η_a, acting as plasticizers. Equation 3.4 shows that lowering the viscosity makes coalescence easier, increasing droplet size.

A telechelic concentration of 5.0 wt.% was chosen as an initial loading level for this study, however the plasticizing effect of the unreacted telechelic chains can be reduced by lowering the amount of telechelics in the blend. Thus a blend of 90% PS/10% PI compatibilized with 37k anh-PS-anh/16k NH_2-PI-NH_2 with a range of telechelic loading (5.0 wt.%, 2.5 wt.%, 1.3 wt.%, 0.5 wt.%, and 0.1 wt.%) was examined. The results of the compatibilization of this blend, melt mixed at 180 °C for 10 minutes, are shown in Figure 3.6 as a plot of $D_n*D_w*D_{vs}$ as a function of annealing time and in Figure 3.7 as a plot of the relative D^3 as a function of annealing time. Figure 3.6 shows that the initial size of the droplets is reduced as the telechelic loading decreases, as fewer unreacted telechelics acting as plasticizers are present in the blend. Figure 3.7 clearly demonstrates that reducing the telechelic loading to 1.3 wt.% and 0.5 wt.% retains its ability to compatibilize the blend, as a large reduction in the growth of the droplets still occurs, yet the initial droplet size decreases. At these loading levels, there are sufficient telechelics present in the system for interfacial coverage of the droplets to prevent coalescence, but also not enough to significantly plasticize the blend. When the telechelic loading is further reduced to 0.1 wt.%, however, the coalescence is not suppressed, presumably because too few telechelics are available to saturate the interface and inhibit coalescence. The coarsening constants were determined for the data in Figure 3.6 and Figure 3.7, and are shown in Table 3.5. As previously discussed, $K_{rel}*t_{stable}$ best quantifies the effectiveness of the compatibilizers. With the exception of the 0.1 wt.% blend, which never achieved stabilization, $K*t_{stable}$ decreases as the telechelic loading was

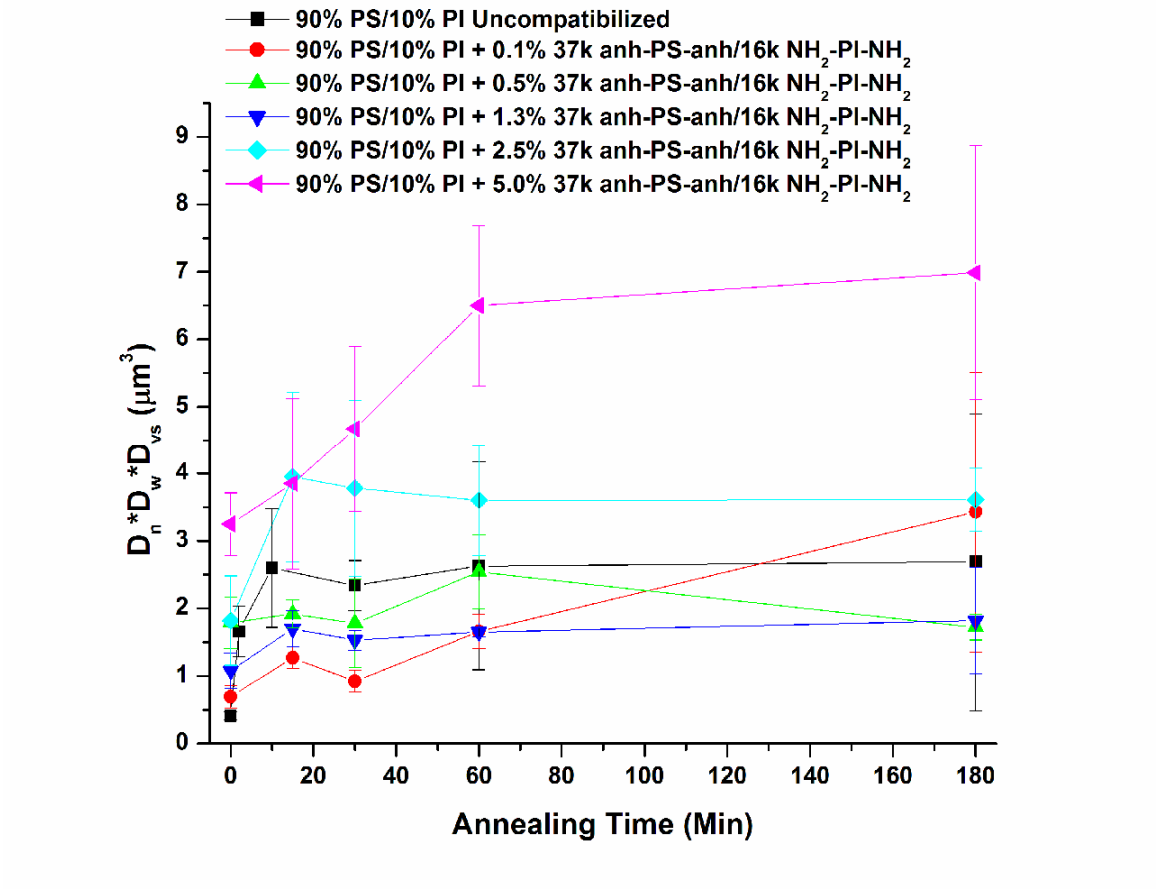

Figure 3.6. D^3as a function of annealing time for 90% PS/10% PI polymer blends compatibilized with various amounts of 37k anh-PS-anh/16k NH_2-PI-NH_2 telechelics.

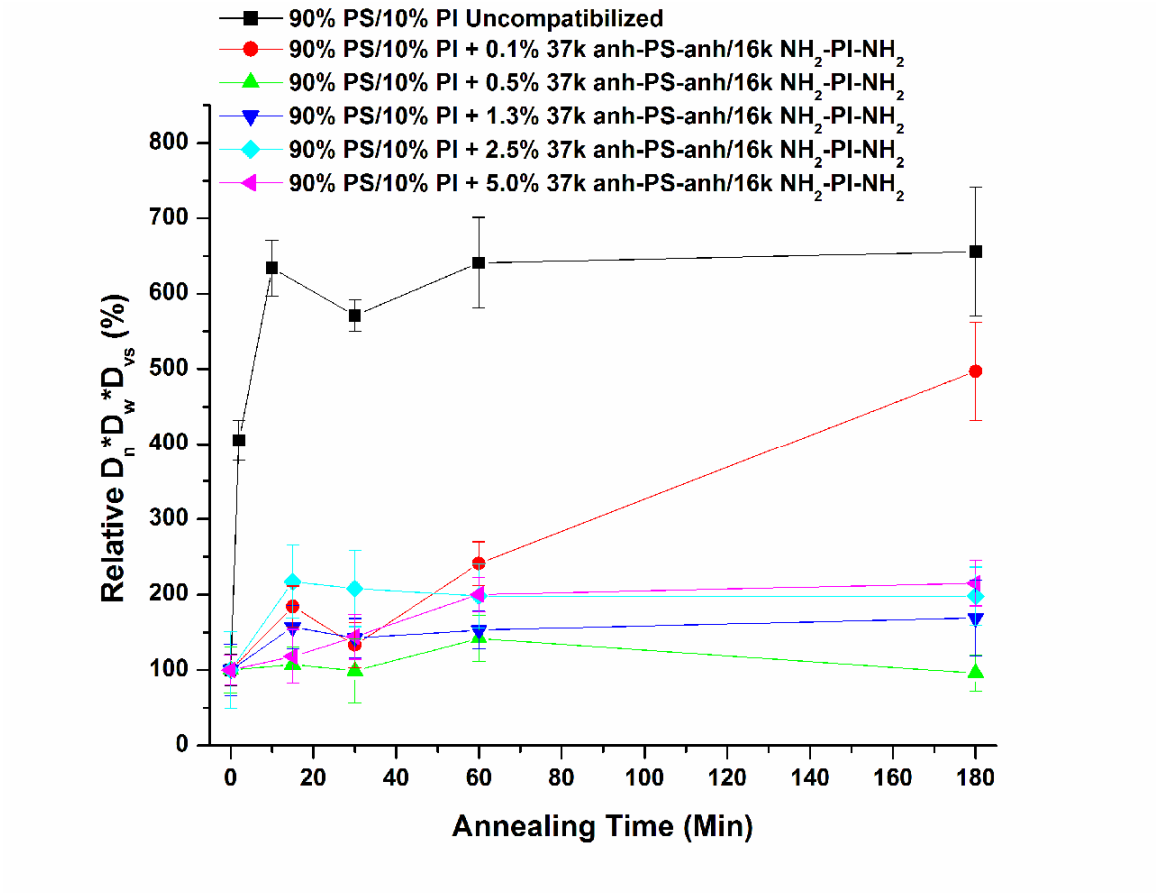

Figure 3.7. Relative D^3 $(D(t)^3/D_0^3)$ as a function of annealing time for 90% PS/10% PI polymer blends compatibilized with various amounts of 37k anh-PS-anh/16k NH_2-PI-NH_2 telechelics.

reduced. Since reducing the telechelic loading reduces the plasticization effect, the initial size of the droplets is also smaller. Thus the increase in absolute size is also reduced. In relative terms, there was no significant difference between $K_{rel}*t_{stable}$ for telechelic loadings of 5.0 wt.% and 2.5 wt.%. When the loading was further reduced to 1.3 wt.% and 0.5 wt.%, a significant decrease in absolute and relative size growth is observed, with the 0.5 wt.% loading clearly showing the slowest growth. These results demonstrate the significant plasticization effects of the unreacted telechelics when large excesses are used. Figure 3.7 and Table 3.5 show that the optimal telechelic loading for 90% PS/10% PI with the 37k anh-PS-anh/16k NH_2-PI-NH_2 telechelic pair is 0.5 wt.%.

The specific interfacial area of these compatibilized blends with variable loading was also calculated as a function of annealing time, where the absolute values are shown in Figure 3.8, and the relative specific interfacial area is plotted in Figure 3.9. Figure 3.8 shows that with the exception of the 0.5 wt.% loading sample, decreasing the telechelic loading increases the initial specific interfacial area. As plasticization is reduced at lower loading, smaller droplet sizes result due to an increase in matrix viscosity which hinders

Table 3.5. Stabilization time, absolute coarsening constant, $K*t_{stable}$, relative coarsening constant, $K_{rel}*t_{stable}$, and R^2 of the linear fit of the data for 90% PS/10% PI blends with various 37k anh-PS-anh/16k NH_2-PI-NH_2 telechelic loading. A * indicates the blend was not stabilized, and values at 180 minutes were used in the calculations.

90% PS / 10% PI 37k anh-PS-anh / 16k NH_2-PI-NH_2	Stabilization (Min)	K (μm^3/Min)	$K*t_{stable}$ (μm^3)	K_{rel} (%/Min)	$K_{rel}*t_{stable}$ (%)	R^2
5.0%	60	6.6E-02	3.9	2.0E+00	122	0.946
2.5%	15	1.4E-01	2.1	7.8E+00	117	1.000
1.3%	15	4.1E-02	0.6	3.8E+00	57	1.000
0.5%	15	8.7E-03	0.1	4.7E-01	7	1.000
0.1%	180*	1.5E-02	2.8	2.2E+00	398	0.948
Uncompatibilized	10	2.3E-01	2.3	5.7E+01	572	0.737

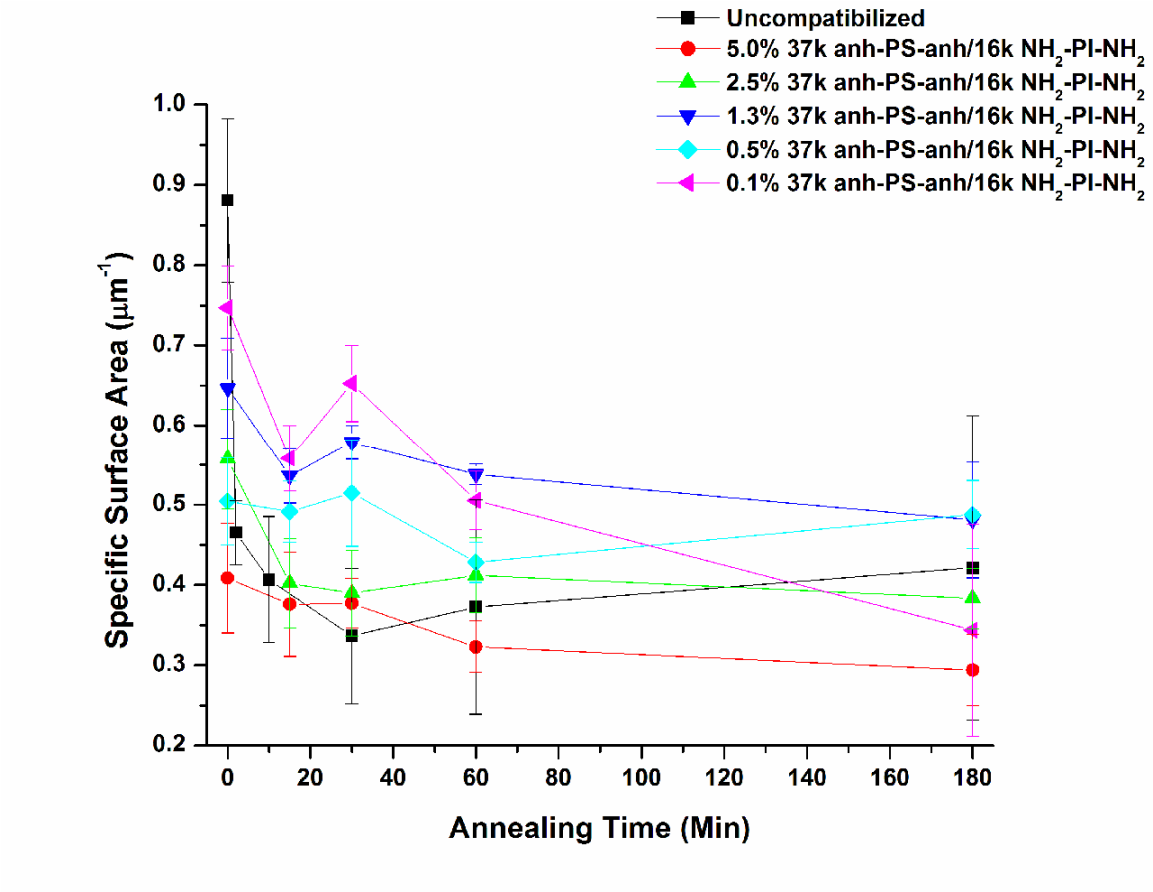

Figure 3.8. The change in the specific surface area as a function of annealing time for blends composed of 90% PS/10% PI with varying amounts of 37k anh-PS-anh/16k NH_2-PI-NH_2 telechelics.

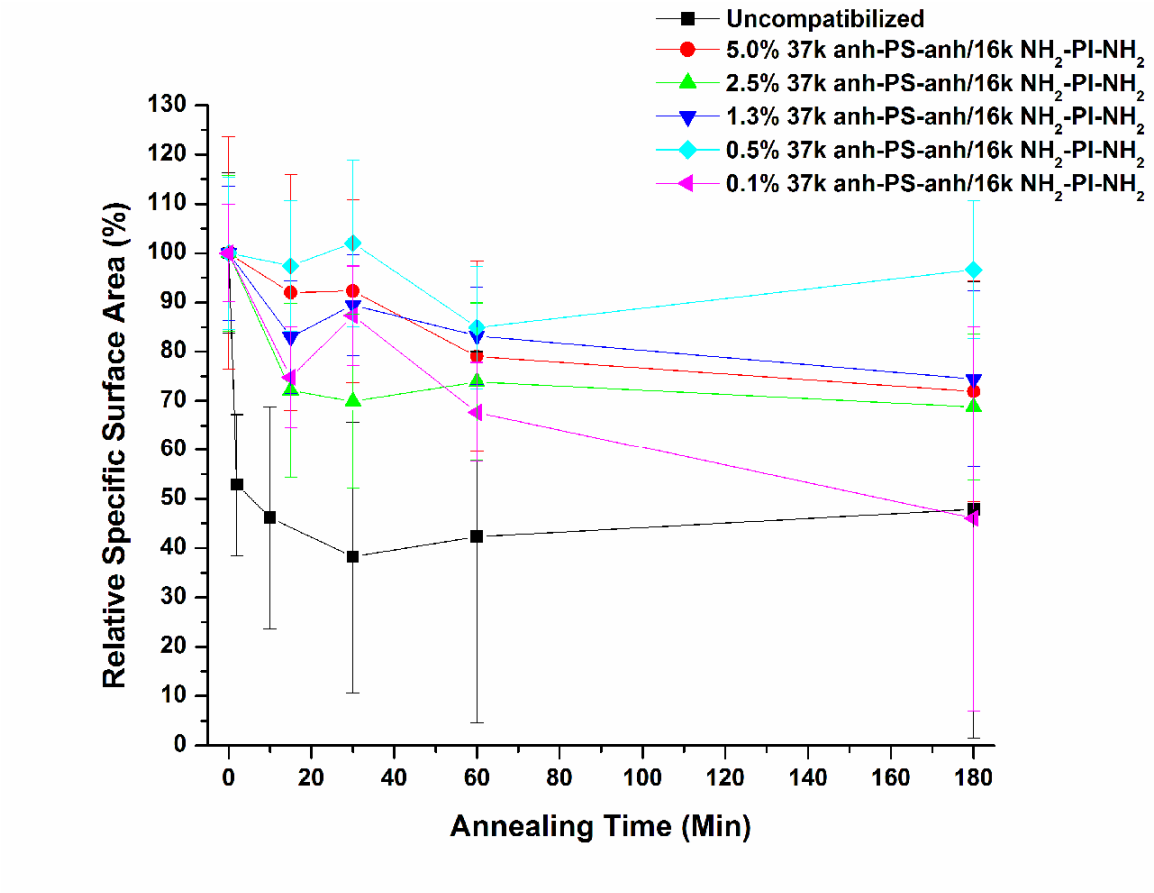

Figure 3.9. The change in the relative specific surface area as a function of annealing time for blends composed of 90% PS/10% PI with varying amounts of 37k anh-PS-anh/16k NH_2-PI-NH_2 telechelics.

droplet coalescence. Figure 3.9 agrees with the observations in Figure 3.7. It is clear that 0.1 wt.% telechelic loading is insufficient to suppress coalescence, as the specific interfacial area constantly decreases during annealing. A loading of 0.5 wt.% shows the least loss of specific interfacial area, ~3%, agreeing with the lowest $K_{rel}*t_{stable}$ value observed for this blend in Table 3.5. The results of the relative specific interfacial area remaining when the blends are stabilized are shown in Table 3.6. It is quite clear that the 0.5 wt.% loading results is the optimal concentration for coalescence suppression, as the interfacial area remains nearly constant during annealing.

The plasticization effects of the unreacted telechelics observed in this study are in agreement with experiments by Chaffin et al., who also discovered that uncompatibilized blends had a smaller initial droplet size than compatibilized blends due to a difference in the melt viscosity ratio.[144] When plasticization effects are minimized in our system at a loading level of 0.5 wt.%, the telechelics reduce the $K_{rel}*t_{stable}$ value by a factor of ~80 and the absolute K value by a factor of ~25 compared to the uncompatibilized blend. In a

Table 3.6. Percent of original relative specific surface area (Rel SA) remaining in 90% PS/10% PI blends with varying amounts of 37k anh-PS-anh/16k NH_2-PI-NH_2 telechelics after droplet stabilization time. A * indicates the blend was not stabilized, and the D_{vs} at 180 minutes was used in the calculation.

37k anh-PS-anh/16k NH_2-PI-NH_2 (Wt. %)	Rel SA (%)	Stabilization Time (Min)
0.5	97.4	15
1.3	83.0	15
2.5	72.1	15
5.0	79.0	60
Uncompatibilized	46.2	10
0.1	46.1	180*

study by Tao et al.,[145] the coarsening constant of a 90% PS/10% HDPE blend was calculated by using SEM to study the domain size of the minor phase after annealing the blend for various times. When the blend was compatibilized with 3.5 wt.% styrene – ethylene butylene – styrene (SEBS) triblock copolymer, the *K* value was reduced by a factor of only 1.7, and significant coarsening was still observed. When a 80% PS/20% HDPE blend was compatibilized with 10 wt.% SEBS triblock copolymer, the *K* value was reduced by a factor of 45. Fortelny et al.[146] calculated the coarsening constant from experimental data by Chen et al.[147] Blends were 71.25/23.75/5.00 wt.% PS/PET/ES, where PET is polyethylene terephthalate and ES is a styrene-ethylene terephthalate or styrene-butylene terephthalate block copolymer. The number of blocks and the copolymer molecular weight are not divulged. When different ES copolymers were used, the coarsening constant was reduced by a factor of ~180 – 830 compared to an uncompatibilized blend of 75/25 wt.% PS/PET which had an extremely large *K* value. Although we cannot make direct comparisons, our results show that multiblock copolymers formed *in situ* are very effective in suppressing droplet coalescence, as only small loading levels are required to achieve a significant reduction in *K*. This is likely explained by the fact that a multiblock copolymer has a larger surface area than a di- or triblock copolymer, requiring lower loading levels to achieve the same interfacial coverage.

3.5 Surface Coverage

Additional insight into the process of coalescence suppression can be gained by determining the percent of the interface covered with multiblock copolymers and this parameter's role in the compatibilization process. For a blend to be compatibilized,

complete saturation of the interface is not required; there only needs to be sufficient chains present at the interface to sterically hinder the droplets from recombining. Macosko et al. reported that an interfacial coverage of ~20% by a 85k PS/PMMA diblock copolymer was sufficient to stabilize a blend of 70% PS/30% PMMA.[49] Lyu et al. reported that 80% interfacial coverage by a 20k PS/20k PE diblock copolymer, 40% interfacial coverage by a 50k PS/50k PE diblock copolymer, and 20% interfacial coverage by a 100k PS/100k PE diblock copolymer was needed to stabilize a system of 87% PS/13% HDPE.[54]

Similar data for this system will further aid in using this process to compatibilize other systems. To determine the number of chains at the interface, it is assumed that all of the copolymer is located at the interface. With this assumption, the number of copolymer chains per nm^2 of interfacial area, Σ, can be calculated as:[49]

$$\Sigma = \frac{\text{chains/vol}}{\text{interfacial area/vol}} = \frac{N_A \rho_{cop} \varphi_{cop}}{M_{n,cop} S_{sp}} = \frac{N_A \rho_{cop} \varphi_{cop} D_{vs}}{M_{n,cop} 6 \varphi_{minor}} \quad (3.5)$$

where N_A is Avogadro's number, ρ_{cop} is the density of the copolymer, φ_{cop} is the volume fraction of the copolymer, $M_{n,\ cop}$ is the number average molecular weight of the copolymer, S_{sp} is the specific interfacial area, D_{vs} is the volume to surface area diameter, and φ_{minor} is the volume fraction of the minor phase. The density of the copolymer is calculated using the temperature-dependent density of PS:[148]

$$1/\rho_{PS} = 0.9199 + 5.098E\text{-}4*(T) + 2.354E\text{-}7(T)^2 + [(32.46 + 0.1017*(T))/M_{w,PS}] \quad (3.6)$$

and the temperature-dependent density of PI:[149]

$$1/\rho_{PI} = 1.0771 + 7.22E\text{-}4*(T) + 2.346E\text{-}7(T)^2 \quad (3.7)$$

where T is the temperature in °C and $M_{w,\ PS}$ is the weight average molecular weight of polystyrene. The copolymer molecular weight and the volume fraction of copolymer in the blend are estimated by GPC with fluorescence detection.

The copolymer volume fraction is calculated as:

$$\varphi_{cop} = \frac{\left(vol_{anh-PS\text{-anh}} + vol_{NH_2-PI\text{-}NH_2}\right)}{\text{total blend vol}} \tag{3.8}$$

where $vol_{anh\text{-}PS\text{-}anh}$ and $vol_{NH2\text{-}PI\text{-}NH2}$ are the volume of telechelics which have reacted to form the copolymer. The volume of the fluorescently labeled NH_2-PI-NH_2 in the copolymer is:

$$vol_{NH_2-PI\text{-}NH_2} = C * m_{NH_2-PI\text{-}NH_2} * \frac{1}{\rho_{PI}} \tag{3.9}$$

where C is the conversion of NH_2-PI-NH_2 into copolymer, $m_{NH2\text{-}PI\text{-}NH2}$ is the total mass of NH_2-PI-NH_2 in the blend, and ρ_{PI} is the density of PI at 180 °C. Determination of the conversion C by GPC with fluorescence detection is described in Chapter 5.8. As the system is designed to contain stoichiometric amounts of equally reactive end groups, the moles of anh-PS-anh in the copolymer are equal to the moles of NH_2-PI-NH_2 in the copolymer. The volume of anh-PS-anh in the copolymer is therefore:

$$vol_{anh-PS\text{-anh}} = C * m_{NH_2-PI\text{-}NH_2} * \frac{1}{M_{n\ NH_2-PI-NH_2}} * \frac{1.9\ \text{endgroups NH}_2}{\text{mol NH}_2 - PI - NH_2} * \frac{1.6\ \text{endgroups anh}}{1.9\ \text{endgroups NH}_2} * \frac{1\ \text{mol anh - PS - anh}}{1.6\ \text{endgroups Anh}} * M_{n\ \text{anh-PS-anh}} * \frac{1}{\rho_{anh-PS-anh}} \tag{3.10}$$

To determine the percent of the interface that is covered by *in situ* formed copolymer, the maximum amount of interface that can be covered with the copolymer must be determined. The maximum interfacial coverage, Σ^*, expressed as number of copolymer chains per nm^2 of interfacial area,[49] is given by:

$$\Sigma^* = \frac{\text{thickness of copolymer monolayer}}{\text{vol/chain}} = \frac{h}{M_{\text{n, cop}} / \rho_{\text{cop}} N_{\text{A}}} \tag{3.11}$$

where h is the height of the copolymer across the interface. With maximum coverage, the copolymer will be in a stretched state to allow more chains to pack at the interface. In previous studies, the thickness of a diblock or graft copolymer layer in the stretched state is estimated to be one half of the lamellar spacing of a symmetric diblock copolymer,[49,68,150,151] which is proportional to $M_n^{2/3}$. This calculation assumes the copolymer aligns perpendicular to the interface. However, Noolandi has shown that multiblock copolymers lie mostly flat in the interfacial plane, forming a pancake structure.[18] Monte Carlo simulations have also shown that block copolymers have a larger radius of gyration (R_g) along the interfacial axis than across it, forming flat cylinder-shaped structures.[26]

To the best of our knowledge, no experimental results of the maximum interfacial coverage using multiblock copolymers have been reported. To a first approximation, the copolymer can be treated as an isotropic chain,[26] similar to PS. The height of a PS chain, h, is $2*R_g$, where the radius of gyration of PS in the bulk, given in nm, is:[152]

$$R_{g,\,PS} = 0.029 M_w^{0.5} \tag{3.12}$$

This approximation places no restriction on the chain conformation. In order to account for the cylindrical shape of the copolymer at the interface, the extension of a chain across the interface is restricted such that ½ of each block expands into its respective bulk phase. One half of a PS block and one half of a PI block (1 diblock equivalent) are therefore used to estimate R_g using Equation 3.12, which is the corresponding height of the flat cylinder that the copolymer occupies at the interface. A pictorial depiction of this

structure is shown in Figure 3.10. This geometric restriction decreases Σ^* and conversely increases $1/\Sigma^*$, the surface area per chain. Since the chain is more compressed in a cylindrical shape along the interfacial plane, each copolymer chain occupies a larger interfacial area. Thus fewer multiblock copolymers are needed to saturate an interface relative to di- and triblock copolymers. The value Σ/Σ^* represents the percent of interface that is covered. As the samples are annealed, the PI droplets coalesce, decreasing the amount of surface area present. Thus there is less available interfacial area to cover as the droplets recombine, and correspondingly, Σ/Σ^* increases with annealing time. As will be discussed in Chapter 5, the accurate determination of the conversion of telechelics into copolymer and their corresponding molecular weight is problematic. Another attempt was made to calculate the conversion of tagged PI telechelics into copolymers by using n-hexane (Acros, HPLC) as a selective solvent to extract the copolymer, telechelic PI, and PI from the blend, in order to avoid the PS fluorescence problems. However, the results were not reproducible for different samples of the same blend. Regardless, the conversion required for stabilization can be determined, which provides insight into this process. The interfacial height, h, is calculated from $2*R_g$ of the equivalent diblock. The D_{vs} droplet size is determined by SEM analysis. From the calculated polymer densities given by Equation 3.5 and Equation 3.6, the volume fraction of each phase is calculated. The copolymer molecular weight in Equation 3.4 and Equation 3.10 for Σ and Σ^*, respectively, cancel each other out, and this value is therefore not required. Using Macosko's and Lyu's results as a guide, we can estimate that 20% interfacial coverage is required for stabilization, and we can therefore calculate the conversion necessary for this coverage by setting Σ/Σ^* equal

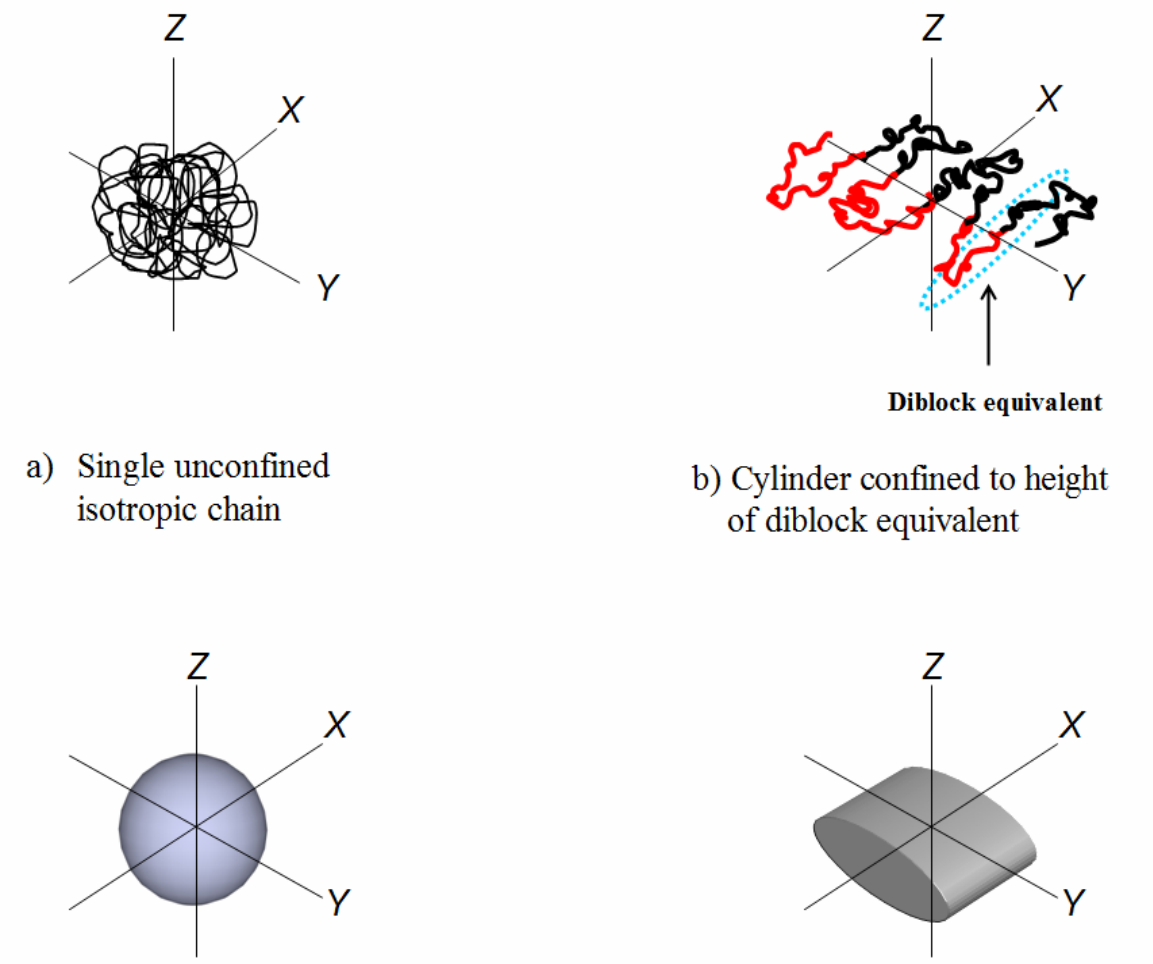

Figure 3.10. When a multiblock copolymer is treated as a single isotropic chain without geometric confinement, its shape is spherical, similar to that depicted in a). Restricting the width to twice the R_g of one diblock equivalent in the chain will result in a flattened cylindrical shape, as seen in scenario b).

to 0.20 and solving for *C*. The conversion required at 5.0 wt.% telechelic loading for 20% surface coverage of both the initial droplet size and stabilized droplet size are shown in Table 3.7. Table 3.7 shows that in order to stabilize the droplets at their initial size, a conversion of ~1.5% – 2.5% is required for the anh/NH_2 blends and ~3% is required for the epoxy/COOH reactive pairs. A larger conversion is required for the latter pair because the initial droplet size is smaller, yielding a larger interfacial area that must be covered. As the blends are annealed, the PI droplets coalesce, reducing their surface area. That is, less copolymer is needed to cover the interfacial area because the area itself has been reduced and Σ/Σ^* increases. The results show a conversion of ~1% – 1.5% is sufficient to stabilize the anh/NH_2 blends, and about 2% conversion is required for the stabilization of the epoxy/COOH blends. Since the latter pair is of lower reactivity than the former, these results indicate that all the stabilized blends have a conversion greater than 2%. Results in Chapter 5.8 suggest that ~5% – 10% conversion is achieved in anh/NH_2 pairs at 5.0 wt.% telechelic loading. Therefore this calculation seems reasonable.

The conversion required for 20% coverage at various loading levels of 37k anh-PS-anh/16k NH_2-PI-NH_2 is also calculated, and shown in Table 3.8. The results in Table 3.8 show that even for telechelic loading as low as 0.5 wt.%, only a moderate level of conversion is required for 20% surface coverage. It is evident that the 0.1 wt.% loading sample cannot stabilize the blend since the amount of telechelics required for stabilization is ~20% more than is present. The conversion required decreases as the blend is annealed and the droplets coalesce. The 0.1 wt.% sample was not stable even after 180 minutes of annealing, so this calculation shows that the conversion is less than the 54% required for

Table 3.7. Conversion at 5.0 wt.% telechelic loading required for a surface coverage of 20% of the initial droplet size and stabilized droplet size. A * indicates the blend was never stabilized, and D_{vs} at 180 minutes of annealing was used in the calculation.

90% PS / 10% PI 5.0 wt % Telechelics	D_{vs} 0 Min (μm)	20% Coverage (% C Needed)	Stabilization Time (Min)	D_{vs} Stable (μm)	20% Coverage (% C Needed)
16k anh-PS-anh / 16k NH_2-PI-NH_2	1.92	1.3	180*	2.88	0.9
37k anh-PS-anh / 16k NH_2-PI-NH_2	1.88	1.3	60	2.38	1.0
37k anh-PS-anh / 32k NH_2-PI-NH_2	1.54	2.3	60	2.06	1.7
83k anh-PS-anh / 32k NH_2-PI-NH_2	1.72	2.7	180*	2.59	1.8
18k epoxy-PS-epoxy / 20k COOH-PI-COOH	0.84	3.0	180*	2.61	1.0
44k epoxy-PS-epoxy / 20k COOH-PI-COOH	1.11	2.8	15	1.34	2.3
44k epoxy-PS-epoxy / 54k COOH-PI-COOH	1.25	3.0	30	1.71	2.4

stabilizing a droplet of that size. At 0.5 wt.% loading, the conversion required for 20% coverage of the stabilized blend remains nearly the same as the initial droplet size. This demonstrates how the droplets can be rapidly stabilized due to the high reactivity of the anh/NH_2 pair and the reduced plasticization effect of lower loading levels discussed earlier. This also implies that the 37k anh-PS-anh/16k NH_2-PI-NH_2 system can achieve over 15% conversion at this loading level in 10 minutes of melt blending at 180°C and 100 rpm. The results show that the initial 5.0 wt.% telechelic loading was excessive; only ~1% of the telechelics were required to react for 20% coverage while the vast majority remained unreacted in the homopolymer phase. The unreacted telechelics acted as plasticizers that decreased the viscosity of the blend, leading to a larger initial droplet size. Decreasing the telechelic loading decreased the initial droplet size as the plasticization effect was reduced. A concentration of 0.5 wt.% telechelics provides the optimal loading level for this system. At this amount, the plasticization effect is minimized while enough telechelics are present for sufficient conversion.

3.6 Conclusion

We have proven that difunctional reactive polymers with anh/NH_2 and epoxy/COOH complementary end groups form multiblock copolymers *in situ* at the

Table 3.8. Conversion at various 37k anh-PS-anh/16k NH_2-PI-NH_2 telechelic loading required for a surface coverage of 20% of the initial droplet size and stabilized droplet size. A * indicates the blend was never stabilized, and D_{vs} at 180 minutes of annealing was used in the calculation.

90% PS / 10% PI 37k anh-PS-anh / 16k NH_2-PI-NH_2	D_{vs} 0 Min (μm)	20% Coverage (% C Needed)	Stabilization Time (Min)	D_{vs} Stable (μm)	20% Coverage (% C Needed)
5.0%	1.88	1.3	60	2.38	0.9
2.5%	1.34	3.3	30	1.86	2.3
1.3%	1.12	7.4	15	1.35	6.1
0.5%	1.39	14.5	15	1.43	14.1
0.1%	0.93	117.5	180*	2.02	54.1

interface between immiscible PS and PI homopolymers via melt blending. By using SEM to measure the minor phase domain size upon sample annealing, we have shown that these copolymers compatibilize the blend by sterically hindering droplet coalescence. To quantify the copolymer's ability to inhibit coalescence, the coarsening constant K for a variety of blends composed of 5.0 wt.% telechelic pairs of various molecular weights was determined. The most accurate way to quantify the effectiveness of the telechelics is to analyze K_{rel}*t_{stable}. Both reactive pairs suppressed coalescence similarly at 5.0 wt.% loading, with the optimal molecular weight pairs being slightly above the critical molecular weight of the polymer, M_c. When the telechelic molecular weight is slightly above M_c, the analogous copolymer blocks can become well entangled with the homopolymer, and sterically hinder coalescence. Concomitantly, this chain length is low enough to exhibit favorable characteristics of low molecular weight telechelics, namely a high end group concentration and the ability to quickly approach the interface.

The larger initial droplet size observed in the compatibilized blends is due to the plasticization effect of the unreacted telechelics. The blend viscosity is reduced by adding these low molecular weight telechelics, making coalescence easier. Variable telechelic loading experiments on the 37k anh-PS-anh/16k NH_2-PI-NH_2 pair showed that

0.5 wt.% telechelics yielded the lowest $K_{rel}*t_{stable}$ value. At this loading level, there is a sufficient quantity of telechelics to react and form multiblock copolymers, but the concentration is low enough to minimize plasticization effects.

The absolute and relative specific interfacial area of blends provided complementary data to the coarsening constant calculations. These results show that the four most effective telechelic pairs lose ~15% – 25% of their interfacial area at 5.0 wt.% loading before stabilization. The telechelic loading studies on the 37k anh-PS-anh/16k NH_2-PI-NH_2 system show that 0.5 wt.% loading results in a relative specific interfacial area loss of only 3%. Further analysis indicates that only ~1.5% – 3.0% conversion was required to attain 20% interfacial coverage of multiblock copolymers at 5.0 wt.% telechelic loading, indicating a large excess of telechelics were used. In the reduced loading experiments, a conversion of ~15% was required for the optimal 0.5 wt.% loading. Telechelic conversion determination by GPC with fluorescence detection proved to be difficult for the systems studied here. It would be interesting to conduct further studies on the epoxy/COOH system at variable loading concentrations to determine the optimal loading conditions for these reactive pairs.

Chapter 4

Quantifying the Grafting of Polymer Loops to the Surface of Multiwall Carbon Nanotubes

4.1 Introduction

Carbon nanotubes have been used extensively to improve the physical properties of materials.[91,92] The fact that nanotubes have an extremely large tensile strength (~0.5 TPa – 4 TPa)[153] and yet are highly flexible[154] and lightweight makes their use for these applications very practical. In order for the nanotubes to be effective, they must be homogeneously dispersed throughout the material[93] and also be able to interact well with the matrix in order to efficiently transfer stress. However, nanotubes tend to form bundles in polymer matrices, and are not easy to separate into individual tubes.[94] One way to alleviate this problem is to graft polymer chains onto the nanotube. This serves two purposes. First, improved nanotube-matrix interaction is achieved due to the grafted chains becoming well entangled with the matrix. Polymer nanocomposites made with small amounts of grafted nanotubes have been shown to greatly improve the mechanical properties of the blend, and are more effective than ungrafted pristine nanotubes in this regard.[155-160] This is due to an efficient load transfer between the polymer chains and the nanotubes.[161] Secondly, the grafted chains help suppress the aggregation of the nanotubes by steric hindrance.[95,96] There is a very short but steep attractive potential between nanotubes. However, the addition of even short polymer chains can produce a long enough repulsive potential to hinder nanotube aggregation.[162] The fact that optically transparent polymeric nanocomposites can be made when grafted nanotubes are incorporated into the polymer matrix demonstrates good nanotube dispersion.[163,164] The

grafting of polymer chains to nanotubes can be achieved by functionalizing the nanotube in order to introduce reactive groups onto the surface, followed by reaction with a polymer chain possessing complementary reactive end groups. Using a difunctional reactive polymer allows for the possibility of the chain to be grafted at both ends to the same nanotube, forming a "loop". However, not all chains will react at both ends, and polymers that are grafted at only one end will instead form a "tail". It is also possible for a difunctional polymer to have both ends grafted to different nanotubes, forming a "bridge".

In our group, we have conducted a series of studies that examine the formation of polymer loops formed on hard surfaces[138,165] and at soft interfaces.[78,166-168] Our group has also conducted experimental studies which show that loops are more effective at strengthening soft interfaces than tails. In one such study, premade block copolymers with a similar molecular weight but different number of blocks were used to compatibilize polystyrene (PS) and poly(methyl methacrylate) PMMA.[84] In this study, it was found that the interfacial strength increased as the interfacial modifier was changed from pentablock > triblock > diblock > heptablock. These results show that increasing the number of blocks in the copolymer increases the number of interfacial crossings which form loops, strengthening the interface, except for the heptablock copolymer which provided the least increase in interfacial strength despite having the most interfacial crossings. This was attributed to the fact that the block size of this copolymer was below its entanglement weight. Therefore, the copolymer blocks in the heptablock were not sufficiently long to effectively entangle with the homopolymers, decreasing its ability to strengthen the interface.

One method to form polymeric loops at a surface is to covalently bond the two ends of a telechelic polymer to a functionalized surface. However, in this process, not all telechelic chains will form loops, as some chains will only react at one end and form tails. This was studied by Huang et al.,[138] where telechelic COOH-PS-COOH was spin coated onto the surface of an epoxy functionalized silicon wafer and annealed above the glass transition temperature to result in a condensation reaction between complementary functional groups, and the subsequent grafting of the PS to the surface. A fluorescent tag was used to monitor the evolution of dangling chain ends into loops as a function of annealing time. It was found that the fluorescence intensity in the early stages of the reaction increased due to polymer chains grafting to the functionalized surface at one end. At further times, the fluorescence intensity was constant, indicating a balance between new chains being grafted to form tails, and singly bound tails continuing to attach to the surface to form loops. At later reaction times, the fluorescence intensity decreased, as the buildup of grafted polymers prevented any new telechelics from grafting to the surface, while existing tails continued to form loops.

In this grafting reaction, it is also important to understand the limiting process in the reactions. The reaction will be limited by either the reaction of the functional groups to the surface or by the diffusion of the polymer to the interface. Fredrickson and Milner conducted a theoretical study of the time-dependent *in situ* formation of diblock copolymers at the interface of immiscible homopolymer phases.[169] In this study, there was an extremely low concentration of reactive polymers dispersed in each homopolymer phase, such that $\rho_0 R_g^3 << 1$, where ρ_0 is the number density of reactive chains in the bulk homopolymer and R_g is the radius of gyration of the reactive polymer. The reaction

between complimentary groups was assumed to be instantaneous and irreversible, making the process of diblock copolymer formation diffusion controlled. They found that the number of copolymer chains per interfacial area that were formed depended on the reaction time regime, and followed a power law equation. Initially, copolymer concentration increases as a function of reaction time, *t*. There is no depletion of reactive polymers or buildup of copolymers at the interface to limit the reaction rate. In the intermediate time regime, the interface is not yet saturated with copolymer chains, but the concentration of reactive polymers near the interface becomes depleted. This time regime is dominated by polymer diffusion to the interfacial area, and the copolymer concentration grows as a function of $t^{0.5}$. At the late time regime, sufficient copolymer buildup at the interface creates a barrier for approaching reactive polymers. Further increase in copolymer concentration is very slow in this time regime, as the concentration grows as a function of $(\ln t)^{0.5}$. To expand this understanding, Müller conducted a Monte Carlo simulation that modeled the reactions of polymers at interfaces in a system similar to Fredrickson and Milner.[170] Müller's results for the diffusion controlled intermediate time regime were in agreement with Fredrickson and Milner.

Kramer conducted a theoretical study of the grafting kinetics of end-functionalized polymers at melt interfaces.[171] He considered both a diffusion controlled case where end-functionalized polymers had to diffuse through the previously grafted chains, and a reaction controlled case where the amount of grafted polymer was determined by the kinetics of the interfacial reaction itself. In this model, the rate of chain grafting for both the diffusion controlled and reaction controlled cases could be calculated by the same general mathematical expression, which is inversely proportional

to the characteristic time τ. For the diffusion controlled reaction $\tau_D = aR_g/D$, where a is the monomer length, R_g is the radius of gyration, and D is the self diffusion coefficient. In a reaction controlled process, second order kinetics are assumed, and $\tau_R = R_g/ak_f[B]$. Here, a is the distance from the interface, k_f is the rate constant, and $[B]$ is the concentration of reactive species in excess. It is therefore demonstrated that the grafting rates for diffusion controlled and reaction controlled processes have different time dependences. Oyama et al. also showed that the reaction of functionalized polymers at soft interfaces could be described by a reaction-controlled model.[73] Experimentally, Rice et al. showed that grafting polymer loops to soft surfaces is reaction controlled.[78] When telechelics of similar molecular weight but different end groups were used, the rate of loop formation was greatly altered, exhibiting strong evidence of reaction controlled kinetics. Similarly, our group has compared experimental results of grafting epoxy-PS-epoxy polymers to a hard surface with both of Kramer's models,[165] which shows that the kinetics of chain grafting are clearly reaction controlled. Even at the shortest reaction times observed, between 2 – 10 minutes, the time dependence on the grafting is much less than $t^{0.5}$.

Bond-fluctuation Monte Carlo simulations by Smith et al. were used to study the irreversible adsorption of telechelic polymers onto solid substrates.[81] An important discovery of this study was the observation of primarily singly bound telechelics at short reaction times, followed by loop formation at longer reaction times. The fraction of loops formed at long times is ~95% for low grafting density, ~90% for intermediate grafting density, and ~80% for high grafting density. The study also showed that the concentration of grafted chains grows very slowly at long reaction times, as the grafting

is controlled by the ability of the free telechelic to penetrate into the previously grafted chains. It was observed that the chain height does not change much with increasing surface coverage, meaning the chains are not in a highly stretched configuration. The reduction in reaction rate at high grafting density was therefore attributed to steric hindrance due to the grafted chains, and not thermodynamic barriers associated with highly stretched chains. It was noted by Smith et al. that thermodynamic barriers would become dominant at very high grafting densities which are not achievable in simulations or experiments. Our experimental fluorescence results agreed well with this model. Similarly, Monte Carlo studies by Yang and Char[172] also used bond-fluctuation Monte Carlo simulations to study the fraction of loops formed as a function of polymer grafting density at an immiscible polymer interface. The results of this study showed that ~90% of the difunctional polymers form loops at low grafting density, and ~85% form loops at intermediate grafting density. At high grafting density, the loop content decreases more rapidly to ~70%, as crowding hinders chain ends from grafting at both ends.

In this study, the formation of grafted loops on carbon nanotubes is monitored to provide insight into the ability of this process to form a modified nanoparticle that can most effectively strengthen the nanoparticle-polymer interface. FT-IR is used to monitor the grafting of telechelic epoxy-PS-epoxy to COOH functionalized nanotubes. The reaction between a carboxylic acid and epoxide forms an ester.[74,114] FT-IR is used to monitor the aromatic ester peak as a function of reaction time, which verifies the telechelic is grafted and not simply adsorbed to the nanotube surface. In addition, FT-IR is used to quantify the amount of telechelic grafted to the nanotube by monitoring the aromatic ring vibrational mode of the telechelic polymer. By annealing the samples, it is

shown that grafted tails continue reacting to form loops. In addition, the absolute and relative amount of tails is determined with FT-IR by amplifying the signal of unbound grafted chain ends ("tails") by further reacting the grafted nanotube sample with monocarboxy terminated poly(4-methylstyrene) (COOH-P4MS), where only unbound telechelic ends can react with the monofunctional polymer. The time-dependent grafting rates are determined from these experiments. Thermogravimetric analysis (TGA) is used in conjunction with FT-IR to quantify the amount of telechelic polymer grafted to the nanotubes.

4.2 Experimental

A. COOH Functionalized Nanotubes

Carbon nanotubes with > 50% single wall content and < 35% multiwall content were purchased from Cheap Tubes, Inc., and are referred to as MWNT in this study. To oxidize the nanotubes and thereby introduce COOH groups to the nanotube surface, 1500 mg of MWNT were added to a two neck round bottom flask containing 500 ml of 6 M HNO_3 (Fisher, Certified ACS Plus). The nanotubes were stirred and refluxed under dry nitrogen at 120 °C for 16 hours. The nitric acid not only introduces oxygen-bearing functional groups, but also removes metal catalysts and amorphous carbon from the nanotubes.[118,119] After cooling, the solution was diluted with 500 ml of deionized water. The nanotubes were then centrifuged (Eppendorf 5702 Centrifuge) for 8 minutes at 4400 RPM. The collected nanotubes were then placed in approximately 200 ml of a 0.5 M NaOH solution and stirred for 30 minutes at room temperature. The NaOH is used to remove carboxylated amorphous carbon impurities in the nanotubes, which are soluble in aqueous metal hydroxide solutions.[119-121] After centrifugation, the nanotubes were rinsed

with approximately 300 ml of nanopure water and centrifuged again. The nanotubes were then placed in a two neck round bottom flask containing 400 ml of piranha solution, which is composed of 3 parts H_2SO_4 (Fisher, Certified ACS Plus) to 1 part H_2O_2 (Fisher, 30 vol. %, sodium stannate stabilized). The nanotubes were then stirred and refluxed under dry nitrogen at 70 °C for 30 minutes. This step is used to introduce defect sites on the nanotubes and to further cut the tubes.[118] After cooling the piranha solution, 500 ml of deionized water was used to dilute the solution. The functionalized nanotubes were centrifuged for 3 minutes at 4400 RPM. After collection, the nanotubes were again placed in approximately 200 ml of 0.5 M NaOH and stirred for 30 minutes at room temperature in order to remove any additional amorphous carbon impurities. The functionalized nanotubes were then rinsed with nanopure water and centrifuged repeatedly until the pH of the solution was neutral. The nanotubes were then dried in a vacuum oven at 80 °C overnight. The functionalized multiwall nanotubes are referred to COOH-MWNT in this study.

B. Grafting Telechelics to Functionalized Nanotubes

To study the grafting of loops on a nanotube surface, telechelic epoxy-PS-epoxy anionically synthesized at the University of Tennessee by Haining Ji (M_n = 17,800, PDI = 1.05, functionality = 1.9) was reacted with the COOH-MWNT in solution. Approximately 500 mg of COOH-MWNT were added to a two neck round bottom flask containing ~250 ml of 1-methyl-2-pyrrolidinone (NMP) (Sigma, Chromasolve Plus HPLC). The solution was sonicated for 15 minutes to disperse the nanotubes. Then ~500 mg of epoxy-PS-epoxy which was dissolved in ~50 ml of NMP was added to the round bottom flask. The solution was stirred and refluxed under dry nitrogen at 150 °C.

50 ml aliquots were removed from the reaction flask at time intervals of 1, 2, 3, and 6 days. After the solution was cooled, the nanotubes were collected by centrifugation at 4400 RPM for 3 minutes. The NMP supernatant was then decanted from the centrifuge tube and collected. To ensure any remaining unreacted epoxy-PS-epoxy was removed, 50 ml of N,N-dimethylformamide (DMF) (Acros, HPLC) was added to the centrifuge tube. The tube was shaken to redisperse the nanotubes, and after subsequent centrifugation, the DMF supernatant was decanted and collected. To test for the presence of unreacted epoxy-PS-epoxy, both the NMP and DMF supernatant were precipitated in cold methanol (-20 °C). After centrifugation, a white precipitate formed in the NMP supernatant indicating the presence of epoxy-PS-epoxy, but no precipitate was visible in the DMF supernatant. It was therefore assumed that 50 ml of DMF was adequate for rinsing the nanotubes to remove excess telechelic PS. The reacted nanotubes were then dried in a vacuum oven at 80 °C overnight to remove the residual solvent. A temperature below the T_g of polystyrene was used to ensure no further grafting reaction occurred during this step of the experiment.

To examine the ability to increase loop formation with heating, the grafted nanotubes were annealed in a vacuum oven at 150 °C for 1 – 6 days. This allows grafted polymer chain end diffusion, allowing any untethered telechelic chain ends to form loops upon reaction with COOH groups on the nanotube surface. In order to quantify the amount of telechelics that formed tails, a new reaction of ~100 mg of COOH-MWNT and epoxy-PS-epoxy was conducted for 1 day in NMP at 150 °C. After removal of the unreacted epoxy-PS-epoxy, the grafted nanotubes were redispersed in ~50 ml of NMP by sonication for 15 minutes, and ~100 mg of monocarboxy terminated poly(4-

methylstyrene) (COOH-P4MS) (Scientific Polymer Products, Inc.) (M_n = 19,400, PDI = 1.09) was dissolved in ~100 ml NMP. The polymer solution was added to the dispersed nanotubes, and the polymer grafting reaction in NMP proceeded at 150 °C under dry nitrogen as previously described for the epoxy-PS-epoxy reaction. At time intervals of 1, 2, 3, and 6 days, 50 ml aliquots were removed from the reaction flask for analysis. The unreacted COOH-P4MS was removed in the same manner as the unreacted epoxy-PS-epoxy. To determine if there was any reaction between the COOH-P4MS and the various functional groups introduced onto the nanotubes, COOH-MWNT and COOH-P4MS were reacted for 1 day at 150 °C. The sample preparation was the same as the previously described samples.

C. Analysis of Grafted Nanotubes

The vibrational mode peak position and intensity for the oxidized nanotubes and the CNT with grafted polystyrene were measured with a Varian 4100 Fourier Transform Infrared Spectrometer (FT-IR). Pellets were made for analysis using FT-IR grade KBr (Sigma, 99+%). The total sample size was 100 mg. The carbon nanotube content was ~0.75 wt.%. For each sample, 8192 scans were collected at a resolution of 4 cm^{-1}. A KBr background sample was analyzed in order to automatically subtract out the matrix contribution of the absorption. All samples were dried in a vacuum oven at 80 °C for at least one hour prior to analysis in order to remove atmospheric water.

The weight change of the functionalized nanotubes, telechelic PS, and grafted nanotube samples as a function of temperature was measured with a TA Instruments Q50 Thermogravimetric Analyzer (TGA) to determine the amount of grafted PS. All samples

were heated in a nitrogen atmosphere at 10 °C/min from room temperature to 550 °C, and then 20 °C/min from 550 °C to 900 °C.

4.3 Quantification of Telechelic Polymer Grafted to Nanotubes

FT-IR absorbance spectra of the as received MWNT and COOH-MWNT were first compared in order to verify oxidation of the nanotubes. Figure 4.1 shows a comparison of the two samples. The as received nanotubes exhibited very weak peak absorbances. After the nanotubes are oxidized, new peaks centered at 1175 cm^{-1}, 1356 cm^{-1}, 1580 cm^{-1}, and 1709 cm^{-1} are observed. The broad peak centered at 1175 cm^{-1} is associated with the C–O stretch of COOH groups, and may also be due to C–OH stretching.[173,174] It is not known what vibrational mode the peak at 1356 cm^{-1} is associated is associated with.[175] The strong peak observed at 1580 cm^{-1} is due to the aromatic C=C asymmetric stretch near oxygenated groups.[174,175] This peak remains present even when the oxygenated functional groups are removed by heating to very high temperatures.[175] The peak centered at 1709 cm^{-1} is associated with the C=O stretch of aromatic COOH groups.[174,176,177] The results in Figure 4.1 therefore provide evidence of successful nanotube carboxylation.

To accurately monitor the grafting of PS onto the oxidized nanotube, the overlap between the vibrational modes associated with epoxy-PS-epoxy and those associated with COOH-MWNT was examined so that a calibration curve for the quantification of grafted telechelic PS could be created using a vibrational band exclusive to epoxy-PS-epoxy. We had anticipated using the aromatic C-H stretching bands, ν(C-H), of the aromatic PS ring, which are typically observed in the 3050 cm^{-1} – 3000 cm^{-1} region.[178] However, instrumental artifacts prevented these bands from being used for quantification of grafted

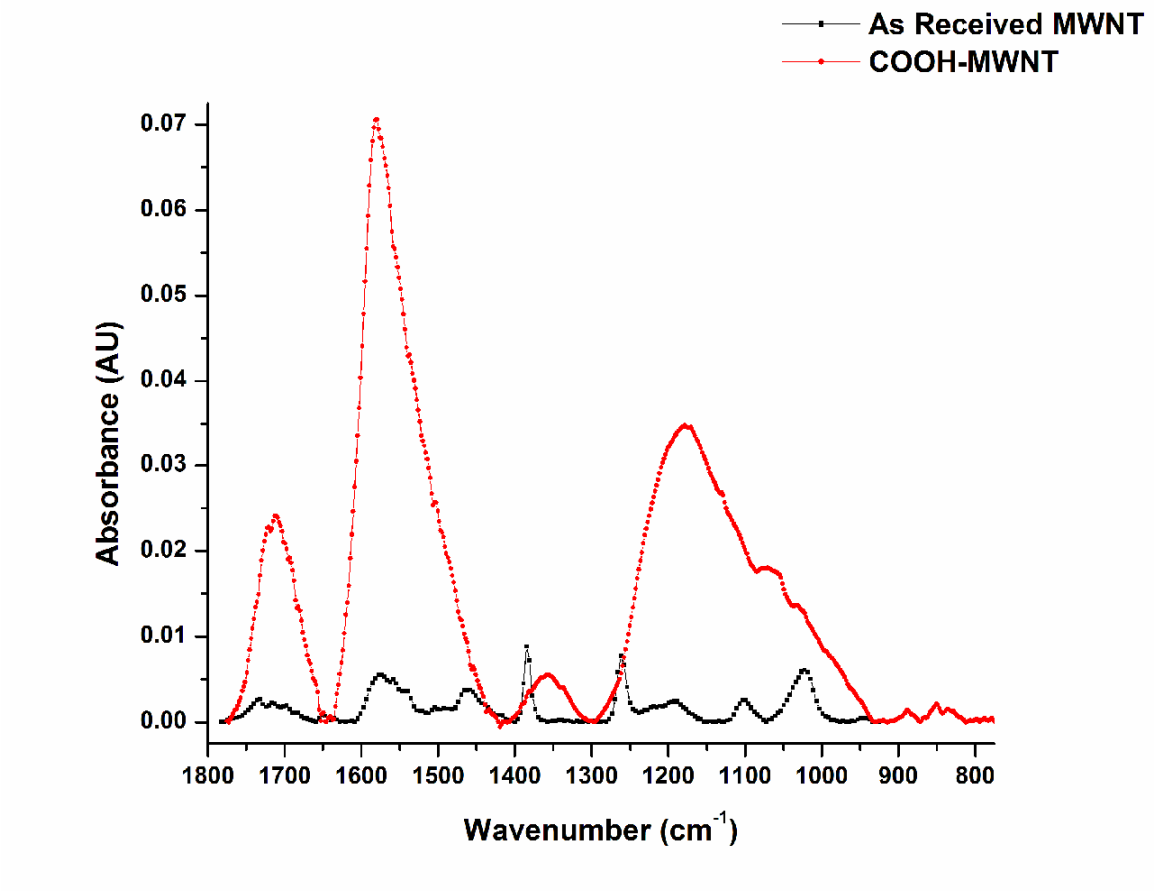

Figure 4.1. FT-IR spectra of MWNT as-is and after functionalization.

PS because when pure KBr was analyzed, random absorption peaks were observed in this region. Therefore other vibrational bands had to be considered. A comparison of COOH-MWNT and epoxy-PS-epoxy peaks in the 1800 cm^{-1} – 600 cm^{-1} range is shown below in Figure 4.2. Many bands in Figure 4.2 overlap, but this comparison shows that the most promising candidates are peaks at 839 cm^{-1}, 822 cm^{-1}, and possibly 1443 cm^{-1}. A comparison between epoxy-PS-epoxy and unfunctionalized PS which was anionically synthesized at the University of Tennessee by Haining Ji (M_n = 105,000, PDI = 1.08) was made to determine which vibrational modes were present in both species and which modes were only associated with the functionalized telechelic PS. Figure 4.3 shows the FT-IR spectra of the two PS polymers. Examination of Figure 4.3 shows there are some differences between the unfunctionalized PS and the epoxy-PS-epoxy. To confidently use epoxy-PS-epoxy for quantification of grafted chains, we need to use peaks that are associated with the aromatic ring, and not the epoxide groups that react. In addition, we need to find vibrational bands that do not overlap with COOH-MWNT signals. For instance, the peaks at 1492 cm^{-1} and 1443 cm^{-1} are found in both polystyrene samples. These bands are associated with the aromatic ring distortion.[176] However, the epoxy-PS-epoxy contains an additional band at 1420 cm^{-1}. The band observed at 839 cm^{-1} in both samples is associated with the C-H bend of aromatic rings.[179] An additional band at 820 cm^{-1} is observed in the epoxy-PS-epoxy sample, which should also correspond to the C-H bend of aromatic rings as well. The C-H bending modes of the oxirane ring are expected to be found at 920 cm^{-1} and 864 cm^{-1}.[180] In the telechelic PS, peaks at 914 cm^{-1} and 868 cm^{-1} are observed. The whole ring stretch of the oxirane is expected to be found near 1250 cm^{-1}, [181-183] and a very weak peak in the telechelic PS is observed at 1261 cm^{-1}. In

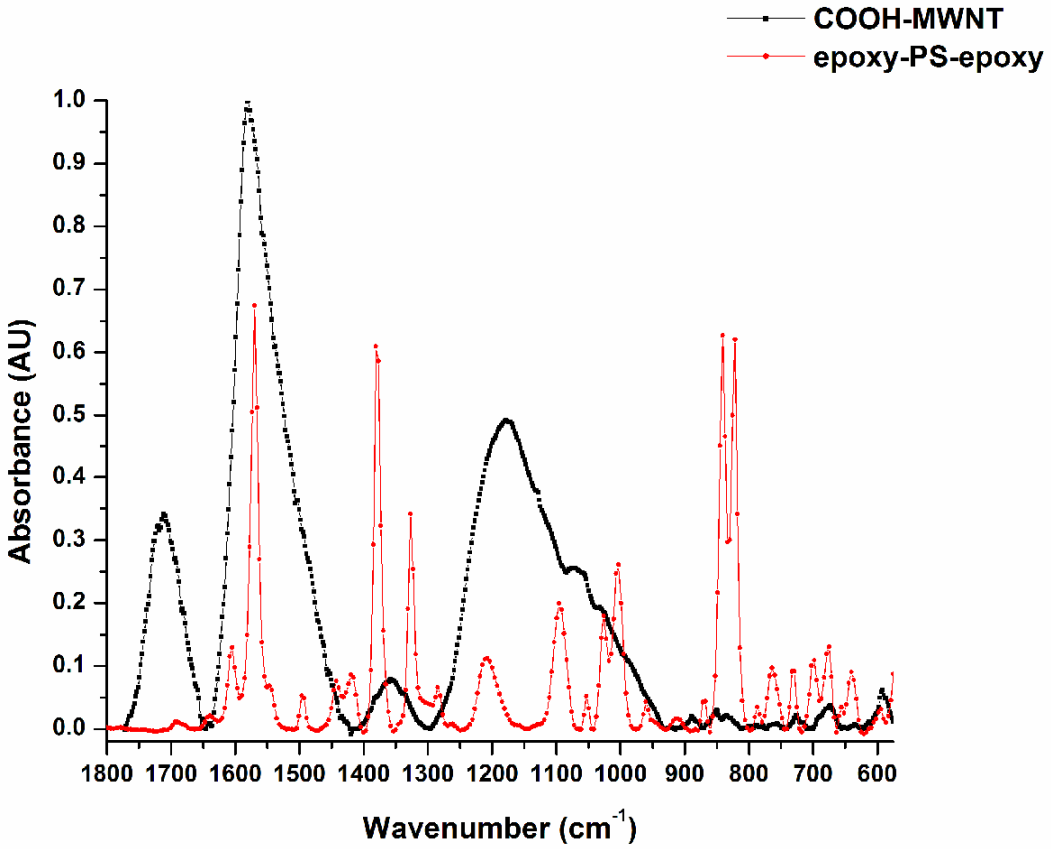

Figure 4.2. FT-IR spectra of COOH-MWNT and epoxy-PS-epoxy.

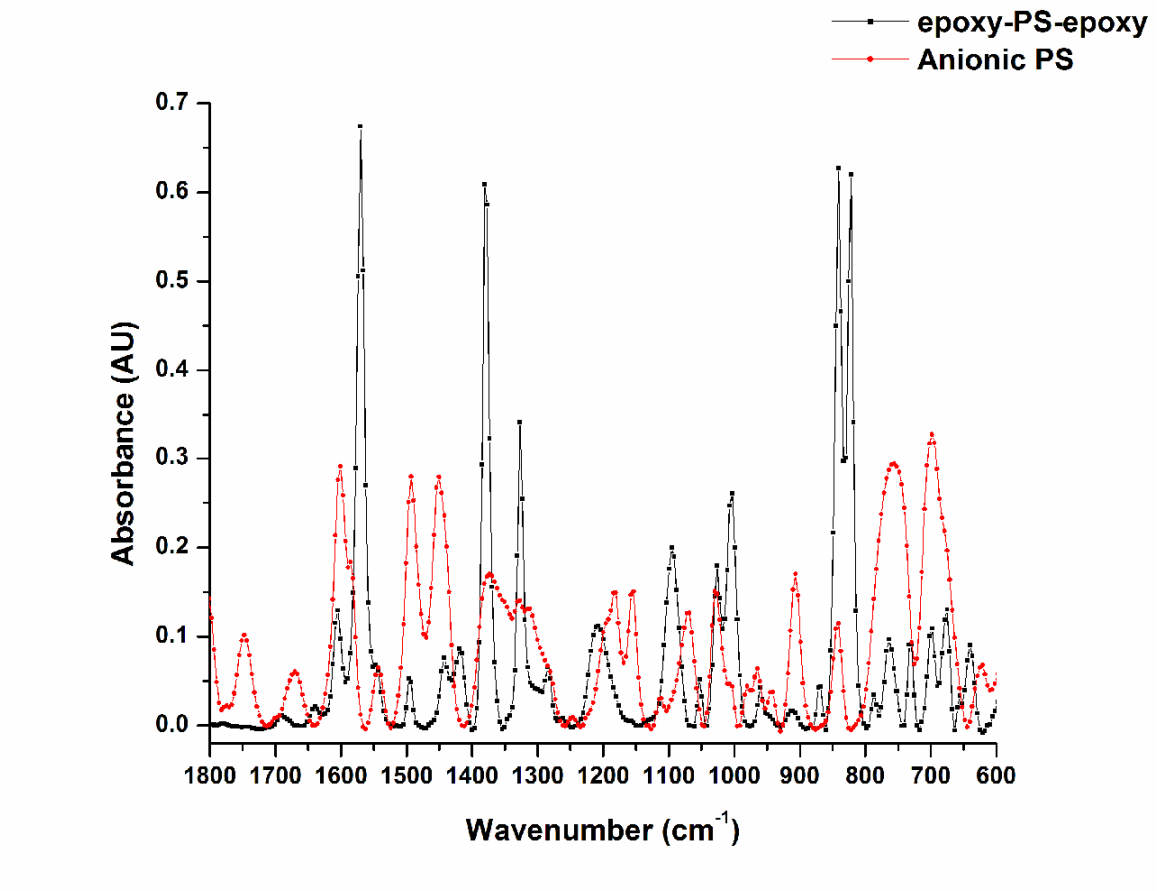

Figure 4.3. FT-IR spectra of 18k epoxy-PS-epoxy and 105k PS synthesized by anionic polymerization.

the synthesis of epoxy-PS, Quirk et al. reported using FT-IR vibrational bands at 1269 cm^{-1} to monitor the epoxide ring and 828 cm^{-1} to characterize the PS aromatic ring.[111]

Upon reaction of an epoxide and –COOH at elevated temperatures, the main product is an ester containing a secondary alcohol. This is demonstrated in Figure 4.4. When an aromatic ester is formed, the asymmetric C-O-C stretching band, ν_{as}(C-O-C), is expected to be located at 1300 cm^{-1} – 1250 cm^{-1}, while the symmetric C-O-C stretching band, ν_s(C-O-C), band is expected to be in the 1200 cm^{-1} – 1050 cm^{-1} range.[178] The ν(C-O) of a secondary alcohol appears near 1085 cm^{-1}, and the ν(C=O) a carbonyl adjacent to an aryl group is expected to be found between 1725 cm^{-1} – 1715 cm^{-1}.[177,178] Since the functionalization of the nanotubes produces not only COOH groups, but likely OH groups as well, it is also possible for an epoxide to react with an alcohol.[114,184] In this case, an aryl alkyl ether will form. The symmetric and asymmetric C-O-C stretching vibrational modes of this ether are found in the same region as the aromatic ester.[177] However, we expect the reaction to form mostly esters even if hydroxyl groups are present on the nanotube surface, since the etherification reaction is about 10 – 20 times slower than esterification.[185,186]

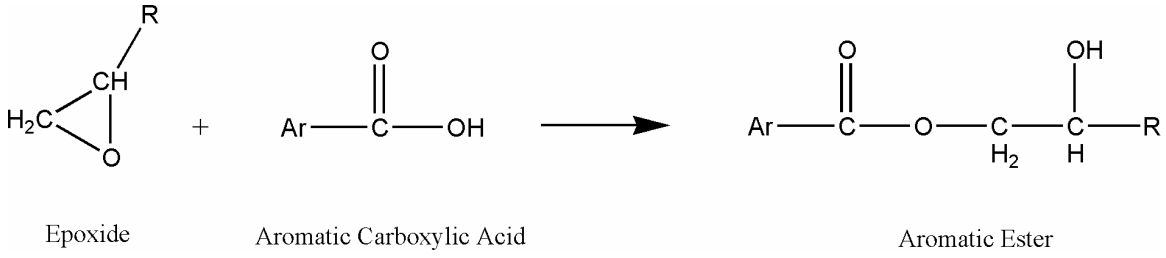

Figure 4.4. Reaction between an epoxide and aromatic carboxylic acid yields an aromatic ester with a secondary alcohol group.

To follow the progress of the grafting, the time evolution of the attachment of the telechelic to the COOH-MWNT in NMP was first monitored. Figure 4.5 shows the FT-IR spectra of COOH-MWNT that has reacted with epoxy-PS-epoxy in NMP for 1, 2, 3, and 6 days. The samples were normalized to the nanotube C=C stretching peak at 1580 cm^{-1}. It should be emphasized that the signal intensity of the neat epoxy-PS-epoxy has been magnified for clarity in Figure 4.5. The epoxy-PS-epoxy has a peak centered at 1570 cm^{-1}, which contributes a small absorbance at 1580 cm^{-1}. This will introduce a small error when normalizing to the 1580 cm^{-1} peak, but remains the best choice available for normalization. Figure 4.5 gives a strong indication that aromatic esters are being formed. Prior to the grafting reaction, the COOH-MWNT has a ν(C=O) peak centered at 1709 cm^{-1}, which is the expected value for aromatic COOH groups. Upon reaction, the ν(C=O) peak is broadened. It appears that a new species is formed that results in a new peak centered near 1720 cm^{-1},which is the expected peak position of ν(C=O) in aromatic esters. The peak intensity at 1680 cm^{-1} also increases with reaction time, but not in a linear fashion. This is most likely not due to the formation of a new species, as this peak is associated with –COOH dimers.[177] The presence of epoxy-PS-epoxy is also confirmed in Figure 4.5 by the increase in absorbance intensity of the aromatic ring distortion band at 1443 cm^{-1} as a function of reaction time.

Inspection of the IR spectrum in the 1280 cm^{-1} – 940 cm^{-1} range further corroborates the grafting of the telechelic PS to the MWNT. This region of the normalized spectrum for samples reacted in NMP for 1 – 6 days is shown in Figure 4.6. The strongest sign of aromatic ester formation is the increase in peak intensity at 1258 cm^{-1} the ν_{as}(C-O-C) vibrational mode, which squarely falls in the range of aromatic

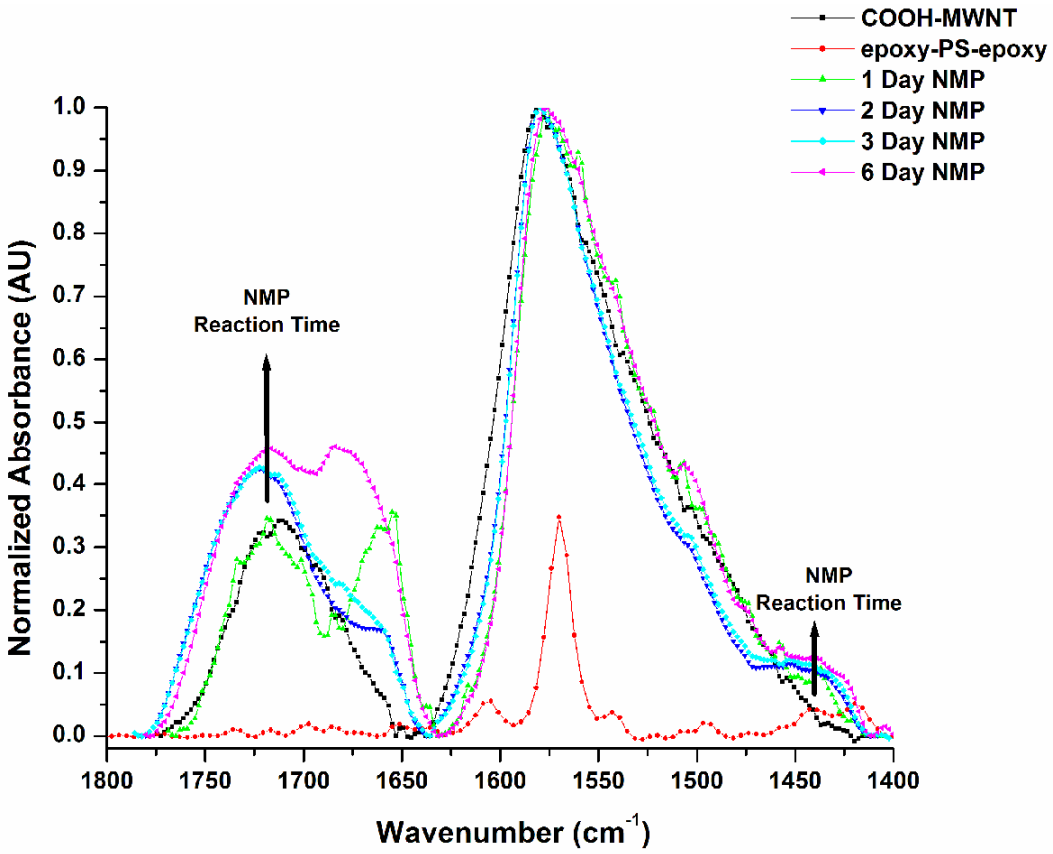

Figure 4.5. Normalized FT-IR spectra of grafted nanotube samples reacted in NMP for 1 – 6 days in the 1800 cm^{-1} – 1400 cm^{-1} range. The epoxy-PS-epoxy signal has been magnified for clarity.

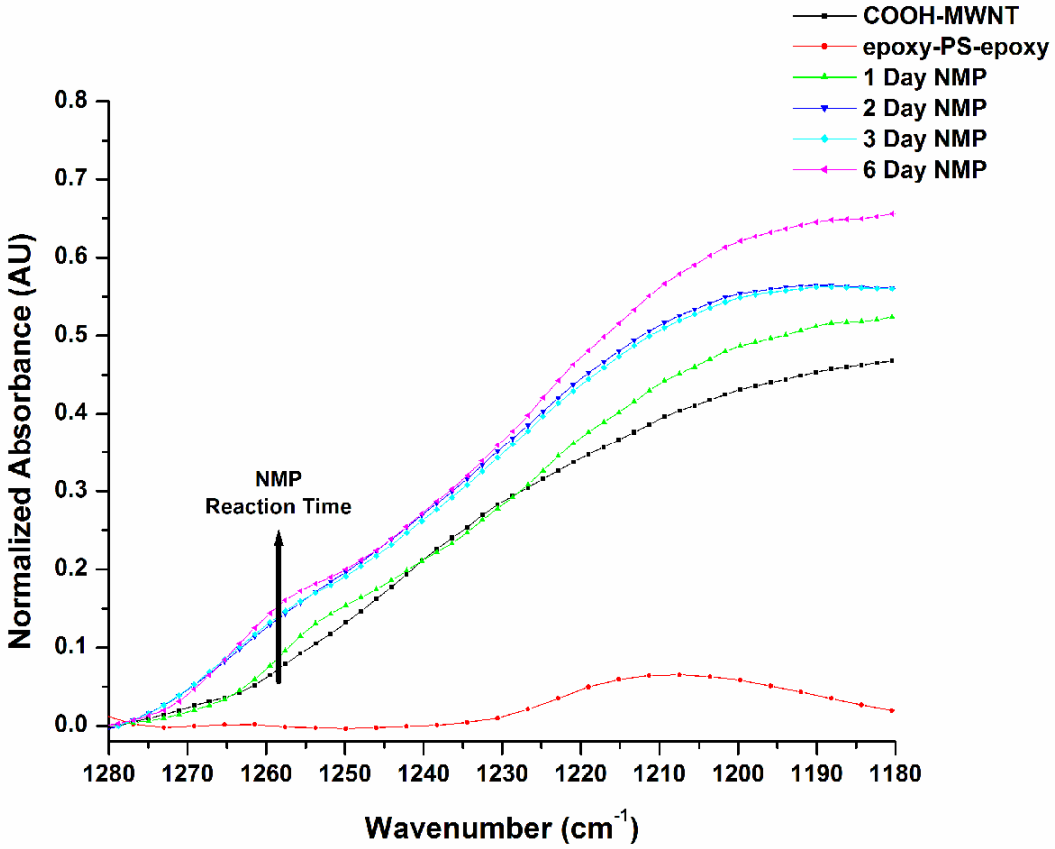

Figure 4.6. Normalized FT-IR spectra of grafted nanotube samples reacted in NMP for 1 – 6 days in the 1280 cm^{-1} – 940 cm^{-1} range.

esters peaks, 1275 cm^{-1} – 1250 cm^{-1}. After reacting for one day, the peak intensity slightly increases and the band slightly broadens. Reaction for two days broadens and intensifies the peak further, and the peak continues to grow for the entire reaction time. With the goal of quantifying the amount of epoxy-PS-epoxy grafted to the nanotubes, the aromatic ring distortion band at 1443 cm^{-1} and the out-of-plane C-H bending signal of the aromatic ring at 839 cm^{-1} and 822 cm^{-1} were also analyzed. Only the band at 822 cm^{-1} proved to be viable for quantification, due to significant band overlap with the other bands. The growth of the 822 cm^{-1} band as a function of reaction time in NMP is shown in Figure 4.7. In Figure 4.7, the peak for the neat epoxy-PS-epoxy peak is centered at 822 cm^{-1}, while the peak shifts to 820 cm^{-1} in the grafted nanotube samples. The peak grows rapidly during the first day of reaction, and then approaches a maximum value after 2 days of reaction. Therefore, the peak at 822 cm^{-1} is interpreted to be associated with the aromatic ring of the PS chain and not the epoxy groups, as the signal intensity increases and reaches a limiting value as the reaction time is increased.

To quantify the amount of epoxy-PS-epoxy that is grafted to the nanotubes, a calibration curve was first made by mixing together known amounts of unreacted epoxy-PS-epoxy and COOH-MWNT and their IR spectra collected. It should be emphasized that in these spectra, the intensity of the 820 cm^{-1} aromatic ring C-H bending absorbance was normalized by dividing its absorbance by that of the nanotube ν_{as}(C=C) at 1580 cm^{-1}. This accounts for any variability due to different sample thicknesses.

Calibration curves correlating this signal intensity *y* to telechelic PS concentration *x*, as shown in Figure 4.8, can then be used to quantify the amount of epoxy-PS-epoxy grafted to the COOH-MWNT. The linear fit of the data in Figure 4.8 yields the equation

$$y = 4.89E\text{-}3*x + 1.60E\text{-}3 \quad (4.1)$$

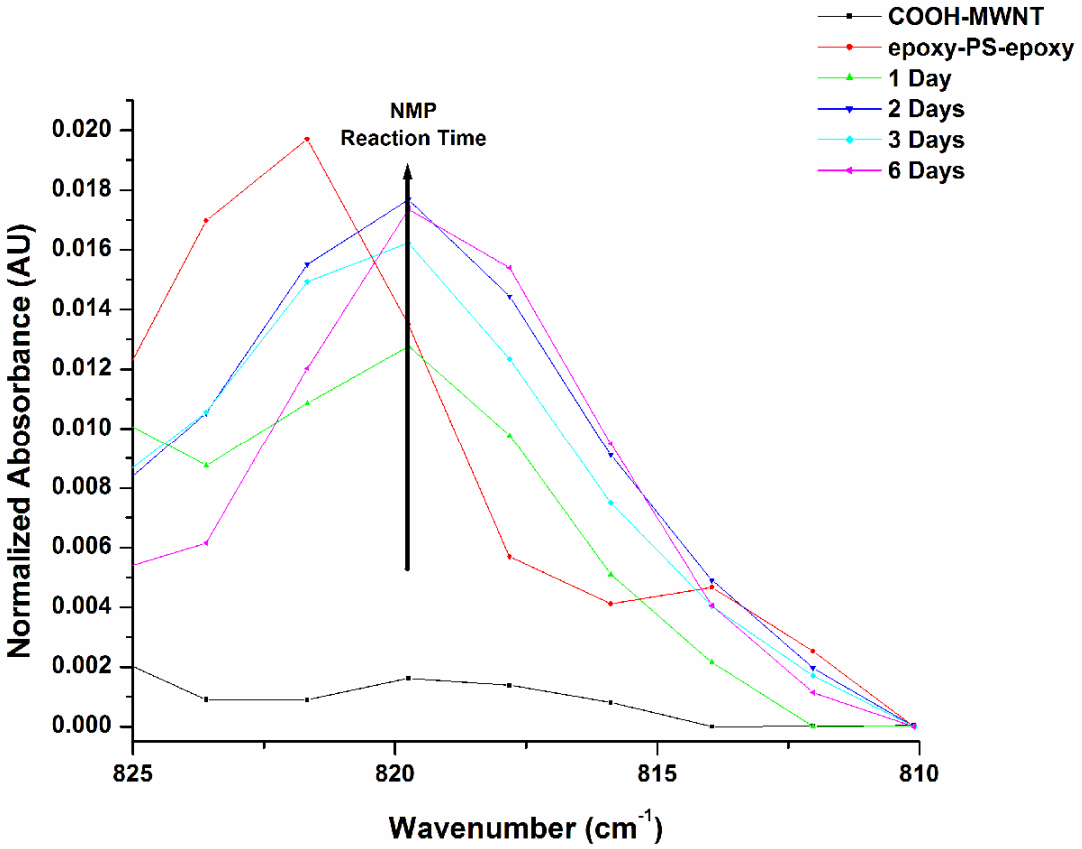

Figure 4.7. Normalized FT-IR spectra of grafted nanotube samples reacted in NMP for 1 – 6 days in the 845 – 810 cm^{-1} range.

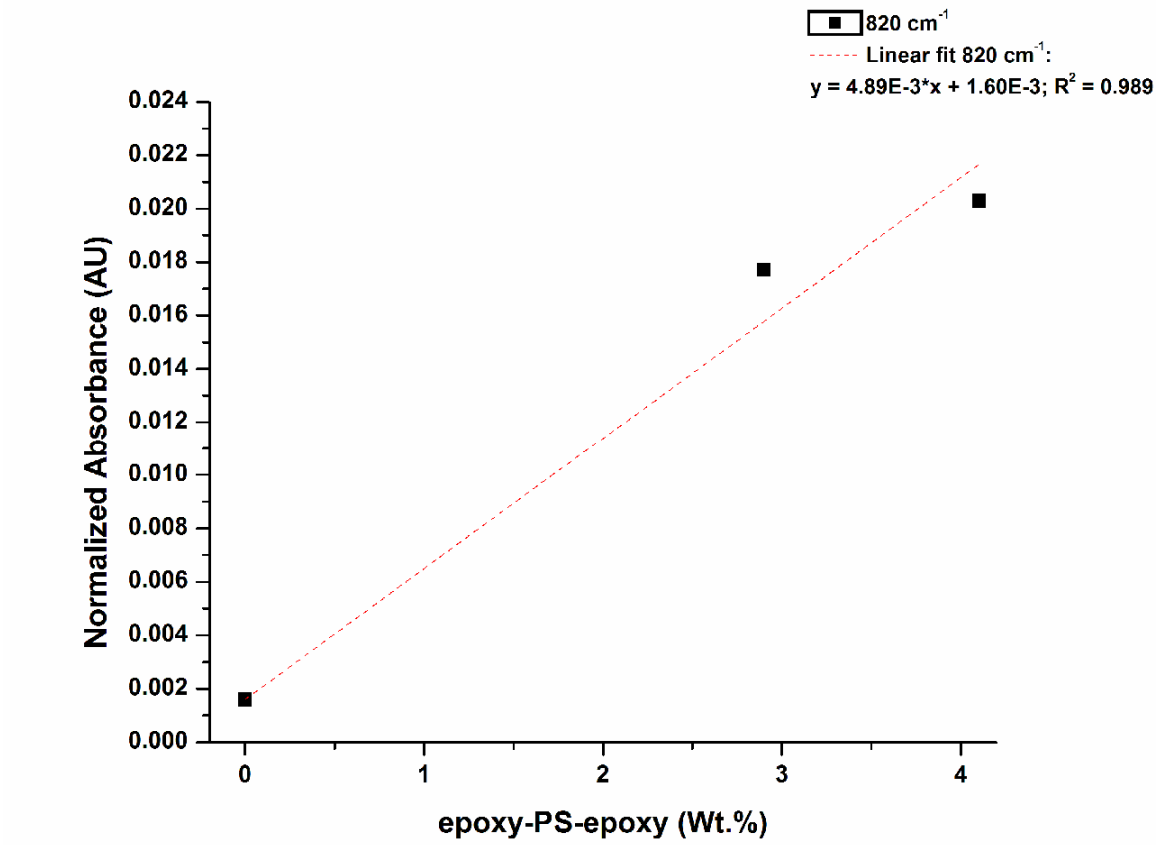

Figure 4.8. An epoxy-PS-epoxy calibration curve of the normalized 820 cm^{-1} signal intensity as a function of unreacted epoxy-PS-epoxy added to COOH-MWNT. A linear fit of the data was used to determine the amount of grafted epoxy-PS-epoxy.

with an R^2 value of 0.989, indicating a good linear correlation. The y-intercept is non-zero due to the small absorbance of IR light by the nanotubes at this wavenumber.

TGA was also used to monitor and quantify the success of the grafting reaction. TGA quantifies the weight percent of grafted PS. First the decomposition of neat epoxy-PS-epoxy was analyzed, indicating that PS weight loss occurs in the 350 °C – 500 °C region under a nitrogen atmosphere. Next the weight change in this temperature region was determined for the COOH-MWNT. Then the grafted nanotube samples were analyzed, with the weight fraction of PS grafted, estimated by

$$\text{Wt.\%}_{\text{PS}} = \Delta\text{Wt.\%}_{\text{Grafted } 350-500} - \Delta\text{Wt.\%}_{\text{COOH-MWNT } 350-500} \tag{4.2}$$

Typical TGA thermograms are shown in Figure 4.9. The weight percent of epoxy-PS-epoxy grafted to the nanotubes determined by FT-IR and by TGA is shown in Table 4.1. When possible, duplicate samples from the same batch were examined by TGA. The FT-IR results indicate that ~2 wt.% epoxy-PS-epoxy grafts to the COOH-MWNT surface in 1 day. The time evolution of the grafting reaction as monitored by FT-IR indicates that the grafted amount reaches a maximum of ~3 wt.% at 2 days and then levels off with further reaction. The TGA and FT-IR results, however, do not quantitatively match. Moreover, there is more scatter in the TGA results that in the FT-IR, which is not surprising when the analysis entails subtracting two large numbers to obtain a small number. Therefore, given this uncertainty in the TGA results and the fact that duplicate samples analyzed by FT-IR exhibited a 5% – 10% variation in absorbance, only the FT-IR results are quantitatively analyzed to provide insight into the grafting reaction.

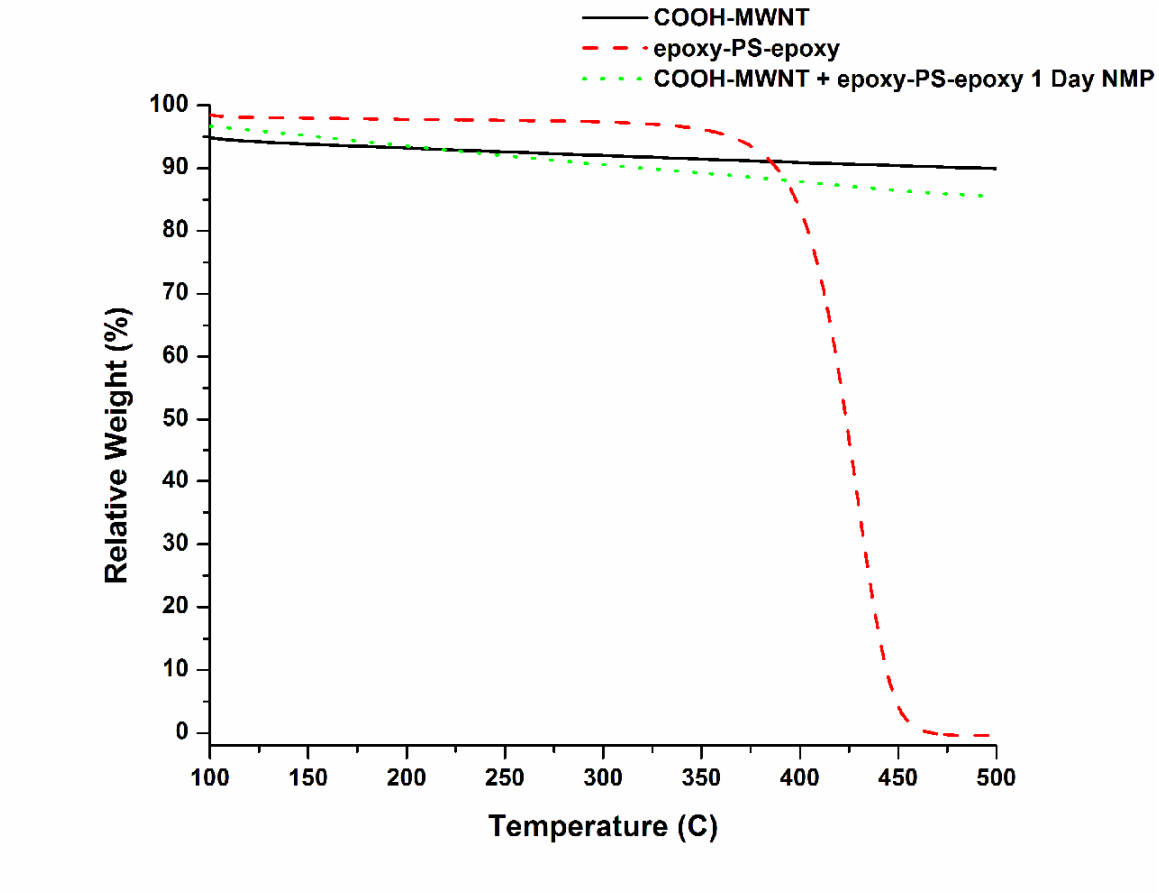

Figure 4.9. TGA thermograms of COOH-MWNT, epoxy-PS-epoxy, and COOH-MWNT + epoxy-PS-epoxy reacted in NMP for 1 Day. The difference in weight percent in the 350 °C – 500 °C range between the grafted and ungrafted COOH-MWNT is attributed to the amount of epoxy-PS-epoxy present.

Table 4.1. Weight percent of epoxy-PS-epoxy grafted to COOH-MWNT determined by FT-IR and TGA.

Reaction Time in NMP (Days, Sample #)	FT-IR 820 cm^{-1} (epoxy-PS-epoxy Wt. %)	TGA (epoxy-PS-epoxy Wt. %)
1 (#1)	2.3	2.1
1 (#2)		2.3
2 (#1)	3.3	4.6
2 (#2)		5.7
3	3.0	0.8
6 (#1)	3.2	2.2
6 (#2)		2.9

4.4 Monitoring the Evolution of Loop Formation

In the grafting process, the epoxy-PS-epoxy initially reacts at one chain end, forming tails. The free end of this grafted chain can then find the MWNT surface to form a loop. Our previous studies of loop formation suggest that the free chain end can readily react with the surface with further annealing in the absence of additional unbound telechelic. To monitor this process, the COOH-MWNT with grafted PS were annealed in a vacuum oven in the absence of free telechelic and in the melt at 150 °C for 1, 2, 3, and 6 days, with the goal of allowing free PS chain ends to diffuse and react with –COOH groups on the nanotube surface. This process is monitored by an increase in the FT-IR aromatic ester peaks while the telechelic PS aromatic ring intensity remains constant. The absorbance of the epoxy-PS-epoxy aromatic ring peaks at 820 cm^{-1} before and after annealing did not change with this annealing process, while Figure 4.10 shows the changes in the 1258 cm^{-1} aromatic ester ν_{as}(C-O-C) peak upon annealing. In Figure 4.10, the x-axis labeling is designed to first indicate the number of days that the MWNT reacts with the telechelic PS in NMP followed by the amount of time that the grafted chain is allowed to react to form loops in the melt. For example, *1NMP + 1A* refers to the sample that reacted for 1 day in NMP followed by annealing in the melt for 1 day in a vacuum oven. The sample *24hr NMP* is a separate batch of COOH-MWNT and epoxy-PS-epoxy reacted for 1 day in NMP that was completed to test for reproducibility. The results indicate that the samples that reacted with epoxy-PS-epoxy in NMP for 2 or more days exhibited a change in the 1258 cm^{-1} absorbance with one day of annealing in a vacuum oven, but this peak did not change with further melt annealing. Therefore, for visual clarity, only the results for 1 day annealing in a vacuum oven are shown for these

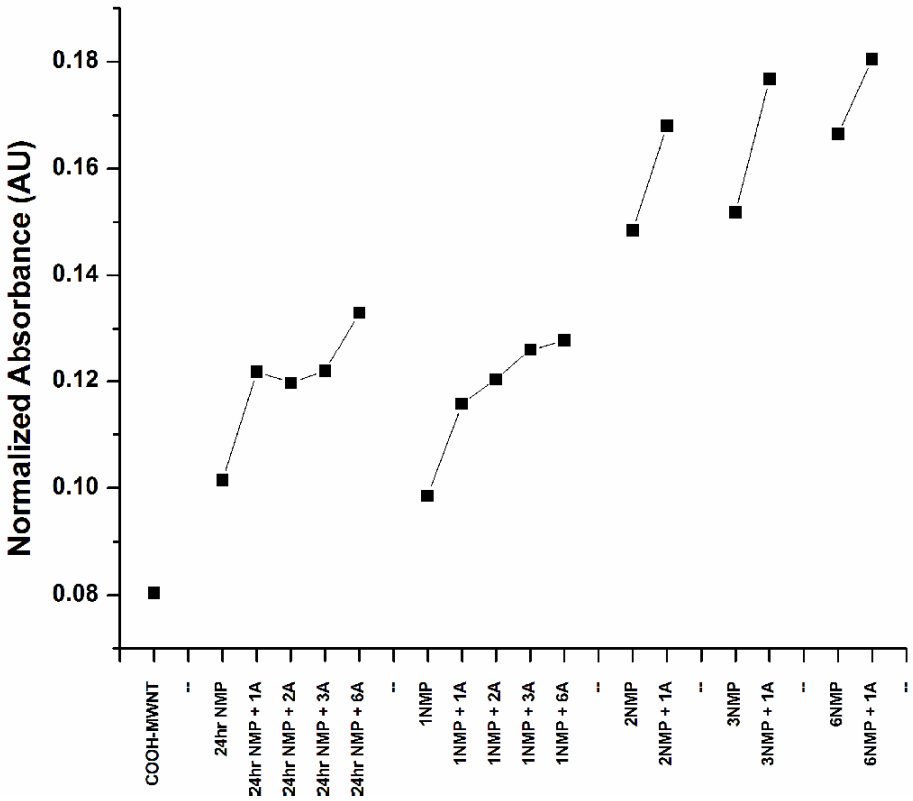

Figure 4.10. Normalized aromatic ester ν_{as}(C-O-C) peak at 1258 cm^{-1} as a function of reaction time in NMP and annealing time under vacuum. In the x-axis, the number in front of *NMP* indicates the number of days the reaction was conducted in solution, while the number in front of *A* indicates how many days the sample was annealed in the melt under vacuum. The *24 hr NMP* series is a separate batch used for duplication which was reacted in NMP for one day and subsequently vacuum annealed in the melt.

samples. Figure 4.10 shows that the COOH-MWNT that was reacted with the telechelic PS in NMP for 1 day resulted in continual growth of aromatic ester peak at 1258 cm^{-1} upon annealing in a vacuum oven in the melt for 6 days, indicating that unbound epoxy chain ends continue to react with –COOH groups on the nanotube surface to form new aromatic esters. In addition, the results appear to be reproducible. For the samples that were reacted in NMP for at least 2 days, there is a much smaller increase observed in the 1258 cm^{-1} peak upon annealing in a vacuum oven in the melt. This suggests that few new loops are formed upon this annealing process, suggesting that a significant number of loops are already formed during the reaction in NMP. The fact that the peak at 820 cm^{-1}, which quantifies the amount of polymer chain bound to the MWNT, remains constant while the aromatic ester peak increases upon annealing verifies that the further reaction is the result of dangling chain ends forming loops.

4.5 Quantifying Loops and Tails

To more fully understand the grafting and loop formation process, the quantification of the fraction of telechelics grafted as tails and loops is desired. Due to the low concentration of dangling ends of bound PS chains, it is not possible to quantify this by monitoring the remaining epoxy groups spectroscopically. To overcome this, a protocol where the number of epoxy groups is amplified by grafting a different polymer chain to the dangling ends whose content can be quantified spectroscopically. To realize this, a new batch of COOH-MWNT was reacted with epoxy-PS-epoxy in NMP for 1 day, isolated, and then further reacted with carboxy terminated poly(4-methyl styrene) (COOH-P4MS) in NMP for 1, 2, 3, and 6 days. This reaction is designed to allow unbound ends of the grafted telechelic to react with the COOH-P4MS, and FT-IR is used

to quantify the amount of COOH-P4MS present. In addition, a separate reaction of COOH-MWNT with COOH-P4MS was conducted in NMP for 1 day to verify that the functionalized polymer (COOH-P4MS) does not react with the carboxylated nanotubes. Figure 4.11 shows the FT-IR spectrum of COOH-P4MS and other components in the grafted MWNT, providing insight into which peaks can be analyzed to quantify the amount of P4MS in the system. Figure 4.11 suggests that the out-of-plane aromatic C-H stretch peaks centered at 813 cm^{-1} and possibly the aromatic ring distortion peak at 1447 cm^{-1} can be used for quantification without significant interference from other species. The peak intensities of COOH-P4MS reacted with COOH-MWNT + epoxy-PS-epoxy as a function of time are shown in Figure 4.12 and Figure 4.13 for 1447 cm^{-1} and 813 cm^{-1}, respectively. The vibrational bands at 1447 cm^{-1} and 813 cm^{-1} are both associated with the aromatic ring of the reactive polymer, as previously described for the epoxy-PS-epoxy telechelic. Figure 4.12 shows an increase in peak intensity at 1447 cm^{-1} as the reaction time of the grafted nanotube with COOH-P4MS increases in duration, while Figure 4.13 shows the same trend at 813 cm^{-1}. Two samples from the same batch were analyzed to test for reproducibility. It is important to emphasize that these results demonstrate that there is not any measurable reaction between COOH-MWNT and COOH-P4MS. Therefore we equate any COOH-P4MS detected to COOH-P4MS covalently bound to the epoxy-PS-epoxy chain, and not to the nanotube surface. Since there was still a significant absorbance at 813 cm^{-1} by the grafted epoxy-PS-epoxy itself, the COOH-P4MS signal was analyzed off-center at 806 cm^{-1}. A calibration curve was made at 806 cm^{-1} by adding known amounts of unreacted COOH-P4MS to the 1 day reaction of COOH-MWNT + epoxy-PS-epoxy. There was too much signal interference

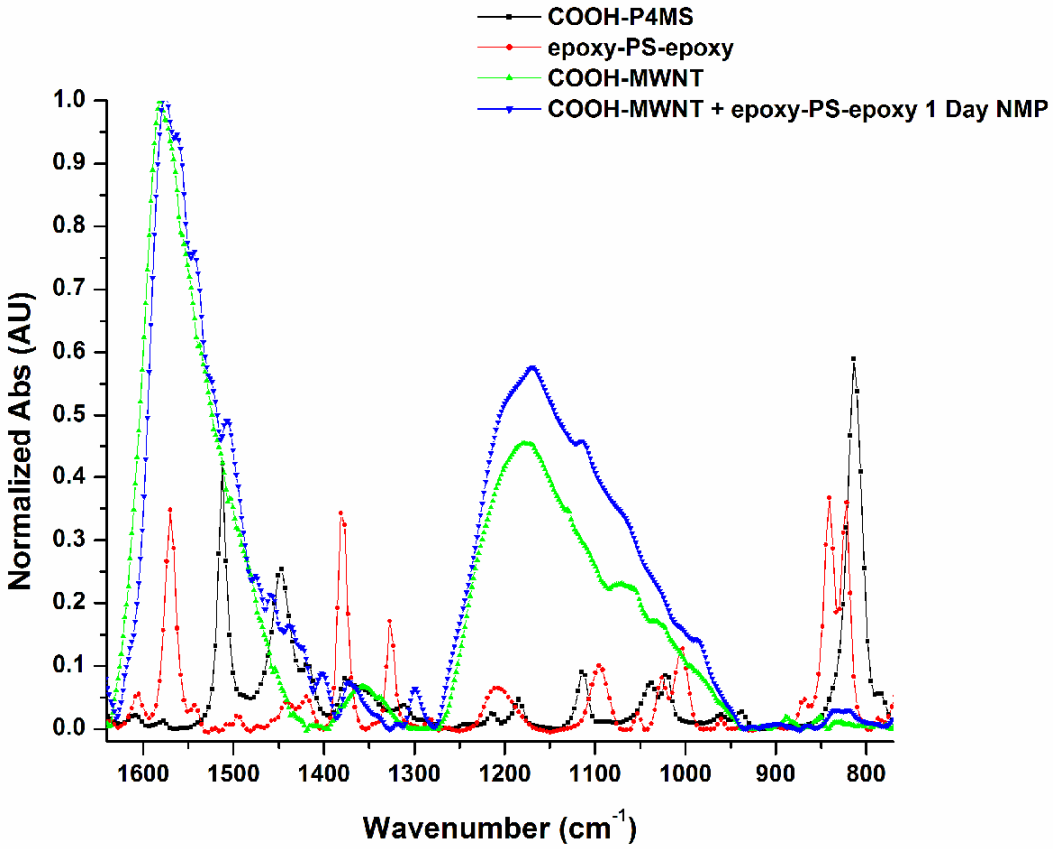

Figure 4.11. FT-IR spectra of COOH-P4MS peaks available for quantification in the 1650 cm^{-1} – 750 cm^{-1} region.

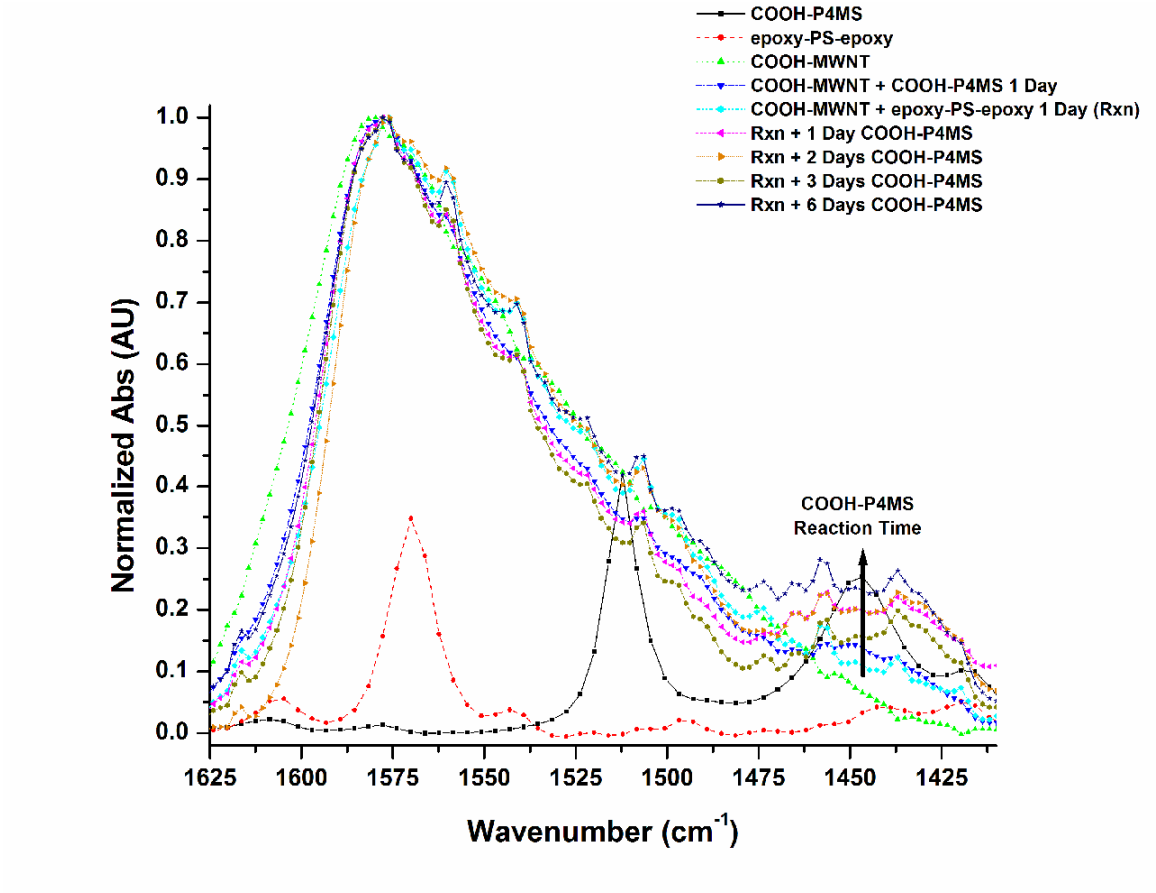

Figure 4.12. Normalized FT-IR spectra of peak intensity at 1447 cm^{-1} as a function of COOH-P4MS reaction time.

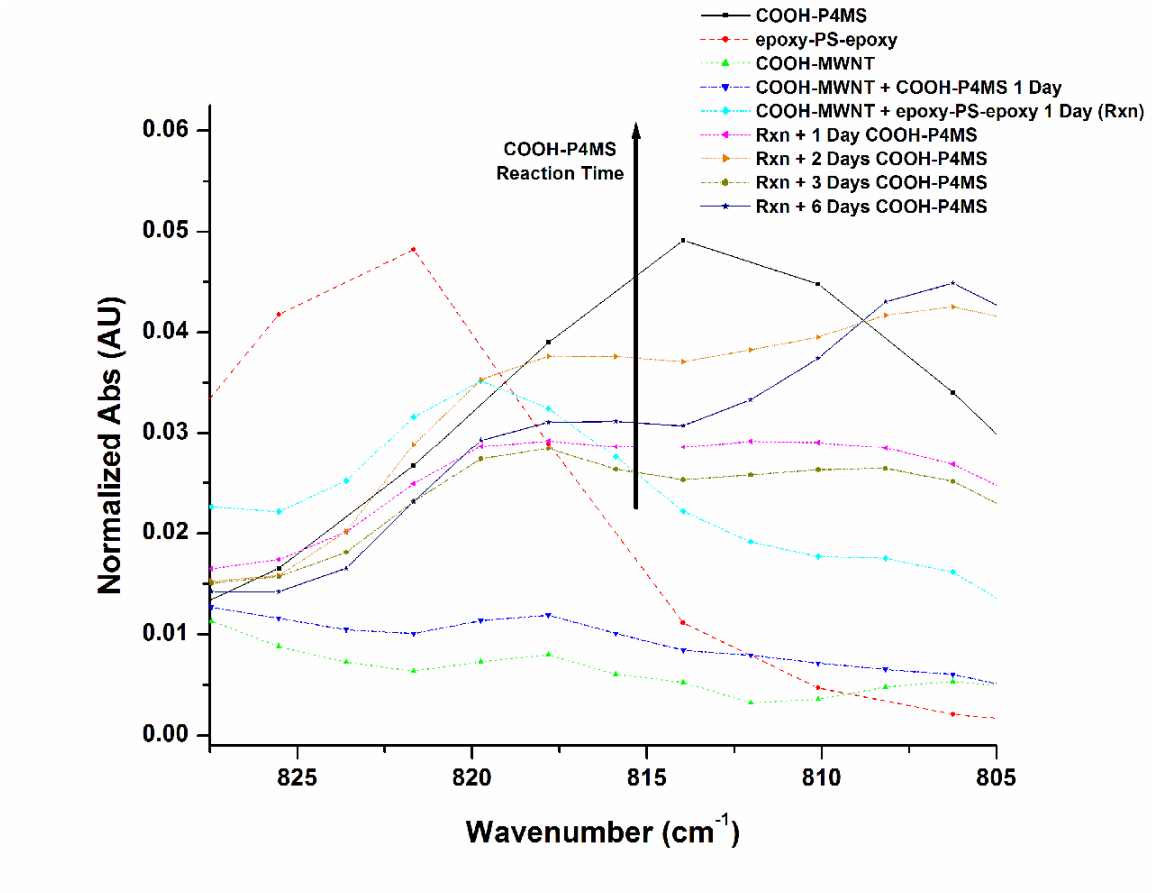

Figure 4.13. FT-IR spectra of normalized peak intensity at 813 cm^{-1} as a function of COOH-P4MS reaction time.

in the 1447 cm^{-1} peak for it to be used for quantification, as results obtained using this wavenumber were consistently higher than the quantification of COOH-P4MS determined from the 806 cm^{-1} signal and TGA. Results for the calibration curve made at 806 cm^{-1} are displayed in Figure 4.14, and the resulting linear fit of the data yields the equation

$$y = 6.35E\text{-}2*x + 3.89E\text{-}2 \tag{4.3}$$

with an R^2 value of 0.984, which is subsequently used to quantify the amount of COOH-P4MS present in the system. The y-intercept value is the absorbance contribution at 806 cm^{-1} due to the nanotubes and the epoxy-PS-epoxy signal.

Quantification of the amount of COOH-P4MS grafted to the MWNT was also estimated from TGA. Duplicate runs from each batch were tested for reproducibility. Table 4.2 shows the weight percent of COOH-P4MS grafted to the MWNT as determined by FT-IR and TGA. The amount of epoxy-PS-epoxy grafted to the nanotubes during this 1 day reaction in NMP (*Rxn*) has a significantly larger amount of grafted PS than the last batch. FT-IR shows that ~4 wt.% of epoxy-PS-epoxy is grafted to the nanotubes. After isolation of the grafted nanotubes and upon further reaction in NMP with COOH-P4MS, Table 4.2 shows that the FT-IR and TGA results generally match. These results also indicate that less than 1 wt.% of COOH-P4MS is grafted onto the MWNT by attaching to dangling epoxy groups when allowed to react.

From this data, the weight percent of telechelics that are singly bound to form tails can be determined by Equation (4.4).

$$\text{Wt.}\%_{\text{Tails}} = \frac{\text{Wt.}\%_{\text{COOH-P4MS}}}{\text{Wt.}\%_{\text{epoxy-PS-epoxy}} + \text{Wt.}\%_{\text{COOH-P4MS}}} \tag{4.4}$$

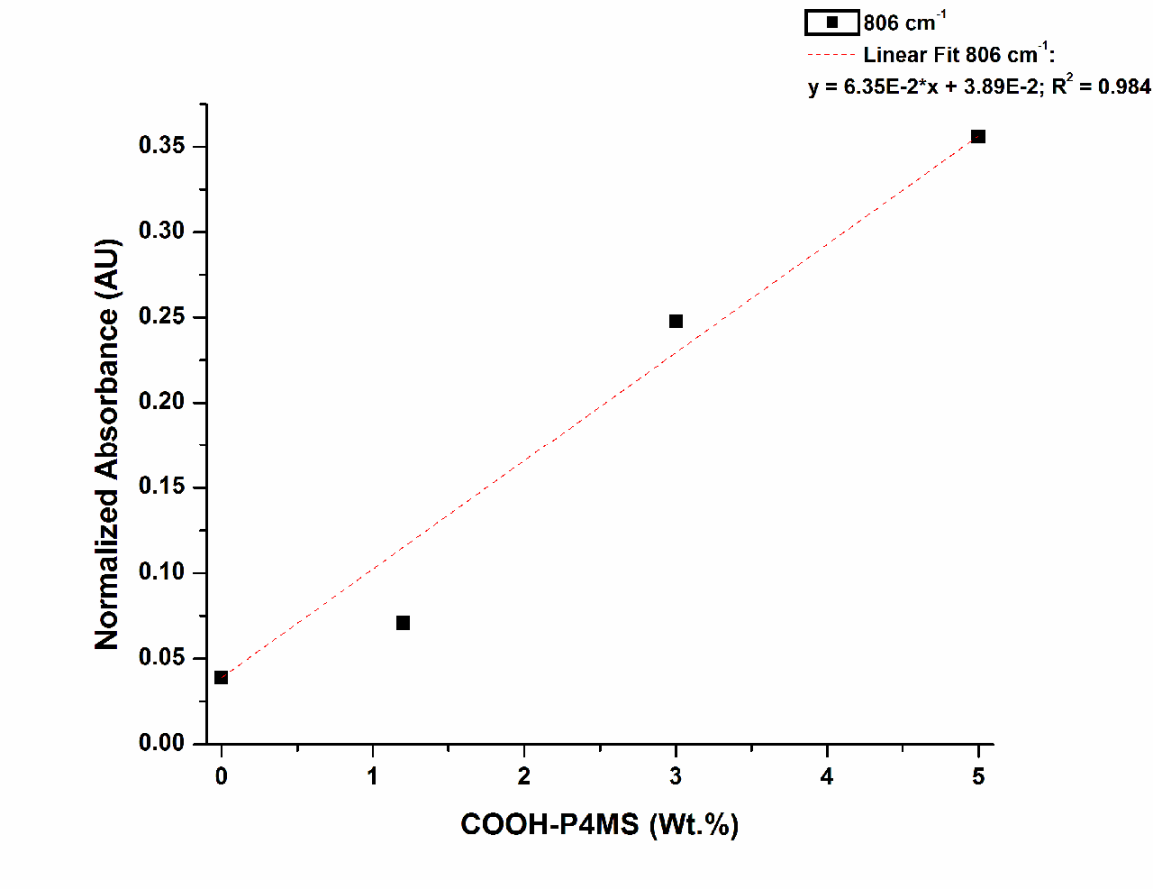

Figure 4.14. Calibration curve of COOH-P4MS constructed at 806 cm^{-1} by adding known amounts of unreacted COOH-P4MS to the 1 day reaction of COOH-MWNT and epoxy-PS-epoxy. The resulting linear fit of the data was used to quantify the amount of reacted COOH-P4MS in the grafted nanotube samples.

Table 4.2. Quantification of COOH-P4MS that reacted with unbound epoxy-PS-epoxy chain ends determined by FT-IR peak intensities at 806 cm^{-1} and by TGA.

	Epoxy-PS-Epoxy 820 cm^{-1} FT-IR (Wt. %)	Epoxy-PS-Epoxy TGA (Wt. %)	COOH-P4MS 806 cm^{-1} FT-IR (Wt. %)	COOH-P4MS TGA (Wt. %)
COOH-MWNT + epoxy-PS-epoxy 1 Day (Rxn) #1	3.7	5.4		
COOH-MWNT + epoxy-PS-epoxy 1 Day (Rxn) #2	4.2	5.8		
Rxn + 1 Day COOH-P4MS #1			0.2	1.0
Rxn + 1 Day COOH-P4MS #2			0.1	0.6
Rxn + 2 Days COOH-P4MS #1			0.4	0.3
Rxn + 2 Days COOH-P4MS #2			0.4	
Rxn + 3 Days COOH-P4MS #1			0.3	0.1
Rxn + 3 Days COOH-P4MS #2			0.1	
Rxn + 6 Days COOH-P4MS #1			0.4	0.6
Rxn + 6 Days COOH-P4MS #2			0.5	
COOH-MWNT + COOH-P4MS 1 Day			**0.0**	**0.0**

The FT-IR data shows that ~9 wt.% of the total grafted polymer is COOH-P4MS after 2 days of reaction in NMP. The number fraction of COOH-P4MS polymer chains can also be calculated by determining the average number of chains in the sample associated with each species of polymer:

$$\text{Wt.\% epoxy - PS - epoxy} \bullet \frac{1\,\text{mole}}{17{,}800\,\text{g epoxy - PS - epoxy}} \bullet \frac{6.02\text{E23 chains}}{1\,\text{mole}} \qquad (4.5a)$$

$$\text{Wt.\% COOH - P4MS} \bullet \frac{1\,\text{mole}}{19{,}400\,\text{g COOH - P4MS}} \bullet \frac{6.02\text{E23 chains}}{1\,\text{mole}} \qquad (4.5b)$$

The FT-IR data show that after 2 days of reaction with COOH-P4MS, ~8% of all the polymer chains present are COOH-P4MS, indicating that ~92% of the grafted telechelics are bound at both ends forming loops. The ~92% loop formation in this study is in agreement with the fraction of loops formed at low to intermediate grafting density in Monte Carlo studies by Smith et al. (~90% – 95%), as well as Yang and Char (~85% – 90%). Previous experimental results from our group indicated that ~80% of difunctional polymers formed loops on a functionalized hard flat surface after a 4 day reaction, at which time the amount of grafted polymer approached an asymptotic value,[81,165] with the experimental and simulation results showing good correlation. The discrepancy in the fraction of polymer loops formed in this study and in our previous study can be explained by variation in the grafting density and surface curvature. Monte Carlo studies show a higher fraction of loops form at lower grafting density. We do not expect COOH-MWNT to have a high surface density of carboxylic acid groups. During the HNO_3 and

piranha treatment of MWNT, the majority of the COOH groups are found on the more reactive amorphous carbon impurities that coat the nanotubes.[120,173] These impurities are then washed away in the subsequent NaOH treatment, leaving a low number of reactive sites on the purified COOH-MWNT. Datsyuk et al.[118] used TGA to investigate the weight loss of acid treated multiwalled nanotubes as a function of temperature in a nitrogen atmosphere, where the weight loss from 150 °C – 350 °C is attributed to loss of COOH groups,[187] and the weight loss from 350 °C – 500 °C corresponds to the loss of OH groups.[188] The TGA results in the decomposition of our COOH-MWNT and as received MWNT under nitrogen in these temperature ranges are shown in Table 4.3. This TGA analysis confirms that the acid treated multiwalled nanotubes used in this study do not contain a large amount of carboxylic acid groups that are able to react with epoxy-PS-epoxy, as COOH-MWNT contains only 2.6 wt.% COOH groups, verifying the low density of grafting sites on the COOH-MWNT.

In this study, it has been assumed that telechelics react at both ends to form loops on an individual nanotube surface. However, it is also possible for a telechelic chain to be grafted between two different nanotubes, forming a "bridge". Testard et al. conducted a Monte Carlo study of the loop and bridge formation between colloidal particles by telechelic polymers.[189] In this study, the ratio of the distance between the particles h to the R_g of the telechelic free chain was varied, where

$$\beta = h/R_g \tag{4.6}$$

The results of this study are shown in Figure 4.15, from ref. 61. It was discovered that approximately 20% – 30% of the telechelics formed bridges from $\beta = 0 – 1$, i.e. for

Table 4.3. TGA results for as received MWNT and COOH-MWNT weight loss from 150 °C – 350 °C (COOH) and 350 °C – 500 °C (OH).

	150C - 350C Wt.%	350C - 500C Wt.%
MWNT	0.6	0.4
COOH-MWNT	2.6	1.6

particle distances ranging from contact up to the R_g of the free telechelic. The fraction of bridges decayed significantly as the value of β increased from 1 to 2. This distance is associated with the end-to-end distance of the grafted chains, which is a factor of $6^{0.5}$ larger than the R_g.[190] The fraction of bridges was found to approach zero beyond $\beta = 3$. The results show that telechelics will exclusively form loops on an individual grafting surface when the particles are far away. When the distance between the particles approaches the end-to-end distance of the telechelics, bridging becomes possible, and the fraction of bridges formed becomes non-trivial.

In these experiments, it is not possible to distinguish between the formation of loops and bridges. Either one of the structures results in the same quantity of epoxy-PS-epoxy aromatic rings and the same number of aromatic esters formed. From the results of the Monte Carlo studies, however, it can be estimated that no more than ~1/3 of the "loops" that were identified in these experiments are actually bridges, which means that these modified MWNT could consist of as many as 30% bridges, with 60% loops and 10% tails, though the number of bridges is probably less than this.

4.6 Determination of Time-Dependent Reaction Rate

Understanding the parameters that control the grafting process is important in developing a full understanding that can be used in the future implementation of this

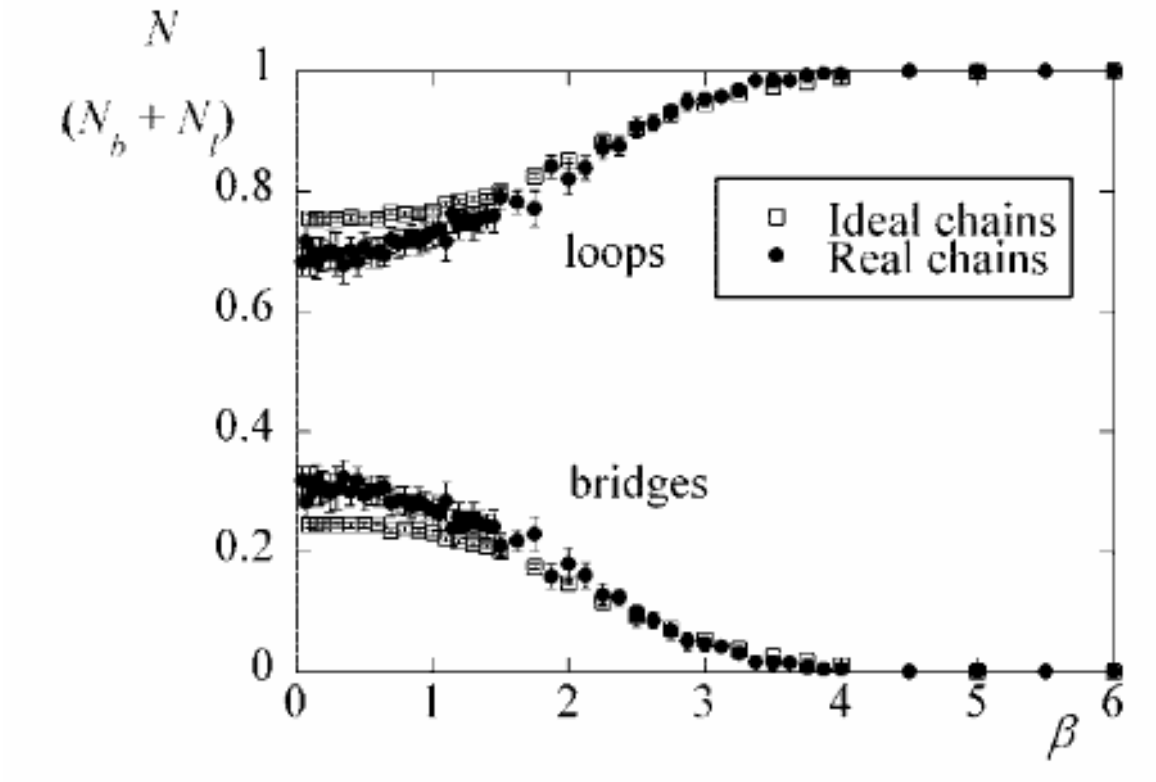

Figure 4.15. Monte Carlo simulations by Testard et al. show that the fraction of telechelic bridges is ~20% – 30% when the particle distance $\beta = h/R_g$ is less than the R_g of the free telechelic, and approaches 100% loops at large particle distances.

protocol. To develop this understanding, whether the grafting reaction is diffusion controlled or reaction controlled is important. As discussed in Chapter 4.1, a diffusion controlled reaction is assumed to have an instantaneous reaction of functional groups. The reaction is limited by how fast the chains can diffuse to the interface, which is proportional to $t^{0.5}$. If the kinetics are reaction controlled, the amount of time the functional groups take to react determines the grafting rate. The grafting rate is significantly less than $t^{0.5}$ in this case.

In order to determine the mechanism limiting the grafting reaction, it is first noted that the rate of a grafting reaction can be described by Equation (4.7)[191]

$$\frac{d\alpha}{dt} = A_0 f(\alpha)\exp(-E_A/RT) \tag{4.7}$$

where α is the extent of reaction after time t, A_0 is a constant, E_A is the activation energy, R is the ideal gas constant, T is the absolute temperature, and $f(\alpha)$ is a function describing the extent of reaction. The extent of reaction can be expressed as[191]

$$f(\alpha) = (1 - \alpha)^m \tag{4.8}$$

where the exponent m is the order of the reaction. Since the extent of reaction α is a function of time, the amount of polymer chains grafted as a function of reaction time can be characterized with a simple power law equation,

$$y = a*t^m \tag{4.9}$$

where a is a constant. To determine the time-dependent power m of the equation, the log of the normalized absorbance y is plotted as a function of the log of the reaction or annealing time t in units of minutes, which becomes a linear equation:

$$\log(y) = m*\log(t) + \log(a) \tag{4.10}$$

Schulze et al. studied the interfacial reaction of NH_2-dPS and anh-PMMA by forward recoil spectrometry.[72] The volume fraction of NH_2-dPS was measured as a function of depth from the surface for various reaction times. The amount of NH_2-dPS at the interface, the interfacial excess, was found to increase with reaction time. Since NH_2-dPS will only react with anh-PMMA at the interface, the reaction will follow a power law. Analyzing the data of Schulze et al., a log-log plot of the interfacial excess as a function of annealing time was plotted to determine the reaction rate given by the slope *m*. Results are displayed in Table 4.4. The fit of the data was found to be linear, with a power law of $\sim t^{0.2}$. This demonstrates the kinetics are reaction controlled, as discussed in Chapter 4.1.

Applying this analysis, the grafting rate of the polymer chains was followed by observing the normalized 820 cm^{-1} absorbance as a function of reaction time in NMP, shown in Figure 4.16. The plot in Figure 4.16 is reasonably linear for the 6 days of reaction in NMP, indicating a slope of 0.279, i.e. the grafting rate is proportional to $\sim t^{0.3}$. The good linear correlation for the entire reaction time also can be interpreted to show that there is no evidence of a decrease in reaction rate with reaction progress, indicating that there is not sufficient polymer buildup on the nanotube surface to hinder further reaction. This again suggests the density of reactive groups on the nanotubes is not very high, as has been previously deduced.

In a similar manner, the growth of the aromatic ester peak follows the reaction of dangling epoxy chain ends to COOH-MWNT in solution and in the melt. In this analysis, the 1258 cm^{-1} ν_{as}(C-O-C) peak was monitored as a function of annealing time to determine the rate of increased absorbance due to tails forming loops, as shown in Figure

Table 4.4. Power law exponent *m* and linear fit R^2 for log-log plot of interfacial excess as a function of annealing time in experiments performed by Schulze et al.

M_n NH_2-dPS	Power Law Exponent (m)	Linear Fit (R^2)
37,000	0.193	0.995
92,000	0.165	0.999

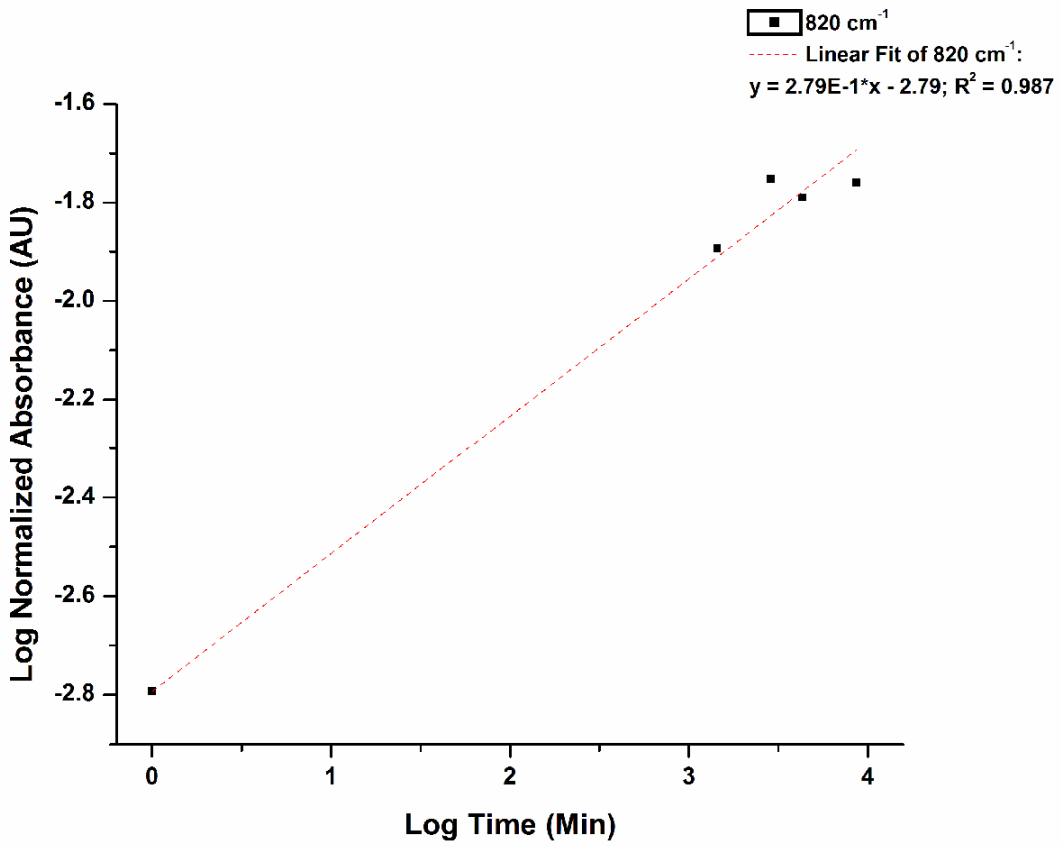

Figure 4.16. FT-IR signal intensity as a function of reaction time in NMP for epoxy-PS-epoxy aromatic ring peak at 820 cm^{-1} plotted on a log-log scale. The slope of the line yields the power law exponent.

4.17. The aromatic ring peak of the telechelic PS at 820 cm^{-1} was also monitored as a function of annealing time, and no significant change in the log-log plot of the signal intensity as a function of annealing time was observed. The data in Figure 4.17 shows that for the sample that initially allowed reaction of the telechelic PS to the COOH-MWNT for 1 day, the initial aromatic ester ν_{as}(C-O-C) signal at 1258 cm^{-1} is small, and continues to grow with time as the sample is annealed for 1 – 6 days. This suggests a small quantity of tails have been grafted to the nanotubes in the NMP reaction, and upon annealing in the melt, they further react to form loops. For the samples reacted in NMP for 2 – 6 days, the initial signal intensity is much greater than the 1 day reaction and in these samples further annealing in the melt only results in a slight increase in the signal intensity. This implies that most of the grafted chains have already formed loops in the NMP reaction, implying that tails are primarily formed at short reaction times in solution, whereas loops are the dominant species at long reaction times. The exponent of the power law dependence for loop formation upon annealing samples in the melt is shown in Table 4.5, where the data was fit over the first 3 days of the annealing regime, as Figure 4.17 indicates a decrease in signal intensity for some samples annealed for 6 days. The results in Table 4.4 demonstrate that the sample that initially allowed reaction of the telechelic PS to the COOH-MWNT for 1 day exhibits the largest power law exponent. This indicates that 1 day of grafting in NMP results in a relatively large fraction of tails being formed, and is insufficient time to achieve significant loop formation. For the samples grafted in NMP for 2 – 6 days, the slope becomes smaller upon annealing with increasing reaction time in NMP. This is interpreted to indicate that longer reaction time

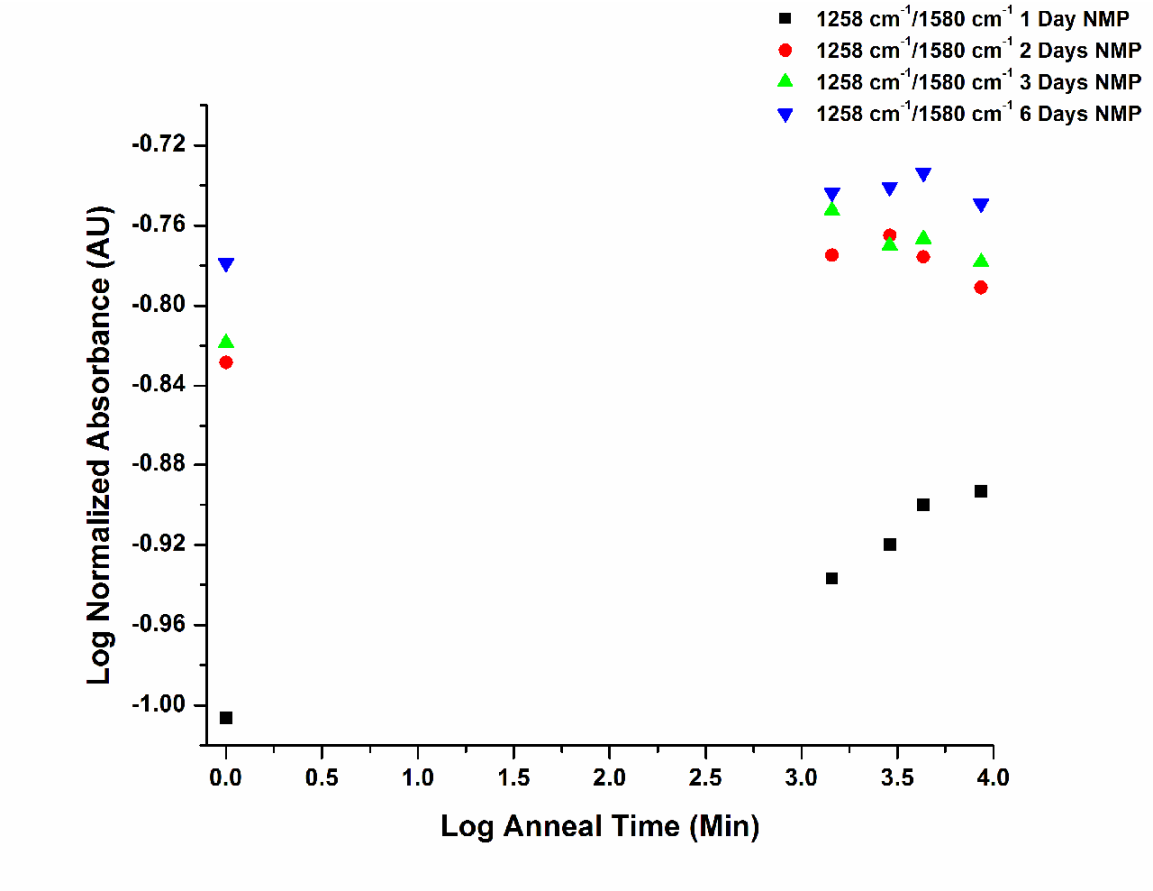

Figure 4.17. Log-log plot of the normalized 1258 cm^{-1} signal intensity as a function of annealing time for COOH-MWNT reacted with epoxy-PS-epoxy for 1 – 6 days in NMP. The large slope of the line for the 1 day reaction in NMP indicates many loops were formed during annealing in the melt, as mostly tails were formed in solution.

Table 4.5. Reaction rate of 1258 cm^{-1} aromatic ester peak as a function of annealing time for COOH-MWNT and epoxy-PS-epoxy reacted in NMP for 1 – 6 days. The slope of the fitted data gives the power law exponent.

1258 cm^{-1}	Slope (Log AU/Log Min)	R^2
1 Day NMP	0.0258	0.953
2 Days NMP	0.0165	0.961
3 Days NMP	0.0142	0.999
6 Days NMP	0.0117	0.987

in NMP allows for an increase in loop formation.

The reaction rate of COOH-P4MS with the unbound epoxy-PS-epoxy chain end was also determined. Figure 4.18 shows the log-log plot of the 1258 cm^{-1} aromatic ester peak and the COOH-P4MS aromatic ring C-H bending signal at 806 cm^{-1} as a function of reaction time with COOH-P4MS in NMP, where Table 4.6 shows the linear fits to this data and the equivalent analysis for the grafting of the telechelic to the COOH-MWNT in solution. Results from Figure 4.18 and Table 4.6 show that the grafting rate of the COOH-P4MS is only about half that of the epoxy-PS-epoxy telechelic grafting rate. One explanation for the lower reaction rate of the monofunctional COOH-P4MS relative to the difunctional epoxy-PS-epoxy is that the COOH-P4MS only has 1/2 the number of reactive groups as the telechelic. Thus the reaction probability will be lower for the former than the latter. This agrees with Monte Carlo simulations by Yang and Char,[172] who showed a higher rate of grafting difunctional polymers than monofunctional polymers with respect to reaction time.

4.7 Effects of Surface Curvature

The 92% loop formation observed in this experiment is significantly higher than the ~80% loop formation found in previous experiments by our group. In Chapter 4.5, the variation was attributed to the large difference in grafting density. Another distinction between these two experiments is that polymer chains were grafted to a highly curved nanotube surface in this case, whereas polymers were grafted to a flat surface in the previous experiment. Here the differences between grafting polymers to a highly curved nanotube surface and a flat planar surface are investigated in order to learn how

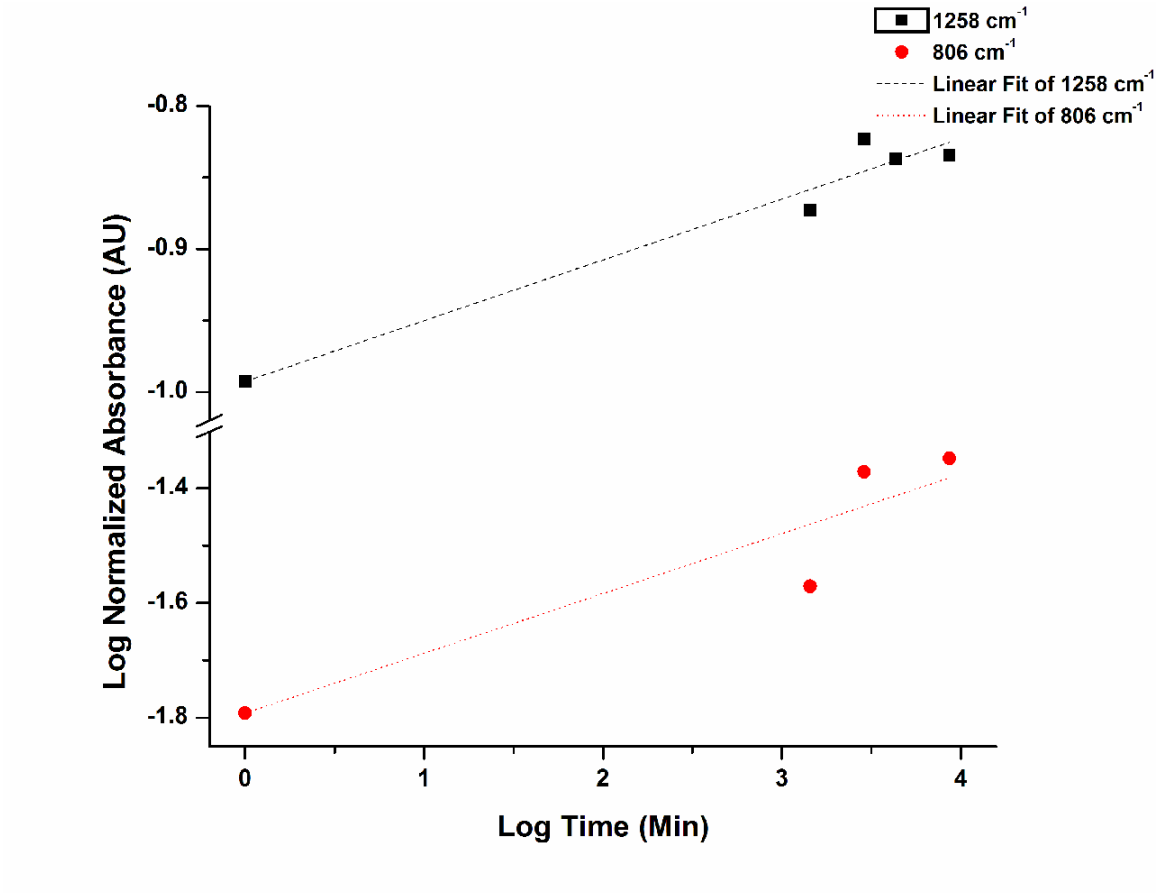

Figure 4.18. Log-log plot of the normalized 1258 cm^{-1} aromatic ester and 806 cm^{-1} aromatic ring intensity as a function of reaction time with COOH-P4MS in NMP. Both plots exhibit a linear response, with the slope of the line corresponding to the power law exponent, which describes the grafting rate.

Table 4.6. Comparison of the reaction rate of the normalized 1258 cm^{-1} aromatic ester peak and 820 cm^{-1} or 806 cm^{-1} aromatic ring intensity as a function of reaction time in NMP for epoxy-PS-epoxy (top) and COOH-P4MS (bottom).

Peak	Reaction	Reaction Time Regime (Min)	Slope (Log AU/Log Min)	R^2
1258 cm^{-1}	epoxy-PS-epoxy	0 - 1440	0.071	1
820 cm^{-1}	epoxy-PS-epoxy	0 - 1440	0.212	1
1258 cm^{-1}	COOH-P4MS	0 - 8640	0.043	0.959
806 cm^{-1}	COOH-P4MS	0 - 8640	0.104	0.872

variations in geometry may also affect the fraction of loops formed.

Murat and Grest performed a molecular dynamics study on polymer chains end-grafted onto a cylindrical surface.[192] Under good solvent conditions, they examined the effects of changing the radius of the cylinder, R. When $R = \infty$, the surface becomes planar, and when $R = 0$, the radius is reduced to a line. Thus, the curvature increases with decreasing radius. Murat and Grest also examined the effects of grafting density ρ, with

$$\rho = M/S_{cylinder} \tag{4.11}$$

where M is the number of polymer chains grafted, and $S_{cylihder}$ is the surface area of the cylinder given by $S_{cylinder} = 2\pi Rl$. Here, l refers to the length of the cylinder. They found that for an equal number of grafted chains and a decreasing cylinder radius R, the brush height increased as a result of the chains becoming more densely packed near the surface. Because a reduction in R results in a smaller surface area, a larger grafting density ensues, as Equation (4.11) demonstrates. Although there is an entropy penalty for stretching, chain extension is preferred because favorable polymer-solvent interactions can be maintained when the chains are not in contact with each other.[193] Murat and Grest also demonstrated that when the cylinder radius is held constant, increasing the grafting density and chain size results in the maximum density of end groups being located at a larger distance from the cylinder surface. A higher grafting density causes the chains to stretch in order to avoid interaction with each other, increasing the distance the chain ends are from the surface. Increasing the chain size increases the average distance the chain ends are from the surface. It stands to reason that for equal numbers of chains grafted to a surface of equivalent dimensions, the chains grafted onto a cylinder will be

less stretched out than the chains grafted onto a planar surface due to a lower grafting density because $S_{cylinder} > S_{plane}$. The surface area of a plane is $S_{plane} = lw$, where w is the width of the planar surface.

At a constant low grafting density, Murat and Grest discovered the monomer density (ρ_m) profile became steeper at short distances from the surface as the cylinder radius decreased, as ρ_m was found to be proportional to $n^{2/3}r^{-4/3}$. Here, n is the number of chains and r is the cylinder radius. This resulted in the maximum density of free ends ρ_e as a function of distance from the grafted surface to shift to shorter distances as well. The results are shown in Figure 4.19, from ref. 65. As the cylinder radius in Figure 4.19 decreases from curve *a* to *c*, the maximum density of chain ends is found closer to the cylinder surface. Cylinders with a large radius, such as curve *a* in Figure 4.19, displayed grafting density profiles identical to a flat surface. So when comparing a polymer chain grafted to a flat surface and a nanotube, Figure 4.19 suggests that the chain end is closer to the nanotube surface than the planar surface for low grafting densities. Since the end group is closer to the surface, it will have a higher probability of finding a reactive complementary group in a random walk than the end group further away in the planar surface case. Therefore a higher percentage of loops are expected to be formed on a nanotube surface than a flat surface.

Since the radius of nanotubes is on the order of 1 nm, the distribution of chain segments is similar to that of polymers grafted to a line[95] rather than a cylinder. At higher grafting densities of polymers grafted to planes, cylinders, and lines, a dead zone evolves near the surface where end groups are not present and subsequently this dead

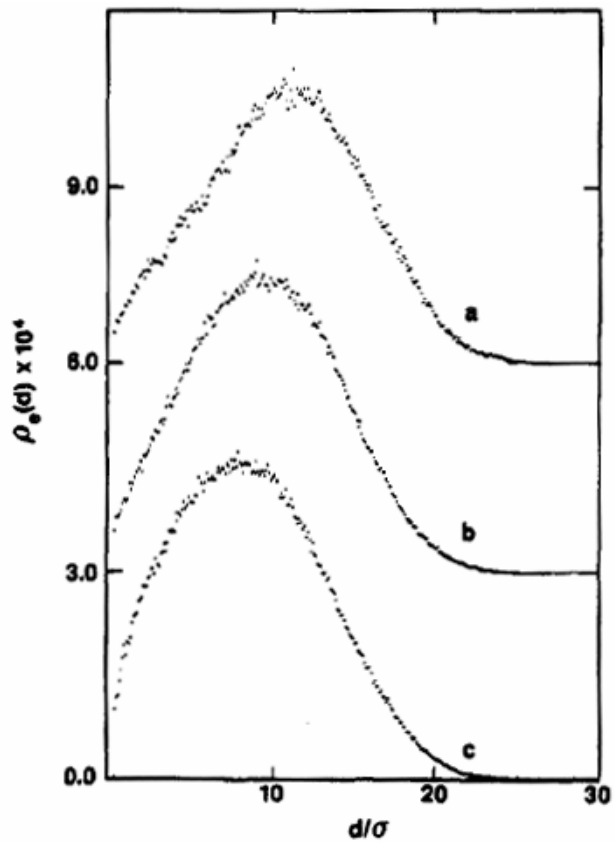

Figure 4.19. Chain end density ρ_e of a grafted polymer as a function of distance from the surface of cylinders with a radius of: a) R = 20σ, b) R = 5σ, c) R = 2σ. The term σ refers to the distance where the Lennard-Jones potential is 0. The grafting density in low in this case, and is the same for all three curves. Curves *a* and *b* have been vertically shifted and scaled for visual clarity.

zone increases with grafting density.[192,194] The grafting densities used to obtain these dead zones were considerably higher than in the case of the cylinders previously described. The density of the free ends as a function of distance from the grafting line for various grafting densities is shown in Figure 4.20, from ref. 65. Figure 4.20 demonstrates how a dead zone evolves where there is zero probability of finding a chain end for increasingly larger distances from the line as the grafting density increases from curves *a* to *d*. The lowest grafting density in curve *a*, $\rho = 0.38$, which is still rather large, shows that end groups can still be found near the surface and no dead zone develops for this condition. The functionalization of MWNT is not expected to create a large density of reactive –COOH groups on the nanotube surface, as TGA results in Chapter 4.5 indicate –COOH groups only consist of 2.6 wt.% (0.7 mol.%) of the COOH-MWNT sample. Thus for an equal number of chains grafted to a cylinder and plane of equal dimensions, a nanotube will have a lower grafting density because a cylinder has a larger surface area than a plane. Therefore tails first grafted on a nanotube surface will have their unreacted end closer to the surface than a telechelic tail on a planar surface. The probability of reaction for the tail closer to the surface will be greater than the planar surface, and a higher percentage of loops will be created on nanotubes than on a planar surface for the same reaction conditions.

However, as previously discussed, carboxylation of nanotubes results in a low surface density of reactive groups, whereas the previous grafting experiment had a planar surface with a higher density of reactive groups. If the planar surface had a smaller amount of reactive groups, the fraction of loops formed should be higher than the 80%

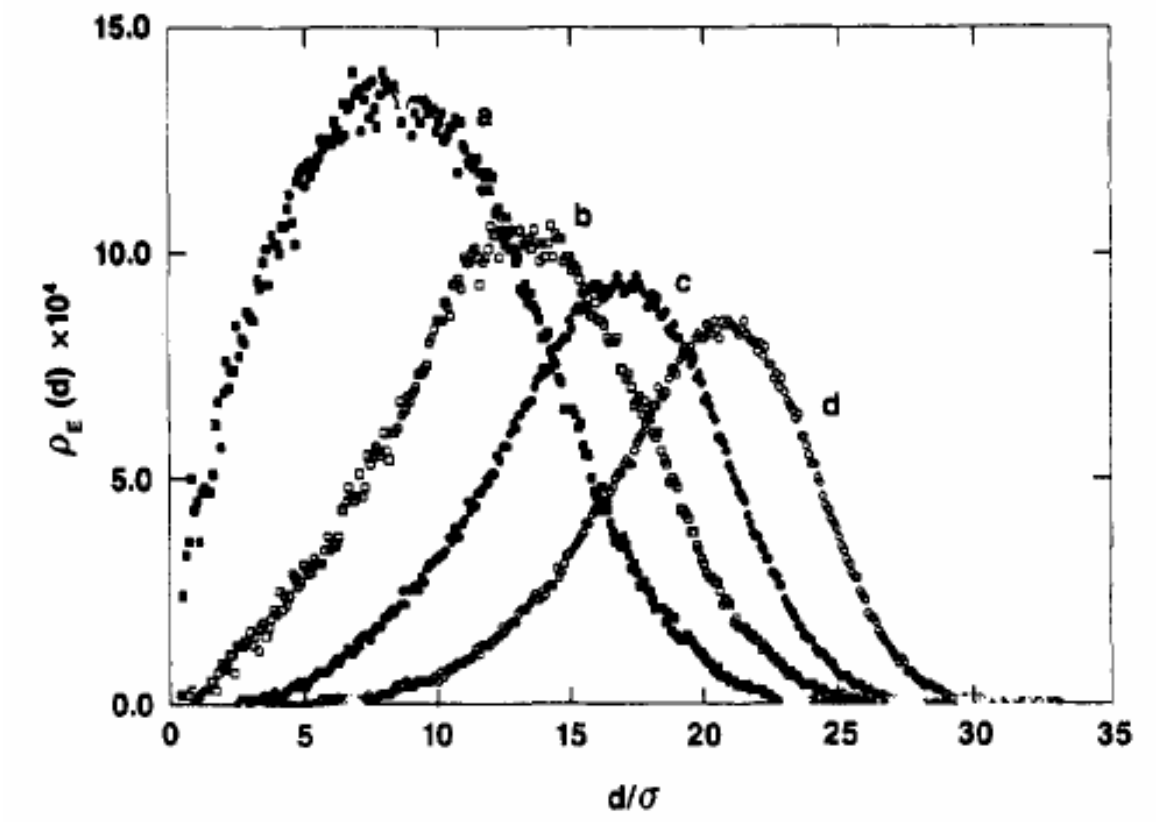

Figure 4.20. End group density of chains grafted to a line as a function of distance from line. The grafting density given in chains/unit length are a) ρ = 0.38, b) ρ = 1.51, c) ρ = 3.14, d) ρ = 6.28.

that was experimentally observed. Therefore the extent that geometry plays in loop formation on different surfaces of low functionalization is not clear. If one wishes to investigate how geometry affects loop formation, the next logical step to extend this project is to change the grafting density of the planar surface. In this manner, it should be possible to determine if > 90% loop formation is achievable on a flat surface at low grafting density. This experiment more clearly demonstrates the influence that the surface geometry has on the fraction of loops formed. Alteration of the density of reactive groups on a planar surface can be achieved by using various combinations of trimethoxysilanes with reactive and inert functional groups. For instance, (3-glycidyloxypropyl)trimethoxysilane (GLYMO) can be used for functionalizing a surface with epoxy endgroups, while hexyltrimethoxysilane (HTMS) can be used to introduce non-reactive alkyl groups to the surface. The contact angle of a monolayer of GLYMO, HTMS, and various combinations of the two trimethoxysilanes is then measured. An epoxy end group is hydrophilic, resulting in a low contact angle, as the surface is easily wetted. If a hexyl endgroup is present, a hydrophobic surface is created, resulting in a large contact angle. The Cassie equation is used to determine the mole fraction that each component contributes to the overall observed contact angle. The Cassie equation is given by[195]

$$\cos(\theta_{obs}) = n_1*\cos(\theta_1) + n_2*\cos(\theta_2) \qquad (4.12)$$

where θ_{obs} is the observed contact angle, θ_i is the contact angle observed using only component i, and n_i is the mole fraction of component i. It is thus theoretically possible to create a planar surface with a similar mole fraction of reactive groups as the

carboxylated nanotubes. This will make the effects of geometry, if any, at this low grafting density more clear.

4.8 Conclusion

It has been experimentally demonstrated that the telechelic polymer epoxy-PS-epoxy can be covalently grafted to the surface of carboxylated multiwall carbon nanotubes, primarily forming loops. FT-IR analysis of the aromatic C-H bending peak was used to quantify the amount of epoxy-PS-epoxy grafted to the nanotubes as a function of reaction time, while the observed evolution of the aromatic ester ν_{as}(C-O-C) peak verifies the success of the grafting reaction. Annealing experiments showed loops can be formed from pre-existing tails, and that loops are the dominant species for long reaction times in solution. By reacting a 1 day reaction of COOH-MWNT + epoxy-PS-epoxy to COOH-P4MS, the amount of telechelics that form tails for this reaction time was quantified, as only unbound epoxy-PS-epoxy chain ends react with the COOH-P4MS. Results from this study show that ~92% of the grafted telechelics form loops, which agrees with Monte Carlo studies of systems with low to intermediate grafting density. The quantitative FT-IR results qualitatively agree with the TGA results and appear to be more reproducible as well, demonstrating how this novel analysis technique allows for the determination of the amount of telechelics that have only reacted at one end to form tails.

The time dependence of grafting polymer chains to a nanotube surface was also determined by fitting FT-IR signal intensity as a function of the reaction time to a power law equation. The aromatic ring C-H bending peak associated with epoxy-PS-epoxy grew as a function of $\sim t^{0.3}$, suggesting the grafting is reaction controlled. The annealing

experiments showed a much smaller growth rate of the aromatic esters for samples reacted in NMP for 2 or more days compared to the reaction conducted for 1 day, implying that most of the loops are formed in NMP within the first 24 hours. In the COOH-P4MS reaction, the aromatic ester and aromatic ring peaks only grew at half of the rate as the epoxy-PS-epoxy. The reduced reaction rate is attributed to the fact that COOH-P4MS is monofunctional, and therefore has a lower reaction probability than the difunctional epoxy-PS-epoxy.

The higher fraction of loops formed on nanotube surfaces in this study compared to planar surfaces in previous studies was associated with a lower grafting density of functional groups on the nanotube surface and the larger surface area of a nanotube relative to a planar surface. High grafting densities found in previous studies encourage polymer chains to stretch out from the surface in order to avoid contact with each other, increasing the distance the unreacted end group is found from the surface. This reduces the reaction probability of the end group, therefore decreasing the fraction of loops formed. The fact that a cylinder has a larger surface area than a comparable planar geometry results in a lower grafting density, encouraging a larger fraction of loop formation.

Chapter 5

Formation of Multiblock Copolymers

5.1 Introduction

In Chapter 1, evidence was presented that indicated that multiblock copolymers are the most efficient compatibilizers to stabilize immiscible homopolymer blends because they cross the interface multiple times, efficiently cover the biphasic interface, and strengthen the interface. Copolymers formed *in situ* have also been shown to be more effective compatibilizers than pre-made copolymers because they are formed from smaller polymers. This allows the reactive polymer to approach the interface more effectively and reduces the amount of copolymer lost as a micelle in one of the homopolymer phases.

As described in Chapter 1, studies have investigated the formation of diblock copolymers in polymer blends *in situ* from monofunctional reactive polymers, demonstrating their ability to compatibilize immiscible homopolymer blends. Similar studies to monitor the formation of multiblock copolymers by reacting telechelic polymers in polymer blends may provide an efficient method to compatibilize phase separated mixtures. We have experimentally investigated the use of difunctional reactive copolymers used to form multiblock copolymers *in situ*. Tagging one of the telechelics with a fluorescent label allows the reaction to be monitored as a function of mixing time by means of GPC equipped with a highly sensitive fluorescence detector. Because only a small amount of telechelics are added to the homopolymer blend to compatibilize them, the concentration of tagged polymer in the sample is very low, making fluorescence detection an ideal analysis method. Since the PI blocks in the formed copolymer contain

a fluorescent label, the amount of tagged telechelic converted and the molecular weight of the copolymer formed *in situ* can therefore be determined using this technique. GPC separates polymers by size, with the larger molecules eluting first. The fluorescence detector should only respond to the copolymer formed *in situ* and the unreacted telechelic, as the homopolymers are minimally fluorescent. Therefore, higher molecular weight copolymers should be observed at shorter elution times, and the unreacted tagged PI telechelic will elute last.

There are several goals of this project. First, the effects of functional groups with different reactivities will be studied. The anh/NH_2 reaction is known to occur very quickly, while the epoxy/COOH reaction is much slower. Since reactive blending needs to produce sufficient copolymers *in situ* on the time scale of minutes for industrial purposes, the ability of the epoxy/COOH reaction to meet this requirement must be verified. Therefore, the conversion of these two reactive pairs as a function of mixing time will be monitored. The other goal of this project is to determine the optimal loading level of compatibilizers for the homopolymer mixture studied, a blend of 90% PS/10% PI. If too few compatibilizers are added, there will be insufficient copolymer produced to suppress coalescence. If an excess of telechelics are added, the quantity that does not react is wasted. In addition, if the molecular weight of the telechelics is lower than the homopolymers, any unreacted telechelics can act as plasticizers. This will reduce the blend viscosity and make coalescence easier, potentially offsetting the advantages of copolymer coalescence suppression.

When multiblock copolymers are formed *in situ*, many different size copolymers are produced. At short reaction times, we expect small copolymers, such as diblocks and

triblocks, to form. The telechelics meet at the interface, first forming a diblock copolymer. Then any other telechelic may react with a complementary telechelic polymer or the diblock at the interface. The copolymer at the interface continues to grow in block size as the reaction time increases, and at longer mixing times the distribution of copolymers should contain a larger amount of higher order blocks. Deconvolution of the copolymer fluorescence signal provides a method to determine the distribution of copolymer sizes present. In order to use GPC with fluorescence detection, the optimal excitation and emission wavelengths of the tagged telechelic must first be experimentally determined.

5.2 Experimental

A. Fluorescence of Tagged Telechelics

The excitation wavelengths of the APE-tagged telechelic PI polymers described in Chapter 2.1 D were determined using a Thermo Spectronic BioMate 5 UV/Vis spectrometer. A 5E-5 molar solution of the polymer in ACS grade THF was placed in a quartz fluorometer cell (Starna). An SLM Aminco SQ-340 Luminescence Spectrometer was then employed to determine the emission (λ_{em}) wavelengths from the maximum excitation wavelength (λ_{ex}) determined from UV/Vis.

The APE fluorescent tag has several excitation and emission wavelengths. According to Yang et al., the maximum intensity for excitation and emission of the APE-tagged model compound C_5H_{11} in THF are λ_{ex} = 363 nm and λ_{em} = 407 nm.[113] When APE was at the junction between PI and PMMA, the excitation and emission wavelengths only shifted 1 nm and 2 nm higher, respectively. For the unreacted APE-tagged telechelics in this study, these optimum wavelengths were not observed. When

the 54k COOH-PI-COOH was excited at λ_{ex} = 364 nm, there was a maximum fluorescence observed at λ_{em} = 412 nm, which was expected. However, the three other telechelics only exhibited a very weak peak at λ_{em} = 409 nm and showed an unexpected broad plateau beyond λ_{em} = 440 nm. This is observed in Figure 5.1. The weak peak observed at 409 nm in three of the telechelics is not attributed to the fluorescent tag, but rather an instrumental artifact, most likely due to stray light emitted from the sample. When HPLC grade THF was excited at various wavelengths, the observed fluorescence emission peak varied in a linear fashion, as shown in Figure 5.2. The most intense excitation wavelength for all four telechelics was 295 nm. Using this excitation wavelength, all four telechelics had a strong fluorescence response, where Figure 5.3 shows the response normalized to the peak at 358 nm. Table 5.1 lists the fluorescence peaks and shoulders observed at the indicated excitation wavelength. For comparison, the excitation and emission values of Yang et al.'s model C_5H_{11}-APE compound are also included. The 16k NH_2-PI-NH_2 and the 18k COOH-PI-COOH have the same spectrum, while the 32k NH_2-PI-NH_2 exhibits more peaks and shoulders at 377 nm, 385 nm, and 406 nm than the former two telechelics. The 54k COOH-PI-COOH exhibits the same fluorescence peaks between ~350 nm and ~375 nm as the other three telechelics, and in addition exhibits the expected APE peaks from ~390 nm to ~450 nm.

In an attempt to identify the origin of the unexpected fluorescence peaks in the tagged telechelics, the fluorescence of pure APE was compared with 54k COOH-PI-COOH. The maximum excitation wavelength of pure APE was observed at 388 nm.

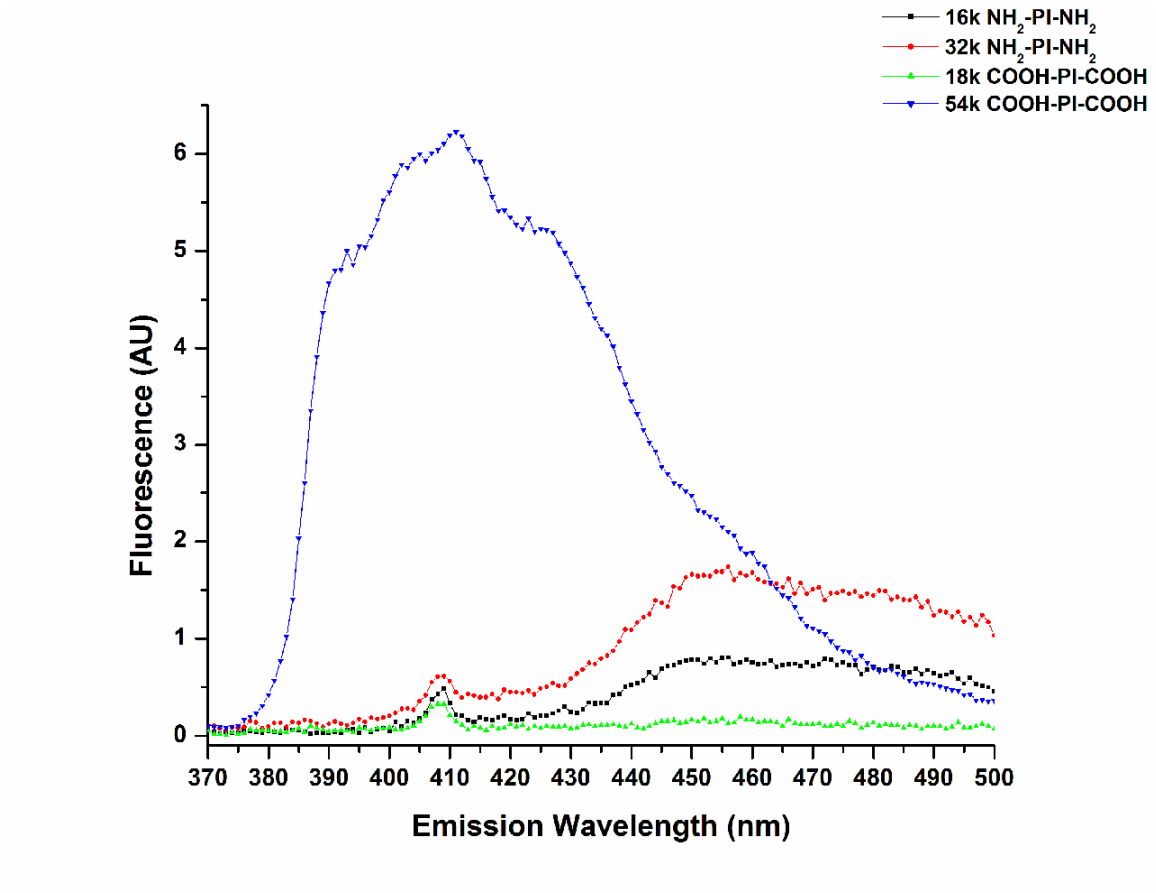

Figure 5.1. The fluorescence of telechelic PI excited at 364 nm.

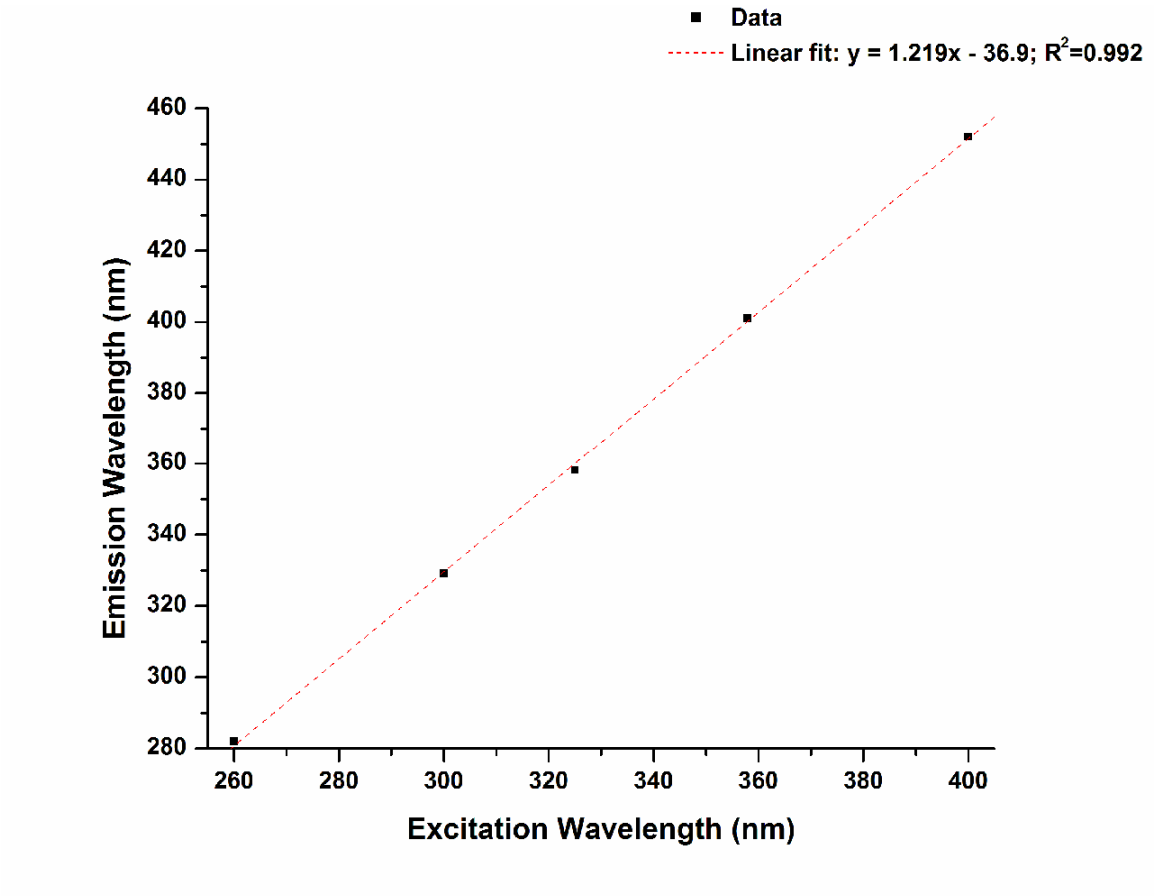

Figure 5.2. Emission wavelength as a function of excitation wavelength for HPLC grade THF.

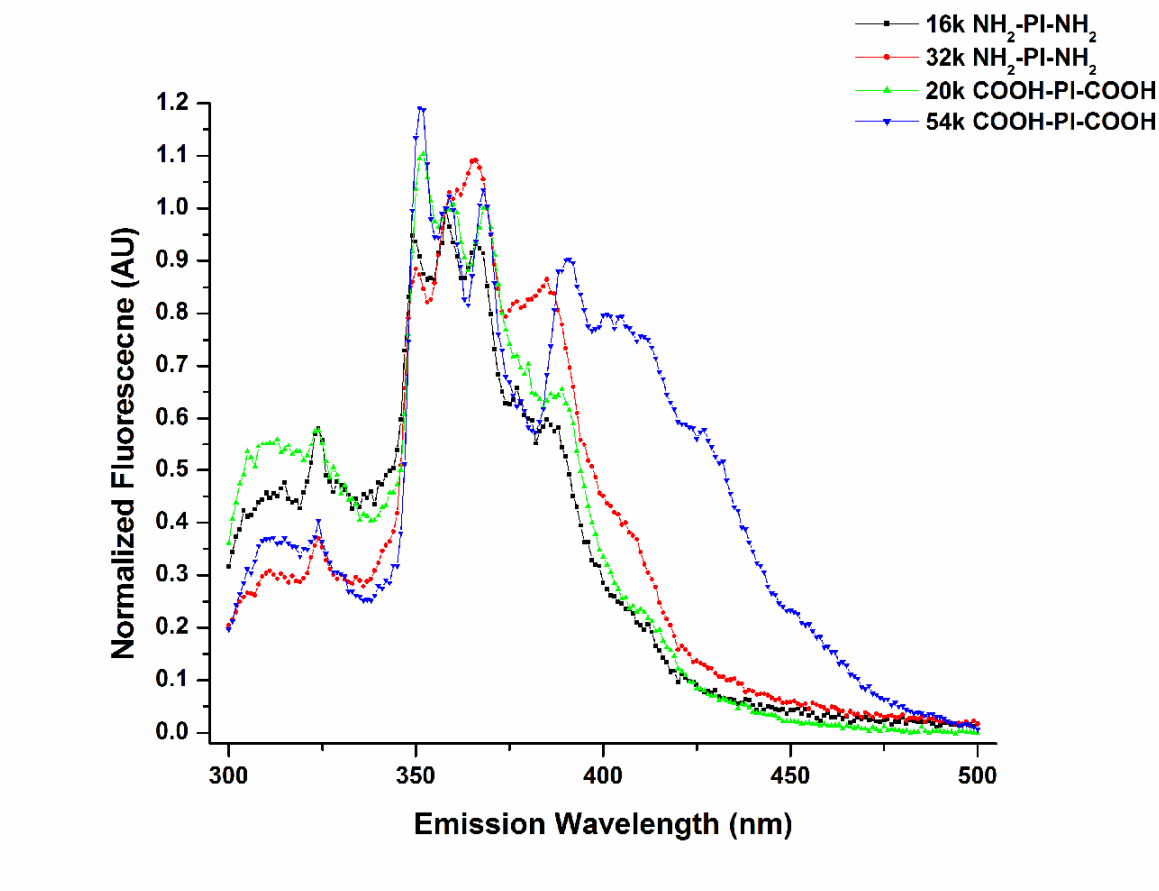

Figure 5.3. The 358 nm normalized fluorescence response of tagged telechelics excited at a wavelength of 295 nm.

Table 5.1. Fluorescence emission (Em) peaks and shoulders observed in the tagged telechelics at the maximum excitation (Ex) wavelength indicated.

Sample	Ex (nm)	Em (nm)	Em (nm)
C_5H_{11}-APE	330	391	
(Yang)	346	411	
	363	431	
	383		
16k NH_2-PI-NH_2	295	349	388
		358	396
		366	399
		377	412
		385	421
32k NH_2-PI-NH_2	295	350	394
		359	399
		366	406
		377	411
		385	421
		387	435
18k COOH-PI-COOH	295	352	389
		360	399
		369	406
		377	410
		380	415
		386	
54k COOH-PI-COOH	295	351	410
	(max)	359	421
		368	427
		378	432
		391	442
		401	450
		405	
54k COOH-PI-COOH	364	391	419
		393	423
		402	425
		405	435
		411	447
		415	451

This was close to the second most intense excitation peak discovered by Yang et al. for the C_5H_{11}-APE model compound, 383 nm. The fluorescence of APE and 54k COOH-PI-COOH normalized to the peak at 412 nm is shown in Figure 5.4 at various λ_{ex}. The emission wavelengths of pure APE excited at either 295 nm or 388 nm show a maximum at 412 nm and no fluorescence at emission wavelengths below 375 nm. The 54k COOH-PI-COOH excited at 295 nm or 364 nm shows a fluorescence response similar to APE between 375 nm – 500 nm. However, when 54k COOH-PI-COOH is excited at 295 nm, new fluorescence peaks are observed between ~300 nm – 380 nm which are not observed in pure APE excited at this same wavelength.

All four telechelics exhibit unexpected fluorescence between 300 nm and 380 nm. What could cause this fluorescence? Figures 5.1 and 5.3 demonstrate that λ_{ex} = 295 nm must be used for all of the telechelics to exhibit fluorescence. It is clear from Figure 5.4 that with λ_{ex} = 295 nm, the fluorescence response between ~300 nm – 375 nm is not from APE itself, as APE does not exhibit any fluorescence response until ~375 nm. However, the fluorescence peaks observed between 340 nm and 380 nm could be caused by a similar conjugated ring system, such as phenanthrene. Phenanthrene has a similar structure to anthracene, as shown in Figure 5.5, but a much different absorption and emission spectrum. A direct energy transfer (DET) experiment by Ni et al. used 1-(9-phenanthry1)-1-phenylethane) as an energy donor and 1-(2-anthryl)-l-phenylethane as an energy acceptor.[196] These compounds are shown in Figure 5.6, and are quite similar to the APE tag used in this study. In a DET experiment, the donor is excited by an external source. The emission spectrum of the donor overlaps the absorption spectrum of the acceptor. If the acceptor molecule is close to the donor molecule, the energy emitted by

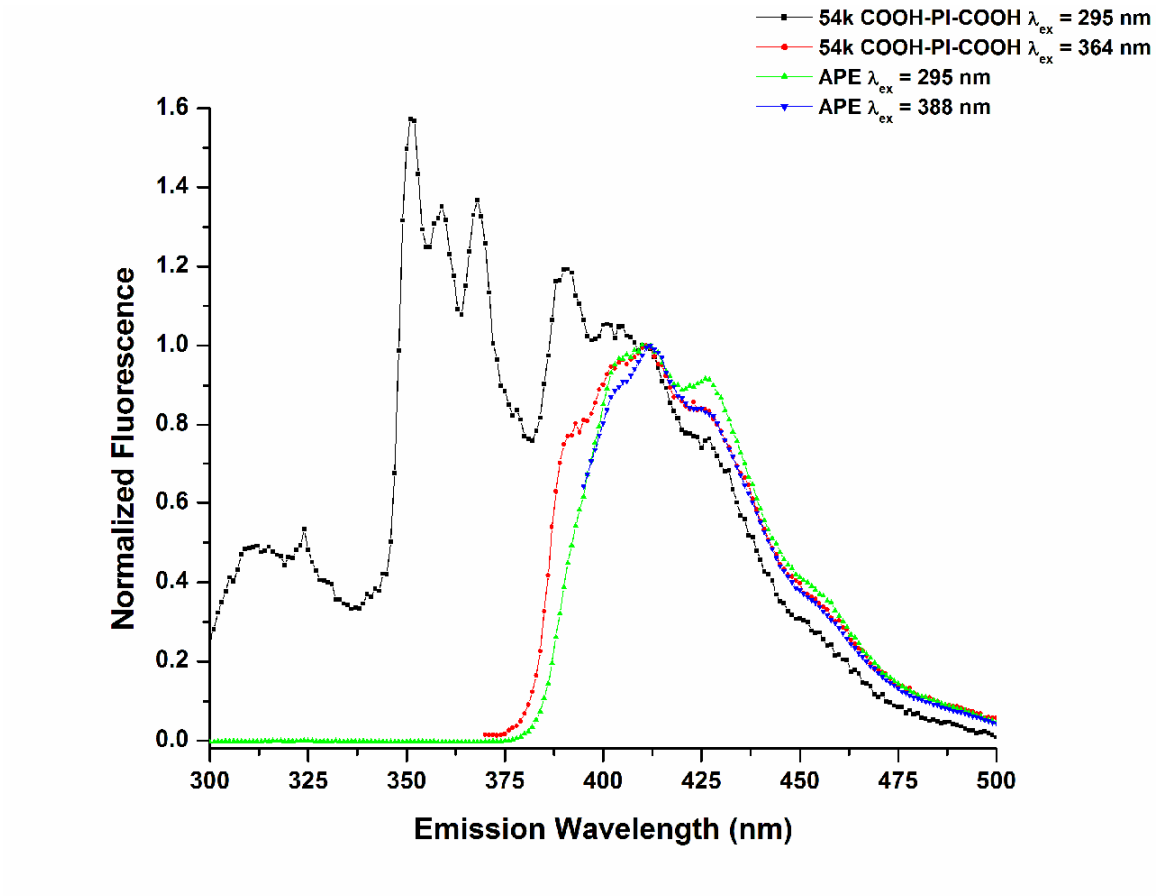

Figure 5.4. The normalized fluorescence of pure APE and APE-tagged 54k COOH-PI-COOH at the expected excitation wavelengths (364nm, 388 nm) and the shorter excitation wavelength (295 nm) found in the other tagged telechelics.

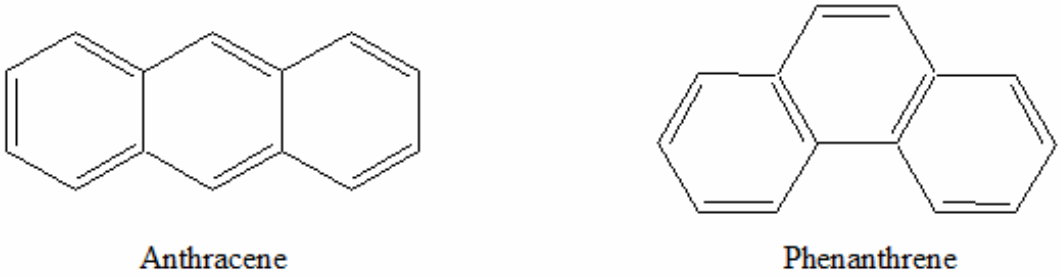

Figure 5.5. Structure of anthracene (left), which is part of the APE tag, and phenanthrene (right).

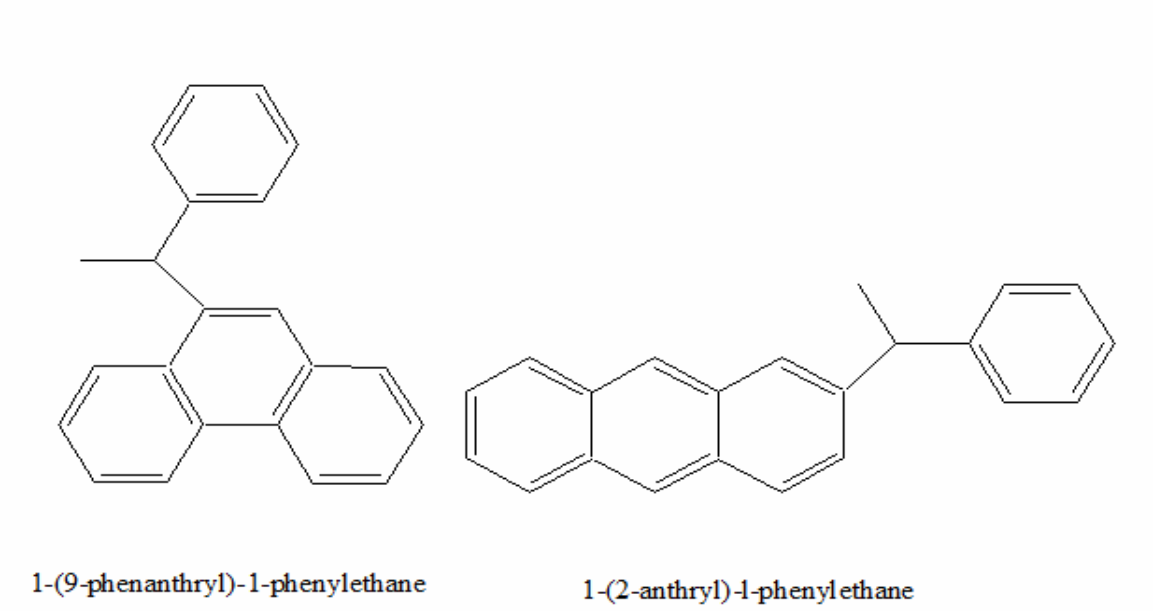

Figure 5.6. Structures of the donor (left) and acceptor (right) compounds used in a DET study by Ni et al.

the donor molecule causes the acceptor molecule to be excited and subsequently fluoresce itself. Thus the acceptor molecule fluoresces by indirect excitation. Ni et al. showed the phenanthryl compound had a maximum excitation wavelength at 298 nm and several emission peaks between ~340 nm – 450 nm. The anthryl compound was found to have strong absorption between ~320 nm – 390 nm, which directly overlaps the region where 1-(9-phenanthry1)-1-phenylethane) fluoresces. The fluorescence region of 1-(2-anthryl)-l-phenylethane is between ~360 nm – 500 nm. The results of this study by Ni et al. are shown in Figure 5.7, from ref. 190. Therefore there may exist phenanthryl or other structurally similar impurities formed in the fluorescently tagged polymers used in this study. Since the fluorescent peaks observed between 300 nm and 380 nm are not found in pure APE, some alteration of the APE tag must have occurred when it was incorporated into the polymer during the synthesis, resulting in the presence of both

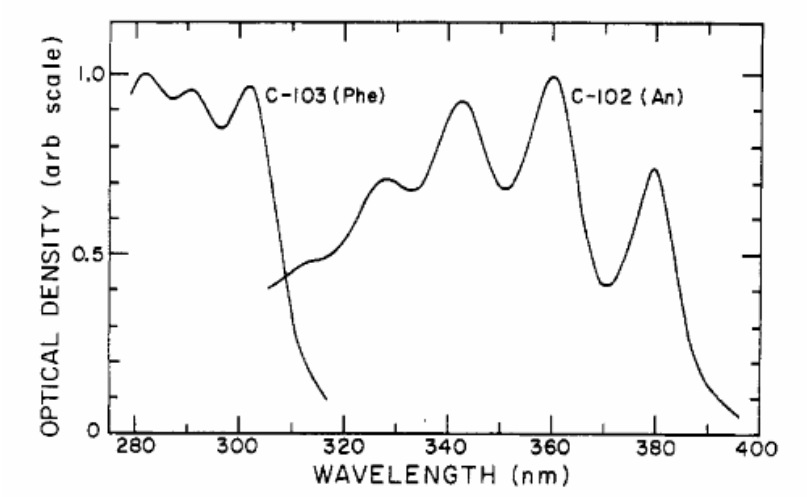

Figure 5.7. UV absorption (left) and fluorescence (right) spectra by Ni et al. for the 1-(9-phenanthry1 phenylethane), shown as C-103, and 1-(2-anthryl)-l-phenylethane, shown as C-102.

phenanthryl and anthryl species. The difference in the fluorescence spectra between a 2-substituted anthryl group, studied by Ni et al., and a 1-substituted anthryl group, such as the tag used in this study, was found to be minimal.[113]

Schillen et al. conducted a DET study in which both 9-phenanthryl and 2-anthryl groups were attached to a phenyl alkane.[197] The 9-phenanthryl compound had a maximum absorption at 300 nm and a maximum emission at 348 nm. When some of the 2-anthryl compound was added to the solution and excited at 300 nm, there was fluorescence from both compounds. The fluorescence in the region of λ_{em} = 345 nm – 360 nm was attributed to the 9-phenanthryl group, while the fluorescence of λ_{em} > 360 was due to the 2-anthryl group. It was also demonstrated that as the mole fraction of the acceptor group, the 2-anthryl compound, was increased, the fluorescence intensity in the region λ_{em} > 360 increased while the fluorescence in the λ_{em} = 345 nm – 360 nm region remained constant.

Polystyrene is known to have absorption peaks at 254 nm, 262 nm, and 269 nm.[198] It has also been shown that for polystyrene, an absorption peak near 260 nm is due to a single phenyl group, while an absorption near 295 nm is due to interaction between a ground state and excited state polystyrene phenyl group,[199] which are known as excimers. An excimer is a conformational structure formed when two aromatic rings are aligned in a coplanar sandwich. Excitation of one of the rings in the pair by absorption of energy in the near-ultraviolet range may lead to an electronically excited dimer, or excimer. The broad structureless fluorescence of the excimer is much different from the structured fluorescence profile of the isolated aromatic ring, or monomer.[200] Polystyrene excimers fluoresce at 335 nm.[198] If the APE tag degrades, a PS-like structure could be formed if the anthracene group was cleaved from the tag. The presence of PS-like excimers could explain the large, unexpected absorbance near 295 and a broad structureless fluorescence near 310 nm, displayed in Figure 5.3. However, one problem with this explanation is that excimer fluorescence of PS at 335 nm is only due to adjacent phenyl rings that are three carbon bonds away. When methanol is added to a solution of polystyrene dissolved in tetrahydrofuran in order to make the polymer interact more with itself than the non-solvent methanol, the excimer contribution to the fluorescence does not increase, indicating that the excimer peak can only be attributed to interaction between phenyl rings three carbon bonds away from each other on the same polymer chain.[199] Since there is no possible way for aromatic rings in the fluorescent tag to be three bonds away from each other in these telechelic samples, the absorption near 295 nm and the broad structureless fluorescence peaks near 310 nm cannot be from PS-like excimers. In

addition, the telechelics were analyzed at lower concentrations in order to avoid excimer formation, and the same fluorescence response was observed as previously described.

B. Optimization of Tagged Telechelic Fluorescence

The cause of the unexpected fluorescence in the telechelics could not be definitely determined. Therefore, an excitation wavelength λ_{ex} = 295 nm and an emission wavelength λ_{em} = 385 nm were used for the fluorescence detection of APE-tagged polymers by GPC. While the most intense absorption wavelength was used for excitation, 385 nm was used for emission rather than the most intense fluorescence emission peaks between 350 nm – 366 nm because the former emission wavelength resulted in a stronger response from the fluorescence detector. This could be due to subtracting the intense fluorescence of the THF mobile phase in the 350 nm – 366 nm range. The fluorescence of THF was monitored in the fluorometer to determine the extent of background fluorescence due to the solvent. The excitation slit width was set to 16 nm, and the emission slit width was set to 8 nm to mimic the specifications of the GPC fluorescence detector described in Chapter 2.4 A. The excitation wavelength was varied while the detector gain was kept constant. The fluorescence response of THF is shown in Figure 5.8, which shows THF has significant fluorescence when excited at wavelengths up to 310 nm. Therefore, at an excitation wavelength of 295 nm, there is still significant solvent fluorescence between 350 nm – 366 nm. By using an emission wavelength of 385 nm, the fluorescence intensity of the tagged telechelic is only reduced slightly, but the solvent fluorescence diminishes significantly.

An excitation wavelength of 257 nm, corresponding to the excitation of a phenyl ring, can also be used to monitor the fluorescence of the APE tag. To examine this

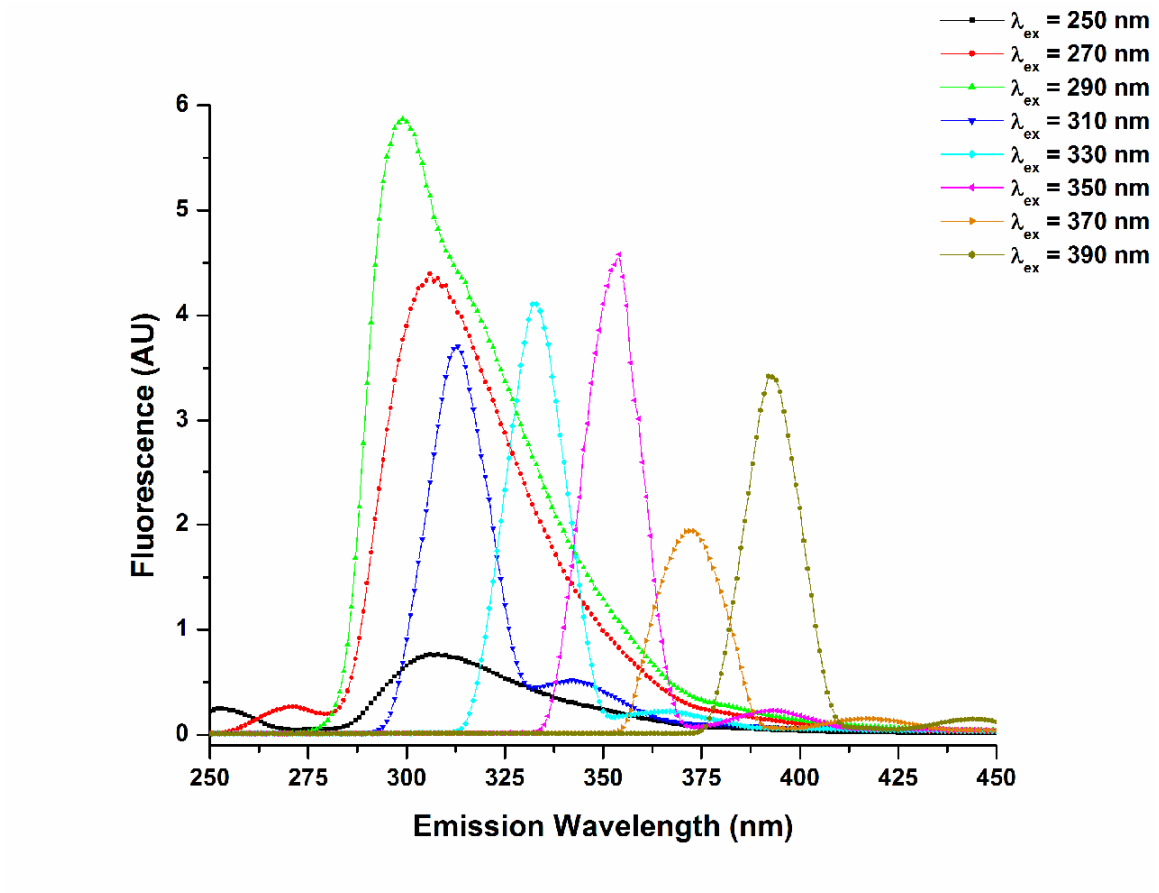

Figure 5.8. Fluorescence of THF excited at various wavelengths.

possibility, a polymer solution containing 97.5 wt.% PS and 2.5 wt.% 32k NH_2-PI-NH_2 was examined at different combinations of excitation and emission wavelengths, with the results shown in Figure 5.9. It is clear that a wavelength that excites the phenyl ring of the APE tag cannot be used to study this blend because the PS fluoresces as well, demonstrated by the detector response between an elution time of 11 and 13.5 minutes. Figure 5.11 also confirms that choosing an emission wavelength of 385 nm produces a much stronger signal than an emission wavelength of 366 nm.

To ensure fluorescence quenching was not occurring, the fluorescence response of 16k NH_2-PI-NH_2 in concentrations ranging from 0.25 - 2.0 mg/ml was monitored at λ_{ex} = 295 nm, λ_{em} = 385 nm, and gain = 100. The response was found to be linear, as shown in Figure 5.10.

5.3 Fluorescence of Compatibilized Blends

A. Monitoring the Reaction of Melt Mixed Telechelics

The reaction between the anhydride and amine telechelics was monitored by melt mixing 37k anh-PS-anh and 16k NH_2-PI-NH_2 together in stoichiometric amounts, as described in Chapter 2.2. The two telechelics were melt mixed under argon at 180 °C with a rotor speed of 100 RPM for 5, 10, 20, and 60 minutes. A small aliquot was taken at each time interval and quenched at room temperature. Samples were then analyzed by GPC with fluorescence detection with λ_{ex} = 295 nm, λ_{em} = 385 nm and gain = 100. The chromatograms of the blends containing the APE-tagged material were normalized to have the same area and the results are shown in Figure 5.11. With the exception of the 60 minute sample, the amount of higher molecular weight copolymers formed, indicated by the increase in signal response from 11 – 14 minutes, increases with mixing time. This

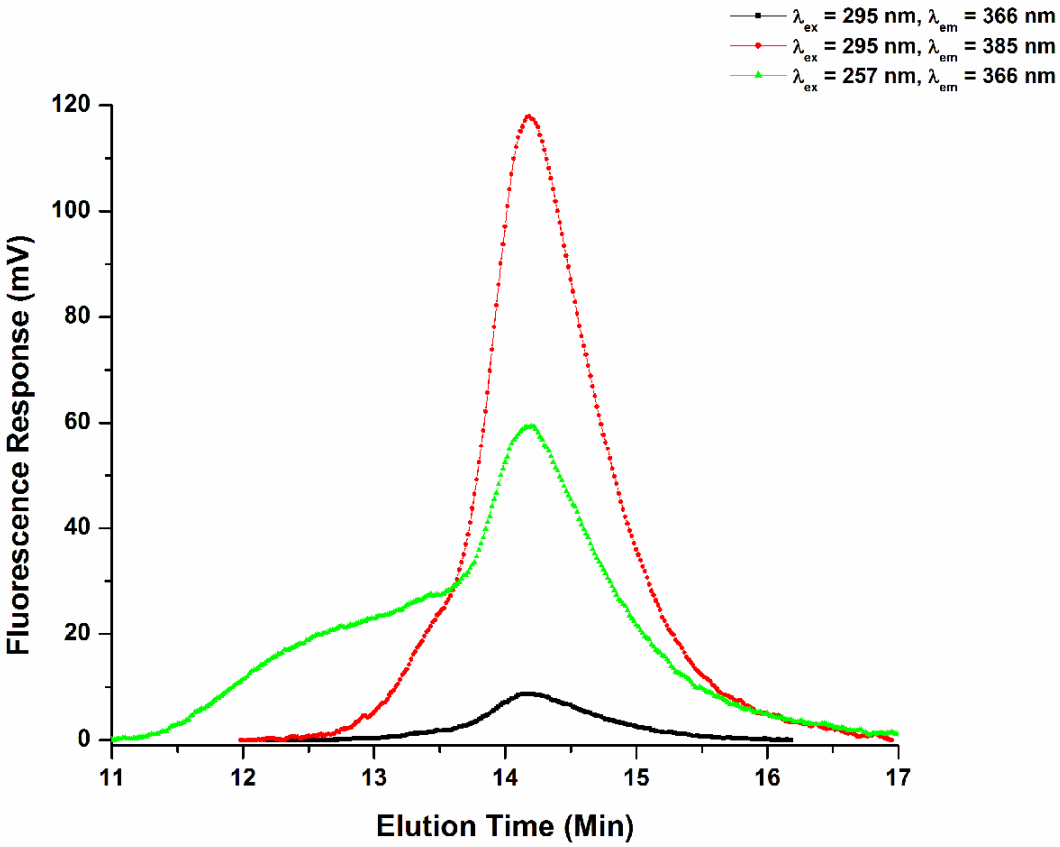

Figure 5.9. GPC fluorescence detector response as a function of elution time for a polymer solution containing 97.5 wt.% 77k PS and 2.5 wt.% 32k NH_2-PI-NH_2.

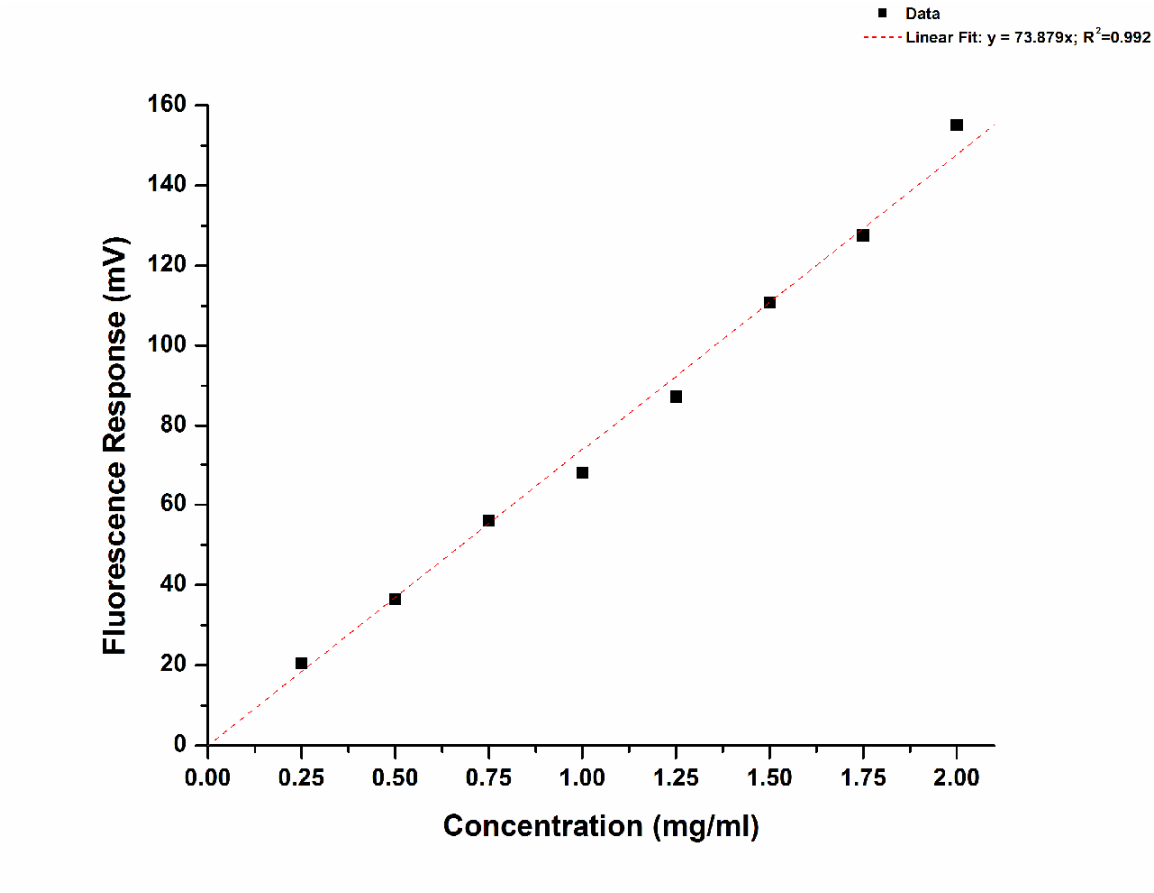

Figure 5.10. 16k anh-PS-anh fluorescence response as a function of concentration.

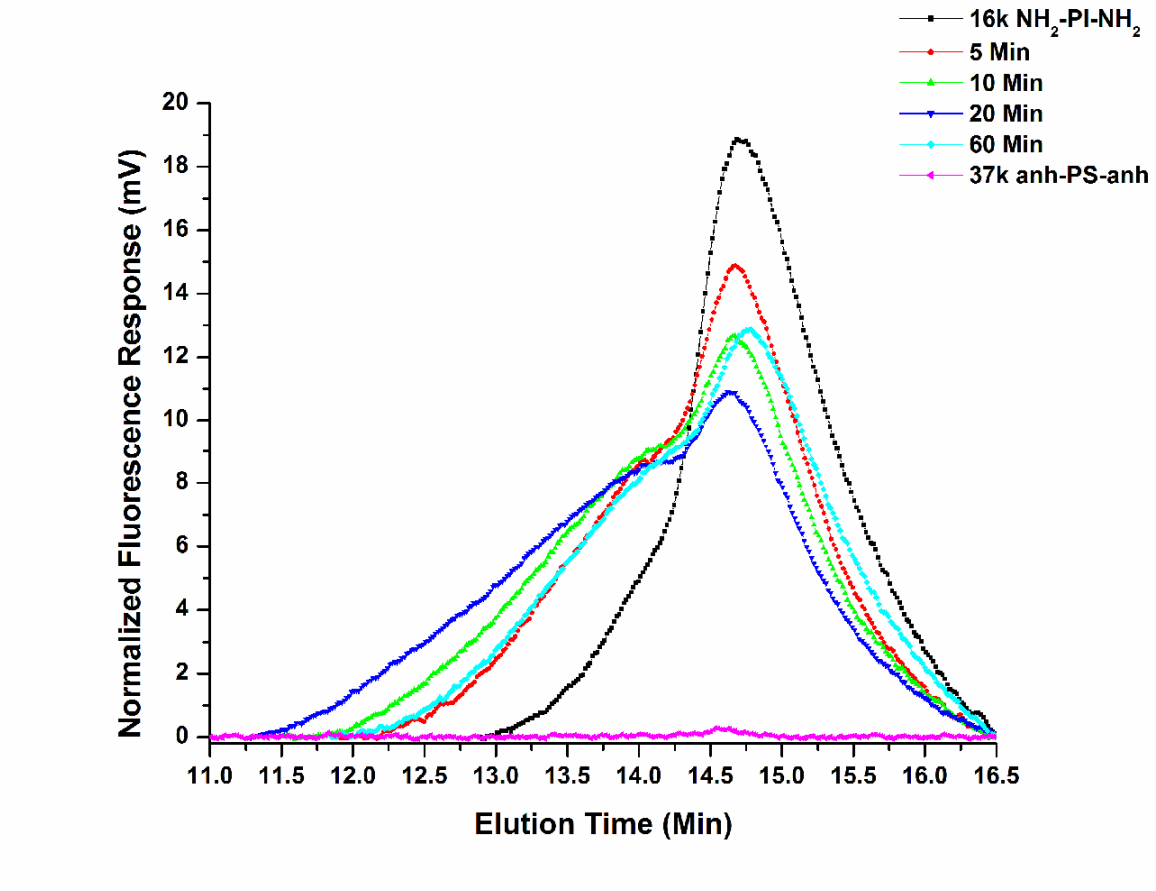

Figure 5.11. Area-normalized fluorescence response of 37k anh-PS-anh/16k NH_2-PI-NH_2 melt mixed blends as a function of elution time for various mixing times.

confirms that larger copolymers are being created *in situ* from smaller starting material. It should be noted that the fluorescence response was truncated after 16.5 minutes because of low intensity fluorescence that continued until an elution time of 18 minutes. These elution times correspond to very low molecular weights. A time of 16.5 minutes was chosen because the GPC refractive index detector (RI) signal of the 16k NH_2-PI-NH_2 approaches zero at an elution time of 15.9 minutes, and there is a 0.6 minute delay time between the RI detector and the fluorescence detector. The fluorescence detector is ~100 times more sensitive than the RI detector, and thus responds to low level impurities, which could account for the low level of fluorescence (< 2 mV) observed beyond 16.5 minutes. Additionally, if the entire fluorescence signal up to 18 minutes was included in the analysis, the polydispersity index of the peak deviates from that of the RI signal. Thus, for the creation of a baseline, the endpoint was taken to be 16.5 minutes.

B. Fluorescence of Compatibilized Polymer Blends

Blends consisting of 5.0 wt.% telechelics and 90% PS/10% PI homopolymers were melt mixed under argon at 180 °C and 100 RPM for 5, 10, 20, and 60 minutes according to the procedures discussed in Chapter 2.2. Figure 5.12 shows a typical fluorescence detector chromatogram for blends made with the anhydride and amine telechelics, represented here by a 90% PS/10% PI + 5.0 wt.% 16k anh-PS-anh/16k NH_2-PI-NH_2 blend melt mixed for 10 minutes. In order to separate the fluorescence contribution due to the copolymer formed *in situ* and the unreacted telechelic from that of the PS and PI, the homopolymer fluorescence contribution was first subtracted from the chromatogram. To accomplish the homopolymer subtraction, a blend containing only homopolymers of the same weight fraction as the compatibilized blend was melt mixed

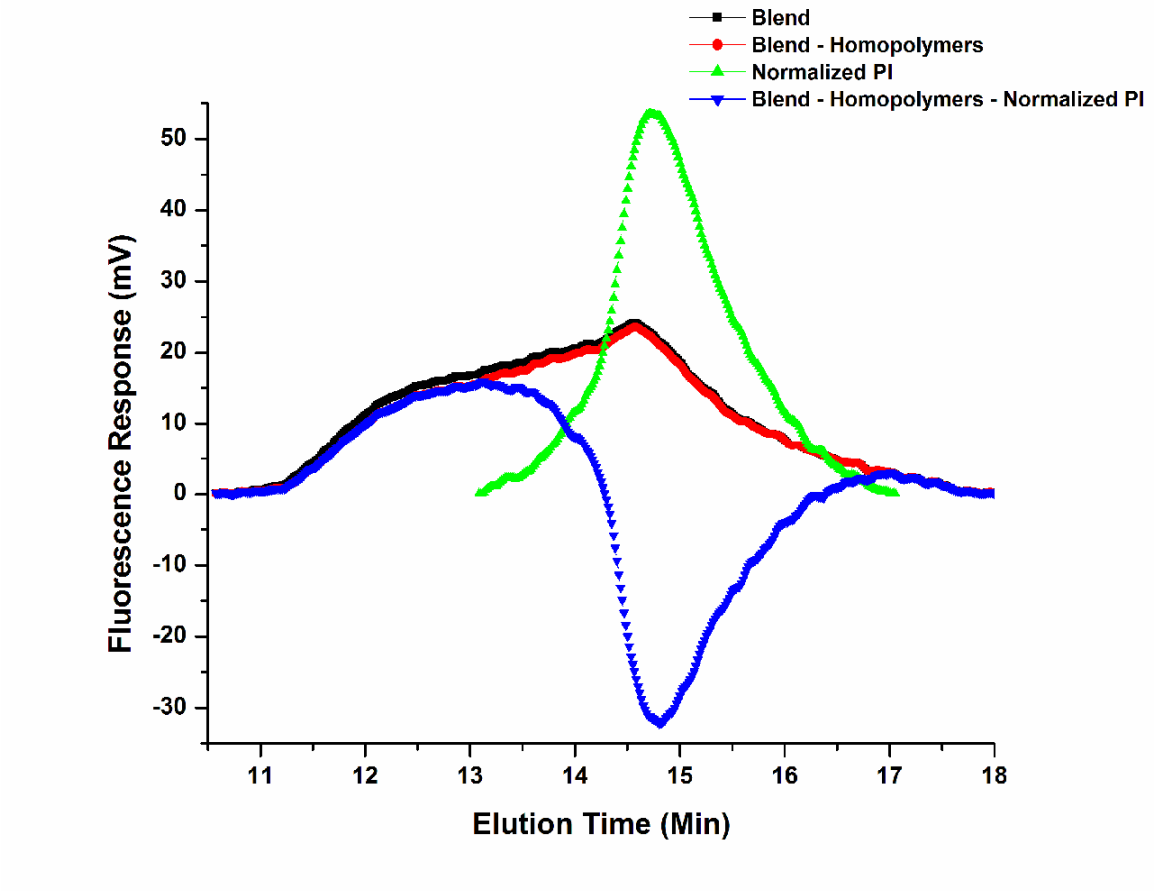

Figure 5.12. Fluorescence response as a function of elution time for the anh-PS-anh/NH_2-PI-NH_2 system.

for various times. This sample was then analyzed by GPC to determine the homopolymer fluorescence contribution. For instance, for a blend compatibilized with 5.0 wt.% telechelics that was analyzed at a concentration of 2.0 mg/ml by GPC, a melt mixed homopolymer sample was analyzed at 1.9 mg/ml. The resulting homopolymer chromatogram was subtracted from the blend chromatogram. This is shown as the red curve in Figure 5.12, whose signal should now only be due to copolymer created *in situ* and the remaining unreacted PI telechelic. The area of the red curve was calculated using Origin 6.0. The area of the pure telechelic PI peak was normalized to have the same area as the red *blend – homopolymers* curve, as both curves contain the same amount of tagged telechelic PI. The normalized PI chromatogram, represented by the green curve in Figure 5.12, is then subtracted from the *blend – homopolymers* curve to yield a chromatogram which represents the fluorescence due only the copolymer formed *in situ*, shown in blue. The positive area of the blue curve in Figure 5.12 at elution times less than that of the unreacted telechelic represents the higher molecular weight block copolymer formed during mixing, while the negative area of the blue curve represents the telechelic PI that was consumed in the condensation reaction between telechelic reactive groups.

Figure 5.13 shows results typical for the epoxy/COOH systems, showing the results for a sample of 90% PS/10% PI + 5.0 wt.% 44k epoxy-PS-epoxy/54k COOH-PI-COOH melt mixed for 10 minutes. As expected, the less reactive epoxy/COOH pair showed a much lower conversion of copolymer, demonstrated by the small peaks observed at elution times of 12 – 13 minutes in Figure 5.13. Additionally, significant peak tailing was observed in all the epoxy/COOH blends, which was unexpected. This

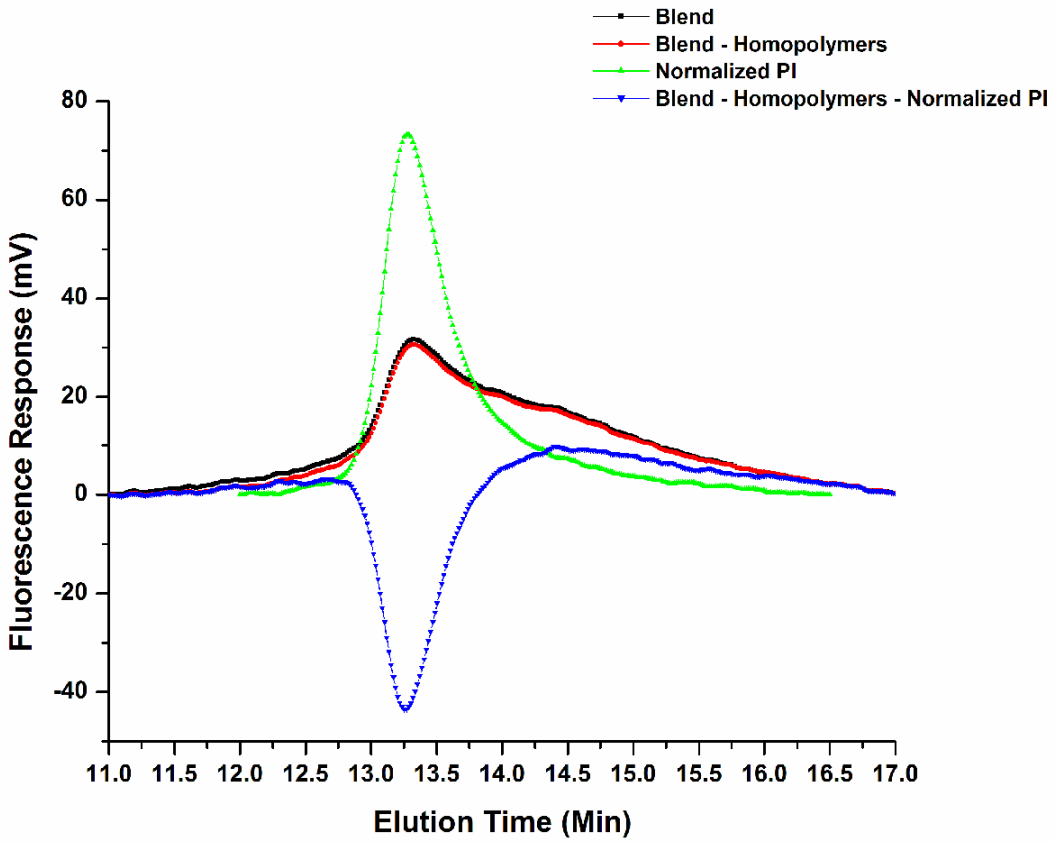

Figure 5.13. Fluorescence response for the epoxy/COOH system. The descriptions of the types of chromatograms shown are the same as in Figure 5.12.

occurred for all mixing times and molecular weight combinations of the epoxy/COOH pair.

5.4 Investigation of Peak Tailing in Fluorescence Spectra

Since unreacted telechelic COOH-PI-COOH showed no signs of tailing, the observed results are not due to COOH groups adsorbing to the column. To examine whether this observation was caused by thermal degradation of the telechelic PI, COOH-PI-COOH samples that were melt mixed for 0 minutes and 10 minutes were compared, with the results shown in Figure 5.14. The chromatograms in Figure 5.14 show no signs of the peak shifting to longer elution times after melt mixing, which would be indicative of degradation. To further investigate the cause of this peak tailing, various components of the blend were combined to identify which mixture contributed most to the tailing. Figure 5.15 shows the components melt mixed individually at 180 °C and 100 RPM for 10 minutes. The results in Figure 5.15 indicate that the primary cause of peak tailing is the interaction between COOH-PI-COOH and PS. Despite the fact that a 90% PS/10% PI homopolymer blend shows very weak fluorescence at all elution times for λ_{ex} = 295 nm and λ_{em} = 385 nm, an increase in the peak tailing occurs when either homopolymer is melt mixed with the fluorescently tagged telechelic. The peak tailing as a result of interactions with the homopolymer PS is the most dramatic. This interaction was observed when the 54k COOH-PI-COOH was melt mixed with bulk PS, ATRP synthesized PS, and anionically synthesized PS at 180 °C at 100 RPM for 10 minutes, as shown in Figure 5.16. It is possible for the COOH group of the telechelic to react with an OH end group of the polystyrene, forming an ester.[114] To confirm that the observed tailing was in fact from an interaction between the PS and COOH groups, pure PS was

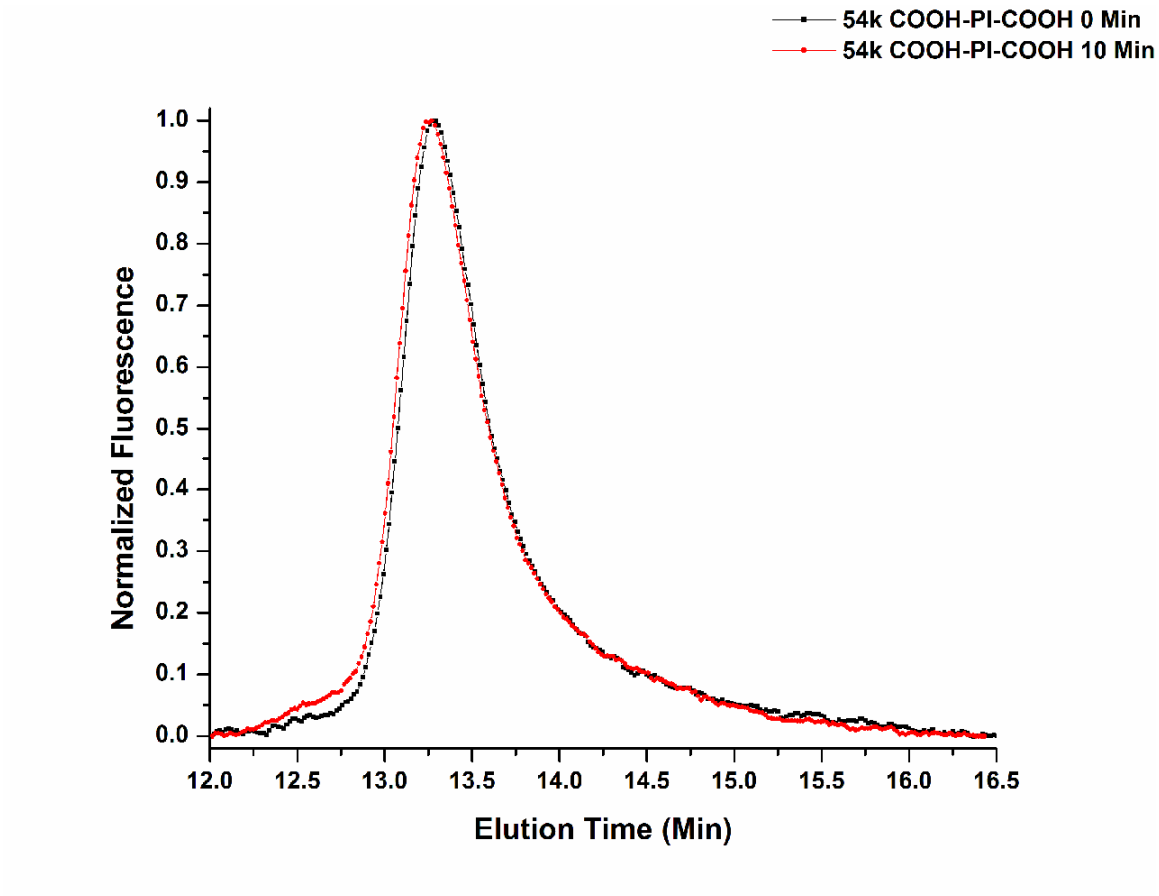

Figure 5.14. Comparison of normalized fluorescence response as a function of elution time for 54k COOH-PI-COOH melt mixed for 0 and 10 minutes at 180 °C and 100 RPM.

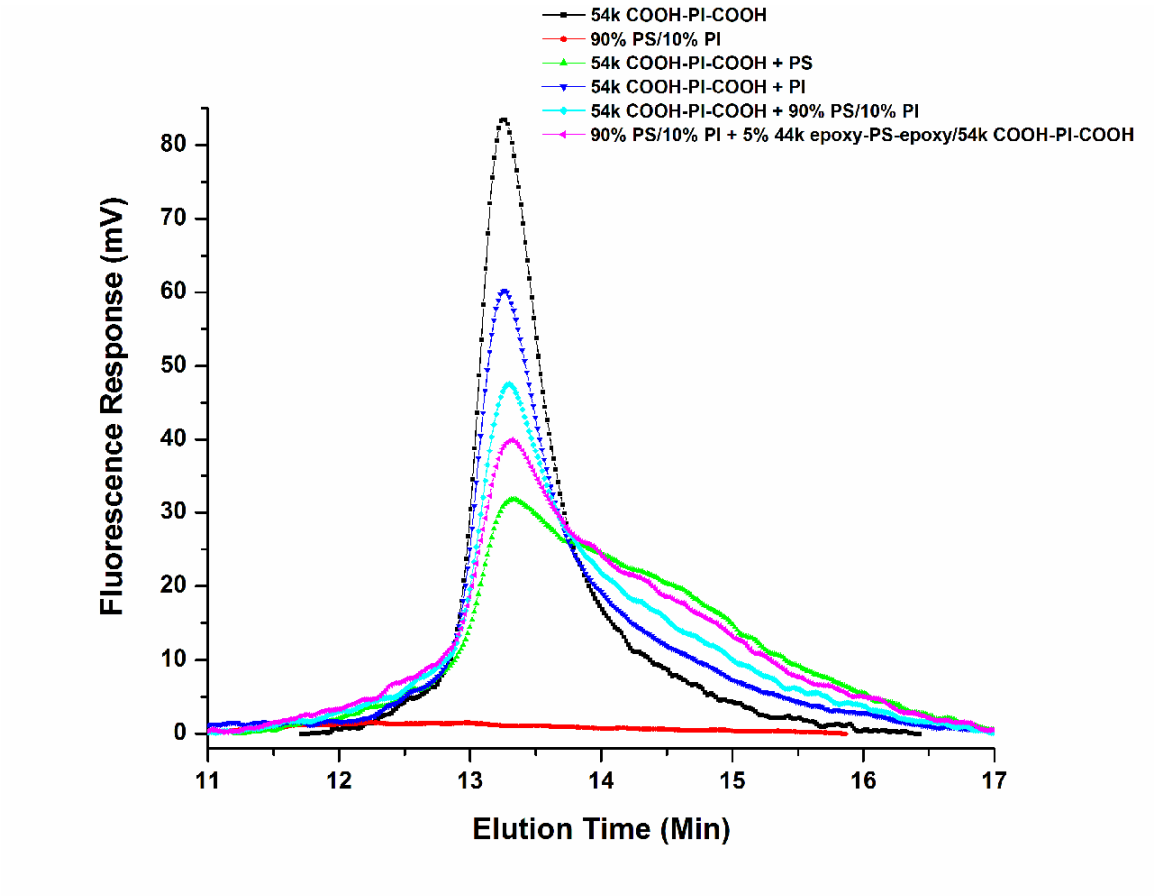

Figure 5.15. Fluorescence response as a function of elution time for 54k COOH-PI-COOH melt mixed with various blend components.

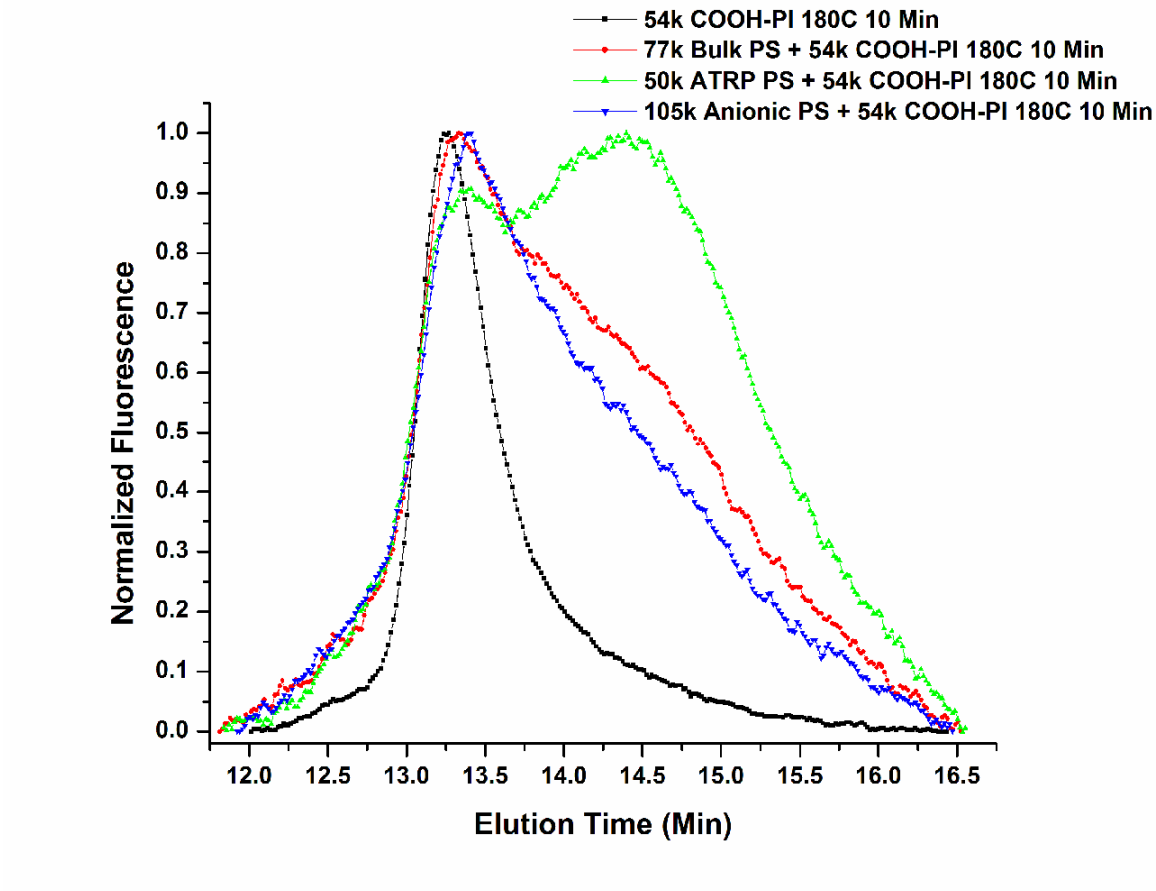

Figure 5.16. Normalized fluorescence as a function of elution time for 54k COOH-PI-COOH melt mixed with PS, ATRP synthesized PS, and anionic synthesized PS at 180 °C and 100 RPM for 10 minutes.

melt mixed at 180 °C for 10 minutes and compared to a sample consisting of 15 mg azelaic acid (HOOC-$(CH_2)_7$- COOH) and 530 mg PS that was melt mixed at 180 °C for 10 minutes. A broad peak resulted when azelaic acid was added to the PS, confirming that the observed tailing is from COOH interactions with PS, as seen in Figure 5.17.

At the same sample concentration of 2 mg/ml, the interaction of azelaic acid with polystyrene increased the fluorescence intensity by approximately a factor of 5. Neither component is strongly fluorescent, so what causes the increase in intensity? Experimental evidence indicates that substituted polystyrene has a more intense fluorescence than unsubstituted polystyrene. It is believed that the disruption of the π bond symmetry of the phenyl ring caused by substitution leads to an increased electronic transition in the polystyrene.[198] While a reaction between a COOH group and a phenyl ring seems unlikely, it has also been shown that benzene preferentially interacts with acidic hydroxyl groups, forming hydrogen bonds.[201] Thus if the symmetry of the π bonds in the PS phenyl ring are disturbed by interaction with a COOH group, it may be possible for the PS to exhibit enhanced fluorescence when it is melt mixed with COOH-bearing compounds. The azelaic acid is a small molecule containing a relatively high end group concentration, thus there exists many COOH – aromatic ring interactions in this sample blend. The small increase in peak tailing of 54k COOH-PI-COOH melt mixed with PI is most likely due to the overlap of PI homopolymer fluorescence between the 13 – 15 minute elution time regime, as Figure 2.1 demonstrates.

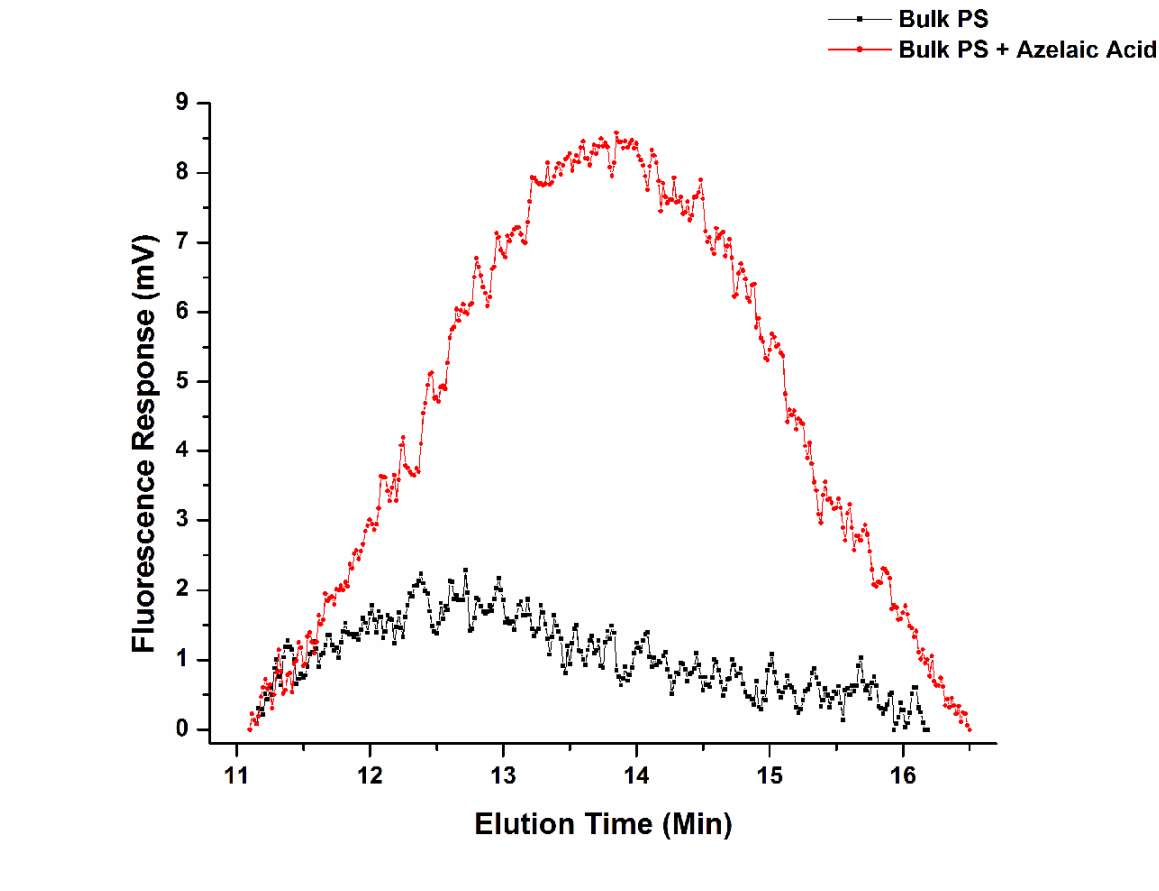

Figure 5.17. Fluorescence response of 2 mg/ml solutions of PS and PS with azelaic acid as a function of elution time. Both polymer samples were melt mixed at 180 °C and 100 rpm for 10 minutes.

5.5 Calculation of Multiblock Copolymer Conversion and Molecular Weight

The chromatograms of the homopolymers, the tagged telechelic PI, and the blend were collected with fluorescence detector settings of λ_{ex} = 295 nm, λ_{em} = 385 nm, and gain = 1000 for various mixing times using Cirrus GPC software. The resulting conversion and molecular weight of the multiblock copolymer formed were determined in the following manner using Origin 6.0 software. First the elution times were corrected for temperature and pump speed fluctuations by multiplying by a correction factor (phenyl isocyanate elution time during calibration divided by elution time during sample collection). Signal responses were smoothed using a Savitzky-Golay filter,[202] which was a 5 point 1st degree polynomial. This resulting data was then baseline corrected. Except for the telechelic PI, the chromatograms of the *homopolymers*, *blend – homopolymers*, and *blend – homopolymers – normalized PI* were obtained at various mixing times as described in Chapter 5.3 B. Conversion of telechelic PI into multi block copolymers was calculated by dividing the positive copolymer area in the *blend – homopolymers – normalized PI* chromatogram by the *blend – homopolymers* area. To calculate the average size of the multiblock formed, the positive signal from the *blend – homopolymers – normalized PI* chromatogram was baseline corrected in Origin and then input into Cirrus GPC software for analysis. Since many different block length combinations are created during copolymer formation, the calculated M_n of the copolymer was therefore used to obtain an estimate of the average number of copolymer blocks formed *in situ*. Adding possible combinations of telechelic PS and PI and comparing them to the value calculated by the software determined the average block size. For example, a tetrablock copolymer formed by reacting 37k anh-PS-anh and 16k NH_2-PI-NH_2 is expected to have

an average molecular weight of 106,000. It should be noted that the GPC software calculates the copolymer molecular weight with polystyrene standards, so the PI molecular weight was multiplied by a factor of 1.6 in the estimation of copolymer blocks to account for the different hydrodynamic radius of this polymer. Thus, the apparent molecular weight of this tetrablock is 125,000 when analyzed using PS standards.

The conversion of various molecular weight telechelic pairs at mixing times of 5, 10, 20, and 60 minutes for both 95% PS/5% PI and 90% PS/10% PI homopolymer compositions with 5.0 wt.% telechelics were determined. The reproducibility of the conversion was verified, where the results show very good reproducibility. Figure 5.18 and Figure 5.19 show the conversion of anh/NH_2 and epoxy/COOH telechelic pairs as a function of mixing time, respectively. In the two graphs, the labels 95/5 or 90/10 refer to the PS and PI weight percent composition of the blend, respectively. The second set of numbers refers to the molecular weight of the telechelic pairs.

With the exception of the 83k anh-PS-anh/32k NH_2-PI-NH_2 samples, Figure 5.20 indicates all blends containing 10 wt.% PI had a higher telechelic conversion than the blends with only 5 wt.% PI. These results can be rationalized by the fact that the blends containing 10 wt.% PI have a larger interfacial area that must be covered by the copolymer. Therefore a larger amount of telechelics is formed with increased minor phase content.

Experimental results by Macosko et al.[49] showed that lower molecular weight telechelics have a higher conversion due to their higher concentration of end groups for a given volume of chains, and can approach the interface easier than high molecular weight telechelics. Based on these observed molecular weight effects, the 16k anh-PS-anh/16k

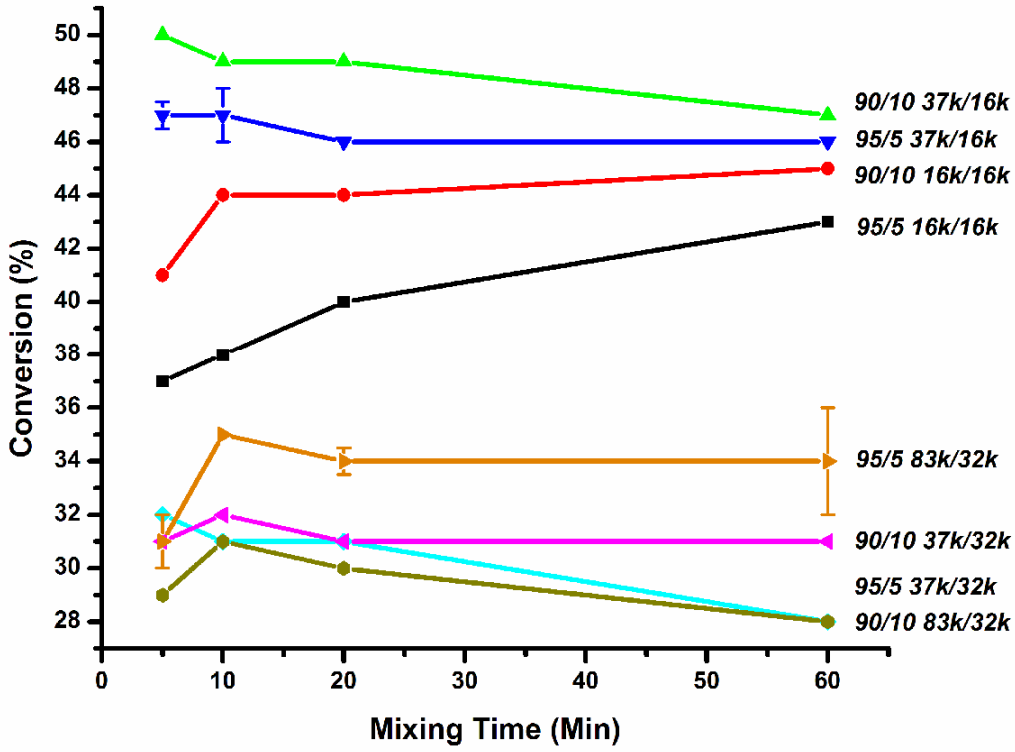

Figure 5.18. Conversion as a function of mixing time for blends containing anh-PS-anh/NH_2-PI-NH_2 telechelic pairs.

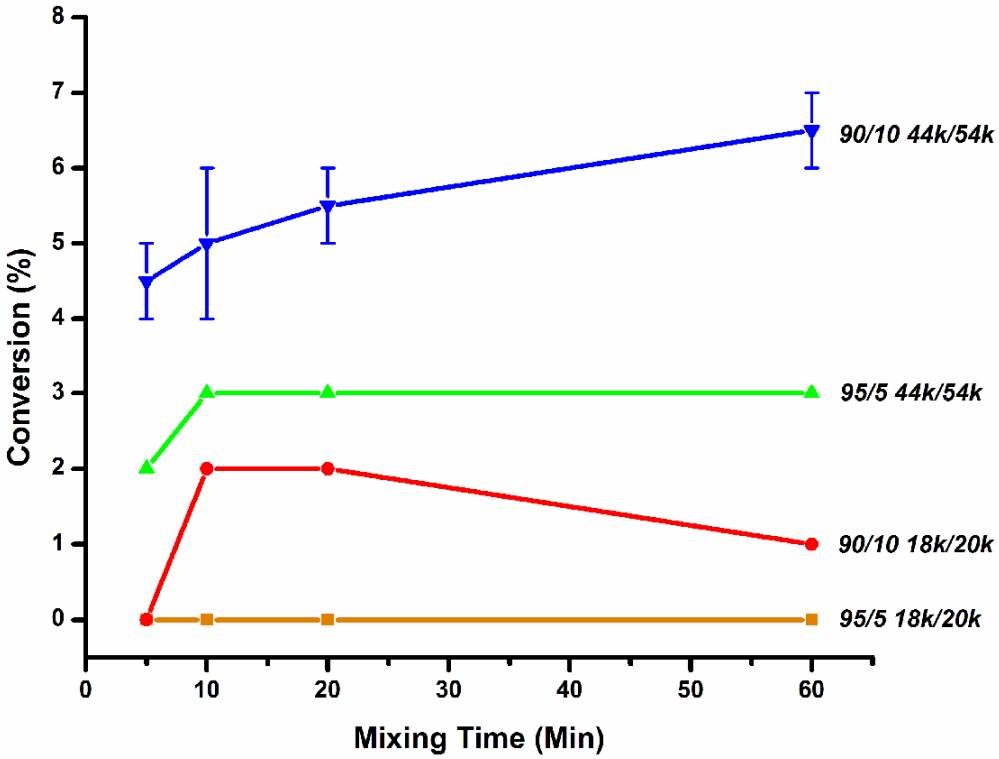

Figure 5.19. Conversion as a function of mixing time for blends containing epoxy-PS-epoxy/COOH-PI-COOH telechelic pairs.

NH_2-PI-NH_2 pair in this study is expected to yield the highest conversion. However, results in Figure 5.18 show that the 37k anh-PS-anh/16k NH_2-PI-NH_2 pair had the highest conversion, rather than the 16k anh-PS-anh/16k NH_2-PI-NH_2 pair. When higher molecular weight 37k anh-PS-anh/32k NH_2-PI-NH_2 and 83k anh-PS-anh/32k NH_2-PI-NH_2 telechelics were used, the conversion decreased. This agrees with previous studies, as larger molecular weight telechelics have lower end group concentrations, and any copolymer formed at the interface will inhibit further reaction by approaching telechelics.[49] The same general trend is observed in the epoxy/COOH system. Figure 5.21 shows that the telechelic conversion is higher in the 44k epoxy-PS-epoxy/54k COOH-PI-COOH blends than in the 18k epoxy-PS-epoxy/20k COOH-PI-COOH blends. Therefore these results appear to be due to a common molecular weight effect and are not dependent on the reactive pairs used.

To explain the lower conversion of the lowest molecular weight telechelics examined, it must be noted that the conversion is controlled by the chemical reactivity of the species, which takes tens or hundreds of seconds to observe, and not the diffusion of the chain to the interface, which occurs on a much faster time scale.[76,74] This means the reactive polymer samples the interface many times before reacting.[72,203] Moreover, the residence time of a chain at the interface will depend on its molecular weight, as a chain that is entangled will reside at the interface longer than an unentangled chain, resulting in a higher reaction probability.[203]

The time a reactive group spends at the interface is determined by the relaxation time of the polymer chain, τ. For an unentangled chain, $\tau \propto N^2$, whereas $\tau \propto N^3$ for an entangled chain, where N is the degree of polymerization.[69] A polymer with a molecular

weight greater than twice the entanglement molecular weight, M_e, exhibits entanglement dynamics.[85,204] The M_e of PS is ~13,000, and the M_e of PI is ~6,000.[142] Thus, the 16k anh-PS-anh chain is not well entangled, while the 37k anh-PS-anh chain is slightly above the critical molecular weight, M_c, required for entangled dynamics. All the telechelic PI used in this study are above M_c. Depending on whether we treat the 37k anh-PS-anh chain as fully unentangled or fully entangled, its relaxation time is ~4 – 30 times greater than the 16k chain, respectively. This results in the 37k chain remaining at the interface longer than the 16k chain, increasing the reaction probability, resulting in a higher conversion. The long reaction time behavior of the two telechelics agrees with this interpretation as the 16k anh-PS-anh/16k NH_2-PI-NH_2 conversion continuously increases and approaches the 37k/16k conversion value after one hour of mixing. With increased mixing time, all chains have sufficiently sampled the interface to achieve maximum conversion.

The average block size of the copolymers formed after 10 minutes of mixing for each reactive telechelic pair is shown in Figure 5.20. With the exception of the 18k epoxy-PS-epoxy/20k COOH-PI-COOH telechelic pair, the general trend is a decrease in the number of blocks formed with increasing telechelic molecular weight. This makes sense, because larger telechelics have a lower concentration of end groups and cause more steric hindrance at the interface, resulting in the formation of smaller copolymers (i.e. fewer blocks).

The average molecular weight of the multiblock copolymers formed after 10 minutes of melt mixing in the 90% PS/10% PI blends compatibilized with 5.0 wt.% telechelics is shown in Table 5.2. The molecular weights of the copolymers reported are

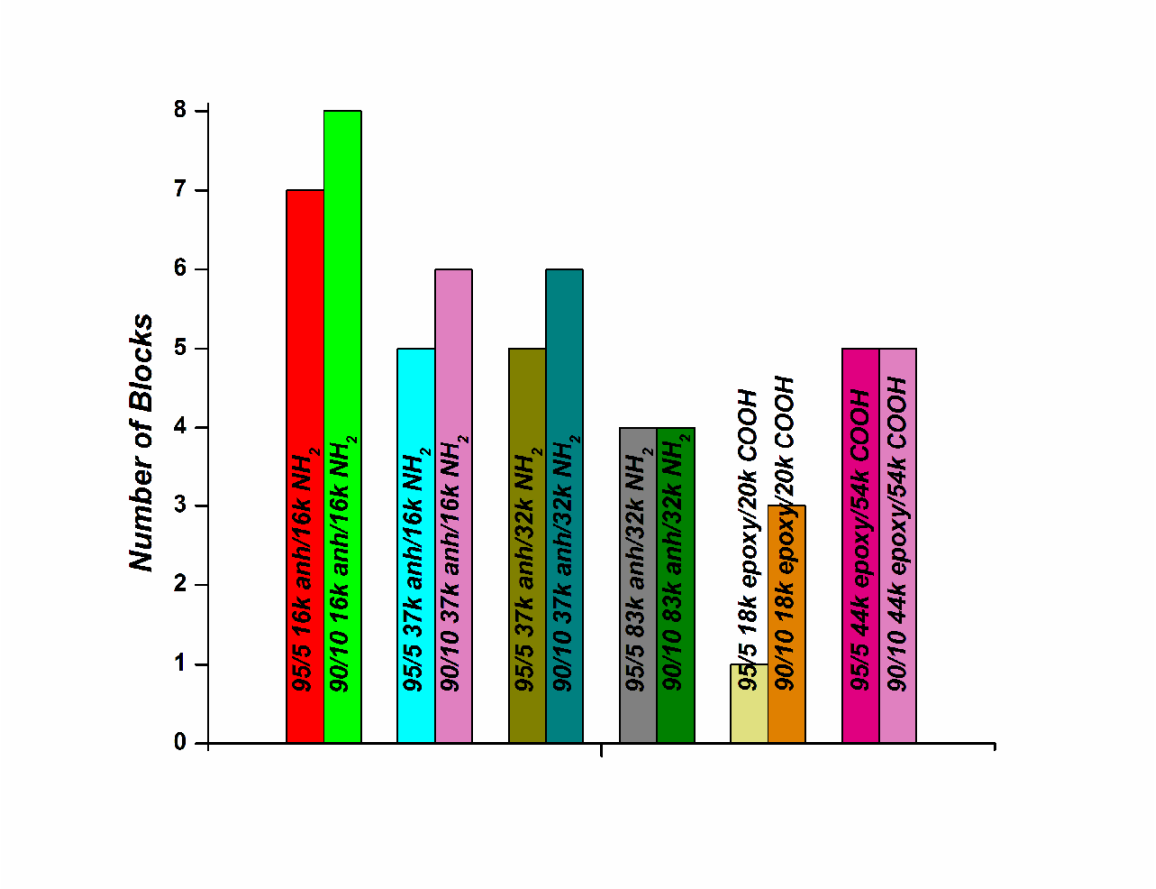

Figure 5.20. The average number of copolymer blocks formed after 10 minutes of mixing for various blend compositions based on the calculated M_n. The first number in the labels refers to the percent composition of homopolymer PS/PI.

Table 5.2. Calculated molecular weight of copolymers formed *in situ* after 10 minutes of melt mixing for 90% PS/10% PI blends compatibilized with 5.0 wt.% telechelics.

90%PS/10% PI + 5.0 wt.% Telechelics	Conversion %	Copolymer M_n	PDI	Blocks Formed
16k anh-PS-anh / 16k NH_2-PI-NH_2	41	128,000	1.62	8
37k anh-PS-anh / 16k NH_2-PI-NH_2	49	159,000	1.73	6
37k anh-PS-anh / 32k NH_2-PI-NH_2	32	207,000	1.57	6
83k anh-PS-anh / 32k NH_2-PI-NH_2	31	230,000	1.42	4
18k epoxy-PS-epoxy / 20k COOH-PI-COOH	2	38,000	2.30	2
44k epoxy-PS-epoxy / 54k COOH-PI-COOH	5	245,000	1.21	5

the corrected values, with the PI molecular weights adjusted to correct the hydrodynamic radius. The results show that large multiblock copolymers are created except when the 18k Epoxy/20k COOH-PI-COOH telechelic pair is used. The polydispersities of the multiblock copolymers are also similar. However, a PDI of 2.30 for the 18k epoxy-PS-epoxy/20k COOH-PI-COOH copolymer is unexpectedly high. This large value was observed at all mixing times as well as for the sample composed of 95% PS/5% PI.

5.6 Telechelic Loading Effects

5.0 wt.% telechelic loading was chosen as an initial starting point in this project. The conversion of the anh/NH_2 and epoxy/COOH pair was considerably less than that reported by Orr. It is quite possible that the conversion observed in our system was lower because an excess of telechelics was used. All of the telechelics that are able to react are located at the interface, while the excess telechelics remain unreacted in the bulk homopolymer phases. To determine if the conversion level changed with telechelic loading, 37k anh-PS-anh/16k NH_2-PI-NH_2 telechelics were added to a 90% PS/10% PI blend at concentrations of 2.5 wt.%, 1.3 wt.%, 0.5 wt.%, and 0.1 wt.% in stoichiometric quantities. The conversion of the tagged telechelic PI into copolymer for various telechelic loading levels in blends melt mixed for 10 minutes is shown in Table 5.3. The results show no significant change in conversion with telechelic loading. If all the telechelics present formed copolymer at the interface, the conversion will increase as the loading levels are reduced. From these results, the validity of our method to determine the conversion is questionable.

The fluorescence of the tagged NH_2 telechelic and an individual component were therefore tested. 16k NH_2-PI-NH_2 was melt mixed for 10 minutes at 180 °C and 100 rpm

Table 5.3. Copolymer conversion after 10 minutes of melt mixing for various loading levels of 37k anh-PS-anh/16k NH_2-PI-NH_2 used to compatibilize a blend of 90% PS/10% PI.

37k anh-PS-anh / 16k NH_2-PI-NH_2 (Wt. %)	Conversion (%)
5.0	47
2.5	45
1.3	44
0.5	48
0.1	43

with PS and PI in amounts similar to that found in the 5.0 wt.% 37k anh-PS-anh/16k NH_2-PI-NH_2 telechelic blends. Samples prepared with a concentration of 2 mg/ml were analyzed with λ_{ex} = 295 nm, λ_{em} = 385 nm, and gain = 1000. These results are shown in Figure 5.21. The results show there is strong long chain fluorescence when the telechelic PI is melt mixed with either homopolymer. The PI blend clearly shows a fluorescence contribution from both the homopolymer and the telechelic. Since the telechelic was added in amounts relative to that contained in the blends with 5.0 wt.% telechelics (6.3 wt.% in PI blend vs. 0.8 wt.% in PS blend), there is a much lower proportion of 16k NH_2-PI-NH_2 in the blend made with PS than the blend made with PI. In addition, the lower molecular weight PS homopolymer species elute at the same time as the telechelic PI. Thus Figure 5.21 shows only strong PS fluorescence in the PS + 16k NH_2-PI-NH_2 blend. It is clear that undesired telechelic PI interactions are occurring in the anh/NH_2 system as well. These results explain the same conversion results for varying telechelic loading. The PS is the major constituent of the bend and its undesired fluorescence peak spans a very long elution time range. Therefore, using this homopolymer becomes problematic for the determination of the conversion of telechelic PI into a copolymer due to the

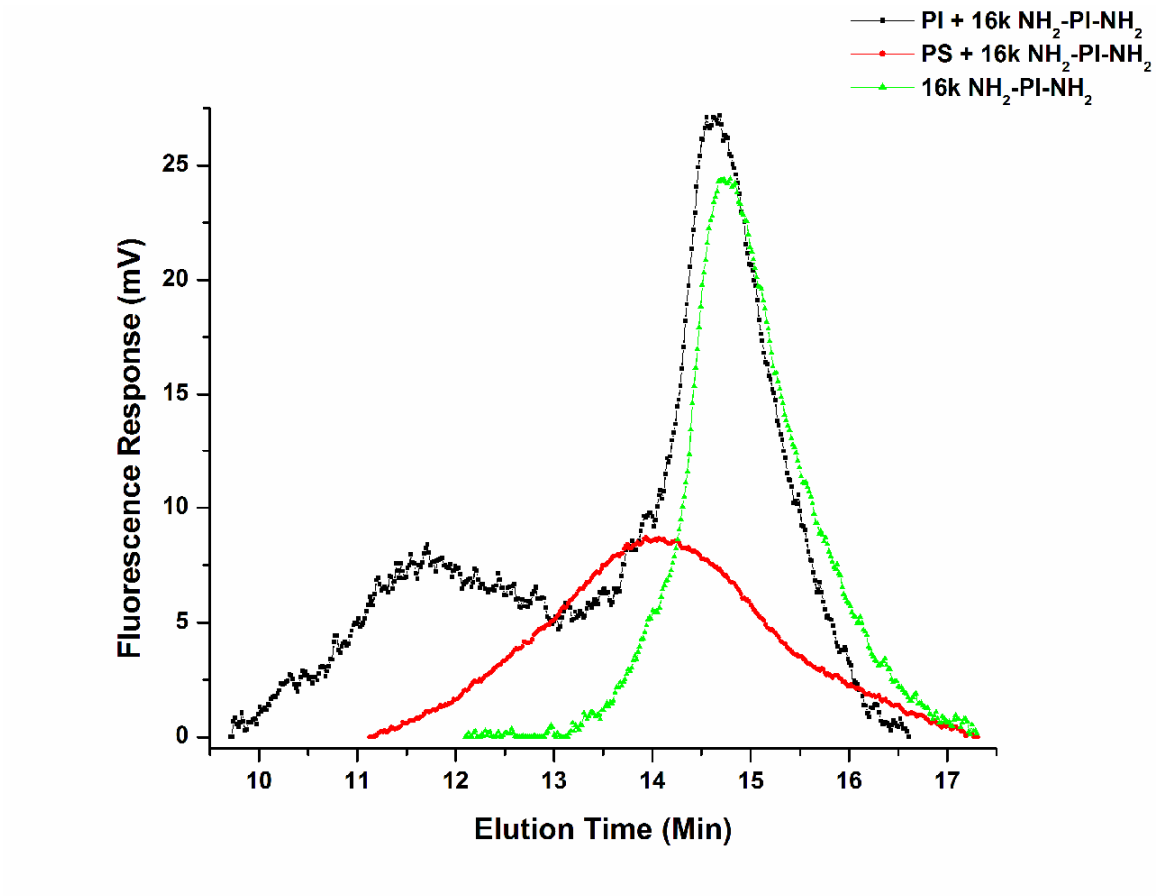

Figure 5.21. Fluorescence response of 16k NH_2-PI-NH_2 melt mixed with PS and PI as a function of elution time.

fluorescence overlap of the different species in the blend. Multiple experiments were completed in an attempt to minimize this fluorescence overlap with limited success. Detailed methodology and results of these tests are shown in Appendix A. Therefore, the precise values reported for conversion of telechelic to multiblock in these studies must be viewed as approximate.

5.7 Mechanical Testing

Preliminary mechanical tests were also performed on the polymer blends to examine the impact of this compatibilization process on the physical properties of the blend and verify its ability to strengthen the interface between the unlike phases. Experiments using an Instron 1122 machine measured the tensile properties of the polymer blends with homopolymer contents of 95% PS/5% PI, 90% PS/10% PI, and 80% PS/20% PI. Each blend composition also contained 5.0 wt.% 37k anh-PS-anh/16k NH_2-PI-NH_2, 5.0 wt.% 83k anh-PS-anh/32k NH_2-PI-NH_2, or no telechelics. Sample preparation and testing methods are described in Chapter 2.3 B. Seven samples from each blend composition were tested. From each stress-strain curve, the modulus (initial stress/strain slope), strain at break, and toughness (area under stress/strain curve) were determined. An example of this analysis is demonstrated in Figure 5.22. The modulus describes a material's stiffness, and is defined by the ratio of the stress to the strain at low strain, as described in Chapter 2.4 B. In Figure 5.22, a toe compensation was applied to ensure the linearity of the initial part of the stress-strain curve. This procedure is described in detail in Chapter 2.3 B. The modulus was calculated in the linear regime of the curve for strain values from 0.000 to 0.010. The average values and standard deviation of the mechanical properties of the blends are shown in Table 5.4. For all the

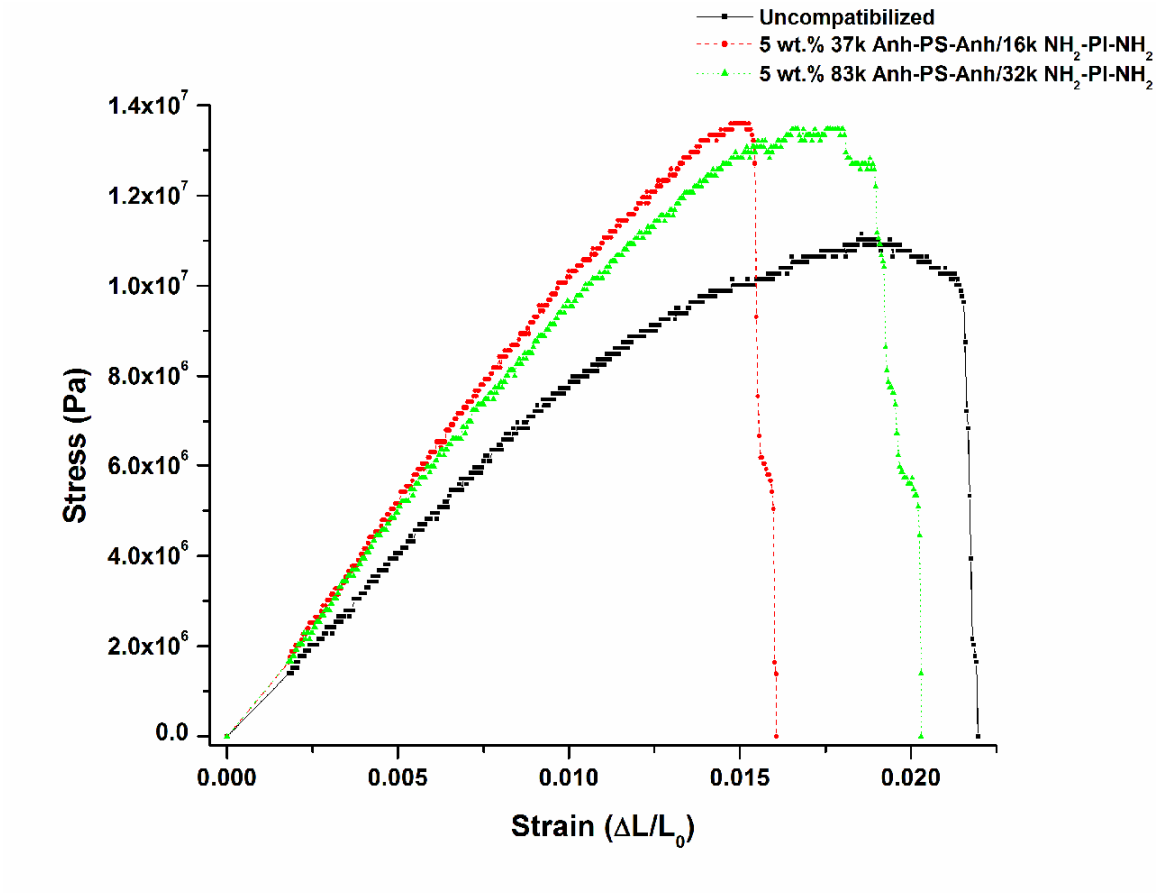

Figure 5.22. Instron tensile strength tests of 90% PS/10% PI blends containing no telechelics, 5 wt% 37k anh-PS-anh/16k NH_2-PI-NH_2, and 5 wt% 83k anh-PS-anh/32k NH_2-PI-NH_2.

Table 5.4. Modulus, strain at break, and area of PS/PI blends of various homopolymer composition and telechelics added.

95% PS/5% PI	Modulus (MPa)	Std Dev (MPa)	Strain at Break	Std Dev	Area (Toughness) (MPa)	Std Dev (MPa)
Uncompatibilized	815	81.7	1.80E-02	3.64E-03	176	62.2
5.0% 37k anh-PS-anh/16k NH_2-PI-NH_2	1001	93.5	1.93E-02	4.99E-03	225	115
5.0% 83k anh-PS-anh/32k NH_2-PI-NH_2	903	137	2.10E-02	3.29E-03	214	39.2

90% PS/10% PI	Modulus (MPa)	Std Dev (MPa)	Strain at Break	Std Dev	Area (Toughness) (MPa)	Std Dev (MPa)
Uncompatibilized	760	150	1.80E-02	3.39E-03	162	62.5
5.0% 37k anh-PS-anh/16k NH_2-PI-NH_2	936	91.3	1.58E-02	1.80E-03	129	16.2
5.0% 83k anh-PS-anh/32k NH_2-PI-NH_2	839	68.5	1.99E-02	5.51E-02	188	90.5

80% PS/20% PI	Modulus (MPa)	Std Dev (MPa)	Strain at Break	Std Dev	Area (Toughness) (MPa)	Std Dev (MPa)
Uncompatibilized	808	133	1.66E-02	2.78E-03	149	39.9
5.0% 37k anh-PS-anh/16k NH_2-PI-NH_2	852	43.0	1.72E-02	2.35E-03	142	26.4
5.0% 83k anh-PS-anh/32k NH_2-PI-NH_2	705	121	1.74E-02	3.44E-03	150	47.4

blend compositions, adding 5.0 wt% telechelics during mixing resulted in a general increase in the modulus, strain at break, and toughness of the blends, indicating the interface between the immiscible phases is strengthened by the incorporation of copolymer into the blend. The optimum telechelic loading was not determined when these experiments were conducted. Experiments conducted after Instron testing clearly indicate that 5.0 wt.% telechelic loading is excessive for this system, as discussed in Chapter 3. Therefore most of the telechelics remain unreacted in the blend. Since their molecular weight is lower than the homopolymers, they reduce the viscosity of the system. Thus, only modest mechanical property improvements are achieved. However, it is still clear that improvements are observed and further optimization should provide additional improvement.

The compatibilized blends were also investigated using dynamic mechanical analysis (DMA). Sample preparation techniques and analysis parameters are described in Chapter 2.3 C. DMA showed a broadening of the *tan* δ peak when the homopolymers were melt mixed with the telechelic polymers. This indicates an increase in stress transfer between phases. Since the homopolymer chains become entangled with each analogous block of the copolymer at the interface, there is an improvement of mixing between the unlike phases, thus stress transfer is improved. The results of these tests are shown in Figure 5.23. Similarly, the loss modulus peaks of each blend component, which correspond to the T_g of the blend component, were slightly broadened upon addition of telechelics to all of the blend compositions. Figure 5.24 demonstrates the differences in the loss modulus of compatibilized and uncompatibilized blends in the temperature range near the T_g of PI. Improved compatibilization results in a shift towards a higher

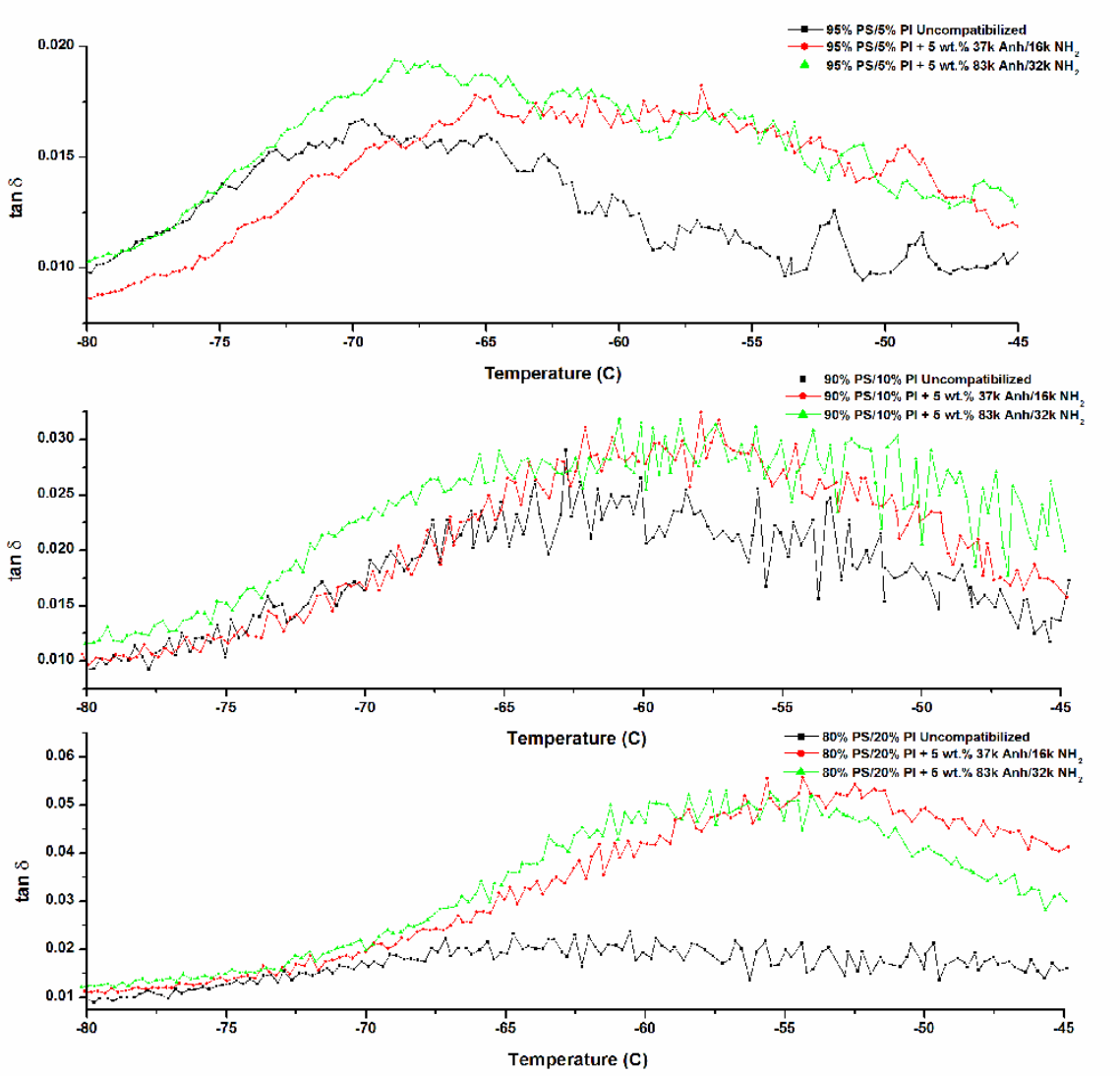

Figure 5.23. DMA *tan δ* as a function of temperature for blends composed of 95% PS/5% PI (top), 90% PS/10% PI (middle), and 80% PS/10% PI (bottom). In each homopolymer composition, the blends contained no telechelics (solid), 5.0 wt.% 37k anh-PS-anh/16k NH_2-PI-NH_2 (dash) or 5.0 wt.% 83k anh-PS-anh/32k NH_2-PI-NH_2 (dot).

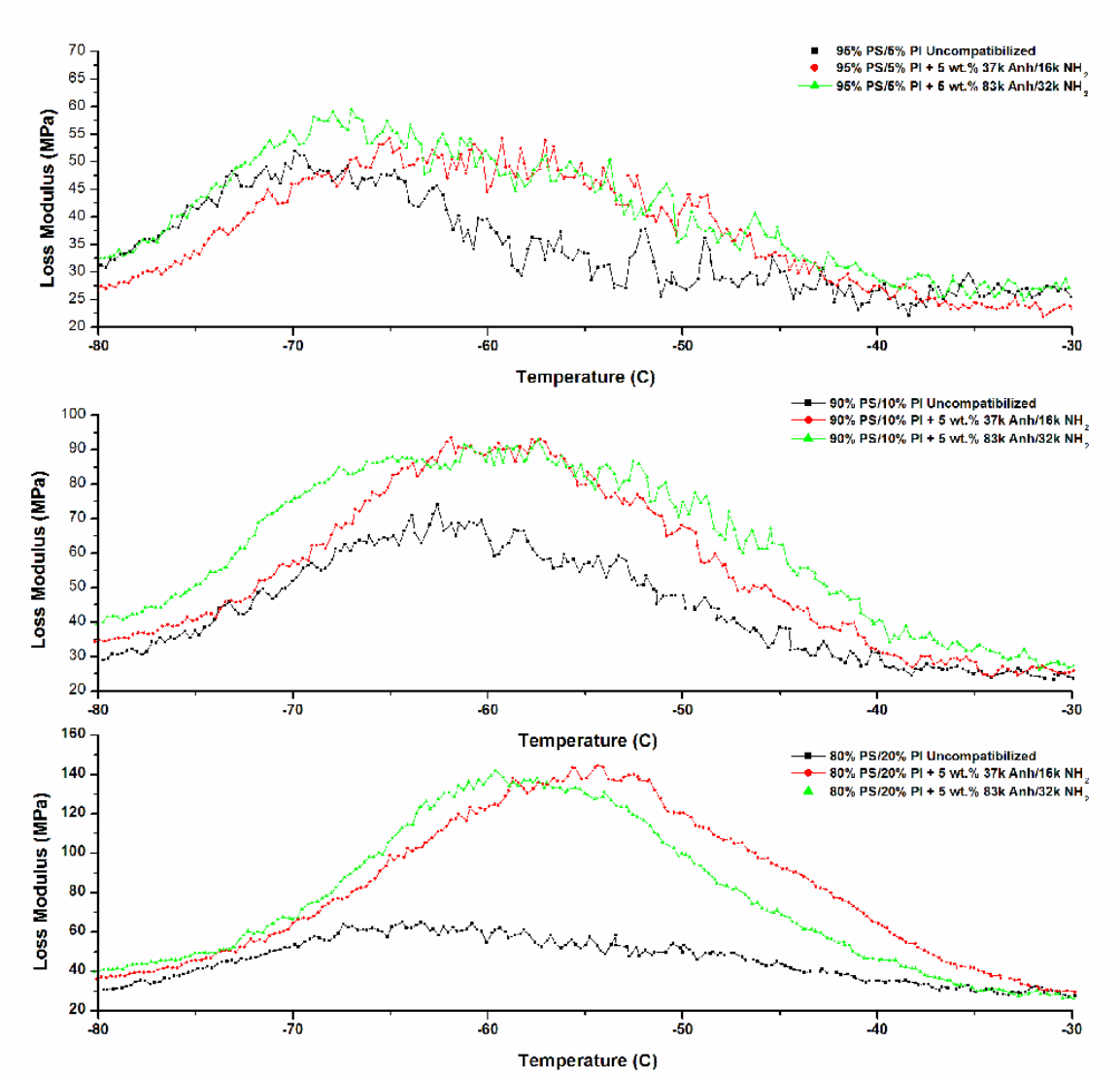

Figure 5.24. DMA loss modulus as a function of temperature for blends composed of 95% PS/5% PI (top), 90% PS/10% PI (middle), and 80% PS/10% PI (bottom). In each homopolymer composition, the blends contained no telechelics (solid), 5.0 wt.% 37k anh-PS-anh/16k NH_2-PI-NH_2 (dash) or 5.0 wt.% 83k anh-PS-anh/32k NH_2-PI-NH_2 (dot).

temperature in the loss modulus peak corresponding to the PI T_g, seen in Figure 5.24, and a shift towards a lower temperature in the loss modulus peak corresponding to the PS T_g (data not shown). The viscous component of the polymer blend is reduced by the presence of a high molecular weight multiblock copolymer present at the interface between the immiscible homopolymers. The increased loss modulus intensity observed in the compatibilized blends can be rationalized by the fact that an excess of telechelics were used in these experiments. These unreacted low molecular weight polymers act as plasticizers, and therefore increase the viscous component of the blend relative to the uncompatibilized blend. When the telechelics are incorporated into the blend, the storage modulus, which describes the elastic component of the polymer, increased slightly for the 90% PS/10% PI blend, but decreased for both the 95% PS/5% PI blend and the 80% PS/20% PI blend (data not shown). An increase in stiffness is expected compared to the uncompatibilized blend, as the copolymer strengthens the interface. Since an excess of telechelics were used, the unreacted polymers will lower the viscosity of the blend and reduce the storage modulus. The observed increase in a system with a non-optimal loading of telechelics, DMA demonstrates that the *in situ* formation of a multiblock copolymer broadens and strengthens the interface between two immiscible polymers on a molecular level.

5.8 Conclusion

GPC with fluorescence detection provides clear evidence of *in situ* multiblock copolymer formation by the reactive mixing of telechelic polymers. Reaction of pure 37k anh-PS-anh and 16k NH_2-PI-NH_2 telechelics resulted in the formation of multiblocks as large as tetrablocks at mixing times of 5 minutes, whereas copolymers as large as

hexablock size were formed *in situ* after 20 minutes of mixing. When the telechelics were incorporated into the homopolymers, there was great difficulty accurately quantifying the conversion of the APE-tagged PI telechelic due to homopolymer fluorescence interference. When a new 9-VA tag with a different λ_{ex} and λ_{em} was incorporated onto the PI telechelic, these fluorescence interference problems persisted when using the bulk homopolymers. New homopolymers with a larger molecular weight and lower polydispersity were made in an attempt to avoid the overlap of fluorescing homopolymer species. The use of FR-PS and CM-PI as homopolymers, described in Appendix A, allowed for the fluorescence chromatogram to be deconvoluted, although not without difficulty and uncertainty.

Conversion was determined by calculating the expected peak elution time and PDI of the different copolymer sizes. Various sizes of these copolymers were incorporated in a fitting program that deconvolutes the chromatogram. From the fitting results, the conversion of tagged PI telechelic into copolymer was determined. Difficulties in calculating the conversion arose from the fact that the PI telechelic also reacted when it was the only telechelic in the blend. The conversion of tagged telechelic into copolymer was calculated by subtracting the conversion determined when only the tagged telechelic was present in the blend from the conversion determined when both telechelics were present in the blend. Using this method, the conversion determined for 5.0 wt.% 83k anh-PS-anh/19k 9-VA NH_2-PI-NH_2 telechelic pairs as well as 5.0 wt.% and 2.5 wt.% 16k anh-PS-anh/19k 9-VA NH_2-PI-NH_2 telechelic pairs was ~5% – 10%. This indicates a large excess of telechelics are present in the blend. Attempts to determine conversion for all other reactive pairs and lower loading levels were not

successful. DMA and Instron tensile tests support the fluorescence data which indicates copolymers are indeed being formed *in situ*. Test results for 5.0 wt.% loading with bulk homopolymers showed a broadening of the *tan δ* peak, indicating an increase of mixing on a molecular level.

Despite the difficulties described here, it is evident that GPC with fluorescence detection provides a sensible means to detect fluorescently tagged polymers at very low concentrations. If future studies of multiblock copolymers formed *in situ* are conducted, it will be imperative to use other polymers, since PI is quite sensitive to thermooxidative degradation and the PS fluorescence is dramatically enhanced when it is melt mixed with the tagged telechelic, apparently from functional groups interacting with the aromatic ring's π electrons. For future experiments, one could use PMMA because it has a much higher degradation temperature than PI. It would also make sense to use PMMA as the matrix as its initial fluorescence response is minimal and is not significantly affected by melt mixing with the tagged telechelic. A preliminary test conducted with 100k bulk PMMA (Polysciences, Inc.) melt mixed with 1.7 wt.% 19k 9-VA NH_2-PI-NH_2 at 180 °C for 10 minutes showed little broadening of the telechelic peak due to homopolymer fluorescence interference. If higher molecular weight PMMA is used as the matrix and PMMA telechelics are available, determining copolymer conversion and molecular weight by this method will be more successful. If PS is used as the minor phase, there will still be problems from the PS fluorescence, but as the minor phase it may not be as dramatic.

Chapter 6

Conclusions and Future Work

6.1 Final Conclusions

A. Motivation for This Study

The goal of this project is to develop methods to modify interfaces with polymeric loops and examine the effectiveness of polymer loops as interfacial modifiers at soft polymer/polymer interfaces and hard nanotube/polymer interfaces. Previous studies in our group investigated the use of premade multiblock copolymers as compatibilizers. The multiple interfacial crossings afforded by these copolymers increases the interfacial strength more than a diblock copolymer, which can only cross the interface once. These interfacial crossings of the copolymer form loops that create entanglement points with homopolymer chains. Other researchers have shown that copolymers made *in situ* are more effective than premade copolymers because the functionalized polymers can approach the interface more quickly than a larger premade copolymer, which diffuses more slowly to the interface and may also become trapped in a homopolymer phase as micelles. In addition, multiblock copolymers cover a larger interfacial area per chain than a diblock copolymer, so fewer multiblock copolymers are required to cover the interfacial area than a diblock copolymer. With this knowledge, we were motivated to investigate the formation of multiblock copolymers *in situ* using difunctional reactive polymers called telechelics. Using these building blocks, it is possible to quickly form copolymers *in situ* that strengthen the interface most effectively and potentially require smaller amounts of compatibilizers.

In order to characterize these telechelics as compatibilizers for immiscible polymers, analytical methods to quantify their effectiveness were developed. By using SEM, the droplet size of polyisoprene (PI) in the polystyrene (PS) matrix after removal by a selective solvent was determined. Since steric hindrance of droplet recombination is one of the copolymer's primary roles in compatibilization, the effectiveness of different telechelic pairs to compatibilize a phase-separated polymer blend was determined by annealing the samples and monitoring the droplet volume as a function of annealing time for different telechelic reactive pairs. The effectiveness of the highly reactive anh-PS-anh/NH_2-PI-NH_2 telechelics was compared with the less reactive epoxy-PS-epoxy/COOH-PI-COOH telechelic pair. Different molecular weight combinations were examined for each pair at 5.0 wt.% loading in blends that were melt mixed for 10 minutes. There were three important discoveries from these experiments. First, the less reactive epoxy/COOH pair was as effective in suppressing droplet growth as the highly reactive anh/NH_2 pair for intermediate molecular weight telechelics. Secondly, the lowest molecular weight combination provided the poorest coalescence suppression for both telechelic pairs. This was ascribed to the fact that the PS block of the copolymer was below the critical molecular weight, so it did not effectively entangle with the PS homopolymer. As such, the copolymer was pushed away from the interfacial region more easily, reducing its effectiveness as a compatibilizer. Finally, it was discovered that the initial size of the droplets was larger in the compatibilized blends than in the uncompatibilized blend. This was attributed to an excess telechelics present at 5.0 wt.% loading. The unreacted telechelics reduce the blend viscosity and make coalescence easier, reducing the steric hindrance effects of the multiblock copolymer formed *in situ* at

the interface. Completion of variable loading experiments confirmed this hypothesis. When the anh-PS-anh/NH_2-PI-NH_2 telechelic pair was added to the blend in concentrations ranging from 0.1 wt.% – 5.0 wt.%, the initial size decreased with a decrease in telechelic loading. The optimal loading for this system was found to be 0.5 wt.%, which provided sufficient telechelic to create a copolymer that covers the interface and suppresses droplet coalescence, but not an excess that leads to a plasticization effect.

In order to quantify the effectiveness of these telechelic pairs, the volume of droplets, as measured by the cubed droplet diameter, was monitored by SEM as a function of annealing time. The rate of volume change gives the coarsening constant. It was discovered that the most appropriate method to quantify the coalescence suppression of these telechelics is to plot the relative droplet volume as a function of annealing time. The slope of this line is therefore the relative coarsening constant, K_{rel}, which gives the percent growth per minute. Since each blend has a different stabilization time, t_{stable}, the quantity $K_{rel}*t_{stable}$ provides the percent growth of the droplets upon coarsening. This quantity takes into account the different absolute size and stabilization times, and allows the direct comparison of different telechelic pairs. The specific surface area (interfacial area per unit volume) and relative specific surface area were also calculated in order to complement the coarsening constant data. The most effective compatibilizers, which had the lowest $K_{rel}*t_{stable}$ value and least relative specific surface area loss upon annealing, were all intermediate molecular weight anh/NH_2 and epoxy/COOH pairs at 5.0 wt.% loading. These blends showed ~100% droplet growth and ~20% relative specific surface area loss after stabilization. Analysis of the variable loading samples clearly indicated that using a loading level of 0.5% wt.% telechelics yielded the smallest percent growth

and smallest loss of relative specific surface area. In this case, the droplets only grew 7% and lost only 3% relative specific surface area upon stabilization. These results plainly demonstrate the deleterious plasticizing effects of excess telechelics.

Although it was not possible to accurately determine the conversion of PI telechelics into copolymer by using GPC with fluorescence detection, the conversion required for 20% interfacial coverage was estimated. This quantity is the approximate coverage that other researchers have determined is required for effective coalescence suppression. The quantity Σ is the number of copolymer chains per nm^2 of interfacial area, and Σ^* is the maximum copolymer coverage. The quantity Σ/Σ^* describes the percent of the interface that is covered with copolymer. Other experimental studies have used the lamellar spacing of diblock copolymers, which align perpendicular to the interface, to determine Σ^*. Because multiblock copolymers form flattened pancake structures along the interface, a new equation for Σ^* was devised. Since the copolymer aligns along the interface, the interfacial width of the copolymer is approximated by the height of one diblock equivalent, which is composed of one half of each telechelic chain. From this approximation, only ~2% – 3% telechelic reaction conversion was required for 20% interfacial coverage at a loading level of 5.0 wt.% for both telechelic reactive pairs. This explains how the less reactive epoxy/COOH system is readily able to sterically hinder droplet coalescence as effectively as the highly reactive anh/NH_2 pair. GPC with fluorescence detection suggested ~5% – 10% conversion was achieved in the anh/NH_2 pair, which indicates there is sufficient conversion to cover the interface. These results also demonstrate that 5.0 wt.% loading is highly excessive. When the conversion calculations were applied to the reduced loading samples, the optimal 0.5 wt.% loading

required a modest 15% telechelic reaction conversion for 20% interfacial coverage. Since this sample was quickly stabilized upon annealing, the results suggest that over 15% of NH_2-PI-NH_2 reacts to form copolymer during 10 minutes of mixing at this loading level.

B. Loops Grafted onto Functionalized Multiwall Nanotubes

Since our group succeeded in forming polymer loops at polymer/polymer soft interfaces and polymer/substrate hard interfaces, our next endeavor was to graft polymer loops onto carboxylated multiwall carbon nanotube (COOH-MWNT) surfaces. As previously discussed, polymer loop formation improves the nanotube/polymer matrix interaction through chain entanglements. The grafted loops will also sterically hinder the nanotubes from aggregation, which decreases their effectiveness in enhancing the physical properties of the polymer. In this project, grafting was achieved via a high temperature condensation reaction in solvent between epoxy-PS-epoxy and COOH-MWNT, forming aromatic esters. Samples were collected at various reaction times. In order to quantify the amount of epoxy-PS-epoxy grafted to the nanotubes, FT-IR was utilized. Because the concentration of epoxy end groups is below the detection limit of the FT-IR instrument, the vibrational mode of the PS aromatic ring was monitored to determine the weight percent of telechelic PS grafted, thereby amplifying the signal associated with the telechelic. The aromatic ester vibrational mode was examined to verify the success of the covalent grafting reaction and that the polymer had not simply adsorbed to the nanotube surface. When the grafted nanotube samples were further annealed in a vacuum oven, the aromatic ester peak increased by a significant amount for the reaction conducted in solution for 1 day. However, samples reacted in solution for 2

or more days showed little growth in the aromatic ester peak upon annealing. These results suggest that at short reaction times, the epoxy-PS-epoxy only reacts at one end to graft to the nanotubes, forming tails. Upon annealing, unreacted end groups further react to form aromatic ester groups, creating a polymer loop that has reacted at both ends. The samples reacted in solution for 2 or more days displayed larger initial aromatic ester peak intensity, and showed little growth in the aromatic ester peak upon annealing. This is interpreted to indicate that most of the loops were formed in solution. The results lead to the conclusion that tails are first formed at shorter reaction times, followed by further reaction to form loops.

In order to determine the fraction of epoxy-PS-epoxy that formed loops, the telechelic PS and COOH-MWNT were reacted in solution for 1 day. After isolation, the grafted nanotubes were further reacted with monocarboxy terminated poly(4-methylstyrene) (COOH-P4MS). FT-IR was used to determine the weight percent COOH-P4MS that reacted with unbound epoxy-PS-epoxy chain ends by monitoring the signal intensity of the COOH-P4MS aromatic ring vibrational mode. Under the conditions that were studied, this study showed that ~93% of the epoxy-PS-epoxy formed loops. The results in this study were significantly higher than previous research in our group, which showed ~80% loop formation when telechelic PS was grafted to a functionalized Si wafer substrate. The grafting density and geometry of the grafting surface is attributed to this difference in loop formation. Monte Carlo simulations have shown that loop formation is favored when the grafting density is low. At higher grafting densities, polymer chains stretch out in order to avoid interaction with each other. Thus, chain ends are far from the reactive group on the surface, resulting in the creation of more

tails. In this study, the density of COOH groups on the nanotube surface is low, which favors loop formation. The highly functionalized Si substrate used in the previous study encourages the formation of more tails. In addition, nanoscale cylindrical surface has a larger surface area than a planar wafer. So, for an equal number of grafted chains, a cylinder has a lower grafting density (chains/surface area) than a planar object of equivalent dimensions, further encouraging loop formation. The separation of the impact of grafting density from geometry in determining loop formation is difficult in these studies. TGA showed COOH groups were only 2.6 wt.% of the COOH-MWNT sample, which is equal to 0.7 mol.%. Thus, the density of surface groups on the nanotubes is expected to be significantly lower than the functionalized Si substrate. It is likely that grafting density plays the primary role in loop formation in this case, as a grafting density of only 0.7 mol.% on a planar surface would most likely result in a large fraction of loops formed as well. In order to study geometric effects in greater detail, the grafting density on the planar surface needs to be similar to the grafting density on the nanotubes surface.

The time evolution of the grafting of polymer chains to functionalized nanotubes was investigated in order to determine if the reaction was diffusion controlled or reaction controlled. For diffusion controlled kinetics, which assumes an instantaneous reaction once the nanotubes and telechelic end groups meet, the grafting process should follow a $t^{0.5}$ power law in the intermediate time regime. If the polymer must first diffuse through a dense layer of grafted polymer chains to reach the interface, grafting then follows a much slower $(ln\ t)^{0.5}$ power law. If the kinetics are controlled by the reactivity of the functional groups, the grafting should follow a power law less than $t^{0.5}$ prior to interfacial crowding. Using the aromatic ring vibrational mode to monitor the grafting process, yielding a

grafting dependence of ~$t^{0.3}$. This power law implies the kinetics are not diffusion controlled. Furthermore, the linearity of the plot for the entire reaction time suggests that the grafting density is low. If there was a buildup of grafted polymer chains on the nanotube surface, they would sterically hinder other telechelic chains from reacting. This would result in a dramatic decrease in the power law. When the kinetics of COOH-P4MS grafting were examined, their grafting rate was found to be half of the epoxy-PS-epoxy grafting rate. This was attributed to the fact that the COOH-P4MS is monofunctional, whereas the telechelic is difunctional, reducing the reaction probability, and therefore the reaction rate.

C. Loops Formed *in situ* at Soft Polymer/Polymer Interfaces

Experiments were also conducted that were designed to monitor the formation of multiblock copolymers *in situ*. The telechelic PI polymers were tagged with a fluorescent label to allow GPC with fluorescence detection to be employed as a sensitive technique to monitor the molecular weight of the copolymer formed and the conversion of the tagged PI telechelic as a function of mixing time. In order to deconvolute the chromatogram containing several different copolymer sizes along with the unreacted tagged PI telechelic, a deconvolution method developed by Shiau was followed. This method calculates the molecular weight and PDI of block copolymers created from reactive polymers having a known molecular weight and PDI. The conversion of the highly reactive anh-PS-anh/NH_2-PI-NH_2 pair without the addition of any homopolymers was also estimated. The results of mixing the pure telechelics showed ~45% conversion of the PI telechelic, with up to tetrablocks being formed after 5 minutes of mixing. After 20 minutes of melt mixing, conversion reached ~65%, and copolymers as large as

hexablocks were formed. This experiment provides clear evidence of *in situ* multiblock copolymer formation. When the anh/NH_2 telechelic pair and the less reactive epoxy-PS-epoxy/COOH-PI-COOH telechelic pair were added at 5.0 wt.% to an immiscible 90% PS/10% PI blend, uncertainty in determining the conversion of PI telechelic developed due to homopolymer fluorescence. The PS and PI fluorescence were greatly increased when only the tagged PI telechelic was added to the blend. The conversion of the tagged telechelic into copolymer was ultimately estimated by subtracting the conversion when only the PI telechelic was added to the blend from the conversion obtained when both telechelics were added to the blend. Results showed that ~5% – 10% of the NH_2-PI-NH_2 was converted at 5.0 wt.% and 2.5 wt.% loading. It was not possible to more accurately determine the conversion at lower loading levels of anh-PS-anh/NH_2-PI-NH_2, or at any loading level of the epoxy/COOH pair.

6.2 Future Work

A. Quantifying Compatibilization Effectiveness of Telechelic Pairs Using SEM

In the SEM studies conducted in this project, the slower epoxy/COOH reaction was found to compatibilize 90%PS/10% PI blends as well as the highly reactive anh/NH_2 telechelics at 5.0 wt.% loading. At this level of loading, calculations showed that only ~3% conversion was required to cover 20% of the interface. At 0.5 wt.% loading, 15% conversion was required for this interfacial coverage using anh/NH_2 telechelics. It would be interesting to do a reduced loading experiment with the epoxy/COOH polymers in order to determine at what loading level the reactivity of the end groups plays an important role. Then the lowest loading levels needed to stabilize the droplets can be

determined and compared to the anh/NH_2 reduced loading results. If the homopolymer fluorescence in the GPC with fluorescence detection studies can be minimized, it will be possible to more accurately determine the conversion at different loading levels.

Another way the SEM study can be expanded is to quantify the $K_{rel}*t_{stable}$ values for the different telechelic pairs at different mixing times. Industrial applications require short mixing times, so it is important to investigate how different mixing times influence the effectiveness of the copolymer's steric hindrance attributes. The results of this study have shown that smaller block copolymers form at shorter mixing times. If experiments were also conducted at 5 minutes of mixing time, it is possible to determine if there is any significant difference in the coalescence suppression ability of hexablocks and tetrablocks, for example. In addition, mechanical studies such as DMA and Instron tests can be performed to determine which telechelic pair and which mixing time strengthens the interface of the immiscible polymer to the greatest extent.

B. Loops Grafted onto Functionalized Multiwall Nanotubes

In this study, ~93% of the grafted epoxy-PS-epoxy formed loops after a 1 day reaction in solvent. Experimental results also showed that when the reaction was conducted in solution for 2 or more days, annealing lead to very little increase in the aromatic ester peak, which was interpreted to mean that most of the chains formed loops in solution. Another area to explore in this study is the fraction of loops formed at reaction times shorter than 1 day. Since Monte Carlo simulations show that tails are the predominant species at short reaction times, experimental studies can verify this observation by conducting a study at shorter reaction times. However, FT-IR sensitivity limits would define the shortest reaction time where a signal from the grafted polymer

can be distinguished. A more sensitive FT-IR than the one used in this study should be used for this purpose if this area is to be explored.

In order to determine the effectiveness of grafted polymer loops to strengthen the polymer/nanotube interface via chain entanglements, mechanical properties can be examined with DMA and Instron tests. Various concentrations of grafted and ungrafted nanotubes can be mixed with a PS polymer matrix, with the ungrafted nanotubes used as the control. To examine how the grafted loops suppress nanotube aggregation, TEM can be employed to monitor the nanotube cluster size. To compare the difference in mechanical properties between loops and tails, a monofunctional polymer with a molecular weight similar to the telechelic can be used in the grafting reaction in order to produce only tails.

C. Loops Formed *in situ* at Soft Polymer/Polymer Interfaces

The experiments performed in this research project have provided strong evidence of multiblock copolymer formation *in situ* at soft interfaces. There are several possibilities to expand this research project in order to improve the detection and characterization of the formed copolymers, as well as to develop further understanding the effects of telechelic functionality. First, it would be beneficial to revisit the determination of conversion and copolymer molecular weight by GPC with fluorescence detection. Fluorescence is a very sensitive method that is able to detect very small telechelic loading levels. Improving upon this detection method can shed more knowledge on *in situ* copolymer formation. In future studies, homopolymer fluorescence needs to be the first consideration. Preliminary tests of 100k bulk PMMA melt mixed with 1.7 wt.% 9-VA NH_2-PI-NH_2 exhibited little broadening of the tagged PI peak. Thus

polymers that show little fluorescence when melt mixed with the tagged telechelics should be considered for the matrix. Secondly, polymers that are sensitive to thermooxidative degradation, such as PI or polybutadiene (PB), should not be used in this study, as high temperatures are required for the condensation reaction to occur. These polymers may form free radicals and oxygen-bearing functional groups at high temperatures, which can subsequently react with other species. Another factor to consider is the choice of fluorescent tag. It is advantageous to use a tag with a longer excitation and emission wavelength in order to reduce homopolymer fluorescence. If these factors are taken into consideration, determining the tagged telechelic conversion and the molecular weight of the multiblock formed *in situ* are expected to be much more precise, even at low telechelic loading levels.

References

References

(1) Koning, C.; van Duin, M.; Pagnoulle, C.; Jerome, R. *Progress in Polymer Science* **1998**, *23*, 707.
(2) Paul, D. R. Background and Perspective. In *Polymer Blends*; Paul, D. R., Newman, S., Eds.; Academic Press: New York, 1978; Vol. 1.
(3) Krause, S. Polymer-Polymer Compatibility. In *Polymer Blends*; Paul, D. R., Newman, S., Eds.; Academic Press: New York, 1978; Vol. 1; pp 132.
(4) McMaster, L. P. *Macromolecules* **1973**, *6*, 766.
(5) Kramer, E. J. *Faraday Discussions* **1994**, *98*, 31.
(6) Fayt, R.; Jerome, R.; Teyssie, P. *Macromolecular Chemistry and Physics* **1986**, *187*, 837.
(7) Bordereau, V.; Shi, Z. H.; Utracki, L. A.; Sammut, P.; Carrega, M. *Polymer Engineering and Science* **1992**, *32*, 1846.
(8) Favis, B. D.; Willis, J. M. *Journal of Polymer Science: Part B: Polymer Physics* **1990**, *28*, 2259.
(9) Kozlowski, M. *Journal of Applied Polymer Science* **1995**, *55*, 1375.
(10) Favis, B. D.; Chalifoux, J. P. *Polymer* **1988**, *29*, 1761.
(11) Heikens, D.; Barentsen, W. *Polymer* **1977**, *18*, 69.
(12) Favis, B. D.; Therrien, D. *Polymer* **1991**, *32*, 1474.
(13) Lyngaae-Jorgensen, J.; Utracki, L. A. *Die Makromolekulare Chemie, Macromolecular Symposia* **1991**, *48/49*, 189.
(14) Scott, C. E.; Macosko, C. W. *Polymer Bulletin* **1991**, *26*, 341.
(15) Scott, C. E.; Macosko, C. W. *Polymer* **1995**, *36*, 461.
(16) Molau, G. E. *Journal of Polymer Science: Part A - Polymer Chemistry* **1965**, *3*, 4235.
(17) Noolandi, J.; Hong, K. M. *Macromolecules* **1982**, *15*, 482.
(18) Noolandi, J. *Makromolekulare Chemie - Theory and Simulations* **1992**, *1*, 295.
(19) Hu, G.-H.; Lambla, M. *Journal of Polymer Science: Part A Polymer Chemistry* **1995**, *33*, 97.
(20) Hu, W.; Koberstein, J. T.; Lingelser, J. P.; Gallot, Y. *Macromolecules* **1995**, *28*, 5209.
(21) Leibler, L.; Pincus, P. A. *Macromolecules* **1984**, *17*, 2922.
(22) Leibler, L. *Physica A* **1991**, *172*, 258.
(23) Tang, T.; Huang, B. *Polymer* **1994**, *35*, 281.
(24) Chattopadhyay, S.; Sivaram, S. *Polymer International* **2001**, *50*, 67.
(25) Fayt, R.; Jerome, R.; Teyssie, P. *Journal of Polymer Science: Polymer Letters Edition* **1986**, *24*, 25.
(26) Dadmun, M. *Macromolecules* **1996**, *29*, 3868.
(27) Ide, F.; Hasegawa, A. *Journal of Applied Polymer Science* **1974**, *18*, 963.
(28) Fayt, R.; Jerome, R.; Teyssie, P. *Journal of Polymer Science: Part C - Polymer Letters* **1981**, *19*, 79.
(29) Fayt, R.; Jerome, R.; Teyssie, P. *Journal of Polymer Science: Part C - Polymer Letters* **1981**, *19*, 1269.
(30) Liu, N. C.; Baker, W. E. *Polymer Engineering and Science* **1992**, *32*, 1695.

(31) Paul, D. R. Interfacial Agents ("Compatibilizers") for Polymer Blends. In *Polymer Blends*; Paul, D. R., Newman, S., Eds.; Academic Press: New York, 1978; Vol. 2; pp 35.
(32) Surface Tension; Wikipedia, 2010; Vol. 2010.
(33) Surface Energy; Wikipedia, 2010; Vol. 2010.
(34) Lepers, J.-C.; Favis, B. D.; Tabar, R. J. *Journal of Polymer Science: Part B: Polymer Physics* **1997**, *35*, 2271.
(35) Granek, R.; Ball, R. C.; Cates, M. E. *Journal de Physique II* **1993**, *3*, 829.
(36) Jiao, J.; Kramer, E. J.; Vos, S. d.; Moller, M.; Koning, C. *Macromolecules* **1999**, *32*, 6261.
(37) Tokita, N. *Rubber Chemistry and Technology* **1977**, *50*, 292.
(38) Anastasiadis, S. H.; Gancarz, I.; Koberstein, J. T. *Macromolecules* **1989**, *22*, 1449.
(39) Inoue, T.; Soen, T.; Hashimoto, T.; Kawai, H. *Journal of Polymer Science: Part A-2* **1969**, *7*, 1283.
(40) Favis, B. D. *Polymer* **1994**, *35*, 1552.
(41) Taylor, G. I. *Proceedings of the Royal Society of London. Series A, Containing Papers of a Mathematical and Physical Character* **1934**, *146*, 501.
(42) Ghodgaonkar, P. G.; Sundararaj, U. *Polymer Engineering and Science* **1996**, *36*, 1656.
(43) Sundararaj, U.; Macosko, C. W. *Macromolecules* **1995**, *28*, 2647.
(44) Beck-Tan, N. C.; Tai, S.-K.; Briber, R. M. *Polymer* **1996**, *37*, 3509.
(45) Crist, B.; Nesarikar, A. *Macromolecules* **1995**, *28*, 890.
(46) Fortelny, I.; Zivny, A. *Polymer* **1995**, *36*, 4113.
(47) Milner, S.; Xi, H. *Journal of Rheology* **1996**, *40*, 663.
(48) Ruckenstein, E. *Colloids and Surfaces* **1993**, *69*, 271.
(49) Macosko, C. W.; Guegan, P.; Khandpur, A. K.; Nakayama, A.; Marechal, P.; Inoue, T. *Macromolecules* **1996**, *29*, 5590.
(50) Lyu, S. P.; Bates, F.; Macosko, C. *American Institute of Chemical Engineers Journal* **2000**, *46*, 229.
(51) Macosko, C. W. *Macromolecular Symposia* **2000**, *149*, 171.
(52) Kim, J. R.; Hutton, S. D.; Jamison, A. M.; Manas-Zloczower, I.; Ishida, H. *Polymer* **2001**, *42*, 4281.
(53) Yin, Z.; Koulic, C.; Pagnoulle, C.; Jerome, R. *Macromolecules* **2001**, *34*, 5132.
(54) Lyu, S.-P.; Jones, T. D.; Bates, F. S.; Macosko, C. W. *Macromolecules* **2002**, *35*, 7845.
(55) Maric, M.; Macosko, C. W. *Journal of Polymer Science: Part B: Polymer Physics* **2002**, *40*, 346.
(56) Jones, T. D.; Schulze, J. S.; Macosko, C. W.; Lodge, T. P. *Macromolecules* **2003**, *36*, 7212.
(57) Lyu, S.-P. *Macromolecules* **2003**, *36*, 10052.
(58) Kim, J.; Gray, M.; Zhou, H.; Nguyen, S.-B.; Torkelson, J. *Macromolecules* **2005**, *38*, 1037.
(59) Van Puyvelde, P.; Velankar, S.; Mewis, J.; Moldenaers, P. *Polymer Engineering and Science* **2002**, *42*, 1956.

(60) Ha, J. W.; Yoon, Y.; Leal, L. G. *Physics of Fluids* **2003**, *15*, 849.
(61) Leal, L. G. *Physics of Fluids* **2004**, *16*, 1833.
(62) Van Hemmelrijck, E.; Van Puyvelde, P.; Macosko, C. W.; Moldenaers, P. *Journal of Rheology* **2005**, *49*, 783.
(63) Van Hemmelrijck, E.; Van Puyvelde, P.; Moldenaers, P. *Macromolecular Symposia* **2006**, *233*, 51.
(64) Yoon, Y.; Hsu, A. *Physics of Fluids* **2007**, *19*, 023102.
(65) Brown, S. B. *Annual Review of Materials Science* **1991**, *35*, 409.
(66) Xanthos, M.; Dagli, S. S. *Polymer Engineering and Science* **1991**, *31*, 929.
(67) Dai, K. H.; Kramer, E. J.; Shull, K. R. **1992**, *25*, 220.
(68) Jeon, H. K.; Zhang, J.; Macosko, C. W. *Polymer* **2005**, *46*, 12422.
(69) Fredrickson, G. H.; Leibler, L. *Macromolecules* **1996**, *29*, 2674.
(70) O'Shaughnessy, B.; Vavylonis, D. *Europhysics Letters* **1999**, *45*, 638.
(71) O'Shaughnessy, B.; Vavylonis, D. *Macromolecules* **1999**, *32*, 1785.
(72) Schulze, J. S.; Cernohous, J. J.; Hirao, A.; Lodge, T. P.; Macosko, C. W. *Macromolecules* **2000**, *33*, 1191.
(73) Oyama, H. T.; Inoue, T. *Macromolecules* **2001**, *34*, 3331.
(74) Guegan, P.; Macosko, C. W.; Ishizone, T.; Hirao, A.; Nakahama, S. *Macromolecules* **1994**, *27*, 4993.
(75) Guegan, P.; Macosko, C. W.; Ishizone, T.; Hirao, A.; Nakayama, S. *Polymeric Materials: Science and Engineering (Proceedings of the American Chemical Society, Division of Polymeric Materials, Science and Engineering)* **1993**, *69*, 187.
(76) Orr, C. A.; Adedeji, A.; Hirao, A.; Bates, F. S.; Macosko, C. W. *Macromolecules* **1997**, *30*, 1243.
(77) Orr, C.; Cernohous, J.; Guegan, P.; Hirao, A.; Jeon, H.; Macosko, C. *Polymer* **2001**, *42*, 8171.
(78) Rice, J. K. The Reaction of Telechelic Polymers at Multicomponent Interfaces: A Molecular Loop Study, University of Tennessee, 2006.
(79) Yin, Z.; Koulic, C.; Jeon, H. K.; Pagnoulle, C.; Macosko, C. W.; Jerome, R. *Macromolecules* **2002**, *35*, 8117.
(80) Lyu, S.-P.; Cernohous, J. J.; Bates, F. S.; Macosko, C. W. *Macromolecules* **1999**, *32*, 106.
(81) Smith, G. D.; Zhang, Y.; Yin, F.; Bedrov, D.; Dadmun, M. D.; Huang, Z. *Langmuir* **2006**, *22*, 664.
(82) Russell, T. P.; Mayes, A. M.; Deline, V. R.; Chung, T. C. *Macromolecules* **1992**, *25*, 5783.
(83) Balazs, A. C.; Siemasko, C. P.; Lantman, C. W. *Journal of Chemical Physics* **1991**, *94*, 1653.
(84) Eastwood, E. A.; Dadmun, M. D. *Macromolecules* **2002**, *35*, 5069.
(85) Creton, C.; Kramer, E. J.; Hadziioannou, G. *Macromolecules* **1991**, *24*, 1846.
(86) Kroeze, E.; Brinke, G. t.; Hadziioannou, G. *Polymer Bulletin* **1997**, *38*, 203.
(87) Retsos, H.; Margiolaki, I.; Messaritaki, A.; Anastasiadis, S. H. *Macromolecules* **2001**, *34*, 5295.
(88) Galloway, J. A.; Jeon, H. K.; Bell, J. R.; Macosko, C. W. *Polymer* **2005**, *46*, 183.

(89) Leibler, L. *Makromolekulare Chemie - Macromolecular Symposia* **1988**, *16*, 1.
(90) Riess, G.; Jolivet, Y. *American Chemical Society Advances in Chemistry Series* **1975**, *142*, 243.
(91) McClory, C.; Chin, S. J.; McNally, T. *Australian Journal of Chemistry* **2009**, *62*, 762.
(92) Moniruzzaman, M.; Winey, K. I. *Macromolecules* **2006**, *39*, 5194.
(93) Coleman, J. N.; Khan, U.; Blau, W. J.; Gun'ko, Y. K. *Carbon* **2006**, *44*, 1624.
(94) Yoon, K. R.; Kim, W.-J.; Choi, I. S. *Macromolecular Chemistry and Physics* **2004**, *205*, 1218.
(95) Szleifer, I.; Yerushalmi-Rozen, R. *Polymer* **2005**, *46*, 7803.
(96) Bandyopadhyaya, R.; Nativ-Roth, E.; Regev, O.; Yerushalmi-Rozen, R. *Nano Letters* **2002**, *2*, 25.
(97) Scobbo Jr., J. J. *Polymer Testing* **1991**, *10*, 279.
(98) Vulic, I.; Vitarelli, G.; Zenner, J. M. *Polymer Degradation and Stability* **2002**, *78*, 27.
(99) Odian, G. *Principles of Polymerization*, 4th ed.; John Wiley & Sons: Hoboken, NJ, 2004.
(100) Stevens, M. P. *Polymer Chemistry: An Introduction*, 3rd ed.; Oxford University Press: New York, 1999.
(101) Bueche, F. *Journal of Applied Polymer Science* **1960**, *4*, 101.
(102) Frenkel, J. *Acta Physicochimica U.R.S.S.* **1944**, *19*, 51.
(103) Doi, M.; Edwards, S. F. *The Theory of Polymer Dynamics*; Clarendon Press: Oxford, 1986.
(104) Atkins, P. *Physical Chemistry*, 6th ed.; W.H. Freeman & Co.: New York, 1999.
(105) Pike, M.; Watson, W. F. *Journal of Polymer Science* **1952**, *9*, 229.
(106) Kauzmann, W.; Eyring, H. *Journal of the American Chemical Society* **1940**, *62*, 3113.
(107) Hirao, A.; Hayashi, M. *Acta Polymerica* **1999**, *50*, 219.
(108) Tung, L.; Lo, G. *Macromolecules* **1994**, *27*, 2219.
(109) Cernohous, J. J.; Macosko, C. W.; Hoye, T. R. *Macromolecules* **1997**, *30*, 5213.
(110) Quirk, R. P.; Lee, Y. *Macromolecular Symposia* **2000**, *157*, 161.
(111) Quirk, R. P.; Zhuo, Q. *Macromolecules* **1997**, *30*, 1531.
(112) Ji, H.; Nonidez, W. K.; Advincula, R. C.; Smith, G. D.; Kilbey II, S. M.; Dadmun, M. D.; Mays, J. W. *Macromolecules* **2005**, *38*, 9950.
(113) Yang, J.; Lu, J.; Winnik, M. *Journal of Polymer Science: Part A: Polymer Chemistry* **2003**, *41*, 1225.
(114) Shimbo, M.; Nakaya, T.; Takahama, T. *Journal of Polymer Science: Part B: Polymer Physics* **1986**, *24*, 1931.
(115) Orr, C. A. Reactive Compatibilization of Polymer Blends, University of Minnesota, 1997.
(116) Padwa, A.; Sasaki, Y.; Wolske, K.; Macosko, C. *Journal of Polymer Science: Part A: Polymer Chemistry* **1995**, *33*, 2165.
(117) Shariatpanahi, H.; Nazokdast, H.; Hemmati, M. *Journal of Elastomers and Plastics* **2003**, *35*, 115.

(118) Datsyuk, V.; Kalyva, M.; Papagelis, K.; Parthenios, J.; Tasis, D.; Siokou, A.; Kallitsis, I.; Galiotis, C. *Carbon* **2008**, *46*, 833.
(119) Rinzler, A. G.; Liu, J.; H.Dai; Nikolaev, P.; Huffman, C. B.; Rodrıguez-Macıas, F. J.; Boul, P. J.; Lu, A. H.; D.Heymann; Colbert, D. T.; Lee, R. S.; Fischer, J. E.; A.M.Rao; Eklund, P. C.; Smalley, R. E. *Applied Physics A: Materials Science & Processing* **1998**, *67*, 29.
(120) Salzmann, C. G.; Llewellyn, S. A.; Tobias, G.; Ward, M. A. H.; Huh, Y.; Green, M. L. H. *Advanced Materials* **2007**, *19*, 883.
(121) Yu, H.; Jin, Y.; Peng, F.; Wang, H.; Yang, J. *Journal of Physical Chemistry C* **2008**, *112*, 6758.
(122) Zhang, J.; Zou, H.; Qing, Q.; Yang, Y.; Li, Q.; Liu, Z.; Guo, X.; Du, Z. *Journal of Physical Chemistry B* **2003**, *107*, 3712.
(123) Chou, A.; Böcking, T.; Singh, N. K.; Gooding, J. J. *Chemical Communications* **2005**, 842.
(124) Martınez, M. T.; Callejas, M. A.; Benito, A. M.; Cochet, M.; Seeger, T.; Anson, A.; Schreiber, J.; Gordon, C.; Marhic, C.; Chauvet, O.; Fierro, J. L. G.; Maser, W. K. *Carbon* **2003**, *41*, 2247.
(125) Masheter, A. T.; Xiao, L.; Wildgoose, G. G.; Crossley, A.; Jones, J. H.; Compton, R. G. *Journal of Materials Chemisty* **2007**, *17*, 3515.
(126) Pumera, M.; Smid, B.; Veltruska, K. *Journal of Nanoscience and Nanotechnology* **2009**, *9*, 2671.
(127) González-Guerrero, A. B.; Mendoza, E.; Pellicer, E.; Alsina, F.; Fernández-Sánchez, C.; Lechuga, L. M. *Chemical Physics Letters* **2008**, *462*, 256.
(128) Dementev, N.; Feng, X.; Borguet, E. *Langmuir* **2009**, *25*, 7573.
(129) Kun, K. A.; Kunin, R. *Journal of Polymer Science: Part A-1* **1968**, *6*, 2689.
(130) Jackson, C.; Chen, Y.-J.; Mays, J. W. *Journal of Applied Polymer Science* **1996**, *61*, 865.
(131) Sebastian, J. M.; Register, R. A. *Journal of Applied Polymer Science* **2001**, *82*, 2056.
(132) Moon, B.; Hoye, T.; Macosko, C. *Journal of Polymer Science: Part A: Polymer Chemistry* **2000**, *38*, 2177.
(133) Standard Test Method for Tensile Properties of Plastics: D638-01. In *Annual Book of ASTM Standards, Vol. 08.01 Plastics (I) D256 - D2343*; ASTM International: West Conshohocken, PA, 2002; Vol. 08; pp 45.
(134) Menard, K. P. *Dynamic Mechanical Analysis: A Practical Introduction*, 2nd ed.; CRC Press: Boca Raton, FL, 2008.
(135) Kato, K. *Journal of Polymer Science: Part B: Polymer Letters* **1966**, *4*, 35.
(136) Mirabella Jr., F. M. *Journal of Polymer Science: Part B: Polymer Physics* **1994**, *32*, 1205.
(137) Alonzo, J.; Huang, Z.; Liu, M.; Mays, J. W.; Toomey, R. G.; Dadmun, M. D.; Kilbey II, S. M. *Macromolecules* **2006**, *39*, 8434.
(138) Huang, Z.; Ji, H.; Mays, J. W.; Dadmun, M. D. *Macromolecules* **2008**, *41*, 1009.
(139) Huang, Z.; Alonzo, J.; Liu, M.; Ji, H.; Yin, F.; Smith, G. D.; Mays, J. W.; Kilbey II, S. M.; Dadmun, M. D. *Macromolecules* **2008**, *41*, 1745.
(140) Fortelny, I.; Zivny, A. *Polymer* **1998**, *39*, 2669.

(141) Hsu, J.-P.; Lin, D.-P.; Tseng, S. *Colloid & Polymer Science* **1995**, *273*, 271.
(142) Fetters, L. J.; Lohse, D. J.; Richter, D.; Witten, T. A.; Zirkel, A. *Macromolecules* **1994**, *27*, 4639.
(143) Zhang, Z.; Qiao, J. *Polymer Engineering and Science* **1991**, *31*, 1553.
(144) Chaffin, K. A.; Bates, F. S.; Brant, P.; Brown, G. M. *Journal of Polymer Science: Part B - Polymer Physics* **2000**, *38*, 108.
(145) Tao, Y.; Lebovitz, A. H.; Torkelson, J. M. *Polymer* **2005**, *46*, 4753.
(146) Fortelny, I.; Zivny, A.; Juza, J. *Journal of Polymer Science: Part B: Polymer Letters* **1999**, *37*, 181.
(147) Chen, C. C.; White, J. L. *Polymer Engineering and Science* **1993**, *33*, 923.
(148) Richardson, M. J.; Savill, N. G. *Polymer* **1977**, *18*, 3.
(149) Han, C. D.; Kim, J.; Kim, J. K. *Macromolecules* **1989**, *22*, 383.
(150) Yin, Z.; Koulic, C.; Pagnoulle, C.; Jerome, R. *Langmuir* **2003**, *19*, 453.
(151) Charoensirisomboon, P.; Inoue, T.; Weber, M. *Polymer* **2000**, *41*, 4483.
(152) *Polymer Handbook*; 3rd ed.; Brandrup, J.; Immergut, E. H., Eds.; Wiley: New York, 1989.
\(153) Treacy, M. M. J.; Ebbesen, T. W.; Gibson, J. M. *Nature* **1996**, *381*, 678.
(154) Yakobson, B. I.; Brabec, C. J.; Bernholc, J. *Physical Review Letters* **1996**, *76*, 2511.
(155) Blake, R.; Coleman, J. N.; Byrne, M. T.; McCarthy, J. E.; Perova, T. S.; Blau, W. J.; Fonseca, A.; Nagyd, J. B.; Gun⁾ko, Y. K. *Journal of Materials Chemisty* **2006**, *16*, 4206.
(156) Blond, D.; Barron, V.; Ruether, M.; Ryan, K. P.; Nicolosi, V.; Blau, W. J.; Coleman, J. N. *Advanced Functional Materials* **2006**, *16*, 1608.
(157) Hwang, G. W.; Shieh, Y.-T.; Hwang, K. C. *Advanced Functional Materials* **2004**, *14*, 487.
(158) Yang, B.-X.; Shi, J.-H.; Pramoda, K. P.; Goh, S. H. *Composites Science and Technology* **2008**, *68*, 2490.
(159) Yang, B.-X.; Shi, J.-H.; Li, X.; Pramoda, K. P.; Goh, S. H. *Journal of Applied Polymer Science* **2009**, *113*, 1165.
(160) Wang, M.; Pramoda, K. P.; Goh, S. H. *Polymer* **2005**, *46*, 11510.
(161) Qian, D.; Dickey, E. C.; Andrews, R.; Rantell, T. *Applied Physics Letters* **2000**, *76*, 2868.
(162) Shvartzman-Cohen, R.; Nativ-Roth, E.; Baskaran, E.; Levi-Kalisman, Y.; Szleiferand, I.; Yerushalmi-Rozen, R. *Journal of the American Chemical Society* **2004**, *126*, 14850.
(163) Lin, Y.; Zhou, B.; Fernando, K. A. S.; Liu, P.; Allard, L. F.; Sun, Y.-P. *Macromolecules* **2003**, *36*, 7199.
(164) Hill, D. E.; Y.Lin; Rao, A. M.; Allard, L. F.; Sun, Y.-P. *Macromolecules* **2002**, *35*, 9466.
(165) Huang, Z.; Ji, H.; Mays, J.; Dadmun, M.; Smith, G.; Bedrov, D.; Zhang, Y. *Langmuir* **2009**, *26*, 202.
(166) Eastwood, E. A.; Dadmun, M. D. *Polymer* **2002**, *43*, 6707.
(167) O'Brien, C. P.; Rice, J. K.; Dadmun, M. D. *European Polymer Journal* **2004**, *40*, 1515.

(168) Ashcraft, E.; Ji, H.; Mays, J.; Dadmun, M. *ACS Applied Materials & Interfaces* **2009**, *1*, 2163.
(169) Fredrickson, G. H.; Milner, S. T. *Macromolecules* **1996**, *29*, 7386.
(170) Müller, M. *Macromolecules* **1997**, *30*, 6353.
(171) Kramer, E. J. *Israel Journal of Chemistry* **1995**, *35*, 49.
(172) Yang, Y.; Char, K. *Macromolecular Theory and Simulations* **2001**, *10*, 565.
(173) Shao, L.; Tobias, G.; Salzmann, C. G.; Ballesteros, B.; Hong, S. Y.; Crossley, A.; Davis, B. G.; Green, M. L. H. *Chemical Communications* **2007**, 5090.
(174) Fanning, P. E.; Vannice, M. A. *Carbon* **1993**, *31*, 721.
(175) Mawhinney, D. B.; Naumenko, V.; Kuznetsova, A.; Yates, J. T., Jr. *Journal of the American Chemical Society* **2000**, *122*, 2383.
(176) Wang, G.; Dong, Y.; Liu, L.; Zhao, C. *Journal of Applied Polymer Science* **2007**, *105*, 1385.
(177) Pavia, D. L.; Lampman, G. M.; Kriz, G. S., Jr. *Introduction to Spectroscopy*; W.B. Saunders: Philadelphia, 1979.
(178) Conley, R. T. *Infrared Spectroscopy*; Allyn and Bacon, Inc.: Boston, 1966.
(179) Magonov, S. N.; Vainilovitch, I. S.; Sheiko, S. S. *Polymer Bulletin* **1991**, *25*, 491.
(180) Evtushenko, Y. M.; Ivanov, V. M.; Zaitsev, B. E. *Journal of Analytical Chemistry* **2003**, *58*, 392.
(181) Patterson, W. A. *Analytical Chemistry* **1954**, *26*, 823.
(182) Decker, C.; Xuan, H. L.; Viet, T. N. T. *Journal of Polymer Science* **1995**, *33*, 2759.
(183) Kumar, R. N.; Woo, C. K.; Abusamah, A. *Journal of Applied Polymer Science* **1999**, *73*, 1569.
(184) Han, S. O.; Drzal, L. T. *European Polymer Journal* **2003**, *39*, 1377.
(185) Park, W. H.; Lee, J. K. *Journal of Applied Polymer Science* **1998**, *67*, 1101.
(186) Martin, P.; Devaux, J.; Legras, R.; van Gurp, M.; van Duin, M. *Polymer* **2001**, *42*, 2463.
(187) Tang, M.; Dou, H.; Sun, K. *Polymer* **2006**, *47*, 728.
(188) Grandi, S.; Magistris, A.; Mustarelli, P.; Quartarone, E.; Tomasi, C.; Meda, L. *Journal of Non-Crystalline Solids* **2006**, *352*, 273.
(189) Testard, V.; Oberdisse, J.; Ligoure, C. *Macromolecules* **2008**, *41*, 7219.
(190) Puech, N.; Mora, S.; Testard, V.; Porte, G.; Ligoure, C.; Grillo, I.; Phou, T.; Oberdisse, J. *The European Physical Journal E* **2008**, *26*, 13.
(191) Piloyan, G. O.; Ryabchikov, I. D.; Novikova, O. S. *Nature* **1966**, *212*, 1229.
(192) Murat, M.; Grest, G. S. *Macromolecules* **1991**, *24*, 704.
(193) Milner, S. T. *Science* **1991**, *251*, 905.
(194) Carignano, M. A.; Szleifer, I. *Journal of Chemical Physics* **1995**, *102*, 8662.
(195) Cassie, A. B. D.; Baxter, S. *Transactions of the Faraday Society* **1944**, *40*, 546.
(196) Ni, S.; Zhang, P.; Wang, Y.; Winnik, M. *Macromolecules* **1994**, *27*, 5742.
(197) Schillen, K.; Yekta, A.; Ni, S.; Farinha, J. P. S.; Winnik, M. A. *Journal of Physical Chemistry B* **1999**, *103*, 9090.
(198) Yousef, Y. A.; Al-Ani, K. E.; Akasheh, T. *Asian Journal of Chemistry* **2006**, *18*, 1675.
(199) Li, T.; Zhou, C.; Jiang, M. *Polymer Bulletin* **1991**, *25*, 211.

(200) Semerak, S. N.; Frank, C. W. *Macromolecules* **1981**, *14*, 443.
(201) Datka, J.; Boczar, M. *Reaction Kinetics and Catalysis Letters* **1993**, *51*, 161.
(202) Savitzky, A.; Golay, M. *Analytical Chemistry* **1964**, *36*, 1627.
(203) Feng, L.-F.; Hu, G.-H. *American Institute of Chemical Engineers Journal* **2004**, *50*, 2604.
(204) Han, C. D.; Baek, D. M.; Kim, J. K. *Macromolecules* **1995**, *28*, 5886.
(205) Shiau, L.-D. *Macromolecular Theory and Simulations* **2001**, *10*, 179.
(206) *Determination of Molecular Weight*; Cooper, A. R., Ed.; John Wiley & Sons: New York, 1989; Vol. 103, pp 526.
(207) Himenz, P. C. *Polymer Chemistry: The Basic Concepts*, 2nd ed.; Marcel Dekker, Inc.: New York, 1984.

Appendix A

A.1. Minimizing Homopolymer Fluorescence Interference

A. Bulk Homopolymers Melt Mixed with 9-VA NH_2-PI-NH_2

The first attempt to minimize the interference of the fluorescence of the homopolymers when melt mixed with the tagged PI telechelic was to use a telechelic PI with a different fluorescent tag. 19k NH_2-PI-NH_2 with a 9-vinyl anthracene (9-VA) fluorescent tag was used in these studies. The excitation and emission wavelengths of this tag are much different from the APE tag. It was experimentally determined that the optimal excitation and emission wavelength were λ_{ex} = 389 nm and λ_{em} = 415 nm. When a blend of 90% PS/10% PI containing 2.5 wt.% 19k 9-VA NH_2-PI-NH_2 was melt mixed at 180 °C and 100 rpm for 10 minutes, there was still significant fluorescence from the homopolymers. Several different excitation and emission wavelengths were tested to determine if the homopolymer fluorescence contribution could be minimized. The results of these experiments are shown in Figure A.1. Figure A.1 shows that using the optimal excitation and emission wavelengths for the 9-VA NH_2-PI-NH_2 in the blend, λ_{ex} = 389 nm and λ_{em} = 415 nm, also yields the largest fluorescence response from the homopolymers. The optimal wavelengths for a strong telechelic PI response and reduced homopolymer fluorescence appear to be λ_{ex} = 389 nm and λ_{em} = 460 nm. However, it is still clear that the homopolymers cause a great amount of interference in the fluorescence response. If the homopolymer and the telechelic are simply dissolved together in a sample, it is possible to separate the two fluorescence signals. Unfortunately upon melt mixing, the signal is broadened and it is not possible to deconvolute the peaks. This is demonstrated in Figure A.2, where a blend consisting of PS and 5.0 wt.% 19k 9-VA NH_2-PI-NH_2 was made. The sample was melt mixed at 180°C and 100 rpm for times

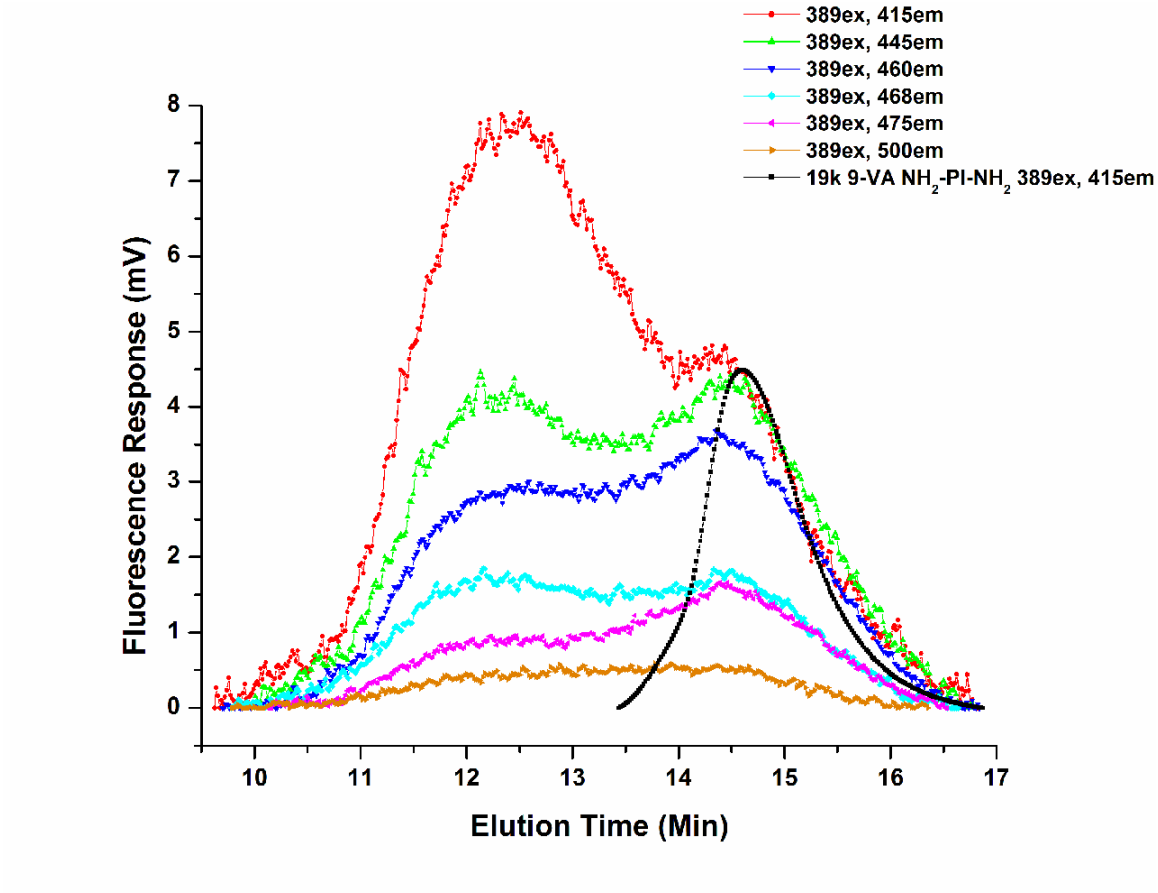

Figure A.1. Fluorescence response as a function of elution time for a blend of 90% PS/10% PI containing 2.5 wt. % 19k 9-VA NH_2-PI-NH_2. The chromatograms show the fluorescence response at various excitation and emission wavelengths.

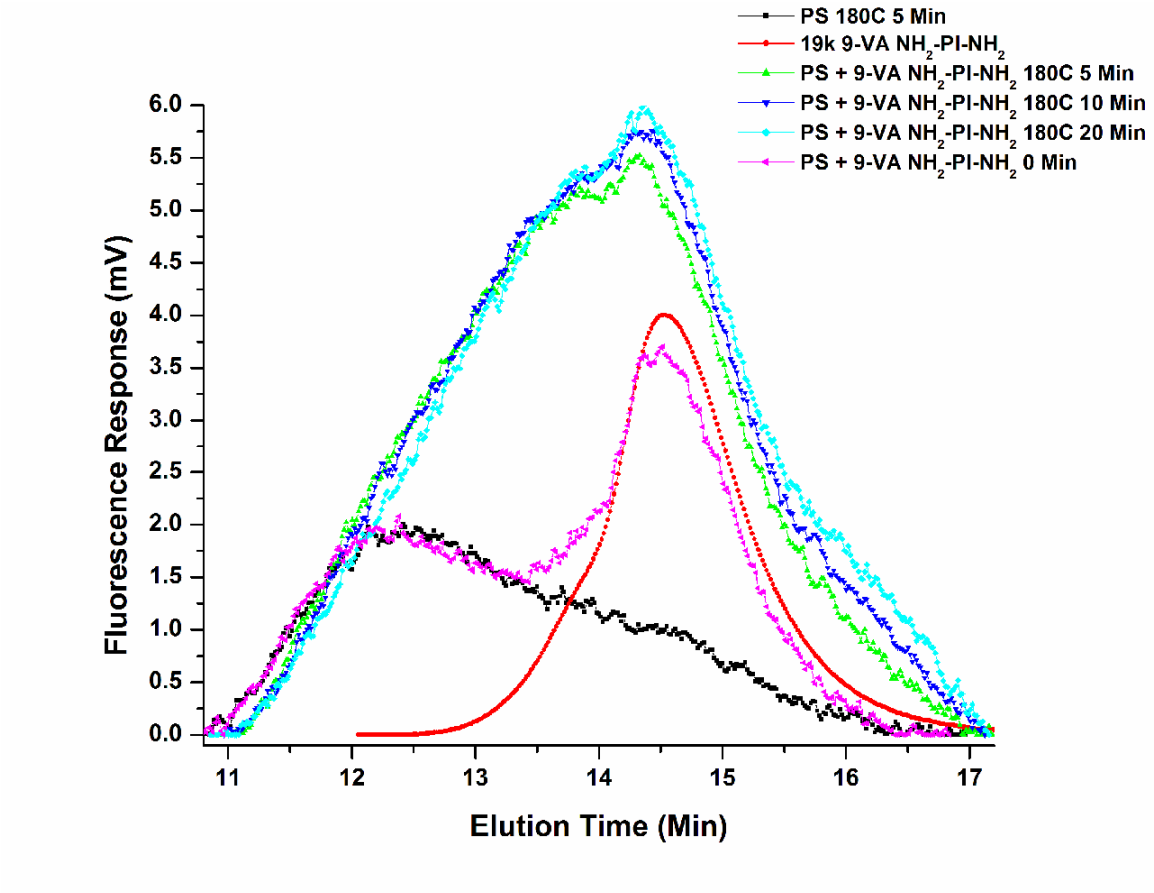

Figure A.2. Fluorescence response as a function of elution time for a blend of PS and 5.0 wt.% 19k 9-VA NH_2-PI-NH_2 melt mixed for 0 – 20 minutes.

ranging between 0 and 20 minutes, and analyzed at λ_{ex} = 389 nm, λ_{em} = 460 nm, and gain = 1000. Figure A.2 clearly shows that the use of the 9-VA tag telechelic will not attenuate the contribution of the bulk homopolymers to the fluorescence.

B. Creating Blends with FR-PS, CM-PI, and 9-VA Telechelic

To try to overcome the fluorescence problems the PS was causing, a decision was made to use a PS homopolymer with a lower PDI and higher molecular weight than the bulk PS. If the PS elutes before the copolymer, then it may still be possible to separate the contribution of the PS to the fluorescence signal, and accurately determine the molecular weight of the copolymer created *in situ* and the conversion of the tagged PI telechelic. The goal of this project is to use a small amount of telechelics in order to compatibilize inexpensive bulk homopolymers. The first attempt to narrow the PDI of the PS was to fractionate a polymer solution of the bulk PS in cold methanol. By using this technique, the lower molecular weight PS and other impurities soluble in methanol remain in solution. The polydispersity of the polymer is subsequently lowered. GPC results of MeOH-precipitated bulk PS showed that the fluorescence intensity actually increased and the PDI was not significantly reduced relative to the previously studies bulk PS. It was then decided to make PS by free radical synthesis (FR-PS). This method is inexpensive and relatively fast, and a PDI as low as ~1.6 can be achieved by using this synthetic technique.

FR-PS1 (M_n = 112,000, M_w = 204,000, PDI = 1.82) was first used as the major constituent of the blend. The synthesis of this polymer is described in Chapter 2.1 B. FR-PS1 and 19k 9-VA NH_2-PI-NH_2 were first dissolved together in a vial with THF, with the telechelic consisting of 2.5 wt.% of the polymer mass. Fluorescence detection at

various emission wavelengths was used to determine the minimum homopolymer fluorescence contribution. Results are shown in Figure A.3. Again, using the most intense emission wavelength of the telechelic, 415 nm, increases the fluorescence of the homopolymer as well. λ_{ex} = 389 nm and λ_{em} = 460 were therefore used for samples containing FR-PS that were compatibilized with 9-VA NH_2-PI-NH_2. When this telechelic was melt mixed with FR-PS1 at 180 °C and 100 rpm, however, a broad peak resulted. Figure A.4 shows the fluorescence response at different mixing times of a blend consisting of 2.5 wt.% telechelic. There is still too much interference in the homopolymer fluorescence for this homopolymer to be used in an experiment that quantifies the conversion of telechelic.

When GPC was used to analyze a blend of PI and 19k 9-VA NH_2-PI-NH_2, new PI was needed. The purchased PI had a much higher molecular weight and PDI than the original PI, thus it had to be broken down to a lower molecular weight and PDI by means of cold mastication. The polyisoprene created in this manner, CM-PI, is described in detail in Chapter 2.1 C. In addition, an even higher molecular weight PS was also synthesized in an attempt to separate the fluorescence contributions of the blend components. The detailed characteristics of these polymers, FR-PS4 – FR-PS7, are listed in Chapter 2.1 B.

When CM-PI1 was melt mixed at 180 °C and 100 RPM for 5 – 60 minutes, the RI and fluorescence peak slightly broadened, as mentioned in Chapter 2.1 C, indicating a small amount of degradation took place. Thus it was not surprising to see that when CM-PI1 was melt mixed with 5.0 wt.% 19k 9-VA NH_2-PI-NH_2, the CM-PI1 fluorescence contribution to the chromatogram increased relative to the telechelic with mixing time.

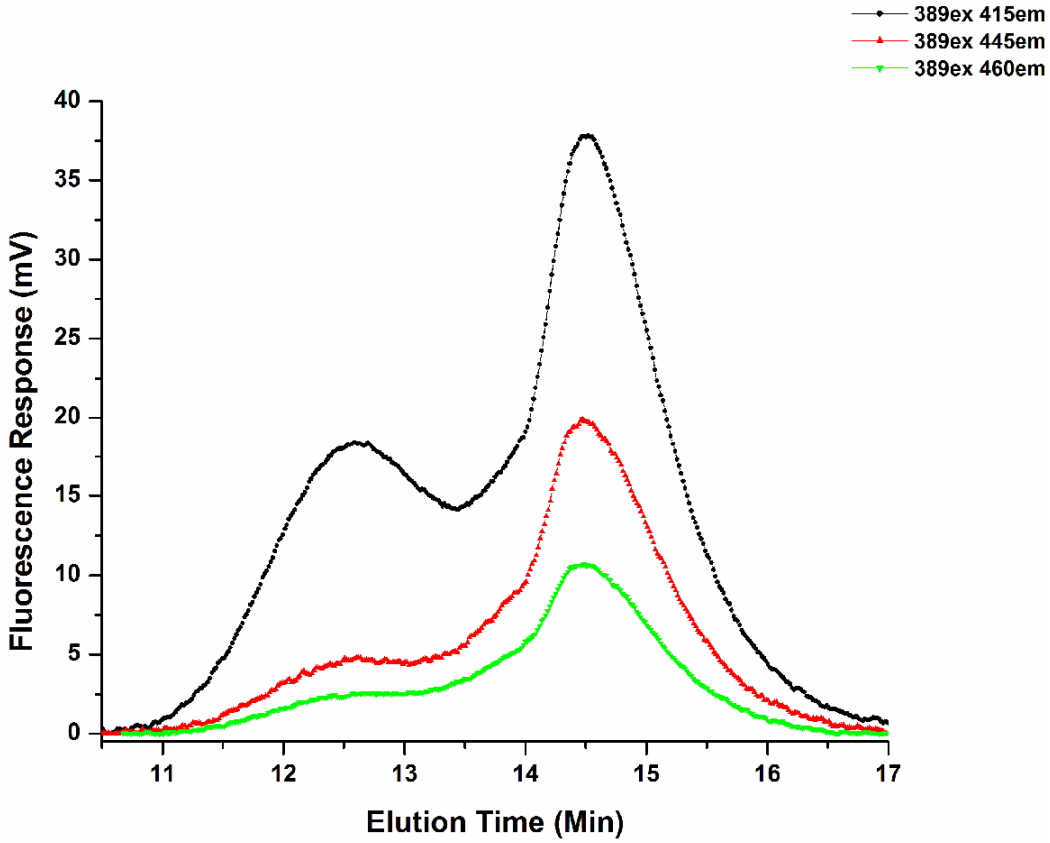

Figure A.3. Fluorescence response as a function of elution time for FR-PS1 co-dissolved with 19k 9-VA NH_2-PI-NH_2.

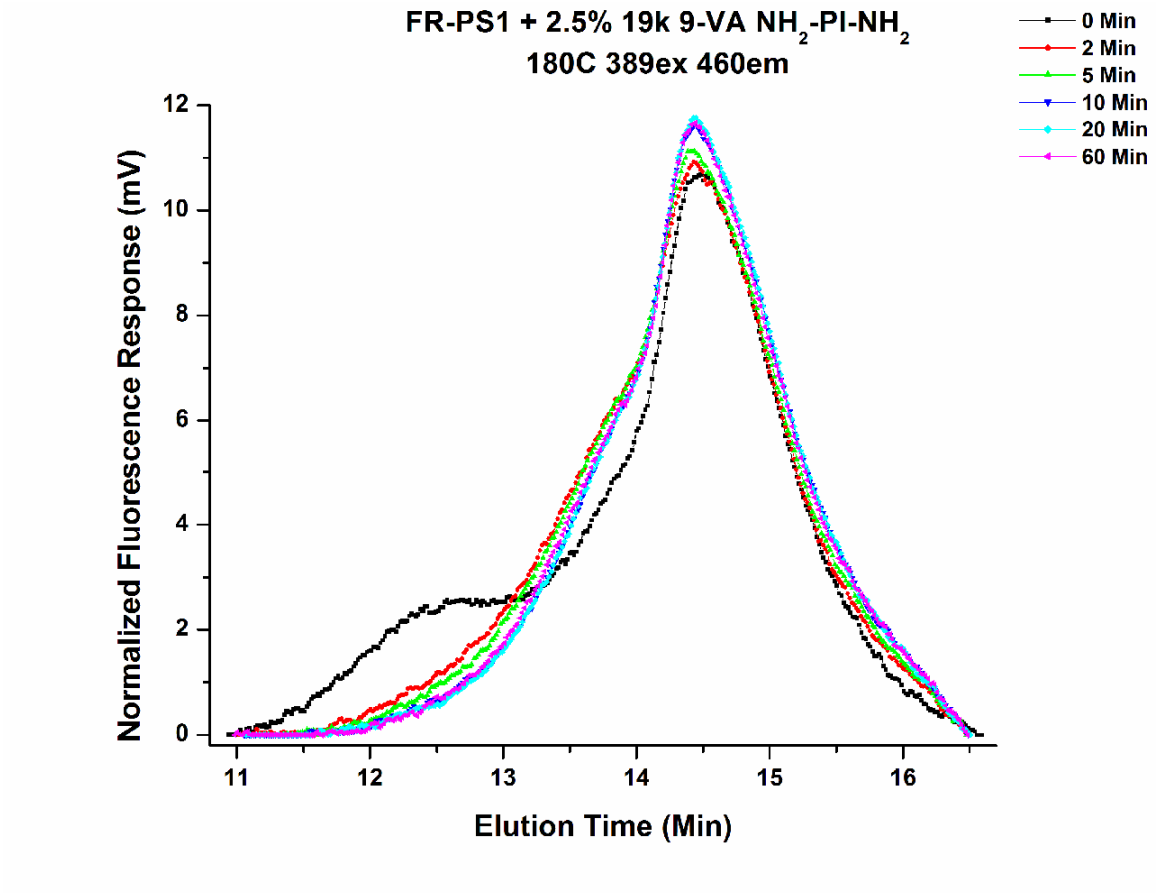

Figure A.4. Fluorescence response as a function of elution time for a blend of FR-PS1 and 19k 9-VA NH_2-PI-NH_2 melt mixed at 180 °C and 100 RPM for various times.

This is shown in Figure A.5, where the area of the melt mixed chromatograms is normalized to contain the same area as the 0 minute chromatogram. The CM-PI1 and telechelic peaks are broadened, but still distinguishable after one hour of mixing. The intensity of the telechelic peak is reduced as a function of mixing time, as some of the telechelic is consumed by reaction with the PI that undergoes thermooxidative degradation. The fact that the peaks can still be deconvoluted after melt mixing proves to be more promising for the determination of the copolymer molecular weight and telechelic PI conversion. In addition, PI only makes up 10% of the homopolymer content in the blends, as opposed to 100% in Figure A.5.

The next progressive step was to analyze a blend of FR-PS/CM-PI with only the 19k 9-VA NH_2-PI-NH_2 to observe how the fluorescence of the homopolymers was affected by melt mixing with the tagged telechelic. In Figure A.6, a representative fluorescence chromatogram of 90% FR-PS5/10% CM-PI1 melt mixed with the appropriate amount of 19k 9-VA NH_2-PI-NH_2 required for 5.0 wt.% of both telechelics (5.0%*) is shown as a function of melt mixing time. From this point forward, when only the required amount of tagged PI telechelic is present in the blend, the telechelic weight percent is denoted with an asterisk. The results in Figure A.6 show that it is possible to deconvolute the chromatogram after 60 minutes of melt mixing at 180 °C and 100 rpm. Therefore if the chromatograms of the tagged telechelic, the homopolymers melt mixed at various times, and the homopolymers with only the tagged telechelic mixed at various times are collected, it should be possible to determine the conversion of the tagged telechelic into a multiblock copolymer when all four components are melt mixed together by separating out the contribution of each component.

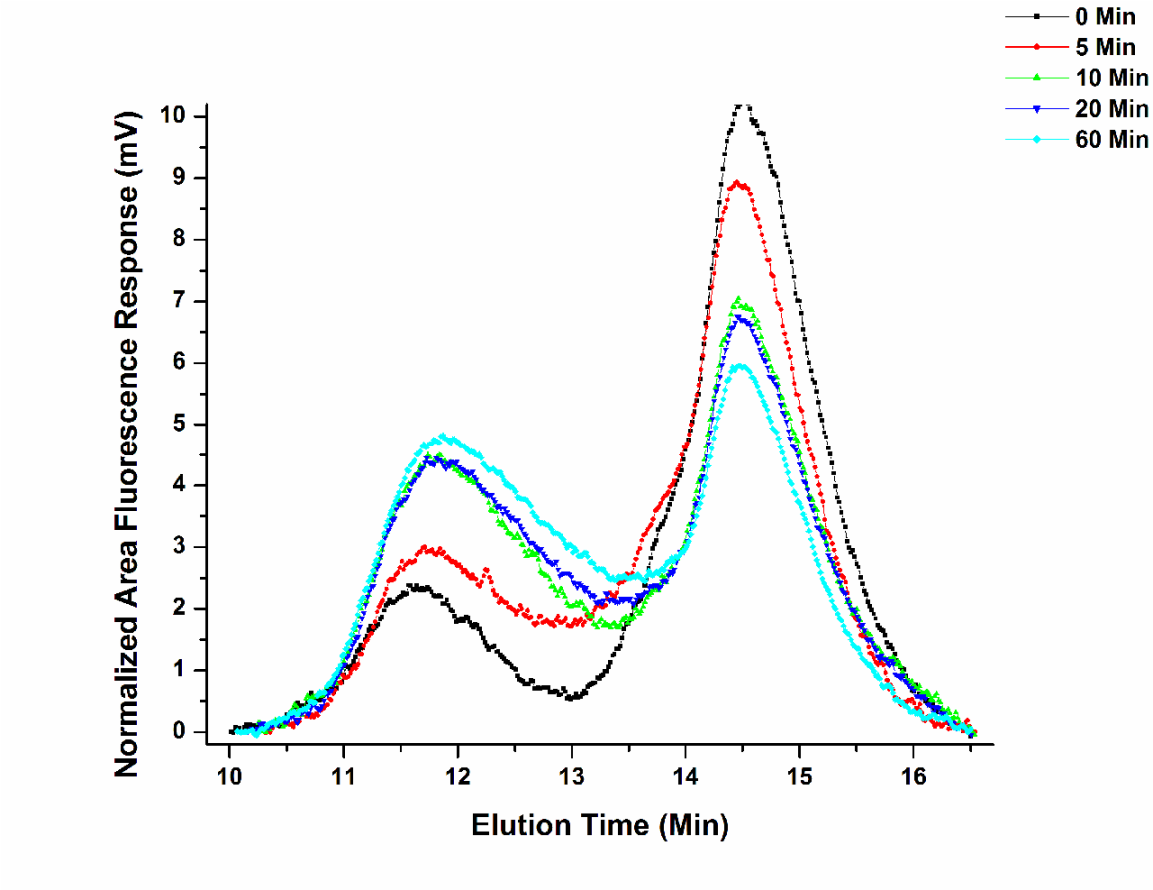

Figure A.5. Fluorescence response as a function of elution time for CM-PI1 + 5.0 wt.% 19k 9-VA NH_2-PI-NH_2 melt mixed for 0 – 60 minutes. The area of each chromatogram is normalized to contain the same area as the 0 minute chromatogram.

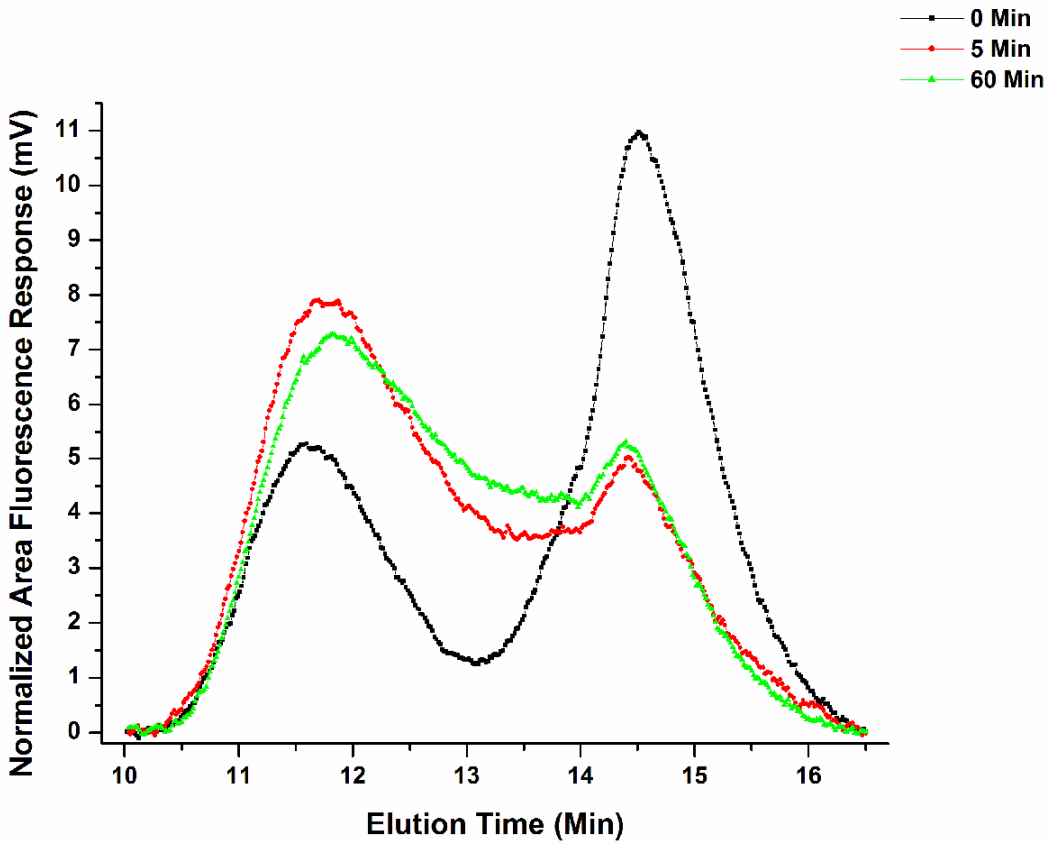

Figure A.6. Normalized fluorescence as a function of elution time for a blend consisting of 90% FR-PS5/10% CM-PI1 + 5.0%* 19k 9-VA NH_2-PI-NH_2 for various mixing times. The chromatogram areas are normalized to contain the same area as the 0 minute chromatogram.

A.2 Appropriate Calculation of Multiblock Copolymer Size

A method to calculate the molecular weight and polydispersity of multiblock copolymers formed *in situ* from reactive polymers from the literature was identified and implemented. From the PDI of the polymer, the Gaussian peak width of its GPC curve can be determined. With knowledge of the peak elution time and peak width of its components, the copolymer chromatogram can be deconvoluted using simple Gaussian peaks that account for diblock, triblock, tetrablock, etc. species. A model developed by Shiau calculates the average properties of block copolymers as a function of reaction conversion without requiring knowledge of the complete molecular weight distribution.[205] The following discussion briefly describes Shiau's method.

In the process to be monitored, two separate polydisperse polymers with reactive end groups react to form multiblock copolymers. Prepolymer *A* has an *A* functional group at each end, and prepolymer *B* has a *B* functional group at each end. Each *A* can react with a *B*, but no reaction among identical groups can occur. It is assumed that all functional groups of the same type have equal reactivity regardless of the size or structure of the polymer it is attached to. Let n_a represent the total moles of prepolymer *A* and n_b represent the total moles of prepolymer *B* in the system. The value α represents the fraction of *A* groups that have reacted and β represents the fraction of *B* groups that have reacted. Therefore the total number of functional groups that have reacted is

$$2n_a\alpha = 2n_b\beta \tag{A.1}$$

Thus $\beta = r\alpha$, where

$$r = n_a/n_b \tag{A.2}$$

The number average molecular weight of the copolymer that is formed, M_n, is defined as the total mass, m_t, divided by the number of molecules, n_t, present at conversion α:

$$M_n = m_t/n_t \tag{A.3}$$

where

$$m_t = n_a M_{n,a} + n_b M_{n,b} \tag{A.4}$$

$$n_t = n_a + n_b - 2\alpha n_a \tag{A.5}$$

$M_{n,a}$ and $M_{n,b}$ are the number average molecular weights of prepolymer *A* and prepolymer *B*, respectively. The value $n_a + n_b$ is the number of moles of prepolymer *A* and prepolymer *B* in the system at the start of the reaction, and $2\alpha n_a$ is the number of bonds formed at conversion α. Each bond combines two molecules into one, so n_t represents the total number of molecules present at conversion α.

The weight average molecular weight of the copolymer, M_w, by definition is

$$M_w = \Sigma[y_a E(W_a) + y_b E(W_b)] \tag{A.6}$$

with

$$y_a = n_a M_{n,a}/(n_a M_{n,a} + n_b M_{n,b}) \tag{A.7}$$

$$y_b = n_b M_{n,b}/(n_a M_{n,a} + n_b M_{n,b}) \tag{A.8}$$

The values y_a and y_b represent the initial weight fraction of prepolymer *A* and prepolymer *B* in the system, respectively. The values $E(W_a)$ and $E(W_b)$ are the expectation values. These expectation values can be expressed as a function of *r*, α, $M_{n,a}$, and $M_{n,b}$, which are known variables. The Shiau paper provides a detailed description of this calculation. The resulting approximation for the weight average molecular weight of the copolymer is

$$M_w = y_a[M_{w,a} + 2(r\alpha^2 M_{n,a} + \alpha M_{n,b})/(1-r\alpha^2)]$$

$$+ y_b[M_{w,b} + 2(r\alpha M_{n,a} + r\alpha^2 M_{n,b})/(1-r\alpha^2)] \quad \text{(A.9)}$$

The polydispersity of the formed copolymer is simply M_w/M_n.

In Shiau's procedure to estimate the copolymer molecular weight, the number of copolymer blocks present is determined by the number of moles of prepolymer *A* and *B*, as well as the fraction of *A* groups that have reacted, α. For copolymers with an odd number of blocks, an average value of the possible permutations is used. For example, a triblock could consist of either an ABA or a BAB structure. For an ABA triblock, $n_a = 2$, $n_b = 1$, and $\alpha = 0.5$. For the BAB triblock, $n_a = 1$, $n_b = 2$, and $\alpha = 1$. The molecular weights of the telechelics are input for $M_{n,a}$, $M_{n,b}$, $M_{w,a}$, and $M_{w,b}$, and always remain the same. These weights are relative to PS standards, so the apparent molecular weights of the PI telechelics are used. After defining the equations and using the mathematical computer program Maple to solve the equations, the copolymer M_n, M_w, and PDI are determined for each diblock, triblock, etc. species.

To deconvolute the multiblock copolymer chromatogram, the experimental curve is fit to a group of Gaussian peaks, where each peak is defined by the following equation

$$y = \frac{A}{\sigma\sqrt{(2\pi)}} \exp\left(\frac{-(x-rt)^2}{2\sigma^2}\right) \quad \text{(A.10)}$$

where *A* is the peak area, σ is the standard deviation, *x* is the retention time, and *rt* is the retention time of the maximum peak height. The median value of a Gaussian peak, *rt*, is calculated by its M_n value.[206] The width of a Gaussian peak is determined by its standard deviation, σ, and can be calculated by[207]

$$\sigma = M_n(PDI - 1)^{0.5} \quad \text{(5.11)}$$

where *PDI* is the polydispersity index calculated by M_w/M_n. To determine the elution time, *rt*, of the copolymer, the calculated M_n value determined by Shiau's method is input into the GPC calibration curve in the Cirrus GPC software.

The Peak Fitting Module in Origin 6.0 was used for peak deconvolution, with the *gauss2* peak function used for fitting. From the GPC results with fluorescence detection, the molecular weights, and therefore the standard deviation, of the telechelics and the homopolymers are determined. The telechelics were analyzed at 0 minutes of melt mixing. The 90% PS/10% PI homopolymer blend was melt mixed for times ranging between 5 – 60 minutes. During fitting, the baseline and standard deviation parameters are locked. It is important to note that the Peak Fitting Module in Origin 6.0 actually uses $(PDI - 1)^{0.5}$ for the standard deviation and not the full equation shown in Equation A.11. After the χ^2 value of the fit is minimized, Origin gives the calculated *rt* and *A* value of the Gaussian curve.

A 90% PS/10% PI blend containing only the PI telechelic and another blend containing both telechelics is melt mixed for 5 – 60 minutes. These blends are carefully weighed to contain the same amount of material. The baseline corrected fluorescence data is then fit in Origin with a series of Gaussian peaks. The baseline, *rt*, and σ values of the unreacted telechelic, the homopolymer blend, and the individual copolymer species determined by Shiau's method are locked, while the area of each curve is allowed to vary. Fits are first made assuming that the copolymers only consist of diblocks, followed by progressively larger multiblocks (i.e. triblocks and diblocks) to compare the quality of fits of each multiblock mixture. The fit with the highest R^2 and lowest χ^2 are deemed the best fit, and an appropriate description of the copolymers formed. Because not all of the

data is used in the fitting, the entire curve of the copolymers may not be fit, and only one half of the Gaussian curve of the unreacted telechelic is fit. To correctly determine the conversion of the telechelic by this fitting method, it is important to use the *AreaFit* value and not *AreaFitT*. The former calculates the entire area of each Gaussian peak by extrapolation, and the latter only calculates the area of the curve that is present in the data fit. The conversion, *C*, is calculated by

$$C = \frac{\text{Area}_{\text{multiblocks}}}{\text{Area}_{\text{multiblocks}} + \text{Area}_{\text{telechelic}}} \tag{A.12}$$

In order to calculate the conversion of PI telechelic due to copolymer creation and not lost due to undesired homopolymer reaction, the conversion into multiblock copolymers C_{cop} is calculated by

$$C_{cop} = C_{2telechelics} - C_{PItelechelic} \tag{A.13}$$

where $C_{2telechelics}$ is the conversion determined when both telechelics are added to the blend, and $C_{PItelechelic}$ is the conversion when only the required amount of PI telechelic is added to the homopolymer blend. In order to determine the conversion where only the PI telechelic is present, the retention time and PDI of the multiblock copolymer with both telechelics is used to make direct comparisons. For example, if the 83k anh-PS-anh/19k 9-VA NH_2-PI-NH_2 system is studied, a diblock is considered to have the same calculated molecular weight and PDI in the blend containing both telechelics and the blend containing only the PI telechelic. A representative fit of a blend with one telechelic and both telechelics is demonstrated in the following figures. The system studied in Figure A.7 is 90% FR-PS5/10% CM-PI1 + 5.0 wt.%* 19k 9-VA NH_2-PI-NH_2 melt mixed for 10 minutes. Figure A.8 is the same system as Figure A.7 except that the blend also includes

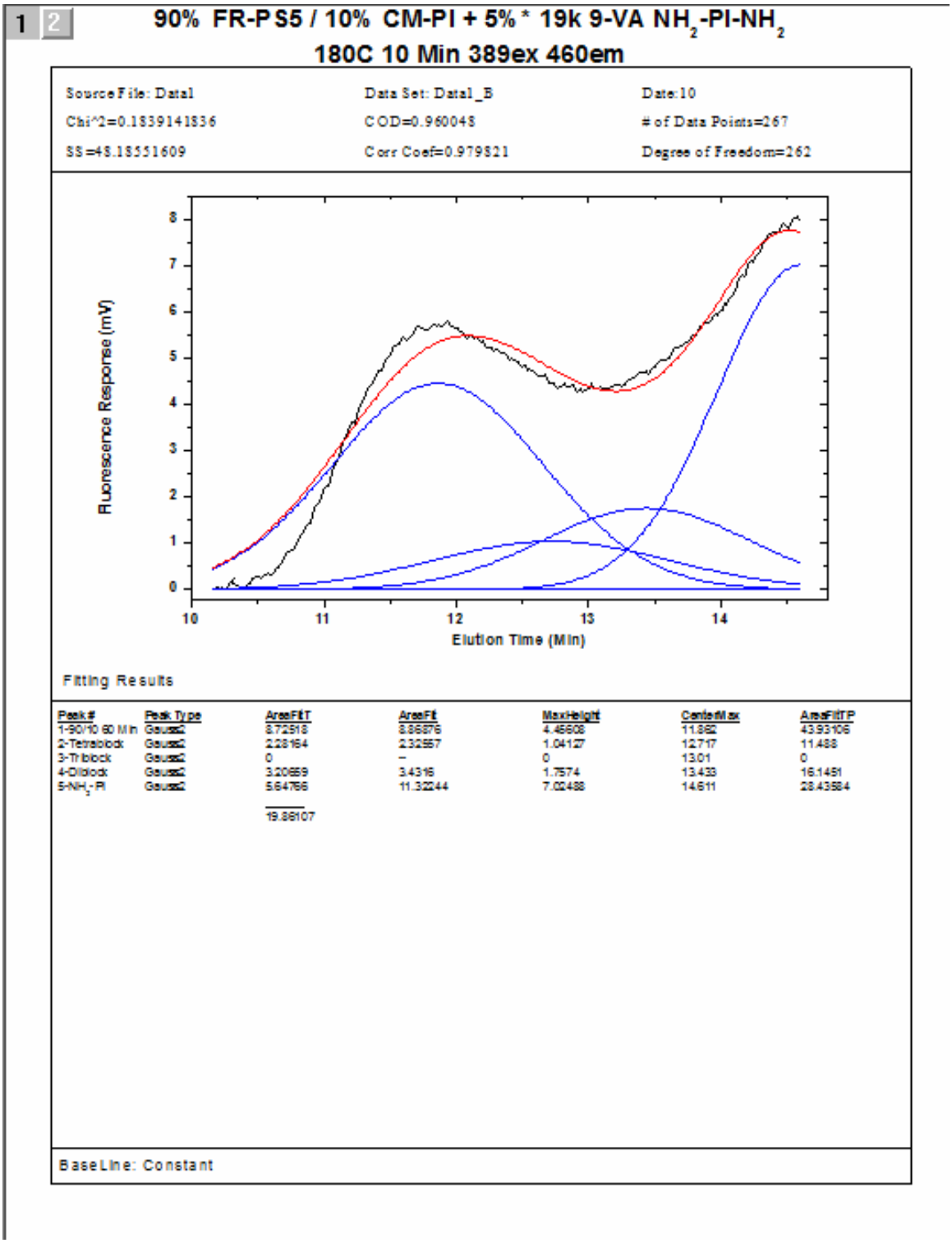

Figure A.7. Deconvolution of a 90% FR-PS5/10% CM-PI1 blend containing 5.0 wt.%* of the 19k 9-VA NH_2-PI-NH_2 telechelic.

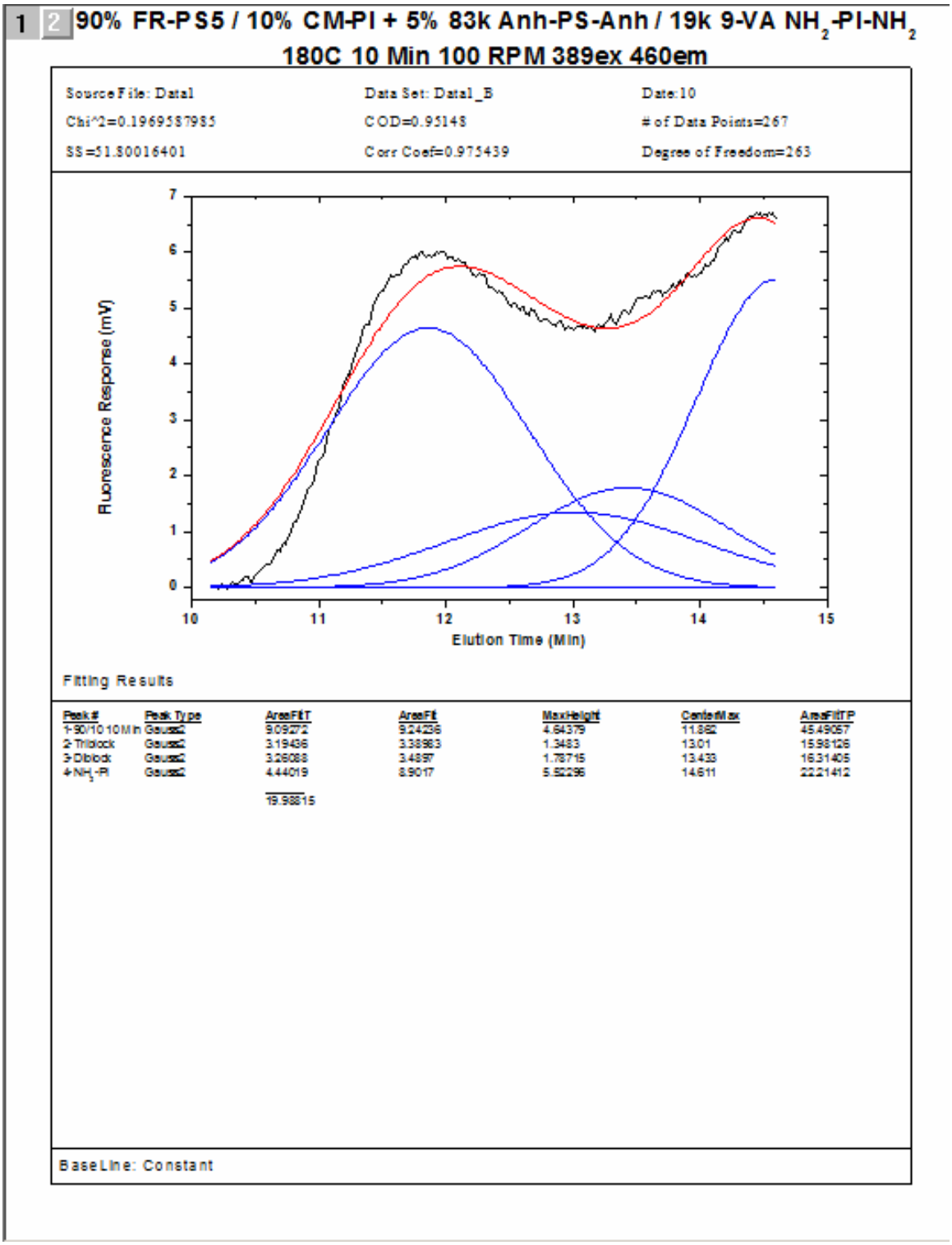

Figure A.8. Deconvolution of a 90% FR-PS5/10% CM-PI1 blend containing 5.0 wt.% of the 83k anh-PS-anh and 19k 9-VA NH_2-PI-NH_2 telechelics.

the 83k anh-PS-anh telechelic. In both figures, the fit is made using multiblock copolymers of tetrablock and smaller sizes. The *AreaFit* data in Figure A.8 shows a conversion of 42.4%, while the conversion in Figure A.7 is 35.7% under the same mixing conditions. Therefore it is concluded that the amount of PI telechelic converted into multiblock copolymers consisting of tetrablocks, triblocks, and diblocks is 8.7%.

If too few multiblock copolymer blocks are used in the fit, the calculated percent area of the homopolymers is too high. As larger and larger multiblock copolymers are used in the fit, their elution time begins to overlap with the homopolymers and "cannibalize" the homopolymer peak area, where the calculated homopolymer peak area becomes too small. To determine the percent of the blend attributed to the homopolymers, the blends were analyzed at 0 minutes mixing time by codissolving the components in THF, and the area fraction of the blend attributed to the homopolymers was calculated. The homopolymer area in the 0 minute blend was normalized so that its contribution to the fluorescence area was equal to its mass fraction in the blend. The homopolymer area in the melt mixed blend was multiplied by the same normalization factor as the 0 minute blend. In this manner, copolymers of increasing block numbers were used in the fit until the percent of the homopolymers in the melt mixed blend was similar to the 0 minute blend as a self-consistent check on the fitting process.

The fitting results of 90% FR-PS5/10% CM-PI1 + 5.0 wt.%* 19k 9-VA NH_2-PI-NH_2 and 90% FR-PS5/10% CM-PI1 + 5.0 wt.% 83k anh-PS-anh/19k 9-VA NH_2-PI-NH_2 blends are shown in Table A.1. In the *Block* column, the Greek prefix refers to the largest multiblock size used in the fit. For example, *Tetra* means tetrablock, triblock, and diblock copolymers were used in the fit. The *90/10 Area%* refers to the fitted percent

area of the homopolymer after multiplying by the normalization factor. The *9-VA %C* (or *APE %C*) refers to the percent conversion of the tagged PI telechelic. R^2 is the fit of the data. *%C Cop* refers to the conversion of the telechelic PI into copolymer, which is calculated by Equation A.15. *Piece #2* indicates cases where a duplication analysis was made. These were different sample pieces from the same batch of blends. Table A.1 shows that the 90% FR-PS5/10% CM-PI1 + 5.0 wt.%* 19k 9-VA NH_2-PI-NH_2 sample which was not melt mixed contained 99.13% homopolymers by mass. To make the homopolymer fluorescence peak 99.13% of the total area, the calculated value was multiplied by 77.05. After multiplying the area of the melt mixed homopolymers by 77.05 in this system, the corresponding *90/10 Area%* values are calculated. None of the blends contained the same homopolymer area as the 0 minute blend. Table 5.4 also shows that no copolymers larger than tetrablocks were formed *in situ*. Using only diblock copolymers in the fitting results in the lowest R^2 value, so it appears at least triblock copolymers are formed. The results show that conversion in different pieces of the same blend varies by as much as 10%, which is observed in blends containing both one and two telechelics. This uncertainty makes determining the conversion into copolymer quite difficult, however Table A.1 suggests that approximately 5 – 10% of the PI telechelics are converted into multiblock copolymers.

The fitting results of 90% FR-PS4/10% CM-PI1 + 5.0 wt.%* 19k 9-VA NH_2-PI-NH_2 and 90% FR-PS4/10% CM-PI1 + 5.0 wt.% 37k anh-PS-anh/19k 9-VA NH_2-PI-NH_2 are shown in Table A.2, which shows that the conversion of the PI telechelic is higher in the blend containing only one telechelic, resulting in a negative copolymer conversion for all melt mixing times. This occurred in the duplication sample as well. Therefore,

Table A.1. Fitting results for blends of 90% FR-PS5/10% CM-PI1 + 5.0 wt.%* 19k 9-VA NH_2-PI-NH_2 and 90% FR-PS5/10% CM-PI1 + 5.0 wt.% 83k anh-PS-anh/19k 9-VA NH_2-PI-NH_2.

90/10 FR-PS5 / CM-PI + 5%* 9-VA for 83/19				**90/10 FR-PS5 / CM-PI + 5% 83/19**				
0 min								
Peak	Wt%	Area	Norm Factor					
90/10	99.13	9.74	77.05					
9-VA	0.87	6.56						
5 Min				*5 Min*				*5 Min*
Block	90/10 Area%	9-VA %C	R^2	Block	90/10 Area%	9-VA %C	R^2	*%C Cop*
Tetra	98.2	32.5	0.9422	Tetra	97.9	31.2	0.9504	-1.3
Tri	98.1	40.5	0.9420	Tri	97.9	30.7	0.9505	-9.8
Di	98.4	31.0	0.9397	Di	98.2	47.5	0.9444	16.5
				Piece #2				
				5 Min				
				Block	90/10 Area%	9-VA %C	R^2	*%C Cop*
				Tetra	98.2	41.6	0.9247	9.1
				Tri	98.2	44.3	0.9244	3.8
				Di	98.6	39.0	0.9192	8.0
10 Min				*10 Min*				*10 Min*
Block	90/10 Area%	9-VA %C	R^2	Block	90/10 Area%	9-VA %C	R^2	*%C Cop*
Tetra	97.6	33.7	0.9601	Tetra	97.8	42.9	0.9516	9.2
Tri	97.5	35.4	0.9598	Tri	97.8	43.6	0.9515	8.2
Di	98.0	32.1	0.9569	Di	98.2	41.0	0.9490	8.9
Piece #2				*Piece #2*				
10 Min				*10 Min*				
Block	90/10 Area%	9-VA %C	R^2	Block	90/10 Area%	9-VA %C	R^2	*%C Cop*
Tetra	98.5	42.9	0.9504	Tetra	98.7	48.3	0.9413	5.4
Tri	98.5	45.2	0.9501	Tri	98.7	49.9	0.9411	4.7
Di	99.0	38.9	0.9295	Di	98.9	46.7	0.9384	7.8
20 Min				*20 Min*				*20 Min*
Block	90/10 Area%	9-VA %C	R^2	Block	90/10 Area%	9-VA %C	R^2	*%C Cop*
Tetra	97.6	43.4	0.9412	Tetra	97.6	47.2	0.9382	3.8
Tri	97.7	43.8	0.9410	Tri	97.6	47.2	0.9383	3.4
Di	98.5	36.9	0.9270	Di	98.4	41.6	0.9286	4.7
60 Min				*60 Min*				*60 Min*
Block	90/10 Area%	9-VA %C	R^2	Block	90/10 Area%	9-VA %C	R^2	*%C Cop*
Tetra	97.9	41.4	0.9401	Tetra	96.6	32.9	0.9611	-8.5
Tri	98.2	46.0	0.9812	Tri	97.1	52.7	0.9556	6.7
Di	98.5	38.1	0.9290	Di	98.2	47.5	0.9444	9.4

Table A.2. Fitting results for blends of 90% FR-PS4/10% CM-PI1 + 5.0 wt.%* 19k 9-VA NH_2-PI-NH_2 and 90% FR-PS4/10% CM-PI1 + 5.0 wt.% 37k anh-PS-anh/19k 9-VA NH_2-PI-NH_2.

90/10 FR-PS4 / CM-PI1 + 5%* 9-VA for 37/19

0 Min

Peak	Wt%	Area	Norm Factor
90/10	98.47	10.52	75.62
9-VA	1.53	12.33	

5 Min

Block	90/10 Area%	9-VA %C	R^2
Octa	97.8	55.1	0.9379
Hepta	98.0	51.6	0.9366
Hexa	98.1	50.0	0.9367
Penta	98.1	49.5	0.9357
Tetra	98.4	47.2	0.9293
Tri	98.6	58.2	0.9214
Di	98.9	79.6	0.8539

10 Min

Block	90/10 Area%	9-VA %C	R^2
Octa	96.6	60.4	0.9549
Hepta	97.2	54.7	0.9539
Hexa	97.4	53.5	0.9541
Penta	97.4	52.6	0.9533
Tetra	97.9	48.2	0.9490
Tri	98.0	59.6	0.9409
Di	98.6	82.5	0.8566

Piece #2

10 Min

Block	90/10 Area%	9-VA %C	R^2
Octa	98.7	69.9	0.9364
Hepta	98.8	66.5	0.9370
Hexa	98.8	66.4	0.9370
Penta	98.8	65.2	0.9365
Tetra	98.9	60.7	0.9355
Tri	98.9	65.1	0.9350
Di	99.2	95.4	0.9097

20 Min

Block	90/10 Area%	9-VA %C	R^2
Octa	97.2	60.6	0.9387
Hepta	97.5	57.0	0.9363
Hexa	97.7	54.9	0.9359
Penta	97.8	54.0	0.9347
Tetra	98.2	50.5	0.9268
Tri	98.4	62.3	0.9184
Di	98.8	86.3	0.8380

60 Min

Block	90/10 Area%	9-VA %C	R^2
Octa	96.9	60.2	0.9426
Hepta	97.3	56.3	0.9399
Hexa	97.6	54.1	0.9393
Penta	97.6	53.8	0.9380
Tetra	98.1	51.4	0.9192
Tri	97.9	71.5	0.9755
Di	98.8	86.3	0.8318

90/10 FR-PS4 / CM-PI1 + 5% 37/19

5 Min

Block	90/10 Area%	9-VA %C	R^2	*5 Min %C Cop*
Octa	97.7	48.6	0.9429	-6.5
Hepta	98.0	44.2	0.9432	-7.4
Hexa	98.0	44.2	0.9432	-5.8
Penta	98.0	43.4	0.9428	-6.1
Tetra	98.1	40.0	0.9418	-7.2
Tri	98.1	42.3	0.9416	-15.9
Di	98.5	57.1	0.9133	-22.5

10 Min

Block	90/10 Area%	9-VA %C	R^2	*10 Min %C Cop*
Octa	97.7	47.2	0.9541	-13.2
Hepta	97.7	47.1	0.9541	-7.6
Hexa	97.8	46.6	0.9541	-6.9
Penta	97.8	46.0	0.9539	-6.6
Tetra	97.9	43.5	0.9536	-4.7
Tri	97.9	45.0	0.9535	-14.6
Di	98.4	61.1	0.9210	-21.4

Piece #2

10 Min

Block	90/10 Area%	9-VA %C	R^2	*%C Cop*
Octa	98.1	62.6	0.9411	-7.3
Hepta	98.3	58.6	0.9416	-7.9
Hexa	98.3	58.9	0.9417	-7.5
Penta	98.3	57.6	0.9411	-7.6
Tetra	98.5	51.5	0.9391	-9.2
Tri	98.2	60.8	0.8568	-4.3
Di	99.0	85.9	0.8943	-9.5

20 Min

Block	90/10 Area%	9-VA %C	R^2	*20 Min %C Cop*
Octa	97.0	51.9	0.9486	-8.7
Hepta	97.3	47.9	0.9390	-9.1
Hexa	97.5	47.3	0.9473	-7.6
Penta	97.5	46.5	0.9467	-7.5
Tetra	97.7	44.1	0.9305	-6.4
Tri	97.9	48.6	0.9412	-13.7
Di	98.4	65.3	0.8926	-21.0

60 Min

Block	90/10 Area%	9-VA %C	R^2	*60 Min %C Cop*
Octa	96.5	56.1	0.9484	-4.1
Hepta	97.0	52.4	0.9462	-3.9
Hexa	97.3	50.4	0.9458	-3.7
Penta	97.3	49.5	0.9449	-4.3
Tetra	97.8	47.3	0.9383	-4.1
Tri	98.0	54.7	0.9333	-16.8
Di	98.5	73.8	0.8667	-12.5

the conversion for this telechelic pair could not be determined using this method.

In Table A.3, the fitting results of 90% FR-PS5/10% CM-PI1 + 5.0 wt.%* 19k 9-VA NH_2-PI-NH_2 and 90% FR-PS5/10% CM-PI1 + 5.0 wt.% 16k anh-PS-anh/19k 9-VA NH_2-PI-NH_2 blends are shown. Table A.3 indicates that although fitting with nonablock and decablock copolymers yields a higher R^2 value than smaller block number copolymers, with these larger copolymers, the area of the homopolymer begins reduce significantly. This is most apparent in the blends melt mixed for 20 minutes and 60 minutes. Although no melt mixed homopolymer area matches the 0 minute homopolymer area, it is very unlikely that copolymers of 9 and 10 blocks are being formed, as the homopolymer area fraction is much lower in these conditions than when smaller blocks are used in the fitting. For the 20 – 60 melt mixing times, there appears to be a significant decrease in homopolymer area when copolymers larger than hexablocks are used. The conversion of telechelics into copolymer is ~6% – 7% when fitting with hexablock and smaller copolymers.

Fitting for reduced telechelic loading was also conducted to see if the conversion of PI telechelic increases due to less excess telechelics present in the blend. The results of 90% FR-PS5/10% CM-PI1 + 2.5%* 19k 9-VA NH_2-PI-NH_2 and 90% FR-PS5/10% CM-PI1 + 2.5% 16k anh-PS-anh/19k 9-VA NH_2-PI-NH_2 blends are shown in Table A.4. Comparison between Table A.4 and Table A.3 shows that when the telechelic loading in the 16k anh-PS-anh/19k 9-VA NH_2-PI-NH_2 is reduced from 5.0% to 2.5%, the conversion slightly increases. It is difficult to determine the actual number of blocks formed in the 2.5% loading blend as well, as the homopolymer area fraction does not approach that of the 0 minute homopolymer area fraction. Again, it still appears that

Table A.3. Fitting results for blends of 90% FR-PS5/10% CM-PI1 + 5.0 wt.%* 19k 9-VA NH_2-PI-NH_2 and 90% FR-PS5/10% CM-PI1 + 5.0 wt.% 16k anh-PS-anh/19k 9-VA NH_2-PI-NH_2.

90/10 FR-PS5 / CM-PI1 + 5%* 9-VA for 16/19

0 Min

Peak	Wt%	Area	Norm Factor
90/10	97.37	33.40	73.92
9-VA	2.63	66.60	

5 Min

Block	90/10 Area%	9-VA %C	R^2
Deca	91.1	59.0	0.9940
Nona	91.5	57.7	0.9940
Octa	91.6	57.4	0.9940
Hepta	91.9	54.5	0.9939
Hexa	92.3	52.5	0.9939
Penta	92.2	51.3	0.9939
Tetra	93.4	48.0	0.9935
Tri	93.4	54.6	0.9934
Di	94.9	98.7	0.9815

10 Min

Block	90/10 Area%	9-VA %C	R^2
Deca	91.7	54.2	0.9931
Nona	92.0	53.1	0.9931
Octa	92.0	53.5	0.9931
Hepta	91.3	47.5	0.9892
Hexa	92.9	47.2	0.9931
Penta	92.7	44.4	0.9930
Tetra	94.2	47.9	0.9917
Tri	94.2	55.2	0.9913
Di	95.4	98.9	0.9758

Piece #2
10 Min

Block	90/10 Area%	9-VA %C	R^2
Deca	91.4	56.2	0.9941
Nona	91.6	55.2	0.9941
Octa	91.5	56.0	0.9941
Hepta	92.3	51.0	0.9941
Hexa	92.5	50.2	0.9941
Penta	92.4	46.4	0.9940
Tetra	94.0	49.7	0.9927
Tri	93.9	57.3	0.9923
Di	95.2	100.0	0.9738

20 Min

Block	90/10 Area%	9-VA %C	R^2
Deca	85.7	57.1	0.9936
Nona	88.6	60.0	0.9919
Octa	90.4	55.5	0.9918
Hepta	90.2	54.6	0.9917
Hexa	92.3	47.1	0.9912
Penta	92.1	44.6	0.9913
Tetra	94.3	49.7	0.9886
Tri	94.3	57.3	0.9881
Di	95.6	100.0	0.9707

60 Min

Block	90/10 Area%	9-VA %C	R^2
Deca	82.5	66.9	0.9921
Nona	86.8	62.2	0.9918
Octa	88.6	60.0	0.9918
Hepta	88.6	55.9	0.9915
Hexa	92.0	47.5	0.9910
Penta	92.2	49.8	0.9907
Tetra	93.8	55.4	0.9883
Tri	94.7	67.2	0.9835
Di	95.4	100.0	0.8787

90/10 FR-PS5 / CM-PI1 + 5% 16/19

5 Min

Block	90/10 Area%	9-VA %C	R^2	*5 Min %C Cop*
Deca	93.5	68.3	0.9879	9.3
Nona	94.3	63.6	0.9878	5.9
Octa	94.2	64.5	0.9878	7.1
Hepta	94.3	61.0	0.9876	6.5
Hexa	94.9	52.3	0.9874	-0.2
Penta	94.9	52.3	0.9873	1.0
Tetra	95.7	50.0	0.9858	2.0
Tri	95.7	58.0	0.9855	3.4
Di	96.3	100.0	0.9624	1.3

10 Min

Block	90/10 Area%	9-VA %C	R^2	*10 Min %C Cop*
Deca	91.4	60.5	0.9943	6.3
Nona	91.7	59.2	0.9943	6.1
Octa	91.6	60.7	0.9943	7.2
Hepta	92.0	56.5	0.9942	9.0
Hexa	92.5	53.9	0.9942	6.7
Penta	92.4	51.6	0.9942	7.2
Tetra	94.0	46.3	0.9932	-1.6
Tri	93.8	60.3	0.9921	5.1
Di	95.0	100.0	0.9555	1.1

Piece #2
10 Min

Block	90/10 Area%	9-VA %C	R^2	*%C Cop*
Deca	96.0	61.3	0.9736	5.1
Nona	96.3	57.8	0.9736	2.6
Octa	96.3	58.0	0.9736	2.0
Hepta	96.6	48.5	0.9730	-2.5
Hexa	96.9	47.5	0.9725	-2.7
Penta	97.0	51.4	0.9715	5.0
Tetra	97.6	54.1	0.9620	4.4
Tri	97.5	70.1	0.9591	12.8
Di	97.4	100.0	0.7475	0.0

20 Min

Block	90/10 Area%	9-VA %C	R^2	*20 Min %C Cop*
Deca	85.4	71.5	0.9943	14.4
Nona	88.4	66.8	0.9940	6.8
Octa	90.1	64.7	0.9940	9.2
Hepta	90.1	61.4	0.9939	6.8
Hexa	92.3	53.5	0.9935	6.4
Penta	93.0	45.6	0.9931	1.0
Tetra	94.3	47.3	0.9915	-2.4
Tri	94.2	61.6	0.9907	4.3
Di	95.2	100.0	0.9495	0.0

60 Min

Block	90/10 Area%	9-VA %C	R^2	*60 Min %C Cop*
Deca	59.1	68.9	0.9947	2.0
Nona	75.8	64.6	0.9945	2.4
Octa	80.4	62.8	0.9945	2.8
Hepta	80.2	58.6	0.9943	2.7
Hexa	88.1	55.1	0.9939	7.6
Penta	88.9	52.8	0.9934	3.0
Tetra	93.3	61.6	0.9863	6.2
Tri	93.3	71.4	0.9849	4.2
Di	95.5	100.0	0.9384	0.0

Table A.4. Fitting results for blends of 90% FR-PS5/10% CM-PI1 + 2.5%* 19k 9-VA NH_2-PI-NH_2 and 90% FR-PS5/10% CM-PI1 + 2.5% 16k anh-PS-anh/19k 9-VA NH_2-PI-NH_2.

90/10 FR-PS5 / CM-PI1 + 2.5%* 9-VA for 16/19

0 Min

Peak	Wt%	Area	Norm Factor
90/10	98.73	53.06	68.50
9-VA	1.28	46.94	

5 Min

Block	90/10 Area%	9-VA %C	R^2
Deca	95.4	60.9	0.9793
Nona	95.7	60.8	0.9793
Octa	95.7	57.8	0.9791
Hepta	95.9	53.6	0.9788
Hexa	96.1	49.6	0.9786
Penta	96.1	47.6	0.9786
Tetra	96.6	46.0	0.9769
Tri	96.6	55.9	0.9765
Di	97.1	100.0	0.9595

10 Min

Block	90/10 Area%	9-VA %C	R^2
Deca	95.4	51.5	0.9792
Nona	95.6	49.6	0.9793
Octa	95.6	49.5	0.9792
Hepta	95.8	44.0	0.9789
Hexa	96.1	38.9	0.9787
Penta	96.1	37.9	0.9786
Tetra	96.7	45.7	0.9750
Tri	96.7	52.7	0.9745
Di	97.1	93.4	0.9559

Piece #2

10 Min

Block	90/10 Area%	9-VA %C	R^2
Deca	95.0	54.1	0.9810
Nona	95.4	52.1	0.9810
Octa	95.4	50.8	0.9809
Hepta	95.6	45.1	0.9805
Hexa	95.6	39.4	0.9803
Penta	96.0	42.6	0.9800
Tetra	96.7	49.3	0.9748
Tri	96.7	57.8	0.9739
Di	97.1	100.0	0.9477

20 Min

Block	90/10 Area%	9-VA %C	R^2
Deca	95.0	49.7	0.9759
Nona	95.5	46.4	0.9756
Octa	95.8	44.6	0.9754
Hepta	95.8	40.4	0.9751
Hexa	96.4	35.3	0.9739
Penta	96.4	38.6	0.9734
Tetra	97.0	44.3	0.9678
Tri	97.0	51.3	0.9672
Di	97.4	89.0	0.9484

60 Min

Block	90/10 Area%	9-VA %C	R^2
Deca	92.9	50.9	0.9814
Nona	93.4	48.1	0.9811
Octa	94.0	44.8	0.9810
Hepta	94.2	40.6	0.9805
Hexa	95.3	38.4	0.9796
Penta	95.4	42.5	0.9787
Tetra	96.4	48.8	0.9719
Tri	96.3	56.6	0.9710
Di	96.9	98.3	0.9476

90/10 FR-PS5 / CM-PI1 + 2.5% 16/19

0 Min

Peak	Wt%	Area	Norm Factor
90/10	98.62	50.60	69.71
9-VA	1.38	49.40	

5 Min

Block	90/10 Area%	9-VA %C	R^2	*5 Min %C Cop*
Deca	95.7	60.4	0.9749	-0.5
Nona	96.0	56.6	0.9747	-4.2
Octa	96.0	56.6	0.9747	-1.2
Hepta	96.1	50.8	0.9743	-2.8
Hexa	96.4	46.1	0.9740	-3.5
Penta	96.4	44.2	0.9739	-3.4
Tetra	96.9	39.9	0.9722	-6.1
Tri	96.8	52.3	0.9718	-3.6
Di	97.2	93.7	0.9557	-6.3

10 Min

Block	90/10 Area%	9-VA %C	R^2	*10 Min %C Cop*
Deca	95.1	59.3	0.9815	7.8
Nona	95.3	56.7	0.9815	7.1
Octa	95.3	56.2	0.9815	6.7
Hepta	95.4	52.2	0.9812	8.2
Hexa	95.8	45.9	0.9811	7.0
Penta	95.7	44.0	0.9811	6.1
Tetra	96.4	42.7	0.9789	-3.0
Tri	96.4	55.8	0.9781	3.1
Di	96.9	99.9	0.9581	6.5

Piece #2

10 Min

Block	90/10 Area%	9-VA %C	R^2	*%C Cop*
Deca	94.5	65.1	0.9819	11.0
Nona	94.8	63.7	0.9820	11.6
Octa	94.8	63.9	0.9819	13.1
Hepta	95.2	55.6	0.9814	10.5
Hexa	95.6	51.2	0.9812	11.8
Penta	95.5	48.7	0.9811	6.1
Tetra	96.4	56.6	0.9763	7.3
Tri	96.4	65.6	0.9754	7.8
Di	96.5	100.0	0.8583	0.0

20 Min

Block	90/10 Area%	9-VA %C	R^2	*20 Min %C Cop*
Deca	93.5	56.9	0.9791	7.2
Nona	94.2	53.0	0.9785	6.6
Octa	94.7	51.4	0.9783	6.8
Hepta	94.7	47.5	0.9779	7.1
Hexa	95.5	40.0	0.9769	4.7
Penta	95.5	42.1	0.9767	3.5
Tetra	96.4	48.7	0.9714	4.4
Tri	96.4	56.3	0.9708	5.0
Di	97.0	99.0	0.9494	10.0

60 Min

Block	90/10 Area%	9-VA %C	R^2	*60 Min %C Cop*
Deca	91.8	60.2	0.9812	9.3
Nona	92.8	56.1	0.9807	8.0
Octa	93.5	53.3	0.9806	8.5
Hepta	93.9	48.3	0.9800	7.7
Hexa	95.0	44.8	0.9790	6.4
Penta	95.2	48.3	0.9782	5.8
Tetra	96.3	50.0	0.9705	1.2
Tri	96.3	64.9	0.9685	8.3
Di	96.6	100.0	0.8883	1.7

about 5% – 10% conversion of telechelic into multiblock copolymer occurs at this loading level.

Telechelic loading levels were further reduced in order to determine if the telechelic PI conversion could be significantly increased. Blends of 90% FR-PS6/10% CM-PI1 + 0.5%* 19k 9-VA NH_2-PI-NH_2 and 90% FR-PS6/10% CM-PI1 + 0.5% 37k anh-PS-anh/19k 9-VA NH_2-PI-NH_2 were made, with the fitting results displayed in Table A.5. Table A.5 indicates that only up to triblock copolymers are formed in the 0.5% 37k anh-PS-anh/19k 9-VA NH_2-PI-NH_2 blend. The homopolymer area fractions in the melt mixed blends are very close to the 0 minute homopolymer area. However, the R^2 in all the blends is poor. The negative copolymer conversion also indicates this data is not useful.

Table A.5. Fitting results for blends of 90% FR-PS6/10% CM-PI1 + 0.5%* 19k 9-VA NH_2-PI-NH_2 and 90% FR-PS6/10% CM-PI1 + 0.5% 37k anh-PS-anh/19k 9-VA NH_2-PI-NH_2.

90/10 FR-PS6 / CM-PI1 + 0.5%* 9-VA for 37/19				**90/10 FR-PS6 / CM-PI1 + 0.5% 37/19**				
				0 Min				
				Peak	Wt%	Area	Norm Factor	
				90/10	99.73	83.60	73.37	
				9-VA	0.27	16.40		
5 Min				*5 Min*				*5 Min*
Block	90/10 Area%	9-VA %C	R^2	Block	90/10 Area%	9-VA %C	R^2	*%C Cop*
Tri	99.5	58.7	0.9212	Tri	99.4	50.1	0.9260	-8.6
Di	99.5	75.6	0.9191	Di	99.5	72.4	0.9221	-3.2
10 Min				*10 Min*				*10 Min*
Block	90/10 Area%	9-VA %C	R^2	Block	90/10 Area%	9-VA %C	R^2	*%C Cop*
Tri	99.4	52.9	0.9118	Tri	99.5	57.0	0.9058	4.1
Di	99.4	73.2	0.9071	Di	99.6	66.7	0.9053	-6.5
20 Min				*20 Min*				*20 Min*
Block	90/10 Area%	9-VA %C	R^2	Block	90/10 Area%	9-VA %C	R^2	*%C Cop*
Tri	99.2	51.6	0.8767	Tri	99.5	53.0	0.8794	1.4
Di	99.3	70.0	0.8695	Di	99.5	62.5	0.8785	-7.5
60 Min				*60 Min*				*60 Min*
Block	90/10 Area%	9-VA %C	R^2	Block	90/10 Area%	9-VA %C	R^2	*%C Cop*
Tri	98.9	57.1	0.8486	Tri	99.2	58.1	0.8435	1.0
Di	99.1	80.1	0.8319	Di	99.4	77.7	0.8376	-2.4

To see if the low block number and conversion in the 0.5% anh/NH_2 blend was the result of using FR-PS6, a very high molecular weight homopolymer, blends of 90% FR-PS6/10% CM-PI1 + 5.0%* 20k COOH-PI-COOH and 90% FR-PS6/10% CM-PI1 + 5.0% 44k epoxy-PS-epoxy/20k COOH-PI-COOH were made because there was not enough 37k anh-PS-anh remaining to conduct further studies. The fitting results of these blends are shown in Table A.6. Again, when FR-PS6 is used as the matrix in the blend, copolymers no larger than tetrablocks are formed. The R^2 value is good, but the homopolymer area fraction of the melt mixed samples is actually higher than the 0 minute blend. In addition, conversion of COOH-PI-COOH into copolymer is positive only for the 60 minute blend.

It appears that the molecular weight of the FR-PS6 is too high to allow for significant reaction between the telechelics. Since viscosity is proportional to $M_w^{3.4}$ for entangled polymers, the viscosity of FR-PS6 is 2.6 times greater than FR-PS4 and 3.3 times greater than FR-PS5 based on this simple approximation. This significantly hinders the telechelic reaction, as they approach the interface much more slowly than in the lower molecular weight matrix. Since there was difficulty reducing the molecular weight of the FR-PS using a new monomer batch, further reduced loading fluorescence studies were not completed.

Although it is difficult to determine the actual conversion of PI telechelic into a multiblock copolymer, we are certain that this conversion occurs. Figure 5.11 in Chapter 5.3 A clearly shows an increase in the fluorescence intensity at shorter elution times when 37k anh-PS-anh and 16k NH_2-PI-NH_2 telechelics are melt mixed without any homopolymers present, indicating the presence of higher molecular weight species. A

Table A.6. Fitting results for blends of 90% FR-PS6/10% CM-PI1 + 5.0%* 20k COOH-PI-COOH and 90% FR-PS6/10% CM-PI1 + 5.0% 44k epoxy-PS-epoxy/20k COOH-PI-COOH.

90/10 FR-PS6 / CM-PI1 + 5%* 20k COOH for 44/20				**90/10 FR-PS6 / CM-PI1 + 5% 44/20**				
				0 Min				
				Peak	Wt%	Area	Norm Factor	
				90/10	98.28	5.35	1010.73	
				9-VA	1.72	94.65		
5 Min				*5 Min*				*5 Min*
Block	90/10 Area%	APE %C	R^2	Block	90/10 Area%	APE %C	R^2	*%C Cop*
Tetra	99.5	19.5	0.9931	Tetra	99.5	17.3	0.9924	-2.2
Tri	99.5	19.7	0.9931	Tri	99.5	17.5	0.9924	-2.2
Di	99.6	19.3	0.9929	Di	99.5	16.9	0.9921	-2.4
10 Min				*10 Min*				*10 Min*
Block	90/10 Area%	APE %C	R^2	Block	90/10 Area%	APE %C	R^2	*%C Cop*
Tetra	99.6	26.1	0.9921	Tetra	99.5	22.0	0.9927	-4.1
Tri	99.5	27.6	0.9936	Tri	99.5	22.4	0.9927	-5.2
Di	99.6	25.7	0.9910	Di	99.6	21.4	0.9915	-4.3
Piece #2				*Piece #2*				
10 Min				*10 Min*				
Block	90/10 Area%	APE %C	R^2	Block	90/10 Area%	APE %C	R^2	*%C Cop*
Tetra	99.6	26.1	0.9923	Tetra	99.5	23.2	0.9926	-2.9
Tri	99.6	26.3	0.9922	Tri	99.5	22.8	0.9917	-3.5
Di	99.6	26.0	0.9920	Di	99.5	27.4	0.9936	1.4
20 Min				*20 Min*				*20 Min*
Block	90/10 Area%	APE %C	R^2	Block	90/10 Area%	APE %C	R^2	*%C Cop*
Tetra	99.6	28.1	0.9920	Tetra	99.5	26.4	0.9935	-1.7
Tri	99.6	28.4	0.9920	Tri	99.5	26.8	0.9935	-1.6
Di	99.6	29.0	0.9918	Di	99.6	26.0	0.9926	-3.0
60 Min				*60 Min*				*60 Min*
Block	90/10 Area%	APE %C	R^2	Block	90/10 Area%	APE %C	R^2	*%C Cop*
Tetra	99.6	35.5	0.9910	Tetra	99.6	42.4	0.9912	6.9
Tri	99.6	36.0	0.9910	Tri	99.6	41.4	0.9905	5.4
Di	99.6	35.1	0.9893	Di	99.6	40.6	0.9906	5.5

summary of the results that use Shiau's method to determine the multiblock copolymer size are displayed in Table A.7. These results show that after only 5 minutes of melt mixing, nearly one half of the APE-tagged PI telechelic is converted into multiblock copolymers containing up to 4 blocks. After 20 minutes of melt mixing, copolymers containing up to 6 blocks are formed. The fact that the poorest R^2 is obtained when fitting the data with diblocks as the only multiblock copolymer present implies that at least triblocks are formed. This is especially apparent for the sample mixed for 20 minutes.

The time dependence of the conversion of telechelic into multiblock copolymer can be determined by the analysis of this data. The time dependence of the conversion can be fit to a power law, $C = a*t^m$. The exponent m can be extracted from a log-log plot of conversion as a function of mixing time. This analysis for the 37k anh-PS-anh

Table A.7. Fitting results of 37k anh-PS-anh and 16k NH_2-PI-NH_2 telechelics.

37k anh-PS-anh / 16k NH_2-PI-NH_2			
5 Min	*Block*	*APE %C*	R^2
	Tetra	45.8	0.9700
	Tri	46.3	0.9698
	Di	46.9	0.9693
10 Min	*Block*	*APE %C*	R^2
	Tetra	56.9	0.9811
	Tri	58.9	0.9805
	Di	63.4	0.9616
20 Min	*Block*	*APE %C*	R^2
	Hexa	64.1	0.9845
	Penta	64.0	0.9844
	Tetra	62.4	0.9841
	Tri	66.2	0.9821
	Di	62.4	0.8877

and 16k NH_2-PI-NH_2 telechelics is shown in Figure A.9. A linear fit to this log-log plot gives a slope of 0.243 with a correlation factor of $R^2 = 0.973$. This indicates the conversion increases as a function of $\sim t^{0.25}$ and the grafting is reaction controlled, as is discussed in Chapter 4.

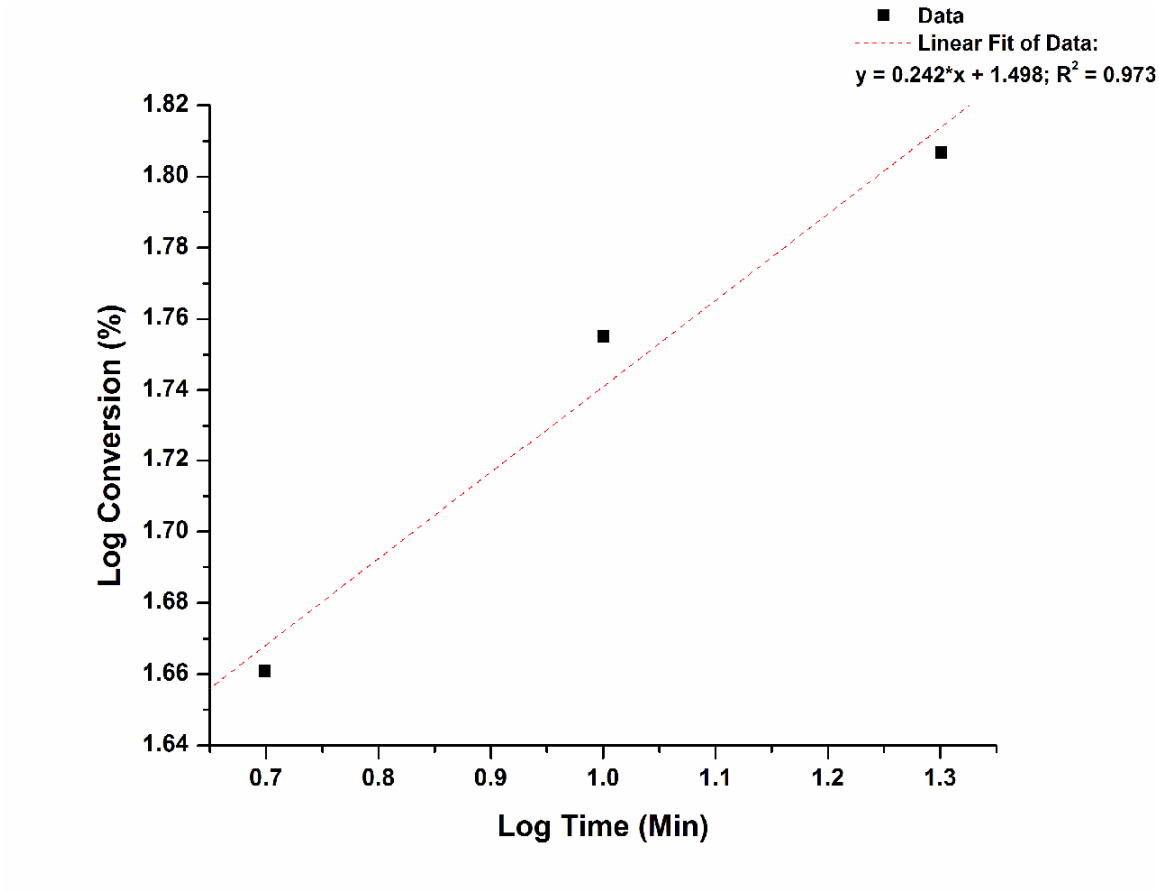

Figure A.9. Log-log plot of conversion as a function of mixing time for 37k anh-PS-anh and 16k NH_2-PI-NH_2 telechelics.

Vita

Earl Ashcraft was born on October 14, 1978 in Red Bank, NJ. From 1979 until 1997, he lived in Towanda, PA, when he graduated from Towanda Area High School. In August of 1997, he moved to Huntingdon, PA, to attend Juniata College for his undergraduate studies. Upon graduating with a BS in chemistry, he moved to Bloomington, IN, where he began his graduate studies in physical chemistry at Indiana University under the direction of Josef Zwanziger. When his advisor moved to Canada in 2003, he completed the experiments and writing required for a MS and returned to Towanda, PA. A MS in physical chemistry was awarded to him by Indiana University in July of 2004. At this time, he moved to Knoxville, TN, to attend the University of Tennessee in order to continue his graduate studies. He joined Mark Dadmun's group, where he studied polymer chemistry. He successfully defended his dissertation on April 27, 2010.